

Cracked naphtha reactivity and its influence on acid catalyst deactivation

by

Giselle Uzcátegui Barrios

A thesis submitted in partial fulfillment of the requirements for the degree of

Doctor of Philosophy

in

Chemical Engineering

Department of Chemical and Materials Engineering

University of Alberta

© Giselle Uzcátegui Barrios, 2022

## Abstract

Acid catalyzed olefin-aromatic alkylation is an alternative process to hydrotreating to reduce the olefin content thermally cracked naphtha produced during the partial upgrading of bitumen. Acid catalysis is not commonly employed for conversion of untreated cracked naphtha. This motivated the study of the reactivity of cracked naphtha and its role on the deactivation of the acid catalyst employed in the olefin-alkylation process.

The instances in which cracked naphtha has led to complications during its processing were reviewed. It was found that oxidative and thermal conditions could trigger the initiation of free radical reactions that promoted the formation of heavy compounds or deposits. It was possible to distinguish between the products from oxidative instability and thermal instability. Compounds with a carbon that is simultaneously in the allylic and benzylic position were found to be particularly reactive and could initiate free radical reactions at 250–350 °C in the absence of oxygen.

The deactivation of the amorphous silica-alumina (ASA) acid catalyst used in the olefin-aromatic alkylation process were first studied by analyzing the deposits of the spent catalysts after reaction with thermally cracked naphtha at different conditions in the range 250–350 °C, WHSV of 0.5–2 h<sup>-1</sup>, in a pilot scale unit. The main cause of deactivation was deposit formation caused by a combination of catalytic and thermal reactions. The location of most of the deposits depended on the operating conditions, including at the reactor outlet. Another outcome was the understanding that nitrogen bases were not the main cause of catalyst deactivation. The nitrogen was only found present in deposits in the inlet of the reactor and at very low concentrations.

To study if free radical chemistry was occurring in cracked naphtha at 200–300 °C, we used a probe molecule,  $\alpha$ -methylstyrene (AMS). AMS facilitated detection of free radical reactions products. Heating of cracked naphtha and AMS mixtures resulted in the formation of compounds linked to free radical termination, like cumene and AMS dimers. Control reactions of AMS ruled out AMS self-initiation as explanation for the observations. The results suggested that compounds in the cracked naphtha initiated the reaction network leading to the observed products, partly because AMS act as a hydrogen acceptor and participate in molecule induced radical formation.

There have been indications that cyclopentenes can undergo reactions that accelerate the formation of carbonaceous deposits. After verifying the existence of cyclopentenes in the cracked naphtha, model compounds were used to investigate how cyclopentene could lead to formation of deposits on an ASA catalyst, and how it compared to the effect of linear olefins. It was found that cyclopentene had a more significant effect on the formation of deposits than 1-hexene. Reactions of cyclopentene on an ASA catalyst at 300 °C yielded bicyclic compounds like decalin and octalin, which indicated that hydrogen transfer was part of the reaction network, since decalin had to be the result of these reactions. It also indicated that cyclopentenes and dienes may share a pathway to bicyclic compounds leading to the formation of deposits on the catalyst surface.

Following the insights gained during the analysis of the spent catalyst samples, it was hypothesized that the adsorption of nitrogen bases was a dynamic process. A series of experiments was done to assess if compounds in the cracked naphtha were competing with nitrogen bases for the adsorption on the acid sites. For this, a pyridine-saturated catalyst was subjected to different temperatures in the presence of cracked naphtha and heptane, and the amount of pyridine desorbed was quantified in the liquid product. It was found that, at all temperatures studied, more pyridine was desorbed towards the cracked naphtha compared to heptane. There were contributions of partitioning of the

previously adsorbed pyridine between the solid and liquid, as well as competitive adsorption in the case of the cracked naphtha. The adsorption of compounds from cracked naphtha was confirmed with diffuse reflectance infrared Fourier transform spectroscopy (DRIFTS), where it was determined that alkyl aromatics were present on the catalyst surface.

## Preface

### (Mandatory due to collaborative work)

Chapter 3 was published as “Uzcátegui, G.; de Klerk, A. Causes of Deactivation of an Amorphous Silica-Alumina Catalyst Used for Processing of Thermally Cracked Naphtha in a Bitumen Partial Upgrading Process. *Fuel* **2021**, *293*, 120479.” I was responsible for concept formation, experimental design, data collection and analysis as well as manuscript composition. I was also the corresponding author, and I was responsible for presenting this research at the International Mexican Congress on Chemical Reaction Engineering (IMCCRE) 2018. Arno de Klerk acted as the supervisory author and corresponding author and was involved in the concept formation, data interpretation and manuscript composition.

Chapter 4 was done in collaboration with Shirley Fong and it was published as “Uzcátegui, G.; Fong, S. Y.; de Klerk, A. Cracked Naphtha Reactivity: Effect of Free Radical Reactions. *Energy Fuels* **2018**, *32* (5), 5812–5823.” I was responsible for concept formation, experimental design, data collection and analysis as well as manuscript composition. I was also the corresponding author, and I was responsible for presenting this research at Canadian Society for Chemical Engineering (CSCChE) conference 2017. Shirley Fong was responsible for data collection and initial interpretation. Arno de Klerk acted as the supervisory author and corresponding author and was involved in the concept formation, data interpretation and manuscript composition.

*To my mom, Antonia, for being there from start to finish.*

*To my grandfather, Marcos, for all the love and support.*

## Acknowledgments

I would like to express my sincere gratitude to Dr. Arno de Klerk. Thank you for believing in me when I first joined the group, for your guidance and patience through the years, and for always supporting me. Your enthusiastic way of viewing science was a great motivation all these years. I greatly appreciate all the learning opportunities you gave me; I am a better engineer thanks to you.

I feel extremely fortunate to have had the opportunity of working in such a wonderful research group. I am confident to say that everyone in the group helped me in one way or another to accomplish what this thesis is today. From discussing experimental strategies or training me on lab equipment, to making light conversation or inviting me for a coffee when I needed a break. Among all these amazing people I would like to specially thank a few: Cibele, for all the support during research activities, and for all the coffees. Natalia, for teaching me those first basics in the lab, and for always being open for a discussion about science or life. Joy, for opening the doors of your home to me when I needed it, and for all the delicious meals. Sima, for always being present, no matter what. Shirley, for making that time in the office/lab more fun. Lina, Yohana, Riya, Cloribel, Sowmya, Tudor, Nuvaaid, Felipe, Shruthi, Adriana, thank you for all the help, support, and friendship.

I want to express my heartfelt gratitude to my mom, for giving me the opportunities that I had, against all odds. Without you, none of this would have been possible. Mi vida, thank you for the unconditional love and support, you are my rock. My aunt Marbelis, for all the support and cheering. My sisters, for always being there for me.

Finally, I thank CNOOC, Alberta Innovates and NSERC for the financial support.

## Table of Contents

|                                                                                                     |    |
|-----------------------------------------------------------------------------------------------------|----|
| Chapter 1. Introduction.....                                                                        | 1  |
| 1.1. Background .....                                                                               | 1  |
| 1.2. Objective .....                                                                                | 6  |
| 1.3. Scope .....                                                                                    | 6  |
| 1.4. References .....                                                                               | 7  |
| Chapter 2. Challenges during processing of cracked naphthas: on the instability and its causes<br>9 |    |
| 2.1. Introduction .....                                                                             | 9  |
| 2.2. Cracked naphtha.....                                                                           | 11 |
| 2.3. Challenges during processing of cracked naphtha .....                                          | 13 |
| 2.3.1. Oxidation products formation during storage.....                                             | 13 |
| 2.3.2. Pressure-drop in hydrotreaters .....                                                         | 15 |
| 2.3.3. Heat exchanger fouling.....                                                                  | 16 |
| 2.3.4. Acid catalyst deactivation.....                                                              | 18 |
| 2.4. Instability of cracked naphthas.....                                                           | 18 |
| 2.4.1. Oxidative stability.....                                                                     | 19 |
| 2.4.2. Thermal stability.....                                                                       | 23 |
| 2.5. Compound classes in the cracked naphtha and their contribution to its instability .....        | 25 |
| 2.5.1. Saturated compounds (alkanes) .....                                                          | 25 |



|                                                                                                                                                                             |                                                                                   |    |
|-----------------------------------------------------------------------------------------------------------------------------------------------------------------------------|-----------------------------------------------------------------------------------|----|
| 2.5.2.                                                                                                                                                                      | Olefins (alkenes) .....                                                           | 26 |
| 2.5.3.                                                                                                                                                                      | Diolfins (dienes).....                                                            | 28 |
| 2.5.4.                                                                                                                                                                      | Aromatics .....                                                                   | 29 |
| 2.5.5.                                                                                                                                                                      | Heteroatom compounds .....                                                        | 31 |
| 2.6.                                                                                                                                                                        | Cracking reactions for cracked naphtha production.....                            | 33 |
| 2.6.6.                                                                                                                                                                      | Naphtha derived from thermal cracking processes.....                              | 35 |
| 2.6.7.                                                                                                                                                                      | Naphtha derived from catalytic cracking processes.....                            | 43 |
| 2.7.                                                                                                                                                                        | Properties expected in cracked naphthas from different cracking processes .....   | 46 |
| 2.8.                                                                                                                                                                        | Crude oil feedstock properties implications for the product cracked naphtha ..... | 47 |
| 2.9.                                                                                                                                                                        | Concluding Remarks .....                                                          | 49 |
| 2.10.                                                                                                                                                                       | References .....                                                                  | 50 |
| <br>Chapter 3. Causes of deactivation of an amorphous silica-alumina catalyst used for processing of thermally cracked naphtha in a bitumen partial upgrading process ..... |                                                                                   |    |
| 3.1.                                                                                                                                                                        | Introduction .....                                                                | 63 |
| 3.2.                                                                                                                                                                        | Experimental .....                                                                | 66 |
| 3.2.1.                                                                                                                                                                      | Materials .....                                                                   | 66 |
| 3.2.2.                                                                                                                                                                      | Equipment and procedure .....                                                     | 67 |
| 3.2.3.                                                                                                                                                                      | Analyses.....                                                                     | 70 |
| 3.3.                                                                                                                                                                        | Results .....                                                                     | 72 |
| 3.3.1.                                                                                                                                                                      | Fresh and spent catalyst characterization.....                                    | 72 |

|            |                                                                            |     |
|------------|----------------------------------------------------------------------------|-----|
| 3.3.2.     | Quantifying Carbonaceous deposits .....                                    | 73  |
| 3.3.3.     | Effect of operating conditions on carbonaceous deposits.....               | 74  |
| 3.3.4.     | Elemental analysis of carbonaceous deposits .....                          | 77  |
| 3.3.5.     | Chemical composition of carbonaceous deposits .....                        | 79  |
| 3.3.6.     | Electron spin resonance spectroscopy of spent catalysts.....               | 80  |
| 3.3.7.     | Infrared spectroscopy of spent catalysts .....                             | 82  |
| 3.3.8.     | FTIR analysis of evolved gases from combustion of deposits during TGA..... | 84  |
| 3.4.       | Discussion .....                                                           | 84  |
| 3.4.1.     | Nitrogen base adsorption and role in deactivation.....                     | 84  |
| 3.4.2.     | Influence of temperature on composition of carbonaceous deposits .....     | 86  |
| 3.4.3.     | Profile of deposit formation .....                                         | 87  |
| 3.5.       | Conclusions .....                                                          | 91  |
| 3.6.       | References .....                                                           | 92  |
| Chapter 4. | Cracked naphtha reactivity: Effect of free radical reactions.....          | 99  |
| 4.1.       | Introduction .....                                                         | 100 |
| 4.2.       | Experimental .....                                                         | 101 |
| 4.2.1.     | Materials .....                                                            | 101 |
| 4.2.2.     | Equipment and procedure .....                                              | 102 |
| 4.2.3.     | Analyses.....                                                              | 103 |
| 4.3.       | Results .....                                                              | 104 |

|                                                                                                                     |                                                                                      |     |
|---------------------------------------------------------------------------------------------------------------------|--------------------------------------------------------------------------------------|-----|
| 4.3.1.                                                                                                              | Free radical content by ESR .....                                                    | 104 |
| 4.3.2.                                                                                                              | Product distribution from GC-MS chromatogram.....                                    | 105 |
| 4.3.3.                                                                                                              | Identification of products through Mass Spectra analysis .....                       | 110 |
| 4.3.4.                                                                                                              | Oxidation products of AMS.....                                                       | 114 |
| 4.3.5.                                                                                                              | Gum content of the feed and product.....                                             | 116 |
| 4.4.                                                                                                                | Discussion .....                                                                     | 118 |
| 4.4.1.                                                                                                              | Free radicals present in the thermally cracked naphtha at 200–300 °C.....            | 118 |
| 4.4.2.                                                                                                              | Comparison of product distribution from thermal and autoxidation of naphtha with AMS | 120 |
| 4.4.3.                                                                                                              | Free radical initiation in thermally cracked naphtha.....                            | 121 |
| 4.5.                                                                                                                | Conclusions .....                                                                    | 124 |
| 4.6.                                                                                                                | References .....                                                                     | 125 |
| Chapter 5. Acid catalyzed reactions of cyclopentene in cracked naphtha and their role on catalyst deactivation..... |                                                                                      |     |
| 5.1.                                                                                                                | Introduction .....                                                                   | 130 |
| 5.2.                                                                                                                | Experimental .....                                                                   | 132 |
| 5.2.1.                                                                                                              | Materials .....                                                                      | 132 |
| 5.2.2.                                                                                                              | Equipment and procedure .....                                                        | 133 |
| 5.2.3.                                                                                                              | Analyses.....                                                                        | 137 |
| 5.3.                                                                                                                | Results .....                                                                        | 138 |
| 5.3.1.                                                                                                              | Identification of cyclopentene species .....                                         | 138 |

|            |                                                                                                                           |     |
|------------|---------------------------------------------------------------------------------------------------------------------------|-----|
| 5.3.2.     | Thermal and catalytic reactivity of cyclopentenes in cracked naphtha .....                                                | 141 |
| 5.3.3.     | Fluorescence spectroscopy of feed and reaction products .....                                                             | 145 |
| 5.3.4.     | Reactions of cyclopentene with Siral30.....                                                                               | 148 |
| 5.3.5.     | Reactions of 1-hexene with Siral30 .....                                                                                  | 154 |
| 5.3.6.     | Electron Spin Resonance (ESR) of the spent catalyst. ....                                                                 | 158 |
| 5.4.       | Discussion .....                                                                                                          | 159 |
| 5.4.1.     | Thermal compared to catalytic conversion of cracked naphtha.....                                                          | 159 |
| 5.4.2.     | Reactivity of different olefinic compounds on an ASA catalyst. ....                                                       | 162 |
| 5.4.3.     | Modification of olefin reactivity by aromatics .....                                                                      | 167 |
| 5.4.4.     | Formation of bicyclic compounds from acid catalyzed reactions of cyclopentene.<br>170                                     |     |
| 5.4.5.     | Role of bicyclic compounds on the formation of deposits on the catalyst surface.<br>173                                   |     |
| 5.5.       | Conclusions .....                                                                                                         | 175 |
| 5.6.       | References .....                                                                                                          | 177 |
| Chapter 6. | Desorption of organic nitrogen bases from an amorphous silica-alumina catalyst<br>used for treating cracked naphtha ..... | 183 |
| 6.1.       | Introduction .....                                                                                                        | 184 |
| 6.2.       | Experimental .....                                                                                                        | 186 |
| 6.2.1.     | Materials .....                                                                                                           | 186 |
| 6.2.2.     | Equipment and procedure .....                                                                                             | 187 |

|                                                                                                    |     |
|----------------------------------------------------------------------------------------------------|-----|
| 6.3. Results and discussion.....                                                                   | 190 |
| 6.3.1. Fresh catalyst characterization.....                                                        | 190 |
| 6.3.2. Desorbed pyridine at different temperatures in cracked naphtha and heptane .....            | 195 |
| 6.3.3. Causes of pyridine desorption.....                                                          | 203 |
| 6.4. Conclusions .....                                                                             | 208 |
| 6.5. References .....                                                                              | 209 |
| Chapter 7. Conclusions.....                                                                        | 213 |
| 7.1. Introduction .....                                                                            | 213 |
| 7.2. Major Conclusions and Insights.....                                                           | 213 |
| 7.3. Recommended future work .....                                                                 | 217 |
| 7.3.1. Contribution of thermal reactions of olefin-alkylation products to deposit formation<br>217 |     |
| 7.3.2. Plug flow reactions of cracked naphtha spiked with cyclopentene and 1-hexene.               | 218 |
| 7.3.3. Pyridine cyclopentene competitive adsorption .....                                          | 218 |
| References.....                                                                                    | 220 |
| Appendix A. Support information for Chapter 4.....                                                 | 242 |
| A.1. Chromatograms of control reactions.....                                                       | 242 |
| Appendix B: Support information for Chapter 5.....                                                 | 244 |
| B1. Dimerization products from the reaction of cyclopentene and Siral30.....                       | 244 |

## List of Tables

|                                                                                                                                                                                            |     |
|--------------------------------------------------------------------------------------------------------------------------------------------------------------------------------------------|-----|
| <b>Table 1.1.</b> Pipeline specifications for crude oil in Canada.....                                                                                                                     | 2   |
| <b>Table 2.1.</b> Typical yields of cracked naphtha for each of the cracking processes. ....                                                                                               | 34  |
| <b>Table 2.2.</b> Characteristics of the cracked naphthas derived from different cracking processes. .                                                                                     | 36  |
| <b>Table 2.3.</b> Product distribution comparison between delayed and fluid coking process using the same feed. ....                                                                       | 42  |
| <b>Table 3.1.</b> Characterization of thermally cracked naphtha.....                                                                                                                       | 67  |
| <b>Table 3.2.</b> Operating conditions of alkene-aromatic test runs from which the spent catalysts were obtained for this study.....                                                       | 69  |
| <b>Table 3.3.</b> Characterization of the fresh and spent amorphous silica-alumina catalyst. ....                                                                                          | 73  |
| <b>Table 3.4.</b> Amount of naphtha feed material converted to carbonaceous deposits on the catalyst at 325 °C in the same time period, but at different weight hourly space velocity..... | 75  |
| <b>Table 3.5.</b> Nitrogen-to-carbon and sulfur-to-carbon ratios of the carbonaceous deposits found on spent catalysts. ....                                                               | 78  |
| <b>Table 3.6.</b> Relative free radical content and g-factors of the carbonaceous deposits in selected spent catalysts. ....                                                               | 81  |
| <b>Table 3.7.</b> Area of the Gram-Schmidt curves for the evolved gases from combustion of the deposits at the inlet and out of the reactor in experiment RS3. ....                        | 84  |
| <b>Table 4.1.</b> Characterization of thermally cracked naphtha.....                                                                                                                       | 102 |
| <b>Table 4.2.</b> Chemicals and cylinder gases used in the study. ....                                                                                                                     | 103 |
| <b>Table 4.3.</b> Gum content of feed and products of conversion performed at the indicated conditions for 1 h.....                                                                        | 117 |

|                                                                                                                                                |     |
|------------------------------------------------------------------------------------------------------------------------------------------------|-----|
| <b>Table 5.1.</b> Chemicals and cylinder gases used in the study. ....                                                                         | 132 |
| <b>Table 5.2.</b> Catalysts textural properties after treatment at 550 °C.....                                                                 | 133 |
| <b>Table 5.3.</b> Characterization of thermally cracked naphtha.....                                                                           | 134 |
| <b>Table 5.4.</b> Solutions for reaction with model compounds.....                                                                             | 136 |
| <b>Table 5.5.</b> Summary identified cyclopentenes .....                                                                                       | 141 |
| <b>Table 5.6.</b> Summary of reactivity of cyclopentene compounds.....                                                                         | 145 |
| <b>Table 5.7.</b> Suggested compounds for the main products from reactions of cyclopentene on Siral30.<br>.....                                | 150 |
| <b>Table 5.8.</b> Relative areas of cyclopentene dimers formed after reaction with Siral 30. ....                                              | 154 |
| <b>Table 5.9.</b> Relative areas of 1-hexene products after reaction on Siral 30 at 300 °C.....                                                | 157 |
| <b>Table 5.10.</b> Free radical content relative to that of the spent catalyst from the reaction with cracked<br>naphtha.....                  | 159 |
| <b>Table 6.1.</b> Characterization of thermally cracked naphtha.....                                                                           | 186 |
| <b>Table 6.2.</b> Chemicals and cylinder gases used in the study. ....                                                                         | 187 |
| <b>Table 6.3.</b> Acid site strength and distribution in Siral 40 from NH <sub>3</sub> -TPD data. ....                                         | 191 |
| <b>Table 6.4.</b> Peak height of infrared absorption bands corresponding to adsorbed pyridine over Siral<br>40 at different temperatures. .... | 193 |
| <b>Table 6.5.</b> Contributing groups for observed absorption bands in each catalyst sample. ....                                              | 201 |
| <b>Table B6.</b> Suggested compounds for the main dimerization products from reactions of<br>cyclopentene on Siral30.....                      | 245 |

## List of Figures

|                                                                                                                                                                                                                                        |    |
|----------------------------------------------------------------------------------------------------------------------------------------------------------------------------------------------------------------------------------------|----|
| <b>Figure 1.1.</b> Simplified block flow diagram of BituMax™. ....                                                                                                                                                                     | 3  |
| <b>Figure 1.2.</b> Formation of an olefin through $\beta$ -scission during thermal cracking. ....                                                                                                                                      | 3  |
| <b>Figure 1.3.</b> Acid catalyzed alkene-aromatic alkylation an alkene dimerization illustrated by the reaction of 1-pentene and toluene. ....                                                                                         | 5  |
| <b>Figure 2.1.</b> Allylic carbon and hydrogen in 1-pentene. ....                                                                                                                                                                      | 27 |
| <b>Figure 2.2.</b> Possible positions of double bonds in pentadiene. ....                                                                                                                                                              | 28 |
| <b>Figure 2.3.</b> Benzylic position in cumene.....                                                                                                                                                                                    | 30 |
| <b>Figure 2.4.</b> Allylic and benzylic position in indene. ....                                                                                                                                                                       | 30 |
| <b>Figure 2.5.</b> Heteroatom compound classes in cracked naphtha. ....                                                                                                                                                                | 32 |
| <b>Figure 2.6.</b> Mechanism of paraffins cracking through the formation of a carbonium ion.....                                                                                                                                       | 43 |
| <b>Figure 2.7.</b> $\beta$ -scission of olefins through the formation of a carbenium ion.....                                                                                                                                          | 44 |
| <b>Figure 2.8.</b> Carbenium ion oligomerization and skeletal isomerization reactions.....                                                                                                                                             | 45 |
| <b>Figure 3.1.</b> Acid catalyzed alkene-aromatic alkylation an alkene dimerization illustrated by the reaction of 1-pentene and toluene. ....                                                                                         | 64 |
| <b>Figure 3.2.</b> Alkene-aromatic alkylation reactors operating in parallel to enable one reactor at a time to be taken off-line for in situ catalyst regeneration. The cycle length will affect the number of reactors employed..... | 65 |
| <b>Figure 3.3.</b> Simplified flow diagram of the laboratory-scale pilot unit used for the alkene-aromatic alkylation. Instrumentation and most valves are not shown. ....                                                             | 68 |
| <b>Figure 3.4.</b> Ammonia temperature programmed desorption curve of fresh (solid line) and spent and calcined (dotted line) amorphous silica-alumina catalyst. ....                                                                  | 72 |



**Figure 3.5.** Spent catalyst mass loss with temperature (solid line) and derivative mass loss with temperature (dotted line) to illustrate the main where regions where mass loss occurred. The data shown is for the spent catalyst sample Exp 1, performed at 325 °C and 1 h<sup>-1</sup>..... 74

**Figure 3.6.** Effect of (a) temperature at a WHSV of 1 h<sup>-1</sup>, and (b) weight hourly space velocity at a temperature of 325 °C, on the amount of carbonaceous deposits found on the spent catalysts in experiments 1–5. The error bars indicate one standard deviation of analyses in triplicate. .... 74

**Figure 3.7.** Carbonaceous deposit content of the spent catalyst from the different sections along the reactor bed in experiments RS1–RS3. The duration of the experiments was different. The error bars indicate one standard ion of analyses in triplicate..... 76

**Figure 3.8.** Chromatograms of the dichloromethane extracts of the spent catalyst samples from the top and bottom of the reactor after experiment RS1, which is compared with that of the naphtha feed material..... 80

**Figure 3.9.** ESR spectra of the spent catalyst samples at a concentration of 6 wt% of organic deposits. .... 81

**Figure 3.10.** Infrared spectra of the fresh catalyst and spent catalysts from the reactor inlet and outlet of experiments RS1 (250 °C) and RS3 (325 °C). .... 82

**Figure 3.11.** Rate of carbonaceous deposit formation calculated from Table 4 showing that there was little change with respect to weight hourly space velocity. .... 90

**Figure 4.1.** ESR spectra of the naphtha sample at room temperature. .... 105

**Figure 4.2.** (a) Complete chromatogram of the thermally cracked naphtha, (b) and comparison of the section of interest of the chromatograms of the feed and product of the control reaction of the naphtha at 300 °C for 1h. .... 106

**Figure 4.3.** Product distribution from reactions of naphtha with AMS at different temperatures. .... 107

|                                                                                                                                                                                                                                                                                           |     |
|-------------------------------------------------------------------------------------------------------------------------------------------------------------------------------------------------------------------------------------------------------------------------------------------|-----|
| <b>Figure 4.4.</b> Cumene production from reactions of naphtha with AMS at different temperatures.<br>.....                                                                                                                                                                               | 108 |
| <b>Figure 4.5.</b> Product distribution from the reaction of naphtha with AMS under 210 kPa of oxygen partial pressure at 300 °C. ....                                                                                                                                                    | 109 |
| <b>Figure 4.6.</b> Effect of the oxygen partial pressure on the product distribution on the reaction of naphtha with AMS at 300 °C. ....                                                                                                                                                  | 110 |
| <b>Figure 4.7.</b> Mass spectra of products (a) P-1, (b) P-4, and (c)P-5. ....                                                                                                                                                                                                            | 111 |
| <b>Figure 4.8.</b> Possible isomers from free radical dimerization of AMS. ....                                                                                                                                                                                                           | 112 |
| <b>Figure 4.9.</b> Mass spectra of products (a) P-2, (b) P-3, and (c) P-6. ....                                                                                                                                                                                                           | 113 |
| <b>Figure 4.10.</b> A possible structure for P-6. ....                                                                                                                                                                                                                                    | 114 |
| <b>Figure 4.11.</b> Chromatogram of the product from the reaction of AMS in <i>n</i> -pentane at 300 °C and 210 kPa oxygen partial pressure. The oxygenates shown (from left to right) are acetophenone, AMS oxide, $\alpha$ -methylbenzeneacetaldehyde, and 2-phenylprop-2-en-1-ol. .... | 115 |
| <b>Figure 5.1.</b> Reaction setup. Thermocouple T01 measured the temperature in the reaction mixture and thermocouple T02 measured the temperature outside of the reactor for control of the heater.<br>.....                                                                             | 135 |
| <b>Figure 5.2.</b> Chromatogram of the cracked naphtha feed.....                                                                                                                                                                                                                          | 139 |
| <b>Figure 5.3.</b> Chromatogram of cracked naphtha feed (black line) and after reaction at 300 °C (blue line). ....                                                                                                                                                                       | 142 |
| <b>Figure 5.4.</b> Chromatogram of cracked naphtha feed (black line) and after reaction with Pural SB at 300 °C (blue line). ....                                                                                                                                                         | 143 |
| <b>Figure 5.5.</b> Chromatogram of the cracked naphtha feed (black line) and product of the reactions with Siral10 (blue line), and Siral30 (red line). ....                                                                                                                              | 144 |

|                                                                                                                                                                                                                                                                   |     |
|-------------------------------------------------------------------------------------------------------------------------------------------------------------------------------------------------------------------------------------------------------------------|-----|
| <b>Figure 5.6.</b> Fluorescence contour plots for (1) cracked naphtha feed, (2) cracked naphtha after 1h at 300 °C with stirring, and cracked naphtha after reaction with (3) Siral10 and (4) Siral30 at 300 °C for 30 min. EX = 200-350 nm. EM = 250-400 nm..... | 146 |
| <b>Figure 5.7.</b> Emission spectra of different samples at excitation wavelength (Ex WL) of 224 and 275 nm. ....                                                                                                                                                 | 147 |
| <b>Figure 5.8.</b> Chromatograms of the reaction products of cyclopentene and Siral30.....                                                                                                                                                                        | 149 |
| <b>Figure 5.9.</b> Cyclopentene dimer, 2-cyclopentyl-cyclopentene. ....                                                                                                                                                                                           | 150 |
| <b>Figure 5.10.</b> Chromatogram of model compounds (black line) and dimerization products of cyclopentene (blue line).....                                                                                                                                       | 152 |
| <b>Figure 5.11.</b> Chromatograms of the reaction products of cyclopentene and ethylbenzene with Siral30. ....                                                                                                                                                    | 153 |
| <b>Figure 5.12.</b> Chromatograms of the reaction products of 1-hexene and Siral30. ....                                                                                                                                                                          | 155 |
| <b>Figure 5.13.</b> Portion of the chromatograms of the reaction products of 1-hexene + ethylbenzene and Siral30. ....                                                                                                                                            | 156 |
| <b>Figure 5.14.</b> ESR spectra of the spent Siral30 after reaction with cracked naphtha and model compounds. ....                                                                                                                                                | 158 |
| <b>Figure 5.15.</b> Possible reaction pathway for the formation of octalin from cyclopentene. ....                                                                                                                                                                | 171 |
| <b>Figure 5.16.</b> Possible bicyclic compounds present after reaction of cyclopentene with Siral 30. ....                                                                                                                                                        | 171 |
| <b>Figure 5.17.</b> Octalin-octalin hydrogen transfer. ....                                                                                                                                                                                                       | 172 |
| <b>Figure 5.18.</b> Production of decahydronaphthalene and naphthalene from tetralin. ....                                                                                                                                                                        | 172 |
| <b>Figure 6.1.</b> NH <sub>3</sub> -TPD curve of Siral 40. ....                                                                                                                                                                                                   | 190 |
| <b>Figure 6.2.</b> Pyridine adsorption in Bronsted and Lewis acid sites. ....                                                                                                                                                                                     | 192 |

|                                                                                                                                                                                   |     |
|-----------------------------------------------------------------------------------------------------------------------------------------------------------------------------------|-----|
| <b>Figure 6.3.</b> Diffuse Reflectance Infrared Fourier Transform Spectroscopy (DRIFTS) of pyridine desorption from Siral 40. Pyridine-free Siral 40 was used as background. .... | 192 |
| <b>Figure 6.4.</b> Chromatogram signal of the GC-NPD, with pyridine eluting at 25 min and internal standard 2-methyl pyridine eluting at 40 min. ....                             | 195 |
| <b>Figure 6.5.</b> Desorbed pyridine in reactions with naphtha and heptane. Analysis in the liquid product. ....                                                                  | 197 |
| <b>Figure 6.6.</b> DRIFTS of pyridine-saturated ASA catalyst after exposure to heptane and cracked naphtha. ....                                                                  | 200 |
| Figure A1. Reactions at 200 °C.....                                                                                                                                               | 242 |
| Figure A2. Reactions at 250 °C.....                                                                                                                                               | 243 |
| Figure A3. Reactions at 300 °C.....                                                                                                                                               | 243 |
| Figure B0.1. Chromatogram of dimerization products from reaction of cyclopentene on Siral30 at 300 °C. ....                                                                       | 244 |

## **Chapter 1. Introduction**

### **1.1. Background**

The oil sands located in Western Canada are one of the largest crude oil reservoirs in the world. Bitumen is produced from these reservoirs through mining or in-situ recovery using methods such as steam assisted gravity drainage (SAGD), and it is taken for further processing before it can be sold in the commodity market.

Bitumen is an extra-heavy type of oil. Thousands of years of bacterial biodegrading turned the once light crude oil into a high density and extremely high viscosity crude oil,<sup>1</sup> with 1015 kg/m<sup>3</sup> and 5000-300000 cSt at 25 °C.<sup>2</sup> These properties are caused by the presence of large molecules and the presence of sulfur, nitrogen, and oxygen. All these characteristics make bitumen an intrinsically difficult feed to process to achieve the desired final fuel products, hence decreasing its value compared to crudes with a lower viscosity, and lower sulfur, nitrogen, and oxygen content.

The ultimate market for most crude oils is a petroleum refinery, in which the desired final products for consumers are produced, such as gasoline, diesel, jet fuel, etc.<sup>3</sup> Although some petroleum refineries are designed to take heavy oil and bitumen, many are not.<sup>4</sup> Bitumen can also be processed in upgraders, which goal is to convert bitumen into a lighter and less viscous crude oil, with lower sulfur, nitrogen, and oxygen content, which would increase its value, but at substantial capital and operating costs.<sup>5</sup>

The main problem faced by bitumen producers is the transportation of this highly viscous fluid to the upgrader or to the refinery from the production site. Transportation can be by rail cars or through pipelines.<sup>5</sup> When transported through pipelines, one way to decrease the viscosity and density of bitumen is by diluting the bitumen using a solvent. But diluting the bitumen has some downsides. There are costs associated to the solvent used, as well as for the total volume of fluid transported in the pipeline.<sup>6</sup> This translates into high operational costs that are significant when considering that, due to its quality, the bitumen is not a high value oil compared to the benchmark crude oil West Texas Intermediate (WTI).<sup>6</sup>

Over the years, an alternative to dilution has been developed in the form of upgrading, of which partial upgrading is a special case.

Partial upgrading has been a topic for substantial research, motivated by the need to replace or decrease dilution as a transportation solution for bitumen, and also to increase the value of the bitumen with minimum processing input.<sup>2</sup> In contrast to full upgrading, the objective of partial upgrading of bitumen is to improve its transportability of the product to decrease or eliminate the use of diluent, while meeting the pipeline specifications (**Table 1.1**) without the capital investment that a full upgrader facility requires. In other words, the aim of partial upgrading is to increase the amount of load of product in the pipelines, since it reduces the diluent needed for transportability, but without the high operational and capital cost of a full upgrader.

Various partial upgrading designs have been suggested,<sup>2</sup> but the design that is relevant for this study is the BituMax™ process.<sup>7</sup> This process is designed to be integrated with a SAGD bitumen extraction site. The process consists of three main elements: solvent deasphalting, thermal cracking, and olefins treating, as seen in **Figure 1.1**.

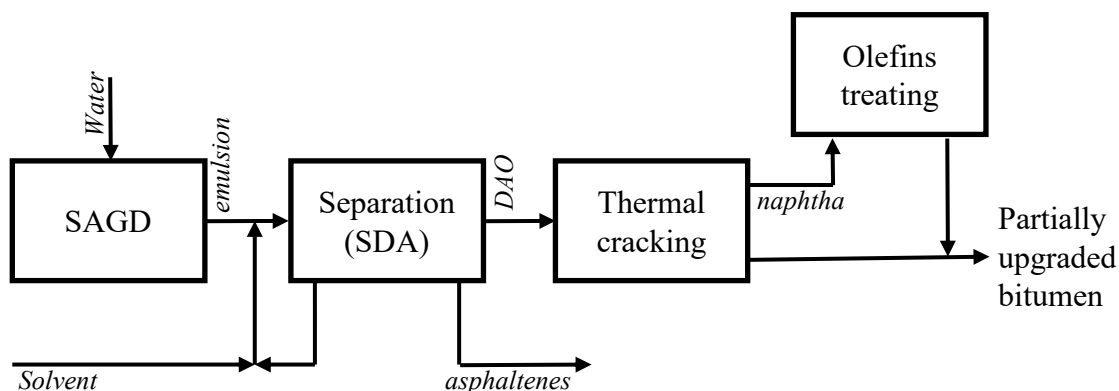
**Table 1.1.** Pipeline specifications for crude oil in Canada.

| Property         | Unit                                 | Value                          |
|------------------|--------------------------------------|--------------------------------|
| Viscosity        | cSt @ 25 °C                          | 350 cSt @ pipeline temperature |
| Density          | kg/m <sup>3</sup>                    | < 940                          |
| Solids and water | vol%                                 | <0.5                           |
| Olefin content   | wt% 1-decene equivalent <sup>a</sup> | <1                             |

<sup>a</sup>Quantification is done using the <sup>1</sup>H NMR spectrum signal corresponding to the olefinic hydrogen, and assuming all olefins are present as 1-decene.

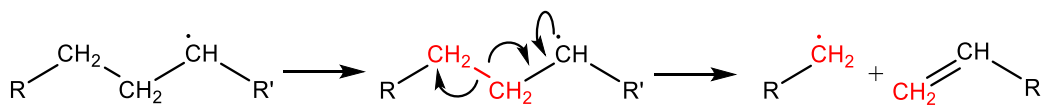
The solvent deasphalting unit deals with the bitumen emulsion coming from the SAGD, and the main objective of this unit is to reject the asphaltenes fraction, which would reduce the viscosity, sulfur and nitrogen content, preparing the feed for the thermal cracker. The thermal cracker envisioned by the process is a coil-and-soaker visbreaking unit. During the thermal cracking, the large molecules that form bitumen (or the deasphalted oil) are broken down. This is an essential step since it yields smaller and lighter molecules that decrease the density and viscosity of the

product.



**Figure 1.1.** Simplified block flow diagram of BituMax™.

An inevitable consequence of cracking of hydrocarbons is the production of olefins.<sup>8</sup> Thermal cracking occurs through a free radical mechanism, and radicals under thermal cracking conditions can undergo different reactions; they can abstract a hydrogen from another molecule, they can add to other molecules, but they can also crack on the  $\beta$  position.<sup>8</sup> The  $\beta$ -scission of a radical yields an olefin and a radical, as illustrated by the cracking of secondary radical in **Figure 1.2**.



**Figure 1.2.** Formation of an olefin through  $\beta$ -scission during thermal cracking.

There is a limitation on the concentration of olefins allowed in the oil to be transported through pipelines, as indicated in **Table 1.1**. Although the restriction was put in place to avoid blending of cracked petrochemical products into the pipeline,<sup>2</sup> it ends up affecting the design of bitumen processing facilities of which the main conversion unit is based on cracking – thus their product will contain olefins.

The conventional way of dealing with the unsaturation of the cracked product of bitumen is hydrotreating. An upgrader would rely on a hydrotreating unit for the removal of sulfur, nitrogen, and metals, as well as the addition of hydrogen to unsaturated molecules already present or produced by cracking.<sup>9</sup> Access to hydrogen in a partial upgrading facility integrated to the SAGD

site, as it is the case of Bitumax™, might not be an option. The addition of a hydrotreater to the partial upgrader infrastructure would require infrastructure for the production of hydrogen. The additional infrastructure would increase capital and operational costs, which would affect the economic target of partial upgrading.<sup>2</sup>

Since cracking of bitumen is a key process to achieve the pipeline specification, the presence of olefins in the product is unavoidable. Trying to keep the partial upgrading process cost efficient, and to meet pipelines specifications in an economical way, has taken part of the research into exploring alternative reaction pathways other than hydrotreating for olefin conversion.

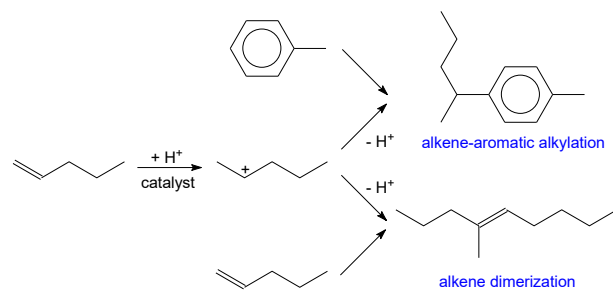
Some of the studies tackling this problem, have looked at alternatives considering the removal of olefins within the cracked naphtha fraction exclusively. Olefins are concentrated in the lighter fraction of the cracked product, progressively decreasing in concentration towards the higher boiling point fractions.<sup>10,11</sup> For this reason, the economic path for reducing olefins from a cracked bitumen product, could consist of separating and treating only the naphtha stream, for it to be blended back into the final product and achieve the pipeline specifications. Based on this, some studies have focused on the reduction of olefins in the cracked naphtha, for example, the transfer addition of hydrogen to olefins using asphaltenes was shown to be plausible.<sup>12</sup>

Another possible alternative conversion pathway to hydrotreating is an olefin reduction technology based on acid catalysis.<sup>13</sup> The technology leverages on the presence of both olefins and aromatics in the cracked naphtha fraction. Using a solid acid catalyst the olefins and aromatics present in the cracked naphtha is converted into alkylaromatics, reducing the unsaturation of the product, and allowing the converted product to meet pipelines specifications. Although the target is olefin-aromatic alkylation, having such a complex mixture as cracked naphtha, it is not the only reaction taking place. Among other, olefins can also react with other olefins through dimerization, as shown in **Figure 1.3**.

Since the process employs a heterogeneous catalyst, premature deactivation of the catalyst is one of the main technological risks. The potential causes of acid catalyst deactivation by cracked naphtha became the focus of this thesis.

Several potential causes for premature catalyst deactivation were identified.





**Figure 1.3.** Acid catalyzed alkene-aromatic alkylation and alkene dimerization illustrated by the reaction of 1-pentene and toluene.

Acid catalysts are susceptible to nitrogen poisoning because of the affinity of nitrogen bases, like pyridine, to the acid sites. Since cracked naphtha from bitumen thermal cracking has nitrogen species present, and pyridines are predominant,<sup>14</sup> it was expected that this could be an issue. Although alkylation of aromatics is favored at lower temperatures, a plausible approach to avoid poisoning, which is an adsorption/desorption process, was to operate at a reaction temperature that favored the desorption step. This was proven to be promising during the alkylation of phenol with 1-hexene at 315 °C in the presence of pyridine.<sup>15</sup> The question that remained was if the same could be achieved with a much more complex feed like cracked naphtha, since operating at a higher temperature would increase the number of molecules undergoing chemical reactions in the process.

It is known that acid sites can catalyze reactions leading to the formation of deposits on the surface.<sup>16</sup> Cracked naphtha has a wide variety of compounds classes that can take part on acid catalyzed processes, but exactly what compounds in the cracked naphtha have a more detrimental effect under the conditions of interest (250-350 °C) has not been extensively studied.

Additionally, cracked products are known to be ‘unstable’.<sup>17</sup> Instability in the cracked naphthas is often manifested by the formation of deposits, like gums during storage,<sup>18</sup> or fouling in hydrotreater reactors.<sup>19</sup> This speaks of the ability of the cracked naphtha to undergo chemical reactions producing heavy compounds, and for this reason, we can also expect a non-catalytic contribution to catalyst deactivation.

Understanding how the cracked naphtha properties and composition contribute to the deactivation of the catalyst, by identifying the compounds reacting, and the catalytic and non-catalytic reactions occurring, is an important step in the development of the technology. The ultimate application of

this knowledge is to have better control over the time-on-stream period of the acid catalyst in the olefin-aromatic alkylation unit of the BituMax™ process. The time-on-stream period between reaction and catalyst regeneration cycles have an impact on process design and cost.

## **1.2. Objective**

The objective of this study was to investigate what molecules and reactions pathways contribute to the deactivation of an amorphous silica-alumina acid catalyst during processing of cracked naphtha derived from thermal cracking of bitumen.

## **1.3. Scope**

The literature on cracked naphtha instability is reviewed in Chapter 2, with a focus on the type of instability often encountered during processing and the reactions that can occur, the molecules present in the cracked naphtha that could possibly contribute to the instability reactions, and how the cracking conditions could give the cracked naphthas their instability.

A series of pilot plant (kg/day capacity) runs were carried out for the study of olefin-aromatic alkylation in thermally cracked naphtha under different conditions, as part of an industrial research project. Chapter 3 covers the extensive characterization of the spent amorphous silica-alumina catalyst samples generated from those pilot plant runs. The interpretation of analyses like coke content and composition at different conditions and at different locations of the reactor helped to understand the causes of catalyst deactivation.

Two questions were meant to be answered experimentally through the model study in Chapter 4. First, if there are free radical reactions occurring in the cracked naphtha upon heating to the temperatures of interest in this study, and second, if these reactions are taking place because of the presence of oxygen in the system, or not. Free radical reactions in the cracked naphtha were explored in the presence and in the absence of oxygen, using a probe molecule to interrogate better the changes.

Olefinic molecules have been the focus of many studies regarding deposit formation of acid catalysts. In Chapter 5, the focus is narrowed down to cyclopentene as a plausible key contributor to deposit formation. After verifying its presence in the cracked naphtha, and the nature of its

reactions, the conversion of cyclopentene was compared to that of 1-hexene over amorphous silica-alumina to determine relative reactivity and impact on deposit formation.

In Chapter 6, desorption of pyridine from amorphous silica-alumina in the presence of cracked naphtha was investigated. The intent was to clarify the role of nitrogen bases on catalyst deactivation. The main question to answer was whether the desorption phenomenon was driven solely by the action of the temperature, or if there was competition for the adsorption on the acid sites between nitrogen bases and compounds in the cracked naphtha.

The main conclusions and outcomes can be found in Chapter 7.

#### 1.4. References

- (1) Gray, M. R. Chemical Composition. In *Upgrading Oilsands Bitumen and Heavy Oil*; The University of Alberta Press: Edmonton, Alberta, 2015; pp 93–142.
- (2) Gray, M. R. Fundamentals of Partial Upgrading of Bitumen. *Energy Fuels* **2019**, *33* (8), 6843–6856.
- (3) Kaiser, M. J.; de Klerk, A.; Gary, J. H.; Handwerk, G. E. *Petroleum Refining: Technology, Economics, and Markets*, Sixth Edit.; CRC Press: Boca Raton, FL, 2020.
- (4) de Klerk, A.; Gray, M. R.; Zerpa, N. Unconventional Oil and Gas. In *Future Energy: Improved, sustainable and clean options for our planet*; Elsevier, 2014; pp 95–116.
- (5) Gray, M. R. Marketing of Bitumen Products. In *Upgrading Oilsands Bitumen and Heavy Oil*; Gray, M. R., Ed.; The University of Alberta Press: Edmonton, Alberta, 2015; pp 209–230.
- (6) de Klerk, A. Processing Unconventional Oil: Partial Upgrading of Oilsands Bitumen. *Energy Fuels* **2021**, *35* (18), 14343–14360.
- (7) de Klerk, A.; Zerpa, N.; Xia, Y.; Abduljawad, O. A. Integrated Central Processing Facility (CPF) in Oil Field Upgrading (OFU). Pat. Appl. US 2014/0138287 A1, 2014.
- (8) Gray, M. R. Upgrading Reactions and Kinetics. In *Upgrading Oilsands Bitumen and Heavy Oil*; Gray, M. R., Ed.; The University of Alberta Press: Edmonton, Alberta, 2015; pp 151–209.

- (9) Gray, M. R. Hydrotreating Processes. In *Upgrading Oilsands Bitumen and Heavy Oil*; Gray, M. R., Ed.; The University of Alberta Press: Edmonton, Alberta, 2015; pp 405–438.
- (10) Gray, M. R.; McCaffrey, W. C. Role of Chain Reactions and Olefin Formation in Cracking, Hydroconversion, and Coking of Petroleum and Bitumen Fractions. *Energy Fuels* **2002**, *16* (3), 756–766.
- (11) Rezaei, M.; Gieleciak, R.; Michaelian, K. H. Determination of Olefin Contents in Liquid Hydrocarbons Using a Quantum Cascade Laser and a Photoacoustic Detector. *Energy Fuels* **2019**, *33* (4), 2859–2866.
- (12) Fong, S. Y.; Montoya Sánchez, N.; de Klerk, A. Olefin Saturation Using Asphaltenes As a Hydrogen Source. *Energy Fuels* **2020**, *34* (4), 4534–4543.
- (13) Zerpa, N. G.; de Klerk, A.; Xia, Y.; Omer, A. A. Olefins Reduction of a Hydrocarbon Feed Using Olefins- Aromatics Alkylation. Canadian Patent application 2916767, 2015.
- (14) Rao, Y.; de Klerk, A. Characterization of Heteroatom-Containing Compounds in Thermally Cracked Naphtha from Oilsands Bitumen. *Energy Fuels* **2017**, *31* (9), 9247–9254.
- (15) Xia, Y. Acid Catalyzed Aromatic Alkylation in the Presence of Nitrogen Bases. MSc Thesis, University of Alberta, Edmonton, AB, Canada, University of Alberta, 2012.
- (16) Guisnet, M.; Magnoux, P. Organic Chemistry of Coke Formation. *Appl. Catal. A: General* **2001**, *212* (1–2), 83–96.
- (17) Yan, Y.; C. Prado, G. H.; de Klerk, A. Storage Stability of Products from Visbreaking of Oilsands Bitumen. *Energy Fuels* **2020**, *34* (8), 9585–9598.
- (18) Pradelle, F.; Braga, S. L.; Martins, A. R. F. A.; Turkovics, F.; Pradelle, R. N. C. Gum Formation in Gasoline and Its Blends: A Review. *Energy Fuels* **2015**, *29* (12), 7753–7770.
- (19) Yui, S. Removing Diolefins from Coker Naphtha Necessary before Hydrotreating. *Oil Gas J.* **1999**, *97* (36), 64–69.

## **Chapter 2. Challenges during processing of cracked naphthas: on the instability and its causes**

### **2.1. Introduction**

Cracking processes, being thermal or catalytic, break down molecules using heat or a combination of heat and a catalyst. Their objective may be to decrease the boiling point of the feedstock, increase the value of heavy products, or just improving properties like viscosity. But along with the desirable changes, a common and undesirable outcome of cracking is the instability or reactivity of the cracking products. Stability in this context refers to the ability of the cracked products to resist further change, which includes phase change and compositional change.

In the absence of blending different materials, instability due to phase change is the result of a change in composition caused by reaction. In heavy materials, the term ‘self-incompatible’ oils were suggested to describe instability in oils that developed insoluble material on their own as a consequence of processing.<sup>1</sup> Instability follows from a compositional change. With this in mind, instability can be more narrowly described as the compositional change that takes place in a material, causing a phase change of part of the material. The phase change may manifest as the formation of additional sediment, fouling, surface deposits, gums, or a dispersed second phase.

Different cracking product fractions present different instability issues that become an operational issue when there is a need for further processing to reach a final refined product’s specifications. For instance, the poorer storage stability of thermally processed oils compared to straight run oils is known, and several studies remarked on the relationship between cracking severity and diminished storage stability.<sup>2,3</sup> Also, cracked deasphalted residue produce new and undesirable asphaltenes after (and even during) reaction.<sup>4,5</sup>

In the case of the lighter fractions produced by cracking, like cracked naphtha, some of same instability problems can be found. Instability is encountered to different extents in naphthas derived from various cracking processes. The instability can manifest during storage when heavy compounds described as gums are formed.<sup>6</sup> The instability can also manifest during processing when the cracked naphtha is subjected to higher temperatures, which may be observed as the

formation of heavier products during distillation,<sup>7</sup> or the formation of particles or deposits on surfaces during catalysis or heat-exchange.<sup>8,9</sup>

If the stability of a liquid is defined in terms of its resistance to change, then the rate of change would be a measure of instability. Compared to straight run or hydroprocessed naphtha, the high rate at which cracked naphthas form heavy compounds during storage, or foul equipment during processing, would classify them as unstable.<sup>10</sup> In these instances, the nature of such changes is compositional, sparked by the reactivity of the compounds present in the cracked naphtha on its own, when in contact with reactants, or when subjected to heat.

The chemistry associated to each instability case is different and deserves a proper description.

The formation of gums during storage of cracked naphtha is the most common example of its instability and has received a lot of attention since the 1920's and continues to be discussed.<sup>11-17</sup> This occurrence has been explained by the autoxidation of the liquid and it is related to its oxidative instability,<sup>16</sup> because of its contact with air in storage tanks, free radical reactions can occur and the formation of heavy compounds or gums is promoted. Instability was reported for cases when oxidation-related free radicals is unlikely to form, and instability was reported even in the presence of hydrogen.

Cracked naphthas have also shown signs of instability where the continuity of the process does not allow for it to be exposed to air. Instability was reported for cases when oxidation-related free radicals is unlikely to form, and instability was reported even in the presence of hydrogen.<sup>18-21</sup> In this case, not only the formation of heavy molecules like those constituting the gums are the way in which the instability of the cracked naphtha is manifested, but we could also expect the formation of particulates or deposition of material on the surfaces in contact with the liquid – including equipment surfaces and catalysts. The reaction mechanisms or the species involved that could describe the phenomena of thermal stability during cracked naphtha processing have not been extensively described in literature.

So, what exactly is happening in the cracked naphtha liquid bulk that causes its notorious instability?

The causes of oxidative and thermal instability of the cracked naphtha have long been pointed to the large content of unsaturated compounds that are accumulated in this fraction from the cracking process,<sup>11,19,22,23</sup> and although these are more reactive than saturated hydrocarbons and undergo addition reactions with ease, this extent of instability is not encountered when refining very olefin-rich materials, such as the products from high temperature Fischer–Tropsch synthesis.<sup>18</sup> It makes one wonder exactly what compounds would initiate or take part of the reactions that contribute to the formation of heavy compounds during cracked naphtha processing.

Breaking down such uncertainties and finding an understanding beyond the presence of double bonds is relevant, since it could allow the tackling of specific problems, and improvement of technologies in the field. Moreover, understanding how such troublesome compounds end up in the cracked naphtha in the first place, by analyzing the catalytic and cracking reactions and the crude oil feedstock used, could allow one to predict the behavior of cracked naphthas derived from different processes.

In this work, we analyze how the properties of cracked naphthas could explain their reactivity under different conditions during their processing, yielding unwanted heavy products. First, we define cracked naphtha and go through some of the instances where its instability has been more commonly reported. Second, we identify the types of instability associated with cracked naphtha processing. Stability, being a broad term, is defined, and oxidative and thermal stability of the cracked naphtha is discussed from a reaction network perspective. The compound classes present in the naphtha are also discussed, exploring the possible reaction pathways they could undergo, to assess their contribution to the formation of heavy material during the processing of cracked naphthas. Lastly, we are going through the most common process for cracked naphtha production and how the process variables can affect the properties of the cracked naphtha leading to its instability.

## **2.2. Cracked naphtha**

Naphtha refers to a boiling fraction. The cut point of naphtha depends on the refinery and broadly speaking it is C<sub>5</sub>–C<sub>10</sub> material in the <175 °C boiling range.

The composition of the stream is a variable that depends on the origin of the naphtha in the first place. For instance, straight run naphthas are the lightest fraction of a crude oil, with no previous processing other than its separation in a distillation column. Cracked naphthas, on the other hand, are the result of a catalytic or thermal process in which a heavy feedstock is converted to a lighter product. In the cracking process, the large molecules of the feed are broken down into lower molecular weight compounds. The cracking process is done to reduce the boiling fraction of a feed, and it is mostly used with heavy crude oils.

There are some key differences between the straight run naphthas, and those produced from a cracking process:

- Cracking produces unsaturated compounds. Olefins, especially short chain alkenes, and diolefins, are found in the cracked naphthas. The unsaturated compounds are more concentrated in the lower boiling material than in the higher boiling material of the cracking product. It is uncommon to find olefins in crude oils/straight run naphthas, since they are reactive,<sup>24</sup> although their occurrence has been documented.<sup>25</sup>
- Cracked naphthas are derived from heavy oils or “bottom of the barrel” oil. Heteroatoms are present at higher concentration in these heavier feedstocks due to the natural increase in abundance of heteroatom-containing species with an increase in boiling point.<sup>26</sup> Once the heavier cuts are cracked, smaller molecules containing heteroatoms are formed, which end in the naphtha fraction. Although nitrogen, sulfur, and oxygen can be found at low concentration in straight run naphthas, cracked naphthas are known to contain a higher concentration of these heteroatoms.<sup>27</sup> The composition of insoluble materials formed during storage implicated heteroatom-containing compounds as contributors to storage instability.<sup>28</sup>
- Cracked naphthas are unstable compared to straight run or hydroprocessed naphthas. The instability of the cracked naphtha is manifested during storage by the formation of gums, or during processing by the formation of particles or deposits on surfaces during catalysis or heat-exchange.<sup>8,9,16</sup>



## **2.3. Challenges during processing of cracked naphtha**

The high complexity of the cracked naphthas translates into the possibility of becoming unstable in different ways and under various conditions. This means that it can easily show signs of change or unwanted reactions at different stages of a process. Several examples of cases in which cracked naphtha instability has become an operational problem are discussed, together with the reported origin or presumed origin in each case.

### **2.3.1. Oxidation products formation during storage**

Naphtha range products are produced and refined to produce blending components for different grades of gasoline. The naphtha range blending components are stored in a tank farm before and after blending to the final products. Once the gasoline is distributed to retail outlets and even after it is sold to customers, gasoline is subject to storage before use. Olefins generally have good research octane numbers (RON), and an olefin-containing blending component is often included in final gasoline blends. The olefinic products from fluid catalytic cracking (FCC), visbreaking and coking are potentially directly useful as blending materials, subject to their sulfur content.

Cracked naphtha streams from FCC may contribute up to 40% of the final gasoline blend and cracked naphtha up to 20% from thermal processes may be included in the final gasoline blend.<sup>15,29</sup>

Cracked materials may be subject to mild selective hydroprocessing to meet sulfur specifications and reduce the concentration of multiply unsaturated compounds.<sup>30-32</sup> During such selective hydrotreating care is taken to limit olefin hydrogenation that would cause a decrease in octane number of the cracked naphtha. Thus, most of the olefin content is retained in the treated cracked naphtha.

The formation of gums has been reported since the early 1900s. It was described as a problem that develops during storage because of the contact of the fuel with air, and it was considered a problem since it could potentially affect engine system function. Moreover, the accumulation of certain oxidation products which are not necessarily gums, could contribute to the corrosive tendencies of a fuel, and could lead to the formation of deposits in metals.<sup>33</sup>

Early studies<sup>11,12,17</sup> identified peroxides as the main cause of gum formation and pointed at diolefins as the compounds with higher oxidation tendencies, followed by olefins. It was highlighted that even small amounts of diolefins could cause the production of substantial quantities of gums.<sup>23</sup> Even though the oxidation of diolefins was faster than that of other molecules, the reaction towards gum formation involved more compounds in the cracked naphtha than just the diolefins.

Gum formation in cracked gasoline continues to be discussed<sup>16</sup> and the cause of this instability is also under continued research.<sup>22</sup> In these studies, the presence of molecules that can form an allylic radical like conjugated diolefins, continue to be the center of attention to explain the autoxidation instability of the cracked gasoline. In a particular study,<sup>22</sup> it was found that primary olefins or isolated primary diolefins, such as 1,5-hexadiene, did not contribute to the formation of gum in the autoxidation tests carried.

Not only diolefins have been found to contribute to the instability of fuels during storage. In different study, it was found that compounds with a benzene ring and a double bond were more unstable than the rest.<sup>33</sup>

Other species have also been implicated in heavy product formation during storage. It has been found that deposits that formed during storage contained nitrogen.<sup>28</sup> Compound class specific analyses found that deposit formation positively correlated with phenolic and pyrrolic species, whereas no strong correlation was found for pyridinic or aniline compounds.<sup>34</sup> Additional support for these observations were independently found.<sup>35</sup> In the review by Batts and Fathoni,<sup>10</sup> several reports that implicated sulfur-containing species were also implicated in oxidative instability.

Hydrogen disproportionation following on oxidation could also lead to the formation of addition products or create species that are olefinic and more susceptible to subsequent addition reactions.<sup>36</sup>

The common theme in all instances of oxidative instability is the formation of heavier products that were not originally present in the fuel product. Furthermore, in all instances it is presumed that the fuel is exposed to O<sub>2</sub> from contact with air.

### 2.3.2. Pressure-drop in hydrotreaters

Not all of the stability issues of cracked naphtha can be attributed to oxidation. Hydrotreating is on the opposite side of the oxidation-reduction spectrum. Yet, in hydrotreating, cracked naphtha may also cause operational issues with catalyst fouling that lead to increased pressure drop over the hydrotreater.

Three explanations for the increased pressure drop in hydrotreaters due to fouling by cracked naphtha are encountered, namely, reactions of multiply unsaturated compounds, pre-existing heavy compounds and reactions unspecified reactive molecules in cracked naphtha. In all these cases the explanation hinges on the presence or the formation of heavy compounds.

Multiple unsaturated compounds, such as diolefins, have been pointed out as the main culprit of the severe pressure drop of cracked naphtha hydrotreaters<sup>19</sup> due to their rapid polymerization and fouling tendencies under the temperature conditions of the unit. Typical start-of-run temperature conditions for naphtha hydrotreaters are 260–300 °C, with end-of-run temperatures being higher.<sup>37</sup> Severe pressure drop that is sometimes encountered may also be due to pre-existing gums in the case of treatment of previously stored cracked naphthas.<sup>19,20</sup> In the case of freshly cracked and distilled feeds, faster fouling of the hydrotreating catalyst is caused by the presence of reactive molecules in the feed.<sup>19,20</sup>

A pretreatment reactor is often used to remove doubly unsaturated and other reactive molecules beforehand to extend the main reactor catalyst life. Such a pretreatment reactor is operated at conditions mild enough to convert only the more reactive species, such as diolefins and acetylenes.<sup>19,30–32,38</sup> For base metal catalyzed hydrotreating in the pretreatment reactor operating temperatures are of the order 105 °C.<sup>31</sup>

Under hydrotreating conditions (250 °C, 3.4 MPa, 2 h<sup>-1</sup>), using a spent sulfided NiMo/ $\gamma$ -Al<sub>2</sub>O<sub>3</sub> hydrotreating catalyst, it was shown that linear, branched, and cyclic conjugated diolefins were prone to addition reactions, whereas isolated diolefins formed no addition products.<sup>39</sup> Although the authors ascribed this to formation of resonance stabilized allylic carbocations,<sup>39</sup> control experiments with co-feeding of 1-octene to increase the olefin content did not support this interpretation. Moreover, sulfided NiMo/ $\gamma$ -Al<sub>2</sub>O<sub>3</sub> hydrotreating catalysts have Lewis acidity, but

not Brønsted acidity. The authors explain that another possible source of the Bronsted acidity could be the sulfur layer of the sulfided NiMo catalyst. But another reaction pathway for the formation of addition products is hydrogen disproportionation of conjugated diolefins with allylic free radical intermediates followed by in cage addition of the radical species. This could explain the negligible impact of added mono-olefins.

Using the same spent sulfided NiMo/ $\gamma$ -Al<sub>2</sub>O<sub>3</sub> hydrotreating catalyst,<sup>38</sup> it was also demonstrated that some non-diolefin species were prone to addition reactions during hydrotreating. Conversion of 4-methyl styrene (250 °C, 3.4 MPa, 2 h<sup>-1</sup>) resulted in significant addition product formation. Over a 30-day time-on-stream period the gum content of the product increased from 2.6 g/100 mL (3 days) to 3.2 g/100 mL (30 days). However, in control experiments with  $\alpha$ -methylstyrene, selectivity to addition products remained low and after 30 days on stream the gum content of the product was 0.01 g/100 mL. The difference in addition product selectivity was explained in terms of steric hinderance.<sup>38</sup> It is again speculated, with reference to the work by Mayo on styrene,<sup>28</sup> that a free radical pathway for addition product formation cannot be discounted.

### **2.3.3. Heat exchanger fouling**

Although fouling of heat exchangers is more commonly associated with heavier oil fractions especially when containing asphaltenes,<sup>40,41</sup> deposits in heat exchangers have been seen to occur when naphtha is the heated fluid. Fouling in heat exchanger represents an operational problem since the heat transfer is affected, and results in lower outlet temperatures. When this occurs, the unit shutdown to the clean the fouled surfaces is necessary. Other solutions may include antifoulant additives to control the fouling reactions,<sup>8</sup> but for this to be effective the reaction mechanism and compound classes taking part need to be identified.

A common element is the formation of heavy compounds. This is most graphically seen in the so-called ‘paradox of the distillation of tars’, which is that cracked products condensed from the vapor phase can only partially be vaporized and distilled again due to formation of heavy products when the liquid is heated for distillation.<sup>7</sup> This is a general problem for previously cracked material. It was expressed as follows for coal liquids from thermal processing with and without hydrogen:<sup>42</sup> “The stability of coal liquids upon storage and/or heating is an important factor which can seriously affect further processing and final product specifications.”

A few specific examples are provided to illustrate the nature of the problem.

An acceleration of the fouling rate of a naphtha hydrotreater effluent heat exchanger was observed after including lighter material in the feed to the hydrotreater.<sup>8</sup> It is noteworthy that in this example the fouling caused by the cracked naphtha took place after hydrotreating. It was determined that the root cause of the deposit formation was free radical polymerization caused by the presence of unsaturated C<sub>4</sub> species and mercaptans (thiols) in the newly included light material.

During pilot plant testing carried out with coker naphtha and in the presence of hydrogen,<sup>21</sup> organic matter was deposited in the heat exchanger of the unit operated at around 400 °C. It was determined that the bottom 15% of the naphtha cut, containing phenols and alkylated nitrogen compounds, were the main precursors for the deposits that formed.

The heat exchanger fouling potential of unsaturated compounds in cracked naphtha is often pointed out and this was evaluated by adding unsaturated naphtha and kerosene range olefinic species to kerosene.<sup>43</sup> It was found that not all olefins contributed to the fouling at the same extent. Shorter chain alkenes, like 1-octene and 1-decene were not found to be contributors to the fouling. But several species with a high fouling potential were identified. These included heavier mono-olefins like 1-hexadecene, cyclic diolefins like 4-vinyl-cyclohexene and dicyclopentadiene, and olefins adjacent to a benzene ring like indene.

A similar remark was reported by Taylor et al.<sup>44</sup>, pointing out that not all olefins contributed in the same extent to deposit formation in heated surfaces. They found that diolefins and indene had the most detrimental effect, even at temperatures of around 100 °C.

In olefin-rich materials, such as naphtha derived from high temperature Fischer–Tropsch synthesis, heat exchanger fouling is not particularly problematic, although the bottom temperature of atmospheric distillation should be kept lower than in petroleum refining.<sup>18</sup>

In conclusion, there are many examples of cracked naphtha in the absence of oxygen and in the absence of a catalyst that can cause heat exchanger fouling even in the presence of hydrogen. Nitrogen-, oxygen-, and sulfur-containing species, as well as several classes of unsaturated compounds were pointed out as culprits causing fouling. Thermally induced free radical addition

appeared to be the common cause for such fouling, irrespective of the nature of the species involved.

#### **2.3.4. Acid catalyst deactivation**

The contribution of unsaturated compound to the instability of cracked naphtha was highlighted by several of the preceding examples. One would therefore anticipate that the processing of a cracked naphtha over a Brønsted acid catalyst would lead to excessive fouling and catalyst deactivation at the inlet of the reactor at short contact time. Curiously, this was not what was found.

After conversion of cracked naphtha over an amorphous silica-alumina catalyst at 325 °C in a pilot scale unit, more carbonaceous deposits were found on the catalyst at the reactor outlet than on the catalyst at the reactor inlet.<sup>9</sup> These observations were made despite the lower olefin content at the reactor outlet. Throughout the tests, the acid catalyst had sufficient Brønsted acidity to perform olefin oligomerization and olefin-aromatic alkylation, the intended reactions of the conversion process.<sup>45</sup> Yet, the cracked naphtha did not cause excessive fouling of the catalyst at the reactor inlet where the olefin and diolefin content was the highest. The anticipated catalyst fouling profile with more deposits found at the catalyst at the reactor inlet was observed only at lower operating temperatures in the range 250–280 °C, when the overall extent of deposit formation was also less.<sup>9</sup> These observations were explained by the sum of the contributions of acid catalyzed addition and free radical addition reactions that led to heavier products retained as deposits on the catalyst. At 325 °C, free radical addition was the main contributor to deposits at the reactor outlet.

Unfortunately, few other studies were found that employed converted untreated cracked naphtha over an acid catalyst. Oligomerization was studied for the removal of the most reactive olefins in visbroken naphtha at 190 °C.<sup>46</sup> Although it was reported that the quality of the treated stream was improved, little mention was made about catalyst deactivation.

#### **2.4. Instability of cracked naphthas**

To define better the cracked naphtha characteristic instability, we need to first define stability itself.

For a liquid to be considered stable, it needs to be resistant to change. If a change can occur with ease, then the liquid is considered unstable. In the case of cracked naphthas, most often the notable

change is physical, described by the formation of a heavier phase that is a consequence of chemical reactions sparked by the conditions at which the liquid is subjected. The change in question can be expressed by the formation of gums, particles, or deposits, depending on the conditions at which it is subjected.<sup>10</sup>

Naphtha is by definition a product of distillation and a finite distillation range. The formation of a second phase is a consequence of heavier products that were formed by reaction and that were not originally present in the cracked naphtha. The heavier phase that forms is a consequence of chemical reactions sparked by the conditions to which the liquid is subjected.

Having reviewed the most common instances where the cracked naphtha tends to behave in unwanted ways in industrial settings (in Section 2.3), we now look at the origin of the reactions that lead to instability. The two most often encountered forms of instability are described as oxidative instability and thermal instability, and they are both driven by a free radical mechanism.

#### **2.4.1. Oxidative stability**

Autoxidation has been the explanation usually provided for the instability of the cracked naphtha during storage when the formation of gums is a problem. Storage tanks where cracked naphtha is kept in refineries offer the conditions for autoxidation to occur.<sup>33</sup> Compounds in the cracked naphtha that are susceptible to oxidation produce radicals that can react at low temperatures acting as the initiators of free radical chain reactions.<sup>47</sup> Once the free radical chain reaction has started, addition reactions are one of the propagation steps, yielding heavy compounds or gum.<sup>48</sup> Addition products can also be formed as a free radical termination step.

The reactivity of a substance to oxygen will determine its oxidative stability. When oxygen is present, and more so when the material is at elevated temperature to accelerate the rate of reaction, many different reactions can take place.<sup>49</sup> Among other, oxidation can cause the formation of oxygenated products and lead to addition reactions with or without oxygen incorporation.

At ambient temperature that is typical of naphtha storage, autoxidation occurs at slow rate. The slow oxidation rate is explained by (i) the low concentration of the diffused atmospheric oxygen from the surface of the liquid to the bulk, (ii) the usually low average temperature of the storage tanks, and (iii) the concentration of reactive molecules at such conditions.<sup>33</sup> There is also evidence

to suggest that for constant temperature and oxygen partial pressure, initiation rate of oxidation is also dependent on the ratio of the gas–liquid interface area per unit volume.<sup>50,51</sup>

The formation of the initial peroxide specie, illustrated in Equations Eq. 2-1-Eq. 2-3 below, is slow.<sup>16</sup> It begins by the abstraction of a hydrogen atom from a molecule (R-H), which could be abstracted by an oxygen molecule forming a hydroperoxyl radical (\*OOH), or by other molecules in the mixture. After abstraction, a carbon centered radical (R\*) if left behind, to which the O<sub>2</sub> can add to form the peroxy radical (ROO\*). Further abstraction of a hydrogen would yield the hydroperoxide molecules (ROOH).



The availability of O<sub>2</sub> in the proximity of the organic free radical species (R\*) formed in Eq. 2-1 or Eq. 2-3 determines the likelihood of Eq. 2-2 taking place. Eq. 2-2 is effectively a reaction in competition with any other reactions that R\* could participate in. These reactions may include addition to olefins (Eq. 2-4), transfer reactions such as hydrogen and methyl transfer (Eq. 2-5) and free radical termination (Eq. 2-5). The presence of unsaturated molecules promotes addition reactions that would form a C-C bond and would continue to propagate the free radical chain reaction.



When R\* participates in an addition reaction (Eq. 2-4 or Eq. 2-6) the heavier product that is formed, is formed without incorporation of oxygen. There is also a potential difference in the selectivity of further reaction of R\* from Eq. 2-1 and Eq. 2-3. The reaction in Eq. 2-1 is more likely to occur at the gas–liquid interface,<sup>51</sup> and selectivity of subsequent reaction of R\* is determined by local conditions at the gas–liquid interface. When R\* is formed by Eq. 2-3, it is likely to occur in the bulk liquid and selectivity is determined by the dissolved oxygen concentration in the bulk liquids



that remains near saturated with dissolved oxygen at low reaction rate,<sup>52</sup> which is typical of storage conditions.

Once the reaction in Eq. 2-2 has taken place, the product from autoxidation will retain oxygen in the product. The oxygen content of gums will therefore depend on whether O<sub>2</sub> was incorporated via Eq. 2-2 or not, because the initiation reaction (Eq. 2-1) does not incorporate oxygen in the product. It is also worthwhile pointing out that Eq. 2-2 may also take place after radical-olefin addition (Eq. 2-4). The reaction sequence following on initiation by autoxidation is more complex than generally described for liquid phase oxidation of hydrocarbons.

The composition of the gums from autoxidation is a result of local oxygen availability.<sup>50</sup> Hydroxyl, ester, carbonyl, carboxylic acid, peroxide and hydroperoxide oxygen functionalities were all identified in gums formed from cracked naphthas.<sup>13</sup> The total oxygen content present in gums from naphtha was reported to be in the range in 14-17 wt%.<sup>13,16</sup> However, it should be noted that these values were for an oxygen content determined by difference calculation to close material balance after CHNS elemental analysis.

The impression is therefore created that on average the oxygen-to-carbon molar ratio in gums from cracked naphtha is 1:6–7. This is a high ratio, because it implies that oxygen is incorporated on an equal molar basis with the naphtha. It would suggest that almost all gums had to be derived from reactions that incorporates O and R in equimolar ratio, such as the termination reaction in Eq. 2-7 or the further oxidation of already oxidized compounds. Such an outcome would require conditions of high oxygen availability, which may be found in some accelerated aging tests.



Eq. 2-7

Another aspect that has to be considered in relation to cracked naphtha, is how the composition of cracked naphtha affects the rate of autoxidation compared to naphthas that are considered stable, such as hydrotreated naphtha.

Molecular structure is the main factor that determines the rate of autoxidation of a compound in the naphtha. Compounds that contain hydrogen that is more easily abstracted are more prone to

autoxidation. In other words, molecules with hydrogen with lower bond dissociation energy are more at risk of autoxidation. Below are mentioned some types of molecules that have a higher autoxidation propensity.

- Molecules with hydrogen activated by  $\pi$ -systems. Allylic and benzylic hydrogen can be easily abstracted, so the molecules can be attacked by oxygen and peroxy radicals. In this group, allylic and benzylic hydrogen within a ring tend to be more reactive than their straight chain analogs, which has been explained by a combination of radical stabilization, steric effects, and polar factors.<sup>53</sup> So, according to this, we can expect tetralin and indane to be more easily autoxidized than ethylbenzene, and cyclohexene and cyclopentene than 3-heptane, for example, which indeed has been observed.<sup>53</sup> When allylic hydrogen is abstracted, there is an even higher chance of addition product formation, because the unsaturated nature of the compound is retained. For example, higher selectivity to addition products was found during the oxidation of indene when compared to that of indane or tetralin.<sup>36</sup>
- Molecules with a hydrogen neighboring 2  $\pi$ -systems correlate with a higher rate of hydrogen abstraction. Dienes, biphenyl compounds, styrenes and indenenes, and allyl benzenes would classify in this group.<sup>53</sup>
- Oxygenated compounds, like ethers, acetals, aldehydes are more readily oxidized.<sup>54-57</sup>

One should anticipate that, depending on the concentration of different compound classes, some cracked naphthas would be more susceptible to autoxidation. This can be illustrated by differences in gum formation between FCC and thermally cracked naphthas in accelerated ageing tests.<sup>58</sup> Although the olefin content in thermally cracked naphthas is generally lower than that of FCC naphthas, thermally cracked naphthas have a higher proportion of cyclo-olefins/diolefins/cyclo-diolefins, which makes them more susceptible to gum formation.

In a model compound study, cyclohexene was identified as the type of olefinic molecule with a higher gum forming tendency, while diolefins were seen to have a promoting effect, increasing gum formation even when present at low concentration, and not leading to peroxide formation.<sup>23</sup>

Another source of radicals is the further decomposition of hydroperoxides,<sup>16</sup> such as those formed by the reaction in Eq. 2-3. Peroxide decomposition follows a unimolecular homolytic bond cleavage. For it to occur, the bond dissociation energy (BDE) needs to be provided to the system.

In the case of peroxides, this energy can be achieved at temperatures of 50-150 °C, because of their weak O-O bond.<sup>59</sup> If peroxides are already present in the mixture, they would start the free radical chain reaction.

In practice, additives or antioxidants are added to the cracked naphthas to limit the propagation step in the free radical chain reaction. Phenolic or amine type molecules can act as radical acceptors and quench the reaction.<sup>14</sup>

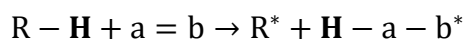
#### **2.4.2. Thermal stability.**

The thermal reactions occurring upon heating of a hydrocarbon mixture have been well documented for the temperatures used for processes like thermal cracking.<sup>60</sup> But at lower temperatures, the reactions that cause the thermal instability of hydrocarbon mixtures like cracked naphtha have been studied less.

Homolytic bond cleavage can occur if the energy in the system is enough to break a bond. In the case of a C-C bond temperatures in the order of 420 °C or higher are needed,<sup>61</sup> whereas C-H bonds are generally weaker. Some functional groups, like peroxides, require much lower temperatures to dissociate, as mentioned in the previous section. However, in the absence of such weak bonds, one has to look more broadly at the type of reactions that can potentially take place to explain the instability of some hydrocarbon mixtures at temperatures well below thermal cracking temperatures.

The abstraction of hydrogen following the reaction of two molecules (not radicals) is what Pryor<sup>62</sup> referred to as molecule-induced homolysis. Molecule-induced homolysis can only take when one molecule can act as a hydrogen donor while the other molecule can act as a hydrogen acceptor. Rüdchard et al.<sup>63</sup> described such reactions when they first observed the transfer hydrogenation from 9,10-dihydroanthracene to  $\alpha$ -methylstyrene. This reaction is an example of what Pryor defined as molecule-induced homolysis and it has been also referred to as molecule-induced radical formation (MIRF), or “retrodisproportionation”.<sup>63,64</sup> This type of reaction can occur at lower temperatures than required for C-H bond dissociation.

Molecule-induced homolysis can be initiated by a hydrogen transfer from a molecule containing a weak R-H bond to an unsaturated acceptor a=b, as shown in Eq. 2-8.<sup>65</sup>



Eq. 2-8

Once a molecule has accepted one hydrogen, a radical is formed, and it can react through addition or hydrogen abstraction. The driving force for the cleavage of the bond is the formation of a stronger bond, and the reaction rate is first order in both molecules involved.<sup>62</sup> Thus, the driving force in this case is a combination of the loss of a weaker C–H bond in the donor molecule, the formation of a stronger C–H bond in the acceptor molecule, and the stability of the two newly formed radicals.

Several examples of such donor and acceptor molecules were reported by Rüchard et al.<sup>65</sup> For example, 9,10-dihydroanthracene, xanthene, acridane, phenalene, are considered good donor molecules, while alkenes of the styrene type, conjugated dienes, azo- and azoxy-, nitro- and nitroso-compounds or quinones are considered suitable hydrogen acceptor molecules.

With this in mind, we should expect that the presence of certain molecules in cracked naphtha could cause the formation of free radicals by molecule-induced homolysis as temperature is increased, thereby affecting the thermal stability.

Hydrogen transfer is known to occur in hydrocarbon mixtures and these can lead to addition product formation. Take for example the reactions between anthracene structures at 300-350 °C, where the reaction between 9,10-dihydroanthracene and 2-ethylanthracene yielded 9,10-dimethyl-9,10-dihydroanthracene as dimeric product.<sup>66</sup> In a different study,<sup>67</sup> the self reaction of dihydronaphthalene at 250 °C yielded tetralin, naphthalene, and dimers. The formation of naphthalene and tetralin indicates that hydrogen donation took place, and the presence of dimers indicated that the free radicals also participated in addition reactions. Although molecules of the type of 9,10-dihydroanthracene are too heavy to be present in the cracked naphtha, dihydronaphthalene is within the boiling range of cracked naphthas.

Adding a hydrogen acceptor molecule like  $\alpha$ -methylstyrene to cracked naphtha, could promote free radical reactions at temperatures of 300 °C and lower, even when cracked naphtha by itself did not show signs of reaction on its own.<sup>68</sup> Considering the effect of the presence of a hydrogen-accepting molecule, and the promotion of radical initiation reaction it can have, we can also look

at these molecules as culprits of the instability of complex mixtures, and not only those with a “weak” hydrogen. In other words, the presence of a hydrogen accepting molecule, can induce radical reactions in an otherwise stable mixture.

The thermal reactions involving molecule-induced homolysis are not limited to disproportionation of hydrogen. Sandhiya et al.<sup>64</sup> have compiled a number of reactions that can enter this group.

## **2.5. Compound classes in the cracked naphtha and their contribution to its instability**

In this section, different compound classes will be evaluated on their possible contribution to the instability of cracked naphtha during the processes mentioned in Section 2.3. For this, their reactivity will be discussed both under autoxidation conditions, i.e., ambient condition with exposure to air, also under temperature conditions up to around 400 °C like those found during in heat exchangers, distillation, hydrotreatment and the oligomerization/aromatic alkylation process that is of specific interest in this study.

### **2.5.1. Saturated compounds (alkanes)**

Paraffins and isoparaffins are alkanes, saturated compounds with formulas of  $C_nH_{2n+2}$ . Paraffins can be present in the naphtha as straight chains or containing branches. Depending on the boiling point distribution of the naphtha cut, paraffins can be present from the very light compounds like butanes ( $C_4$ ), to the  $C_{10}$  long chains. They are stable compounds, and need the presence of a strong reacting agent, catalyst, or high temperatures for them to react. After all, the word paraffin is derived from the Latin, meaning “little affinity”, since chemist attributed their lack of reactivity to a low affinity to other reagents.

Although seemingly innocuous, some paraffins can react through oxidation, given that enough energy is provided to the system. In a study<sup>69</sup> on autoxidation of  $C_8$  isoparaffins, i.e., n-octane, 2-methylheptane, 2,5-dimethylhexane, and 2,2,4-trimethylpentane, at the temperature range of 100-160 °C, it was found that the induction period decreased on increasing number of branches. The induction period was indicative of the consumption of oxygen, meaning that the higher branched molecules reacted more easily with it. This was true for 0-2 branched molecules, since the induction period of 2,2,4-trimethylpentane was similar to that of n-octane. We should note that in this study the conditions were set to obtain accelerated results and do not reflect those of

autoxidation, since pure oxygen was used, and the temperatures were above those found in storage tanks. Nevertheless, the findings speak for the paraffins abilities for hydrogen abstraction, although under severe conditions, and not during autoxidation in storage tanks. Tertiary carbons like those on 2-methylheptane and 2,5-dimethylhexane form a more stable radical, hence the hydrogen in these positions is more prone to be abstracted, and the molecules could react with the oxygen, reporting a higher consumption of oxygen. For the three-branched molecule, the lower oxygen consumption might be related to only be able to form one tertiary radical.

Thermal reactions of paraffins in the absence of oxygen are possible. For a paraffin to crack through homolytic bond cleavage of a C-C bond and form free radicals, temperatures above 400 °C are needed, which is higher than the temperatures seen by the cracked naphtha during its processing and storage. For this reason, it is unlikely that paraffins are responsible of initiating free radical chain reactions in the naphtha during processing and in the absence of oxygen.

Naphthenes or cyclic alkanes, are saturated compounds with formulas  $C_nH_{2n}$ . As paraffins, their relative reactivity is low. They are expected to be in the cracked naphtha mainly as C<sub>4</sub>-C<sub>6</sub> rings. The oxidation reaction of cyclohexane at 100 °C with di-tercbutyl peroxide as initiator was studied to track the behavior of cyclohexane during autoxidation.<sup>70</sup> The main products were cyclohexyl hydroperoxide, with cyclohexanol and cyclohexanone as chain termination products. This indicates the ability of a naphthene molecule likely present in the naphtha to undergo free radical reactions.

### **2.5.2. Olefins (alkenes)**

Olefins are alkenes, unsaturated compounds containing a double bond, with formula  $C_nH_{2n}$ . The unsaturation of olefins is manifested with the presence of a  $\pi$ -bond. The presence of a  $\pi$ -electron pair facilitates the attack of electrophilic reactants which makes olefins a very reactive compound class. They contribute to the known instability of cracked naphthas, because of its easiness to undergo addition reactions ending in heavier compounds. Olefins are not commonly present in crude oils but are present in cracked materials.<sup>24,60</sup> They can be converted during petroleum refining, used as raw material in petrochemical processes, and also be used as high research octane number blending material for gasoline.

The higher reactivity of olefins compared to paraffins is partly due to the added stability of the intermediate product when it can form an allylic radical species.<sup>53</sup> The hydrogen bonded to the allylic carbon, which in turn is the carbon bonded to the carbon containing the double bond, is more easily abstracted. Please refer to Figure 2.1.

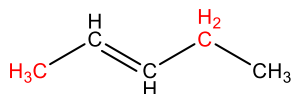


Figure 2.1. Allylic carbon and hydrogen in 1-pentene.

The hydrogen in this position has lower dissociation energy than a hydrogen connected to a carbon in other position. For instance, the dissociation energy of a C-H of a primary carbon in propane is 422 kJ/mol, whereas is 364 kJ/mol in the case of the C-H bond in the allylic position in a propene molecule.<sup>71</sup> This has to do with the free radical that is formed, which is stabilized by resonance.

During oxidation of olefins, once the hydrogen in the allylic positions has been abstracted (Eq. 2-1), the oxygen is added to the newly formed carbon centered radical, forming a hydroperoxide.<sup>53,72</sup>

Not all olefinic molecules are equally reactive to autoxidation. Cyclic olefins show a higher rate during the hydrogen abstraction step than their linear analog. The addition of a second double bond increases such rate, so we can expect that the reactivity of unsaturated compounds to follow the following order: linear olefin < cyclic olefin < linear diolefin < cyclic diolefin.<sup>53</sup> Moreover, the presence of both a double bond and a benzene ring in the structure of an alkenyl aromatic, make a molecule particularly susceptible to hydrogen abstraction.<sup>33</sup>

Under thermal and non-oxidative conditions, depending on the relative stability of the compounds present, some olefins can act as hydrogen donors or hydrogen acceptors during molecule induced radical formation. As an example, the products from the self-reaction of indene show that it can react through hydrogen transfer, by donating or accepting a hydrogen.<sup>4</sup> Linear mono-olefins, like 1-hexene can react with hydrogen donors through a free radical mechanism,<sup>73</sup> yielding the corresponding alkane by hydrogen transfer, but also dimers like dodecenes which are the result of the addition reaction of a hexyl radical to 1-hexene.

Regardless of the way of radical initiation, once free radicals form, one reaction pathway is the addition of a radical to the olefins,<sup>74-76</sup> yielding a radical and allowing the propagation of a chain reaction. For this reason, cracked naphthas with a higher olefin content are considered more prone to formation of heavy compounds, even if such olefinic species are not contributing to the formation of radicals in the first place.

### 2.5.3. Diolefins (dienes)

Diolefins or dienes are molecules that contain two double bonds. Depending on the relative position of the double bonds, dienes can be categorized in cumulated, conjugated, and isolated. The different configurations of pentadiene are shown in Figure 2.2.

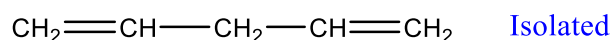


Figure 2.2. Possible positions of double bonds in pentadiene.

Diolefins are usually found at low concentrations in the cracked naphtha,<sup>77</sup> but even low concentrations of these compounds have been found to be harmful for naphtha stability, rapidly increasing the gum potential.<sup>22,23</sup> It is usually recommended that these troublesome molecules be removed before a catalytic process, to deaccelerate coke formation.<sup>19</sup>

Diolefins, like their mono-unsaturated analogs, can also undergo addition reactions when in the presence of free radicals. Diolefins can act as radical acceptor and add to radicals, yielding another radical, allowing the chain reaction to progress. The difference with the mono-olefinic structures is the rates at which this reaction can occur. Addition of a methyl radical was seen to take place almost 3 times as fast in the case of isolated dienes when compared to mono-olefins, while the same addition was slower for cumulated dienes in comparison to other unsaturated molecules, including mono-olefins.<sup>76,78</sup> On the other hand, conjugated diolefins show a very high reactivity towards methyl radical addition, around 2000 times higher than mono-olefins.<sup>74,76,78,79</sup> This is explained by the stability of the allylic radical formed, which is resonance stabilized by the conjugated system.<sup>71</sup>



Less often mentioned in literature is the ability of diolefins of donating a hydrogen during hydrogen abstraction reactions. It was found that besides conjugated diolefins, isolated ones with two single bonds separating the double bonds were particularly reactive to hydrogen abstractions. An example of this kind of molecule is 1,4-pentadiene, structure of isolated diolefin illustrated in Figure 2.2, where the position for the hydrogen abstraction would be the hydrogen in carbon 3, which happens to be the allylic position with respect to both bonds. The rate for hydrogen abstraction for 1,4-pentadiene was 4 times higher than the rate for 1,5-hexadiene.<sup>79</sup> Moreover, in the presence of a good hydrogen donor, diolefins like 1,3-cyclohexadiene and 1,3-cycloheptadiene can accept hydrogen and get hydrogenated to the mono-olefin or the corresponding paraffin.<sup>80</sup>

#### 2.5.4. Aromatics

The oxidation of the aromatic ring is possible. Aromatics also participate in a pre-oxidative step that is of lower energy than hydrogen abstraction.<sup>81</sup> The way in which the pre-oxidation takes place depends on the ring-configuration. Since the aromatic compounds in naphtha is mainly mononuclear aromatics, the substitution pattern may affect how oxygen is added in the pre-oxidation step.

Benzene can react with oxygen to produce maleic anhydride if the aromatic ring cleaves, or benzoquinone if the aromatic ring remains intact,<sup>81</sup> and the same can occur during the oxidation of aromatics with more than one ring. But the conditions to promote oxidation of the aromatic ring are considerably more severe than those experienced by the cracked naphtha in the instances where instability occurs. At mild autoxidation conditions, as those experienced during storage, we can expect the aromatic ring to be unreactive towards the atmospheric oxygen, except for the pre-oxidation step that does not require hydrogen abstraction.

Although the oxidation of the aromatic ring is not expected, the mere presence of a cyclic conjugated  $\pi$ -system contributes to the reactivity of the neighboring atoms within the molecule. The benzylic position (Figure 2.3) is particularly reactive, reason why alkyl aromatics<sup>33,53</sup> and aromatics with a side aliphatic ring<sup>53</sup> are especially prone to autoxidation.

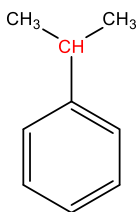


Figure 2.3. Benzylic position in cumene.

The reactivity of alkylaromatics increases with the substitution of the benzylic carbon, as in any radical-forming system. Tertiary benzylic carbons like that on cumene, has a weaker C-H bond, allowing the abstraction of this hydrogen more easily, also helped by the stability of the cumyl radical formed. In a study on rate of autoxidation of diverse compounds,<sup>53</sup> the rate of oxidation of cumene was determined to be approximately 7 times higher than that of ethylbenzene, and 100 times higher than toluene, all of this at 30 °C. At the same time, the rate of oxidation of a secondary benzylic carbon increases if it is contained in ring, to higher rates than that of tertiary benzylic carbons. For instance, in the same study, the rate of oxidation of indane was determined to be slightly higher than that of cumene, and the rate of tetralin was determined to be 1.5 times higher than that of the cumene.

As mentioned in Section 2.5.2, indene has a particular reactivity, which is explained by the presence of a conjugated  $\pi$ -system and a double bond. The highlighted position in the molecule in Figure 2.4 can be considered as both allylic and benzylic, which gives makes the hydrogens in this carbon particularly susceptible to be abstracted.

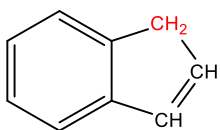


Figure 2.4. Allylic and benzylic position in indene.

The hydrogen transfer ability that makes certain alkyl aromatics prone to oxidation, would also be of high impact during thermal reactions, as it was explained in Section 2.4.2. The hydrogen transfer of benzylic hydrogen has been reported since the 1950's when the tetralin transfer hydrogenation capacity was used during cracking to improve the product quality.<sup>82</sup> The ability of tetralin for hydrogen donation is driven by the formation of a much more stable naphthalene molecule.

### 2.5.5. Heteroatom compounds

Cracked naphtha contains nitrogen, sulfur, and oxygen, present in compound classes with different chemical properties. Characterization of cracked naphthas have helped identifying those compounds containing heteroatoms present in them.<sup>83,84</sup> Generally speaking, the main compound classes are illustrated in Figure 2.5. Note that the compounds in Figure 2.5 were chosen to illustrate the kind of compound class and functionality found, and more compounds with different carbon number and branching are also present.

Oxygenated compounds like ethers, acetals, and aldehydes are particularly reactive and can form peroxides, but they were not found to be present in the cracked naphtha.<sup>84</sup> The oxygen containing compounds present in cracked naphtha are not particularly reactive, according to the literature revised. Although some studies have found that typical phenols present in the cracked naphtha participate in gum and deposit formation,<sup>16,85</sup> some alkylated phenolic inhibitors like 2,6-di-tert-butyl-p-cresol (BHT) and 2,6-di-tert-butylphenol have been tested and their effect on quenching the radical chain reaction has been proven.<sup>14,15</sup>

Sulfur compounds like thioethers and thiophenes have been reported to have little effect on deposit formation during storage and when in contact with heated surfaces, while thiols, in particular thiophenol, have been reported to increase deposit formation.<sup>86,87</sup> Disulfides have also pointed as deposit forming molecules,<sup>86</sup> but their presence in the cracked naphtha is doubtful since they decompose during cracking conditions. On the other hand, compounds of the type of sulfides containing a benzene ring (e.g. benzyl n-propyl sulfide) have been seen to enhanced deposit formation in heated surfaces,<sup>87</sup> although this compounds were not found in the naphtha in the characterization studies cited. The main mechanism used to explain the reactivity of the sulfur compounds is the radical formation by homolytic cleavage of the C-S bond, which is has a lower dissociation energy than the C-C bond (307 kJ and 344 kJ, respectively).<sup>61</sup>

Basic nitrogen present in the naphtha in the form of pyridine or quinoline has been widely discussed and characterized because of its detrimental effect to acid catalysts. Although pyridines have been reported to have a small effect on the instability of fuels,<sup>88</sup> pyrrole has been the nitrogen-containing molecule that has received most attention, since its presence has been related to a major decrease of the fuel stability.<sup>16,85,88-91</sup> Oswald et al.<sup>89</sup> described the contribution of alkylated pyrroles to their ease to form free radicals through the abstraction of the hydrogen in the alkyl chains, which was also observed by Gritter<sup>90</sup> and Li<sup>91</sup>. Moreover, the pyrrole molecule is highly susceptible to radical attack, which has been compared to that of conjugated diolefins because of the conjugated pair present in pyrroles.<sup>90</sup> Indoles, which can be considered pyrrole derivatives, are also expected to have an adverse effect on the stability of fuels. Pyrrole-type molecules, although proven to be present in the cracked naphtha, their concentration is low (quantified at 20 µg/g by Rao et al.<sup>84</sup>).

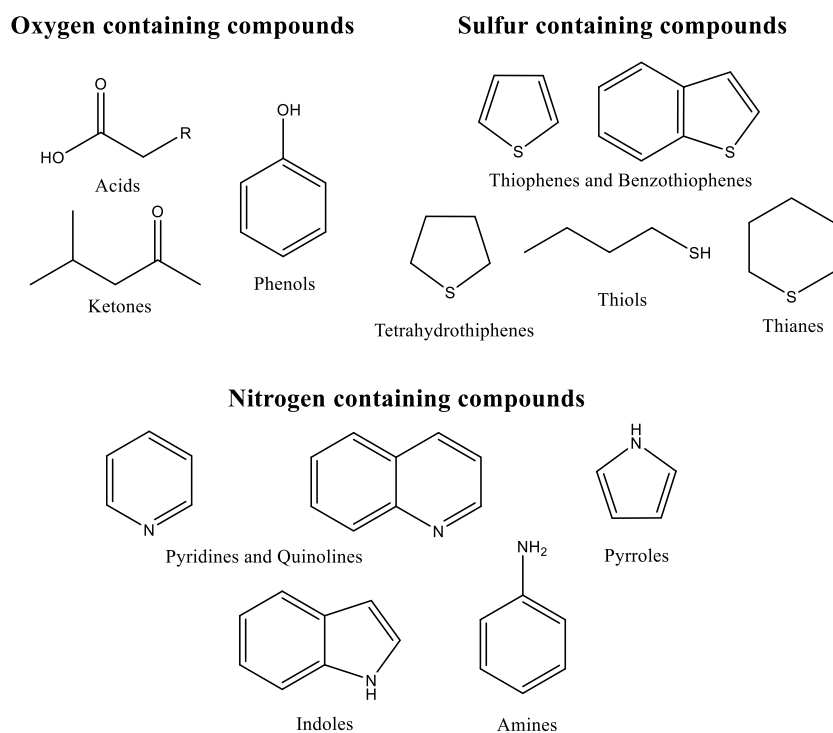


Figure 2.5. Heteroatom compound classes in cracked naphtha.

Amine-type molecules like *N,N'*-Di-*sec*-butyl-*p*-phenylenediamine are used as antioxidants to avoid fuel degradation.<sup>14</sup> It works by acting as radical acceptor and terminating the chain reaction leading to high molecular weight compounds.

## 2.6. Cracking reactions for cracked naphtha production

Up to 2013, the total installed capacity for cracking processes were  $5.5 \times 10^7$ ,  $2.1 \times 10^7$  and  $1.3 \times 10^7$  m<sup>3</sup>/h (14.4, 5.6, and 3.5 MMBPD) for Fluid catalytic cracking (FCC), delayed coking, and other thermal processes, respectively.<sup>92</sup> The yields of the cracked naphtha vary with the initial feedstock used for cracking and with the cracking process used to produce it. **Table 2.1** lists the typical yields of cracked naphtha obtained in different processes. Considering this, we could be talking of approximately  $3.1 \times 10^7$  m<sup>3</sup>/h (8 MMBPD) of cracked naphtha production, considering only FCC and delayed coking processes, which can only increase over time as heavier feedstocks are used more often. These values provide context for the prevalence of cracked naphtha and the possibility of encountering issues related to the instability of cracked naphthas in the refining of heavy crude oils.

The origin of the instability of cracked naphtha as opposed to straight run naphtha, is related to the process of production of cracked naphtha. The feed, the nature of the cracking reactions, and the reaction conditions determines the final composition and the tendency of cracked naphtha to undergo certain reactions that will affect its stability. Hence, we can expect differences between cracked naphthas derived from different processes, and even from similar processes carried out with different feeds or at different operating conditions.

**Table 2.2** lists the characterization of different cracked naphthas, from its physical properties as density, to their elemental and chemical composition.

To understand better such differences, we can look at the reaction network from which the cracked naphtha originated in the first place. From a high-level point of view, there are two main types of cracking reactions that molecules in a crude oil can undergo: thermal and catalytic. The reaction mechanisms are complex for both processes, especially because the feedstock itself it is a highly complex mixture.

The main processes from which cracked naphthas are derived, are discussed from the point of view of their reaction network and process conditions to understand the development of composition and physical properties.

**Table 2.1.** Typical yields of cracked naphtha for each of the cracking processes.

| Row | Process          | Reference               | Feedstock                     | Product naphtha         |             | Yield of other products (wt%) |               |      |
|-----|------------------|-------------------------|-------------------------------|-------------------------|-------------|-------------------------------|---------------|------|
|     |                  |                         |                               | Fraction definition     | Yield (wt%) | Gases and lights              | Other liquids | Coke |
| 1   | Visbreaking      | Gary al. <sup>93</sup>  | et Kuwait Long Resid          | IBP - 165 °C            | 5.9         | 2.5                           | 91.6          |      |
| 2   | Visbreaking      | Jones al. <sup>94</sup> | et VR                         | C5 + 165 °C naphtha     | 4.5         | 2.5                           | 93            |      |
| 3   | Thermal cracking | Jones al. <sup>94</sup> | et AR                         | C5 + 165 °C naphtha     | 7.0         | 4                             | 89            |      |
| 4   | Delayed Coking   | Jones al. <sup>94</sup> | et AR                         | C5 + 165 °C naphtha     | 15.5        | 7.5                           | 59            | 18   |
| 5   | Visbreaking      | Joshi al. <sup>95</sup> | et Bachaquero AR              | C5 - 175 °C             | 6.2         | 2.4                           | 91.4          |      |
| 6   | Visbreaking      | Joshi al. <sup>95</sup> | et Bachaquero VR              | C5 - 175 °C             | 5.5         | 2.0                           | 92.5          |      |
| 7   | Visbreaking      | Joshi al. <sup>95</sup> | et Light Arabian AR           | C5 - 175 °C             | 7.4         | 2.6                           | 90            |      |
| 8   | Visbreaking      | Joshi al. <sup>95</sup> | et Light Arabian VR           | C5 - 175 °C             | 6.2         | 2.3                           | 91.5          |      |
| 9   | Delayed Coking   | Gray. <sup>96</sup>     | Athabasca bitumen             | IBP - 177 °C            | 19          | 3                             | 53            | 25   |
| 10  | Fluid coking     | Gray. <sup>96</sup>     | Bitumen + hydropross. residue | IBP - 177 °C            | 14.1        | 10                            | 55.1          | 21.7 |
| 11  | FCC              | Letzsch. <sup>97</sup>  | Chinese waxy VGO              | C5 + gasoline (<182 °C) | 55.1        | 21.1                          | 19.5          | 4.3  |
| 12  | Thermal cracking | Gary al. <sup>98</sup>  | et                            | C5 + gasoline (<205 °C) | 26.9        | 14.2                          | 58.9          |      |
| 13  | FCC              | Gary al. <sup>98</sup>  | et Similarly topped feed      | C5 + gasoline (<205 °C) | 48.9        | 22.4                          | 23.7          | 5.0  |

## 2.6.6. Naphtha derived from thermal cracking processes

What is common among all thermal cracking processes is that the reactions for the reduction on the size of the molecules of the feed follow a free radical mechanism. What is different among the thermal cracking processes is the extent to which such reactions are allowed to progress. From the “mild” visbreaking to the “severe” delayed coking, temperature and time combinations are selected to convert the heavy feed into different products, with different boiling distributions and different compositions. This has direct implications to the final composition of the products, including that of the cracked naphtha, and the possible characteristics they can display on further processing.

### 2.6.6.1. Thermal cracking reactions

To understand the origin of the typical compounds in thermally cracked products, we can take a look at the nature of reaction that generate them.

Literature explains that for thermal cracking to occur, the energy needed for a chemical bond to be broken needs to be provided. Depending on the molecule, the C-C bond could need temperatures up to 420 °C to go through a homolytic bond cleavage. Once enough molecules crack, free radicals are formed. This is known as the initiation stage, and it is the rate limiting step of the reaction. This is the conventional description of initiation during thermal cracking.

This initiation mechanism, although widely reported, does not explain the role of the already existing persistent radicals present in heavy feedstocks.<sup>100,101</sup> The radical species present in the feed can undergo propagation reactions while other molecules are being cracked through homolytic bond cleavage.

The concentration of free radical species in heavy oil changes with temperature.<sup>102</sup> For the same species, the bond strength of C-C bonds in a non-radical and radical species are different.<sup>103</sup> As a consequence, hydrogen abstraction by free radical species already present in the heavy oil can affect the reaction kinetics and meaningful deviation from a kinetic description relying only on cracking is found at temperatures lower than about 380–400 °C.<sup>104</sup>

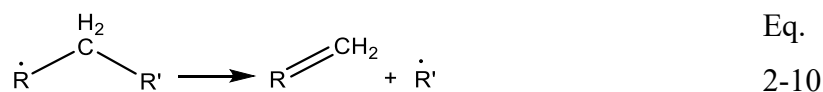
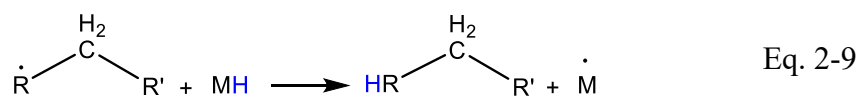
**Table 2.2.** Characteristics of the cracked naphthas derived from different cracking processes.

| <b>Cracking process</b>                            | <b>Visbreaking<sup>6,58</sup></b> | <b>Visbreaking<sup>6,5</sup><sub>8</sub></b> | <b>Coking<sup>6,58</sup></b> | <b>FCC<sup>99</sup></b> | <b>FCC<sup>6,58</sup></b> | <b>FCC<sup>6,58</sup></b> |
|----------------------------------------------------|-----------------------------------|----------------------------------------------|------------------------------|-------------------------|---------------------------|---------------------------|
| <b>Feed</b>                                        |                                   |                                              |                              | Gas oil                 |                           |                           |
| <b>IBP – FBP [°C]</b>                              | 51 – 152                          | 48 – 183                                     | 54.5<br>162.5                | - 34 – 217              | 45 – 155                  | 47 – 144                  |
| <b>Density [kg/m<sup>3</sup>]</b>                  | 727.3                             | 724.0                                        | 714.3                        | 755.9                   | 714.3                     | 706.7                     |
| <b>H/C</b>                                         | 2.13                              | 2.02                                         | 2.08                         |                         | 2.12                      | 2.16                      |
| <b>Sulfur [wt%]</b>                                | 0.80                              | 0.53                                         | 0.088                        | 0.18                    | 0.068                     | 0.033                     |
| <b>Nitrogen [ppm]</b>                              | 9.6                               | 10.7                                         | 19.1                         |                         | 15.8                      | 7.3                       |
| <b>Paraffins [vol%]</b>                            | 42.9                              | 46.1                                         | 39.8                         | 24.69                   | 26.2                      | 32.2                      |
| <b>Cycloparaffins [vol%]</b>                       | 17.8                              | 11.1                                         | 11.4                         | 9.13                    | 7.2                       | 9.0                       |
| <b>Dicycloparaffins [vol%]</b>                     | 0.0                               | 0.9                                          | 0.2                          | 0.85                    | 0.4                       | 0.1                       |
| <b>Olefins [vol%]</b>                              | 18.9                              | 21.1                                         | 24.8                         | 35                      | 40                        | 37.2                      |
| <b>Cycloolefin + Diolefins + Acetylenes [vol%]</b> | 11.0                              | 13.8                                         | 14.9                         | 6.25                    | 14.1                      | 15.0                      |
| <b>Trienes + Cyclo diolefins [vol%]</b>            | 2.2                               | 1.0                                          | 1.9                          |                         | 1.0                       | 0.2                       |
| <b>Dicycloolefin [vol%]</b>                        |                                   |                                              |                              | 0.09                    |                           |                           |
| <b>Alkyl Aromatics [vol%]</b>                      | 7.2                               | 6.0                                          | 7.0                          | 20.51                   | 11.1                      | 6.3                       |
| <b>Alkenyl/cycloparaffin Aromatic [vol%]</b>       |                                   |                                              |                              | 2.18                    |                           |                           |
| <b>Bicyclic Aromatics [vol%]</b>                   |                                   |                                              |                              | 1.30                    |                           |                           |

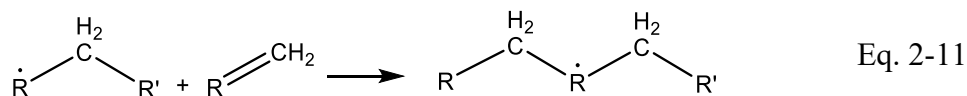


Less discussed in literature, is the fact that hydrogen transfer can also occur with non-radical molecules, acting as a mode of initiation and producing two new radicals. Molecule-induced radical formation or molecule-induced homolysis has been explained by Pryor,<sup>93,95</sup> referring to the transferring of a hydrogen only taking place upon the interaction of certain molecules that could act as hydrogen donors and acceptors. A couple of examples of this reaction have been mentioned in Section 2.4.2, as it can take place at lower temperatures but is not limited to those conditions.

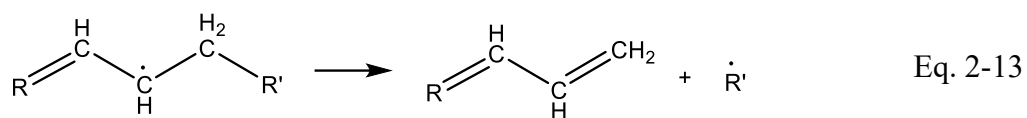
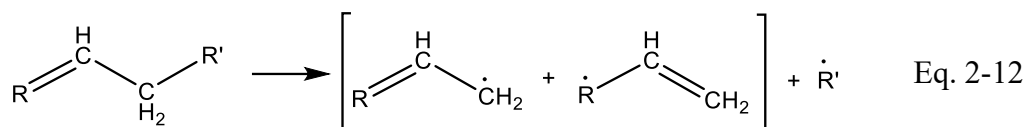
Once a radical is formed, or the conditions for an existing radical to react are in place, the propagation step occurs. This stage of the free radical mechanism proceeds at a higher rate, because energy barriers are lower.<sup>61</sup> During the propagation stage, a free radical can take two reaction pathways. In the first possible route, as shown in Eq. 2-9, the radical molecule would abstract a hydrogen from a molecule MH, and it would yield a saturated bond (RH) and a new radical. The second reaction pathway a radical can undergo during propagation is  $\beta$ -scission, as illustrated in Eq. 2-10, where the radical molecule would cleave at the  $\beta$ -position yielding an  $\alpha$ -olefin and a new radical (R').



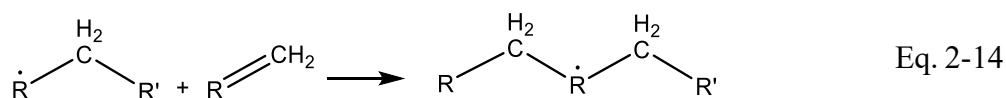
Every radical present or formed during cracking can undergo radical isomerization. Radicals can also add to already formed olefins (Eq. 2-11), with the possibility of yielding larger molecules, step that has been identified as important in the formation of coke in thermal cracking processes.<sup>60</sup>



Besides addition reaction to radicals, olefins can form radicals by cracking – of a C-C bond or a C-H bond (hydrogen abstraction) in the allylic position (see Figure 2.1 in Section 2.5.2). In this case, the driving force is the formation of a resonance-stabilized allylic radical, as that shown in Eq. 2-12. Once the radical is formed, it can crack by  $\beta$ -scission, yielding diolefins (Eq. 2-13), or it can abstract a hydrogen for a proximate molecule yielding an olefin.



The chain reaction approaches the termination stage once the temperature is dropped, since no new radicals are formed and most of the remaining radicals undergo radical addition (Eq. 2-14),<sup>60</sup> or hydrogen disproportionation to form non-radical species (Eq. 2-9).



There will be few radical species that would remain in the liquid products, if stable enough,<sup>101</sup> or that exist as dynamic free radical pairs.<sup>105</sup> These species are generally heavier compounds and no experimental evidence was found for the presence of persistent free radicals in cracked naphtha.<sup>68</sup>

The role of the phase in which the cracking reaction takes place is important since it can favor certain reaction pathways of the molecules. More simply put, the phase affects the probability of monomolecular compared to bimolecular reactions.

The effect of the thermal cracking of *n*-hexadecane both in the liquid and gas phase was studied by Wu et al.<sup>106</sup> When the reaction was carried out in the liquid phase, they found that addition products were favored over cracking products, having a larger proportion of paraffins than olefins. The opposite was found in the gas phase. This was also supported by the work done by Khorasheh et al. on the high-pressure thermal cracking of *n*-hexadecane.<sup>107</sup> What was observed can be explained by the concentration of the reactants on each phase. In the gas phase intramolecular reactions are more likely due to the lower concentration of reactant, whereas that in the liquid phase, intermolecular interactions are favored due to the proximity of the molecules. Hence, we can expect  $\beta$ -scission to be more significant in the gas phase. In fact, the further cracking of olefins into diolefins is more prevalent in the gas phase. For this reason, the phase in which the cracking reactions take place determined by operating pressure and temperature, dictates the reaction pathways and consequently the composition and distribution of the final product.

The specific reaction pathways are dependent of the feed and the conditions, as explained above. Using this background, to better describe the properties of cracked naphthas, we should take a closer look at the industrial processes in which cracked naphtha is produced.

### 2.6.6.2.Visbreaking

The objective of a visbreaker is to reduce the viscosity of a heavy feed. When applied in the refinery industry the target is to reduce viscosity of a vacuum residue to reach the specifications of a more valuable fuel oil. In the context of upgrading of heavy oil and bitumen, the process is aimed to improve the transportability of the feed. The visbroken product tends to be unstable and the olefins produced at higher conversions contribute to this instability.<sup>41</sup>

The severity of the visbreaking process is limited to produce less than 10% of gasoline and gas,<sup>93</sup> as it can be seen in **Table 2.1** with the typical yields for visbreaking. If the feed asphaltene content is high, as is the case in bitumen, then the conversion in the process may be more limited.<sup>96</sup>

The mild conditions of this process are achieved by tuning the temperature and residence time. Temperatures of 455-485 °C are match with residence times of 1-5 min, using a coil visbreaker, where the cracked feed is immediately quenched at the coil outlet to stop the reaction.<sup>93,95</sup> Visbreaking can also take place at lower temperatures and increasing the residence time using a coil-soaker configuration, where most of the conversion occurs in the soaker vessel. Similar conversions to that of the coil visbreaker can be achieved with temperatures lower than 450 °C and residence times of 8-25 min.<sup>93,95</sup>

Since the conversion of the feed is only taken to low values of conversion, only those molecules with bonds weak enough get to be broken, and reactions involving primary products are limited.

In a heavy feed, molecules are diverse, but one of the main structures present are large and heavy alkyl aromatics, interconnected with long carbon chains.<sup>108</sup> These molecules are prone to crack in their aliphatic sections, by carbon-carbon, sulfide (C-S), or disulfide (S-S) bond cleavage. It is the cracking of these molecule what allows the viscosity to drop dramatically, and by it, meet the objective of a visbreaking process.

The radicals formed from the cracking of these molecules can go on to affect other molecules in the neighbourhood, but since the reaction only takes seconds the propagation stage of the reaction is quickly terminated, and most of the products remain as larger molecules. This is notable when seeing the typical yields of a visbreaking process from **Table 2.1**, where it is shown how most the liquid remains in the +175 °C fraction. To explore more on the effect of the feed we can take rows 5 and 6 and 7 and 8 in **Table 2.1**, where the feed processed come from the same crude oil, but different at cut points. The naphtha yield from atmospheric residue (AR) is higher than that of the vacuum residue (VR). This occurs because the atmospheric residue is composed of lighter molecules, that can yield lighter primary products than those produce by the vacuum residue.

Going more in depth in the process, other operational parameters could also affect the resulting products to a minor extent, but data is not readily available. Similar conversion of a heavy oil or residue feed can be achieved at the same temperature by adjusting the residence time, but different composition can be expected. Smaller molecules need a higher energy to break than higher hydrocarbon chains, so we can expect that there is a difference of the type (and hence the amount) of molecules that are affected by homolytic bond cleavage. Additionally, lower temperatures help maintaining the material in the liquid phase, favoring transfer reactions instead of  $\beta$ -scission reactions. In terms of cracked naphtha production and composition, we can expect that the higher temperatures yield a higher amount of the naphtha fraction and a higher concentration of olefins, on the same feed basis. This is reflected also in the coke formation for each configuration, where the rate of carbonaceous deposits is higher for coil visbreaker (higher temperatures) than for the soaker configuration.<sup>95</sup>

### **2.6.6.3. Delayed coking naphtha**

Moving further into the severity of the process there is delayed coking, where coke and distillates are the main desired products. For this reason, the conversion of the heavy feed is taken to the maximum. Taking a look at rows 4 and 9 from **Table 2.1** the high conversion can be seen in terms of the naphtha, gas and coke yields, when compared to the rest of the thermal processes. However, the distribution of products from the delayed coker depends on the feed's propensity to coke, which is measured in terms of Micro-carbon Residue (MCR) or Conradson Carbon Residue (CCR).<sup>96</sup> The yields from the delayed coker can be predicted based on the measure of this property.<sup>93</sup>

The delaying coking process consists of two main units where the thermal cracking reaction occurs: a heater and a coke drum. For analogy with the visbreaking process, the coke drum would be equivalent to the soaker unit. The main difference are the conditions. The feedstock is heated to 480-500 °C,<sup>93</sup> to then fill the coke drum. The coking cycle is a semi-batch process, and the residence time of the feed in the drum is of around 24 h.<sup>93</sup> The delayed coking process is done using up to 4 coke drums, to be able to have a continuous generation of products. After reaction cycle is completed, the coke drum is emptied from liquid and gas products, which are separated in a fractionator. The coking reaction is usually carried at low pressure, 100-600 kPa.<sup>109</sup>

Delayed coking is often called a carbon rejection process, because of the difference of carbon in the different products. But it can be more accurately described as a disproportionation process, increasing the H/C ratio of some products at the expense of the rest.<sup>96</sup> Such degree of disproportionation, as observed in the H/C ratio of delayed coking products is achieved after many H-transfer reactions. Condensed heavy molecules are hydrogen donors, helping increase the H/C ratio of the lighter molecules. Over time, the heavy molecules would be hydrogen depleted and become coke.

The fact that the hydrogen is transferred to the liquid products does not mean that the liquid products are saturated. **Table 2.2** shows the olefin and diolefin content of the coking process, that compared to that of the visbreaking is higher. This can be explained by the low operation pressures and higher temperatures, that allow the evolution of a vapor phase, which in combination with the long residence times promote extensive cracking reactions ( $\beta$ -scission), pushing the product distribution to the lower boiling points.

The disproportionation of the feed goes further than the H/C ratio. Certain molecules are more prone to end up in the coke, limiting their concentration on the liquid products. Take for example the sulfur content of the different cracked naphthas samples in **Table 2.2**. In processes where coke is produced, i.e., delayed coking and FCC, the sulfur content in the naphtha is lower. In visbreaking, where no coke is produced, the sulfur content is high in the naphtha. Nevertheless, the sulfur content of the cracked naphtha also depends on the initial content of the feed, although feedstocks of cracking processes tend to be sulfur rich.

#### 2.6.6.4. Fluid Coking

In contrast with the delayed coking process, which is semi-batch, the fluid coking is a continuous process. The feed is sprayed into a bed of fine coke particles in the reactor, where reaction takes place at temperatures as high as 510-550 °C.<sup>96</sup> Such temperatures are achieved providing the necessary heat by burning part of the coke produced in a burner vessel. The pressure is kept close to atmospheric, which allows part of the feed to vaporize as soon as it is injected. The portion of feed that deposits in the coke will crack to yield gas/liquid products, which will also vaporize, and the coke that remains deposited will enlarge the coke particles.<sup>109</sup> The evolution of vapor products and the injection of steam in the bottom of the bed ensures a good mixing and reduces hot spots. This allows fluid coking units to operate at such a high temperature. Although a vapor phase evolves in the reactor, the low residence time limits vapor phase reactions compared to the delayed coking process. Although product distribution greatly depends on the feed used for the coking process, based on operating conditions and particularly the vapor phase residence time, we could expect slightly lower yields of cracked naphtha in a fluid coker when compared with a delayed coker, even when the temperature in a fluid coker is higher. This can be seen in **Table 2.3**, which shows the product distribution for both coking processes using the same feed.<sup>109</sup>

**Table 2.3.** Product distribution comparison between delayed and fluid coking process using the same feed.

| Process                      | Delayed coking    | Fluid coking |
|------------------------------|-------------------|--------------|
| <b>Feedstock</b>             | Tia Juana Residue |              |
| <b>Product yields (vol%)</b> |                   |              |
| Naphtha (35-220 °C)          | 25.6              | 20.7         |
| Other liquids                | 40.2              | 48.3         |
| Coke                         | 33.0              | 20.0         |

We can also speculate that compounds like diolefins, which are mainly produced in the vapor phase where  $\beta$ -scission prevails, would be present in a lower concentration in the product from the fluid coker.

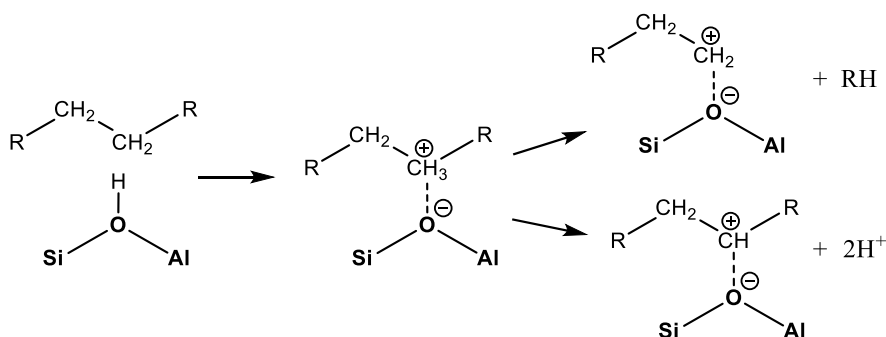
## 2.6.7. Naphtha derived from catalytic cracking processes

Catalytic cracking processes have been optimized over the years to enhance the production of gasoline and light olefinic gases, by tuning reaction conditions and, more importantly, the catalyst properties. Being performed at high temperature, there is a thermal component in the reaction network (free radical reactions), but the main reaction pathway that takes place is through acid-catalyzed chemistry.

### 2.6.7.1. Catalytic cracking reactions

During catalytic cracking, an intermediate carbocation is formed, which lowers the energy necessary for the cleavage to occur, hence requiring lower reaction temperatures than the thermal processes. Catalytic cracking is also a chain reaction mechanism, with initiation, propagation, and termination steps.<sup>110</sup> The initiation step is the formation of the carbocation upon adsorption of reactant on the catalyst, propagation entails the transfer of a hydride ion, and termination is the desorption of a paraffin or olefin.<sup>110,111</sup> Once the carbocation has been formed, besides of hydride transfer, cracking can also occur, yielding more protonated species. Depending on the molecule adsorbing two types of cracking can take place:

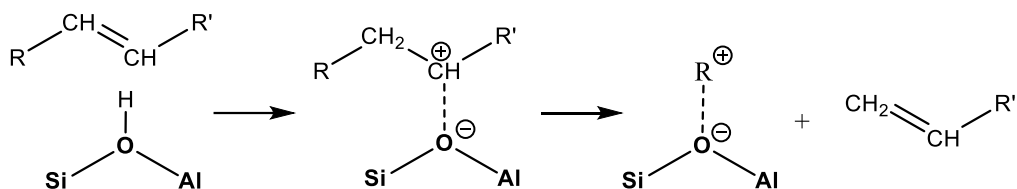
- Protolytic cracking occurs when a penta-coordinated carbocation (or carbonium ion) is formed upon adsorption of a paraffin on the catalyst, on a Bronsted acid site, as shown in **Figure 2.6**.



**Figure 2.6.** Mechanism of paraffins cracking through the formation of a carbonium ion.

This pentavalent carbocation can undergo cracking on the alpha position, producing a paraffin and a carbenium ion which could form an olefin if desorbed. The carbonium ion can also lose the hydrogens necessary to produce a carbenium ion.<sup>112</sup> Rearrangement of the molecules do not occur when this is the cracking step, so more linear products are expected.<sup>110</sup>

- Catalytic cracking by  $\beta$ -scission takes place when a carbenium ion is formed, after an olefin is adsorbed on a Bronsted acid site on the catalyst (Figure 2.7).<sup>112</sup> Cracking occurs at the  $\beta$  position and yields an olefin and a primary carbenium ion. Adsorbed carbenium ions can undergo hydride transfer promoting propagation reactions, and/or it will rearrange through skeletal isomerization possibly giving a branched product since a primary carbocation is highly unstable.<sup>110</sup>



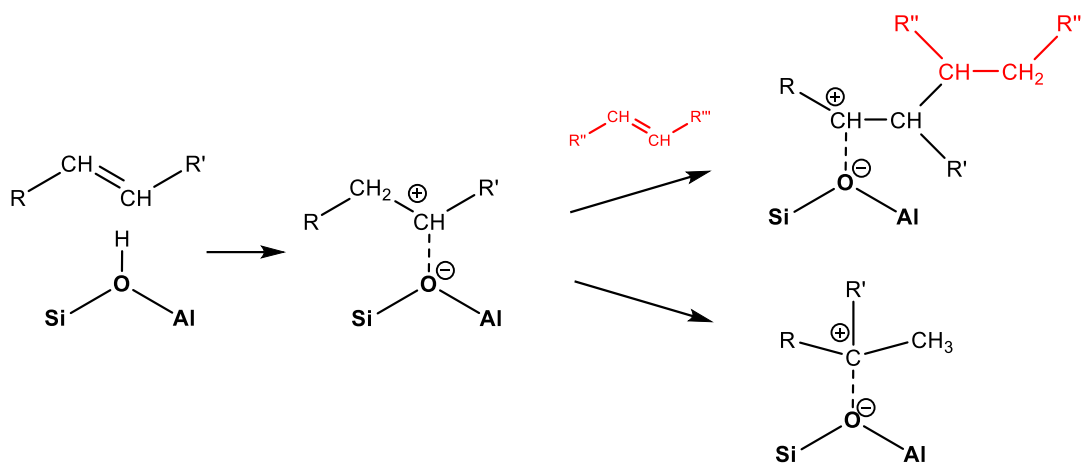
**Figure 2.7.**  $\beta$ -scission of olefins through the formation of a carbenium ion.

Other reactions also take place during catalytic cracking: thermal cracking (free radical chain reactions), double-bond and skeletal isomerization, cyclization, hydrogen transfer, polymerization.<sup>98,110,111</sup>

**Figure 2.8** shows a couple of the reactions a carbenium ion can go through. On the top is the product of an oligomerization reaction when an olefin is added (red). Oligomerization of olefins can continue until a higher molecular weight olefin is desorbed.  $\beta$ -scission of oligomers can yield olefins and diolefins. Cyclization of oligomers can produce cyclic compounds that if dehydrogenated can yield polyaromatics, forming coke.

On the bottom reaction in **Figure 2.8**, skeletal isomerization allows the formation of branched molecules, driven by the formation of a tertiary carbocation. Double bond isomerization is also possible through carbocation intermediary.





**Figure 2.8.** Carbenium ion oligomerization and skeletal isomerization reactions.

### 2.6.7.2. Naphtha from Fluid Catalytic Cracking (FCC)

Fluid catalytic cracking (FCC) is the main conversion process of crude oil to lighter products in refineries since it transforms low value streams like gas oil and residues into valuable products like gasoline and diesel fuels.<sup>98</sup> FCC accounts for nearly 50% of installed capacity of the main conversion processes in refineries – this is including hydrocracking, coking, thermal operations, and resid hydrotreating.<sup>92</sup>

Cracking reactions are endothermic, and in the FCC process the required energy is produced by burning the coke on the spent catalyst during the regeneration step. When the feed enters, it is mixed with the hot catalyst at a typical catalyst-to-oil ratio of 5.5 and a temperature of 550 °C.<sup>92</sup> The mixture then moves along the riser reactor and the reaction proceeds. The contact time is < 10 s, but it is sufficient time for reaction to occur.<sup>97,113</sup> At the exit of the riser reactor the temperature is around 500 °C,<sup>92</sup> and the mixture is then separated into products and spent catalyst.

During the initial contact time of the feed with the catalyst at high temperatures, the reaction network follows mainly a free radical mechanism.<sup>112</sup> At this point gas products and coke deposition on the catalyst are favored.<sup>112</sup>

After the initial contact time, the heavy molecules found in residues (long chain alkyl aromatics) have broken down into molecules that can enter the catalyst pores, and acid catalyzed cracking prevails. Since olefins are products from the cracking reactions, we can expect that at lower conversion levels protolytic cracking dominates, and at higher conversion levels  $\beta$ -scission takes

place predominately, especially because olefins can protonate more easily than paraffins.<sup>112</sup> At any point of the reaction, olefins are being formed, which gives the FCC cracked naphtha a higher content of unsaturated compounds compared to thermal cracking processes (**Table 2.2**). This is desirable from the octane number point of view, and it explains why the FCC cracked naphtha is the main blend component in gasoline.

As it can be observed in **Table 2.1**, the yield of cracked naphtha from catalytic cracking almost doubles the yield obtained by the most severe thermal cracking processes like delayed coker.

Most of the FCC units today use Y-zeolites as primary catalysts. These solids have a high acidity that promotes cracking by  $\beta$ -scission, and the pore size of the zeolite limits (i) the molecules that can enter and (ii) the rearrangements of the protonated species that can form inside, thus limiting the products obtained.<sup>110</sup>

ZSM-5 zeolites are less often used, and only as co-catalyst to the Y-zeolites. Protolytic cracking is more favorable in ZSM-5, used for improving propylene selectivity.<sup>110</sup> Depending on the objectives of the refinery, the ratio between Y-zeolites and ZSM-5 can vary since it can control the ratio of protolytic to  $\beta$ -scission reactions. This is important because it determines the product distribution. Protolytic cracking promoted by a ZSM-5 zeolite additive will favor the production of small olefins in the gas fraction (LPG) and in naphtha but will also decrease naphtha yield and the selectivity to branched products.<sup>110</sup> On the other hand,  $\beta$ -scission contributes to the selectivity of the naphtha. Since  $C_{7+}$  olefins can rearrange into more favorable protons (i.e., tertiary carbocations) they crack at a higher rate through  $\beta$ -scission, yielding mainly  $C_{3+}$  molecules which contribute to the yield increase of the naphtha fraction.<sup>114</sup>

So, cracked naphthas derived from FCC processes driven mainly by Y-zeolites can be expected to have a higher proportion of branch molecules in the  $C_4$ - $C_8$  range. Also, the yield of cracked naphtha is expected to decrease with increased use of the ZSM-5 zeolite, since it promotes the formation of shorter chain molecules that end up in the gas fraction.<sup>110</sup>

## **2.7. Properties expected in cracked naphthas from different cracking processes**

There are some key differences in the reaction pathways followed by thermal and catalytic cracking that result in different properties and different product distribution in the cracked naphtha.

- (i) Skeletal isomerization occurs through a carbocation mechanism. For this reason, we can expect a larger proportion of branched molecules in cracked naphthas derived from a catalytic cracking process. Branch molecules, offering the chance of forming a tertiary radical which is more stable, tend to be more reactive during free radical reactions like those that cause the instability of the fuels.
- (ii) Double bond isomerization also occurs through carbocation chemistry. We can anticipate a wider variety of olefin isomers, especially internal olefins, which tend to be more reactive than terminal olefins<sup>22</sup> in cracked naphthas coming from a catalytic process.
- (iii) Total olefin content is also higher in catalytic processes compared to even the most severe of the thermal processes (delayed coking) as can be observed in **Table 2.2**. Although olefins are an unavoidable result of any type of cracking, the catalytic cracking process has been designed to have a higher conversion and a higher selectivity towards the naphtha fraction, which requires of cracking by  $\beta$ -scission, therefore producing more olefins. In contrast, the thermal cracking processes are not as selective, and olefin yielding reactions can take place in parallel with hydrogen transfer and radical combination, limiting the final content of olefins. Although not all olefins contribute to the instability of the cracked naphtha from an initiation point of view, we can expect that heavy compounds or deposit form at a faster rate in highly unsaturated mixtures due to the participation of olefins in addition reactions (Eq. 2-11).
- (iv) Diolefin content is related to the conditions of cracking. Those conditions that promote intramolecular reactions, like low pressure during thermal cracking reactions, would enhance the production of diolefins.

## **2.8. Crude oil feedstock properties implications for the product cracked naphtha**

Degree of branching as well as the content and type of unsaturated compounds present in the final naphtha product can be correlated to the type of cracking process from where the naphtha was derived. But certain properties given by the presence of some compounds can only be inherited from the feed cracked.

Formation of aromatics compounds can take place during the cracking process since cyclization and hydrogen transfer can readily occur during catalytic and thermal cracking. But a feed that has a higher concentration of aromatics will yield a more aromatic cracked naphtha, as it can be expected when comparing catalytically cracked naphtha derived from bitumen versus one derived from a more paraffinic feed as a Fischer Tropsch wax.<sup>115</sup> The same can be extended to the final concentration of naphthenes.

Also, the final content of nitrogen, sulfur, and oxygen in the cracked naphtha is directly proportional to the content of these same elements in the initial feed. The heteroatom-containing compounds present in the heavy feed will be cracked into smaller molecules, with some heteroatoms making their way into the lighter fraction in the form of those compounds illustrated in Figure 2.5.

Heavy oils and bitumen are high heteroatom containing feedstocks, with nitrogen content ranging from 0.34-1.23 wt%,<sup>116</sup> and a sulfur content of 4.46 wt% for the case of the Athabasca Bitumen in Alberta, Canada.<sup>24</sup> As the heteroatom content increases in the crude oil fractions with increasing boiling point, one needs to consider that the total heteroatom content of a residue feedstock is going to be higher than that of a feedstock containing all its fractions. For instance, the sulfur content of the vacuum residue fraction of the Athabasca Bitumen mentioned before is 5.72 wt%.

Other unconventional feedstocks like biomass, contribute differently to the heteroatom content of its derived cracked products. Although biomass is low in sulfur, is high on oxygenates.<sup>117</sup> This property could have an effect increasing the total acid number of the products. Also, the instability of the products can be if any of the final oxygenates are in the form of ethers, acetals, and aldehydes.

Although mainly dependent on the feed, we can expect variations on the final concentration of heteroatoms in cracked naphthas depending on the cracking process. FCC catalyst, zeolites, being highly acidic have a high affinity to nitrogen bases for which we can expect part of the feed nitrogen ending up on the coke during FCC processing. Part of the sulfur can be present as aliphatic sulfides and disulfides in a heavy oil feed, which are mostly decomposed to H<sub>2</sub>S during cracking, ending in the gas fraction of the product and not in the cracked naphtha.

## 2.9. Concluding Remarks

Two main types of instability of cracked naphtha have been identified after reviewing the most common instances in which this stream is found to cause problems during processing. (i) Oxidative instability during storage, caused by the contact with air over long periods of time. (ii) Thermal instability during processing, caused by the thermal reactions occurring upon heating of the cracked naphtha.

Both types of instabilities are caused by the ability of certain compounds in the feed to start or take part in free radical chain reactions. Compounds with a weakly bonded hydrogen are found to be prone to form the initial peroxides during autoxidation and can also undergo molecule-induced radical formation (MIRF) upon heating in the absence of oxygen when in the presence of a hydrogen acceptor.

A list of the compound classes present in cracked naphtha was reviewed and evaluated in their possible contribution to the naphtha's instability. The instability of the naphtha has been described to its olefin content, but this is an over-simplification of the role of olefins. Although olefins can readily participate of the free radical chain reaction, not all of the unsaturated compounds are able to initiate a free radical reaction or take part of the propagation step with the same ease.

- Compounds with a carbon that is simultaneously in the allylic and benzylic position, like indene and allylbenzenes, or compounds with an allylic carbon shared by two bonds, like 1,4-pentadiene, are particularly prone to hydrogen abstraction and therefore to oxidation and MIRF in the presence of oxygen or a hydrogen acceptor. Linear conjugated diolefins, like 1,3-pentadiene, are more reactive during propagation of a free radical chain reaction but not particularly reactive to hydrogen abstraction. Cyclic diolefins tend to be the most reactive of the olefinic compounds both in hydrogen abstraction and radical addition.
- Alkyl groups in alkyl benzenes are susceptible to hydrogen abstraction, with the alkylaromatics with a double bond in the alkyl chain being more reactive.
- Among the heteroatom compounds known to be present in the cracked naphtha according to the literature reviewed here, pyrroles are the most detrimental to fuel stability.

The presence of the compounds that give cracked naphtha their instability are a direct cause of the cracking process and the feed used to produce the naphtha.

- Catalytic cracking involves a wider range of reactions catalyzed by the carbocation intermediate. The high selectivity towards the naphtha fraction is achieved to the expense of the saturation of the compounds, hence the high olefin content of catalytically cracked naphthas. A higher degree of branching is also a consequence of the acid catalyst, and it relates to a higher availability of tertiary carbons more reactive during radical reactions that affect cracked naphtha stability.
- High severity cracking processes carried at low pressures, like delayed coking, favor  $\beta$ -scission reactions in the vapor phase, increasing the content of diolefins in their products.
- The aromatic content and the heteroatom content are influenced by the feed composition.

### **Acknowledgement**

The study was funded through the NSERC/CNOOC Ltd. Industrial Research Chair program in Field Upgrading and Asphaltenes Processing that is financially supported by the Natural Science and Engineering Research Council (NSERC) of Canada, Alberta Innovates, and CNOOC International.

### **2.10. References**

- (1) Wiehe, I. A. Self-Incompatible Crude Oils and Converted Petroleum Resids. *J Dispers Sci Technol* **2004**, 25 (3), 333–339.
- (2) Rogel, E. Theoretical Approach to the Stability of Visbroken Residues. *Energy Fuels* **1998**, 12 (5), 875–880.
- (3) Zhang, N.; Zhao, S.; Sun, X.; Xu, Z.; Xu, C. Storage Stability of the Visbreaking Product from Venezuela Heavy Oil. *Energy Fuels* **2010**, 24 (7), 3970–3976.
- (4) Tannous, J. H.; de Klerk, A. Asphaltenes Formation during Thermal Conversion of Deasphalted Oil. *Fuel* **2019**, 255, 115786.

- (5) Yan, Y.; C. Prado, G. H.; de Klerk, A. Storage Stability of Products from Visbreaking of Oilsands Bitumen. *Energy Fuels* **2020**, *34* (8), 9585–9598.
- (6) Nagpal, J. M.; Joshi, G. C.; Rastogi, S. N. Stability of Cracked Naphthas from Thermal and Catalytic Processes and Their Additive Response. Part I. Evaluation of Stability and Additive Response. *Fuel* **1995**, *74* (5), 714–719.
- (7) Loison, R.; Foch, P.; Boyer, A. *Coke. Quality and Production*; Butterworth: London, 1989.
- (8) Wright, B.; Hughes, B. Mitigation of Heat Exchanger Fouling. *Digital refining* **2012**, 1–5.
- (9) Uzcátegui, G.; de Klerk, A. Causes of Deactivation of an Amorphous Silica-Alumina Catalyst Used for Processing of Thermally Cracked Naphtha in a Bitumen Partial Upgrading Process. *Fuel* **2021**, *293*, 120479.
- (10) Batts, B. D.; Fathoni, A. Z. A Literature Review on Fuel Stability Studies with Particular Emphasis on Diesel Oil. *Energy Fuels* **1991**, *5* (1), 2–21.
- (11) Brooks, B. T. The Chemistry of Gasolines 1: Particularly with Respect to Gum Formation and Discoloration. *Ind. Eng. Chem.* **1926**, *18* (11), 1198–1203.
- (12) Walters, E. L.; Minor, H. B.; Yabroff, D. L. Chemistry of Gum Formation in Cracked Gasoline. *Ind. Eng. Chem.* **1949**, *41* (8), 1723–1729.
- (13) Kawahara, F. K. Composition of Gum in Cracked Naphtha. *Ind. Eng. Chem. Prod. Res. Dev.* **1965**, *4* (1), 7–9.
- (14) Nagpal, J. M.; Joshi, G. C.; Rastogi, S. N. Stability of Cracked Naphtas from Thermal and Catalytic Processes and Their Additive Response. Part I. Evaluation of Stability and Additive Response. *Fuel* **1995**, *74* (5), 720–724.
- (15) Nagpal, J. M.; Joshi, G. C.; Rastogi, S. N. Stability of Cracked Naphthas from Thermal and Catalytic Processes and Their Additive Response. Part II. Composition and Effect of Olefinic Structures. *Fuel* **1995**, *74* (5), 720–724.

- (16) Pradelle, F.; Braga, S. L.; Martins, A. R. F. A.; Turkovics, F.; Pradelle, R. N. C. Gum Formation in Gasoline and Its Blends: A Review. *Energy Fuels* **2015**, *29* (12), 7753–7770.
- (17) Dryer, C. G.; Lowry, C. D.; Morrell, J. C.; Egloff, Gustav. Mechanism of Gum Formation in Cracked Gasoline - Formation of Peroxide, Aldehyde, and Acid in Storage. *Ind. Eng. Chem.* **1934**, *26* (8), 885–888.
- (18) de Klerk, A. Sasol 2 and 3 Facilities. In *Fischer-Tropsch Refining*; Wiley-VCH: Weinheim, Germany, 2011; pp 181–216.
- (19) Yui, S. Removing Diolefins from Coker Naphtha Necessary before Hydrotreating. *Oil Gas J.* **1999**, *97* (36), 64–69.
- (20) Shaban, H. I.; Khan, A. R. Pressure-Related Operational Problems and Their Remedies in Hydrotreating Reactors in Petroleum Refineries. *J. Pet. Sci. Eng* **1995**, *14* (1–2), 79–88.
- (21) Galya, L. G.; Cronauer, D. C.; Painter, P. C.; Li, N. C. Thermal Instability of Coal-Derived Naphtha. *Ind. Eng. Chem. Fundam.* **1986**, *25* (1), 129–135.
- (22) Pereira, R. C. C.; Pasa, V. M. D. Effect of Mono-Olefins and Diolefins on the Stability of Automotive Gasoline. *Fuel* **2006**, *85* (12–13), 1860–1865.
- (23) Nagpal, J. M.; Joshi, G. C.; Singh, J.; Rastogi, S. N. Gum Forming Olefinic Precursors in Motor Gasoline, a Model Compound Study. *Fuel Science and Technology International* **1994**, *12* (6), 873–894.
- (24) Gray, M. R. Chemical Composition. In *Upgrading Oilsands Bitumen and Heavy Oil*; The University of Alberta Press: Edmonton, Alberta, 2015; pp 93–142.
- (25) Curiale, J. A.; Frolov, E. B. Occurrence and Origin of Olefins in Crude Oils. A Critical Review. *Org. Geochem.* **1998**, *29* (1–3), 397–408.
- (26) Altgelt, K. H.; Boduszynski, M. M. *Composition and Analysis of Heavy Petroleum Fractions*; CRC Press: Boca Raton, FL, 1994.



- (27) Kokayeff, P.; Zink, S.; Roxas, P. Hydrotreating in Petroleum Processing. In *Handbook of Petroleum Processing*; Treese, S. A., Pujado, P. R., Jones, D. S. J., Eds.; Springer International Publishing: Cham, 2015; pp 361–434.
- (28) Hardy, D. R.; Wechter, M. A. Characterization of Soluble Macromolecular Oxidatively Reactive Species (SMORS) from Middle Distillate Diesel Fuels: Their Origin and Role in Instability. *Energy Fuels* **1994**, *8* (3), 782–787.
- (29) Gary, J. H.; Handwerk, G. E.; Kaiser, M. J. *Petroleum Refining*, Fifth.; CRC Press: Boca Raton, FL, 2007.
- (30) Jin, Y.; Liu, T.; Ma, J.; Wang, H. Selective Hydrogenation Catalyst of Ni-Mg/Al<sub>2</sub>O<sub>3</sub> for FCC Light Gasoline. *Petrol. Sci. Technol.* **2005**, *23* (2), 109–117.
- (31) Havran-Mueller, V.; Blommel, J.; Nedohin, G. J. Selective Hydrogenation Processes. In *Handbook of petroleum refining processes*; Meyers, R. A., Ed.; McGraw-Hill: New York, 2016; pp 365–373.
- (32) Mirzoeva, L. M. Low-Temperature Hydrofining of Catalytically Cracked Light Gasoline Fraction. *Chem. Technol. Fuels Oils* **2014**, *50* (3), 225–229.
- (33) Chertkov, Ya. B.; Zrellov, V. N. The Oxidation of Hydrocarbon Fuels under Storage Conditions. In *The Oxidation of Hydrocarbons in the Liquid Phase*; Emanuel, N. M., Ed.; Elsevier, 1965; pp 351–361.
- (34) Balster, L. M.; Zabarnick, S.; Striebich, R. C.; Shafer, L. M.; West, Z. J. Analysis of Polar Species in Jet Fuel and Determination of Their Role in Autoxidative Deposit Formation. *Energy Fuels* **2006**, *20* (6), 2564–2571.
- (35) Aksoy, P.; Gül, Ö.; Cetiner, R.; Fonseca, D. A.; Sobkowiak, M.; Falcone-Miller, S.; Miller, B. G.; Beaver, B. Insight into the Mechanisms of Middle Distillate Fuel Oxidative Degradation. Part 2: On the Relationship between Jet Fuel Thermal Oxidative Deposit, Soluble Macromolecular Oxidatively Reactive Species, and Smoke Point. *Energy Fuels* **2009**, *23* (4), 2047–2051.

- (36) Siddiquee, M. N.; de Klerk, A. Hydrocarbon Addition Reactions during Low-Temperature Autoxidation of Oilsands Bitumen. *Energy Fuels* **2014**, *28* (11), 6848–6859.
- (37) Heinrich, G.; Kasztelan, S. Hydrotreating. In *Petroleum Refining. Vol. 3. Conversion processes*; Leprince, P., Ed.; Editions Technip: Paris, 2001; pp 533–573.
- (38) Alzaid, A.; Wiens, J.; Adjaye, J.; Smith, K. J. Catalyst Deactivation and Reactor Fouling during Hydrogenation of Conjugated Cyclic Olefins over a Commercial Ni–Mo–S/ $\gamma$ -Al<sub>2</sub>O<sub>3</sub> Catalyst. *Energy Fuels* **2018**, *32* (5), 6213–6223.
- (39) Alzaid, A.; Wiens, J.; Adjaye, J.; Smith, K. J. Impact of Molecular Structure on the Hydrogenation and Oligomerization of Diolefins over a Ni-Mo-S/ $\gamma$ -Al<sub>2</sub>O<sub>3</sub> Catalyst. *Fuel* **2018**, *221*, 206–215.
- (40) Watkinson, A. P.; Wilson, D. I. Chemical Reaction Fouling: A Review. *Exp. Therm. Fluid Sci.* **1997**, *14* (4), 361–374.
- (41) Xing, T.; Ali, M.; Alem, T.; Gieleciak, R.; Chen, J. Fouling Tendency of Bitumen Visbreaking Products. *Fuel* **2021**, *289*, 119735.
- (42) Stiegel, G. J.; Shah, Y. T.; Krishnamurthy, S.; Panvelker, S. v. Refining of Coal Liquids. In *Reaction engineering in direct coal liquefaction*; Shah, Y. T., Ed.; Addison-Wesley: Reading, MA, 1981; pp 285–381.
- (43) Asomaning, S.; Watkinson, A. P. Heat Exchanger Fouling by Olefin-Kerosene Mixtures. *Can. J. Chem. Eng.* **1992**, *70* (3), 444–451.
- (44) Taylor, W. F. Kinetics of Deposit Formation from Hydrocarbons. Fuel Composition Studies. *Ind. Eng. Chem. Prod. Res. Dev.* **1969**, *8* (4), 375–380.
- (45) Zerpa, N.; de Klerk, A.; Xia, Y.; Omer, A. A. Olefins Reduction of a Hydrocarbon Feed Using Olefins Aromatics Alkylation. Patent Application WO2015000061A1, 2015.

- (46) Usmanov, M. R.; Batyrov, N. A.; Galimov, Z. F.; Khairullin, R. N.; Bilalov, R. T. Treatment of Visbreaker Naphtha Fraction by Oligomerization. *Chem. Technol. Fuels Oils* **1999**, 35 (1), 4–6.
- (47) Mayo, F. R. Some New Ideas on Oxidation. *Ind. Eng. Chem.* **1960**, 52 (7), 614–618.
- (48) Al-Malaika, S. Chapter 2. Autoxidation. In *Atmospheric Oxidation and Antioxidants. Volume I*; Scott, G., Ed.; Elsevier, 1993; pp 45–82.
- (49) Emanuel, N. M.; Denisov, E. T.; Maizus, Z. K. *Liquid-Phase Oxidation of Hydrocarbons*; Plenum Press: New York, 1967.
- (50) Siddiquee, M. N.; Wu, Y.; de Klerk, A.; Nazemifard, N. The Impact of Microfluidic Reactor Configuration on Hydrodynamics, Conversion and Selectivity during Indan Oxidation. *J. Flow Chem* **2020**, 10 (4), 647–660.
- (51) Siddiquee, M. N.; de Klerk, A. Reaction Engineering Related to Initiation in Liquid Phase Hydrocarbon Autoxidation. *Unpublished*.
- (52) Siddiquee, M. N.; de Klerk, A. In Situ Measurement of Liquid Phase Oxygen during Oxidation. *Ind. Eng. Chem. Res.* **2016**, 55 (23), 6607–6618.
- (53) Howard, J. A.; Ingold, K. U. Absolute Rate Constants for Hydrocarbon Autoxidation. VI. Alkyl Aromatic and Olefinic Hydrocarbons. *Can. J. Chem.* **1967**, 45 (8), 793–802.
- (54) Clark, D. E. Peroxides and Peroxide-Forming Compounds. *Chemical Health and Safety* **2001**, 8 (5), 12–22.
- (55) Jackson, H. L.; McCormack, W. B.; Rondestvedt, C. S.; Smeltz, K. C.; Viele, I. E. Control of Peroxidizable Compounds. *J. Chem. Educ.* **1970**, 47 (3), A175.
- (56) Howard, J. A.; Ingold, K. U. Absolute Rate Constants for Hydrocarbon Autoxidation. XVII. The Oxidation of Some Cyclic Ethers. *Can. J. Chem.* **1969**, 47 (20), 3809–3815.

- (57) Zaikov, G. E.; Howard, J. A.; Ingold, K. U. Absolute Rate Constants for Hydrocarbon Autoxidation. XIII. Aldehydes: Photo-Oxidation, Co-Oxidation, and Inhibition. *Can. J. Chem.* **1969**, *47* (16), 3017–3029.
- (58) Nagpal, J. M.; Joshi, G. C.; Singh, I. D.; Kumar, K. Studies on the Nature of Gum Formed in Cracked Naphthas. In *6th International Conference on Stability and Handling of Liquid Fuels*; Vancouver, Canada, 1997; pp 543–550.
- (59) Parsons, A. F. *Introduction to Free Radical Chemistry*; Blackwell Science: Oxford, 2000.
- (60) Gray, M. R.; McCaffrey, W. C. Role of Chain Reactions and Olefin Formation in Cracking, Hydroconversion, and Coking of Petroleum and Bitumen Fractions. *Energy Fuels* **2002**, *16* (3), 756–766.
- (61) Gray, M. R. Upgrading Reactions and Kinetics. In *Upgrading Oilsands Bitumen and Heavy Oil*; Gray, M. R., Ed.; The University of Alberta Press: Edmonton, Alberta, 2015; pp 151–209.
- (62) Pryor, W. A. Part II The Production of Radicals. In *Free radicals*; McGraw-Hill: New York, 1966; pp 57–145.
- (63) Rüchardt, C.; Gerst, M.; Ebenhoch, J. Uncatalyzed Transfer Hydrogenation and Transfer Hydrogenolysis: Two Novel Types of Hydrogen-Transfer Reactions. *Angew. Chem., Int. Ed. Engl.* **1997**, *36* (1314), 1406–1430.
- (64) Sandhiya, L.; Jangra, H.; Zipse, H. Molecule-Induced Radical Formation (MIRF) Reactions—A Reappraisal. *Angew. Chem. Int. Ed.* **2020**, *59* (16), 6318–6329.
- (65) Rüchardt, C.; Gerst, M.; Nölke, M. The Uncatalyzed Transfer Hydrogenation of  $\alpha$ -Methylstyrene by Dihydroanthracene or Xanthene—a Radical Reaction. *Angew. Chem., Int. Ed. Engl.* **1992**, *31* (11), 1523–1525.
- (66) Billmers, R.; Griffith, L. L.; Stein, S. E. Hydrogen Transfer between Anthracene Structures. *Am. J. Phys. Chem.* **1986**, *90* (3), 517–523.

- (67) Payan, F.; de Klerk, A. Hydrogen Transfer in Asphaltenes and Bitumen at 250 °c. *Energy Fuels* **2018**, *32* (9), 9340–9348.
- (68) Uzcátegui, G.; Fong, S. Y.; de Klerk, A. Cracked Naphtha Reactivity: Effect of Free Radical Reactions. *Energy Fuels* **2018**, *32* (5), 5812–5823.
- (69) Chatelain, K.; Nicolle, A.; ben Amara, A.; Starck, L.; Catoire, L. Structure–Reactivity Relationships in Fuel Stability: Experimental and Kinetic Modeling Study of Isoparaffin Autoxidation. *Energy Fuels* **2018**, *32* (9), 9415–9426.
- (70) Hendry, D. G.; Gould, C. W.; Schuetzle, D.; Syz, M. G.; Mayo, F. R. Autoxidations of Cyclohexane and Its Autoxidation Products. *J. Org. Chem.* **1976**, *41* (1), 1–10.
- (71) Ouellette, R. J.; Rawn, J. D. Conjugated Alkenes and Allylic Systems. In *Organic Chemistry*; Ouellette, R. J., Rawn, J. D., Eds.; Elsevier, 2018; pp 321–351.
- (72) Sergeev, P. G.; Ivanova, L. A. The Oxidation of Hexenes. In *The Oxidation of Hydrocarbons in the Liquid Phase*; Emanuel, N. M., Ed.; Elsevier, 1965; pp 211–218.
- (73) Fong, S. Y.; Montoya Sánchez, N.; de Klerk, A. Olefin Saturation Using Asphaltenes As a Hydrogen Source. *Energy Fuels* **2020**, *34* (4), 4534–4543.
- (74) Gresser, J.; Rajbenbach, A.; Szwarc, M. Methyl Affinities of Some Cyclic Olefins and Polyenes. *J. Am. Chem. Soc.* **1961**, *83* (14), 3005–3008.
- (75) Cvetanović, R. J.; Irwin, R. S. Rates of Addition of Methyl Radicals to Olefins in the Gas Phase. *J. Chem. Phys* **1967**, *46* (5), 1694–1702.
- (76) Buckley, R. P.; Szwarc, M. The Addition of Methyl Radicals to Ethylene, Propylene, the Butenes and Higher 1-Olefines. *Proceedings of the Royal Society of London. Series A. Mathematical and Physical Sciences* **1957**, *240* (1222), 396–407.
- (77) Paez, N. Identification, Conversion and Reactivity of Diolefins in Thermally Cracked Naphtha. MSc. Thesis, University of Alberta, 2016.

- (78) Rajbenbach, A.; Szwarc, M. Methyl Affinities of Dienes. *J. Am. Chem. Soc.* **1957**, *79* (23), 6343–6344.
- (79) Rajbenbach, A.; Szwarc, M. Addition of Methyl Radicals to Isolated, Conjugated and Cumulated Dienes. *Proceedings of the Royal Society of London. Series A. Mathematical and Physical Sciences* **1959**, *251* (1266), 394–406.
- (80) Morgenthaler, J.; Rüdhardt, C. Bimolecular Formation of Radicals by Hydrogen Transfer, 11. Transfer Hydrogenation of Conjugated Cyclic Dienes and Trienes. *Liebigs Annalen* **1996**, *1996* (10), 1529–1532.
- (81) Montoya Sánchez, N.; de Klerk, A. Autoxidation of Aromatics. *Appl. Petrochem. Res* **2018**, *8* (2), 55–78.
- (82) Carlson, C. S.; Langer, A. W.; Stewart, J.; Hill, R. M. Thermal Hydrogenation. Transfer of Hydrogen from Tetralin to Cracked Residua. *Ind. Eng. Chem.* **1958**, *50* (7), 1067–1070.
- (83) Martin, P.; McCarty, F.; Ehrmann, U.; Lima, L. de; Carvajal, N.; Rojas, A. Characterization and Deposit Forming Tendency of Polar Compounds in Cracked Components of Gasoline. Identification of Phenols and Aromatic Sulfur Compounds. *Fuel Science and Technology International* **1994**, *12* (2), 267–280.
- (84) Rao, Y.; de Klerk, A. Characterization of Heteroatom-Containing Compounds in Thermally Cracked Naphtha from Oilsands Bitumen. *Energy Fuels* **2017**, *31* (9), 9247–9254.
- (85) Epping, R.; Kerkering, S.; Andersson, J. T. Influence of Different Compound Classes on the Formation of Sediments in Fossil Fuels During Aging. *Energy Fuels* **2014**, *28* (9), 5649–5656.
- (86) Thompson, R. B.; Druge, L. W.; Chenicek, J. A. Stability of Fuel Oils in Storage: Effect of Sulfur Compounds. *Ind. Eng. Chem.* **1949**, *41* (12), 2715–2721.
- (87) Taylor, W. F.; Wallace, T. J. Kinetics of Deposit Formation from Hydrocarbons. Effect of Trace Sulfur Compounds. *Ind. Eng. Chem. Prod. Res. Dev.* **1968**, *7* (3), 198–202.

- (88) Thompson, R. B.; Chenicek, J. A.; Druge, L. W.; Symon, T. Stability of Fuel Oils in Storage - Effect of Some Nitrogen Compounds. *Ind. Eng. Chem.* **1951**, *43* (4), 935–939.
- (89) Oswald, A. A.; Noel, F. Role of Pyrroles in Fuel Instability. *J. Chem. Eng. Data* **1961**, *6* (2), 294–301.
- (90) Gritter, R. J.; Chriss, R. J. Free-Radical Reactions of Pyrroles. *J. Org. Chem.* **1964**, *29* (5), 1163–1167.
- (91) Li, J. Storage Stability of Jet Fuels. *Fuel* **1985**, *64* (8), 1041–1046.
- (92) Vogt, E. T. C.; Weckhuysen, B. M. Fluid Catalytic Cracking: Recent Developments on the Grand Old Lady of Zeolite Catalysis. *Chem. Soc. Rev.* **2015**, *44* (20), 7342–7370.
- (93) Gary, J. H.; Handwerk, G. E.; Kaiser, M. J. Chapter 5. Coking and Thermal Processes. In *Petroleum Refining*; CRC Press, 2007.
- (94) Jones, D. S. J. Upgrading the Bottom of the Barrel. In *Handbook of Petroleum Processing*; Treese, S. A., Pujado, P. R., Jones, D. S. J., Eds.; Springer International Publishing: Cham, 2015; pp 531–564.
- (95) Joshi, J. B.; Pandit, A. B.; Kataria, K. L.; Kulkarni, R. P.; Sawarkar, A. N.; Tandon, D.; Ram, Y.; Kumar, M. M. Petroleum Residue Upgradation via Visbreaking: A Review. *Ind. Eng. Chem. Res.* **2008**, *47* (23), 8960–8988.
- (96) Gray, M. R. Thermal Cracking and Coking Processes. In *Upgrading Oilsands Bitumen and Heavy Oil*; Gray, M. R., Ed.; The University of Alberta Press: Edmonton, Alberta, 2015; pp 295–346.
- (97) Letsch, W. Fluid Catalytic Cracking (FCC) in Petroleum Refining. In *Handbook of Petroleum Processing*; Treese, S. A., Pujadó, P. R., Jones, D. S. J., Eds.; Springer International Publishing: Cham, 2015; pp 261–316.
- (98) Gary, J. H.; Handwerk, G. E.; Kaiser, M. J. Chapter 6. Catalytic Cracking. In *Petroleum Refining*; CRC Press: Boca Raton, FL, 2007.

- (99) Melpolder, F. W.; Brown, R. A.; Young, W. S.; Headington, C. E. Composition of Naphtha from Fluid Catalytic Cracking. *Ind. Eng. Chem.* **1952**, *44* (5), 1142–1146.
- (100) Tannous, J. H.; de Klerk, A. Quantification of the Free Radical Content of Oilsands Bitumen Fractions. *Energy Fuels* **2019**, *33* (8), 7083–7093.
- (101) Zhang, Y.; Siskin, M.; Gray, M. R.; Walters, C. C.; Rodgers, R. P. Mechanisms of Asphaltene Aggregation: Puzzles and a New Hypothesis. *Energy Fuels* **2020**, *34* (8), 9094–9107.
- (102) Dappe, V.; ben Tayeb, K.; Vezin, H.; Mariette, S.; Serve, O.; Livadaris, V. Effect of Thermal Treatment of Different Petroleum Fractions: Characterization by In Situ EPR Spectroscopy. *Energy Fuels* **2020**, *34* (10), 12026–12032.
- (103) Blanksby, S. J.; Ellison, G. B. Bond Dissociation Energies of Organic Molecules. *Acc. Chem. Res.* **2003**, *36* (4), 255–263.
- (104) de Klerk, A. Thermal Conversion Modeling of Visbreaking at Temperatures below 400 °C. *Energy Fuels* **2020**, *34* (12), 15285–15298.
- (105) Alili, A. S.; Siddiquee, M. N.; de Klerk, A. Origin of Free Radical Persistence in Asphaltenes: Cage Effect and Steric Protection. *Energy Fuels* **2020**, *34* (1), 348–359.
- (106) Wu, G.; Katsumura, Y.; Matsuura, C.; Ishigure, K.; Kubo, J. Comparison of Liquid-Phase and Gas-Phase Pure Thermal Cracking of n -Hexadecane. *Ind. Eng. Chem. Res.* **1996**, *35* (12), 4747–4754.
- (107) Khorasheh, F.; Gray, M. R. High-Pressure Thermal Cracking of n-Hexadecane. *Ind. Eng. Chem. Res.* **1993**, *32* (9), 1853–1863.
- (108) Cheshkova, T. v.; Sergun, V. P.; Kovalenko, E. Y.; Gerasimova, N. N.; Sagachenko, T. A.; Min, R. S. Resins and Asphaltenes of Light and Heavy Oils: Their Composition and Structure. *Energy Fuels* **2019**, *33* (9), 7971–7982.
- (109) Speight, J. G. Thermal Cracking. In *The Refinery of the Future*; Speight, J. G., Ed.; Elsevier, 2020; pp 161–195.



- (110) Corma, A.; Orchillés, A. V. Current Views on the Mechanism of Catalytic Cracking. *Microporous Mesoporous Mater.* **2000**, *35–36* (3 (76)), 21–30.
- (111) Bartholomew, C. H.; Farrauto, R. J. Petroleum Refining and Processing. In *Fundamentals of Industrial Catalytic Processes*; John Wiley & Sons, Inc.: Hoboken, NJ, USA, 2010; pp 635–704.
- (112) Dupain, X.; Makee, M.; Moulijn, J. Optimal Conditions in Fluid Catalytic Cracking: A Mechanistic Approach. *Appl. Catal. A: Gen* **2006**, *297* (2), 198–219.
- (113) Sadeghbeigi, R. Process Description. In *Fluid Catalytic Cracking Handbook*; Sadeghbeigi, R., Ed.; Elsevier, 2012; pp 1–42.
- (114) Buchanan, J. S.; Santiesteban, J. G.; Haag, W. O. Mechanistic Considerations in Acid-Catalyzed Cracking of Olefins. *J. Catal.* **1996**, *158* (1), 279–287.
- (115) Dupain, X.; Krul, R. A.; Makkee, M.; Moulijn, J. A. Are Fischer–Tropsch Waxes Good Feedstocks for Fluid Catalytic Cracking Units? *Catal. Today* **2005**, *106* (1–4), 288–292.
- (116) Prado, G. H. C.; Rao, Y.; de Klerk, A. Nitrogen Removal from Oil: A Review. *Energy Fuels* **2017**, *31* (1), 14–36.
- (117) Shan Ahamed, T.; Anto, S.; Mathimani, T.; Brindhadevi, K.; Pugazhendhi, A. Upgrading of Bio-Oil from Thermochemical Conversion of Various Biomass – Mechanism, Challenges and Opportunities. *Fuel* **2021**, *287*, 119329.

### **Chapter 3. Causes of deactivation of an amorphous silica-alumina catalyst used for processing of thermally cracked naphtha in a bitumen partial upgrading process**

#### **Abstract**

Thermally cracked naphtha represents a challenging feed for many catalytic processes. Its contaminant content and reactivity cause the deactivation of catalysts. Nevertheless, the use of an amorphous silica-alumina acid catalyst to convert and reduce the alkene content in thermally cracked naphtha was possible. The purpose of this study is to determine the cause(s) of catalyst deactivation by analysis of spent catalysts after conversion of cracked naphtha at different conditions in the range 250–350 °C, 6 MPa and WHSV of 0.5–2 h<sup>-1</sup>. It was found that nitrogen bases, suspected to be important acid catalyst poisons, were not the main cause of catalyst deactivation. Nitrogen was more abundant in deposits on the catalyst at the inlet compared to the outlet of the reactor, but the accumulated nitrogen in deposits represented only a minor fraction of the total amount of basic nitrogen to which the catalyst was exposed. Carbonaceous deposits were the main cause of catalyst deactivation and the profile of the deposition on the catalyst changed with temperature. At 325 °C the amount of deposits at the reactor outlet was higher, with lower H/C ratio and higher persistent free radical content than at the reactor inlet. Although some of the precursor species that formed deposits were present in the feed, some of the precursor species that formed deposits were produced during the conversion process. Although the contribution of acid catalysis was not ruled out, many observations in the study indicated that carbonaceous deposits formed mainly due to free radical reactions.

**Keywords:** Cracked naphtha, acid catalysis, amorphous silica-alumina, catalyst deactivation, nitrogen bases, carbonaceous deposits.

### 3.1. Introduction

Thermally cracked naphtha is produced by the thermal conversion of heavy feed materials in processes such as visbreaking and delayed coking. Naphtha represents the lightest atmospheric distillation fraction of the liquid cracked products. The cracked naphtha is a mixture of alkanes (paraffins), cycloalkanes (naphthenes), alkenes (olefins), dienes (diolefins), aromatics, and heteroatom containing compounds. The exact composition of the cracked naphtha depends both on the nature of the heavy feed material that was cracked and the severity of the thermal conversion.

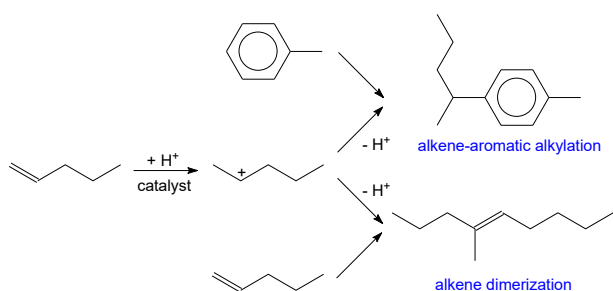
Refining of cracked naphtha is usually performed by hydrotreating <sup>1</sup>. Hydrotreating reduces the heteroatom content and saturates the alkenes. In the case of light naphtha, the preference is to partially hydrogenate the dienes, but limit the alkene saturation to retain the octane number value of the alkenes in the light naphtha, to enable direct blending into motor-gasoline <sup>2,3</sup>.

In the present investigation, the context in which thermally cracked naphtha is treated, is different to what is found in a petroleum refinery. When oilsands bitumen is upgraded <sup>4</sup>, or partially upgraded <sup>5</sup>, the aim is to produce pipeline transportable oil. Raw bitumen is too viscous for pipeline transport. Thermal conversion is central to bitumen upgrading. In bitumen upgraders, hydrotreating the cracked naphtha has the specific aim of reducing the alkene content in the naphtha to meet pipeline requirements <sup>6,7</sup>, and the hydrotreating objective is therefore different to that in a petroleum refinery.

However, unlike in bitumen upgrader facilities, hydrogen is not necessarily available in facilities for partial upgrading or field upgrading of bitumen. Other potential process pathways to reduce the alkene content without the aid of hydrogen include conversion processes such as oligomerization <sup>8</sup>, aromatization <sup>9</sup>, hydrogen transfer from asphaltenes <sup>10</sup>, and alkene-aromatic alkylation <sup>11</sup>.

This study deals with the alkene-aromatic alkylation process that is used to reduce the alkene content in thermally cracked naphtha produced by visbreaking bitumen-derived feed. Alkene-aromatic alkylation is an acid catalyzed process. The alkene is protonated by the acid catalyst and

then alkylates an aromatic to produce an alkyl aromatic (**Figure 3.1**) or dimerizes with another alkene to produce a heavier alkene as product.



**Figure 3.1.** Acid catalyzed alkene-aromatic alkylation and alkene dimerization illustrated by the reaction of 1-pentene and toluene.

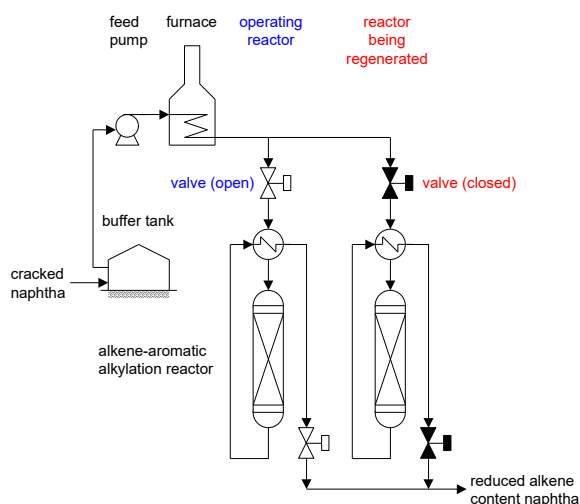
Alkene-aromatic alkylation is industrially practiced to produce products such as ethyl benzene and cumene<sup>12</sup>. When the petrochemical application of alkene-aromatic alkylation is compared to its application for bitumen partial upgrading, there are important differences that affect the catalysis and catalyst deactivation, namely, feed purity and composition control.

(a) Feed purity. The feed materials to petrochemical alkylation processes are purified alkene and purified aromatic streams, with heteroatom containing compounds rigorously removed prior to reaction. For example, for the production of cumene, the feed materials are purified propene and purified benzene. The feed material to the alkene-aromatic alkylation process for partial upgrading is cracked naphtha. The cracked naphtha is not purified in any way and it contains, among other, alkenes, dienes, aromatics, and heteroaromatics that include basic compounds, like pyridines<sup>6,13-15</sup>.

(b) Composition control. Petrochemical alkylation processes make use of an excess of aromatics to moderate the reaction, reduce dimerization and suppress catalyst deactivation by coking. This is possible, because the alkene and aromatic feeds are available as separate feed streams. This type of control is not possible for the application of alkene-aromatic alkylation in a partial upgrader. The cracked naphtha contains both the alkenes and the aromatics. The ratio of alkenes to aromatics is determined by the thermal conversion process by which the cracked naphtha was produced. By adjusting the distillation cut point of the cracked naphtha, limited control of the alkene to aromatic

ratio is possible. Within the naphtha, the alkenes are more concentrated in the lighter boiling material, whereas the aromatics are more concentrated in the heavier boiling material.

It was anticipated that the acid catalyst used for alkene-aromatic alkylation of the thermally cracked naphtha would deactivate with time-on-stream. As a consequence, the reactor design for the alkene-aromatic alkylation process made use of reactors in parallel to enable one reactor at a time to be taken off-line for catalyst regeneration (**Figure 3.2**). It was important to understand the primary causes for deactivation, since this could potentially indicate a form of pretreatment to extend the length of the on-stream period, or cycle length, before regeneration would be necessary.



**Figure 3.2.** Alkene-aromatic alkylation reactors operating in parallel to enable one reactor at a time to be taken off-line for in situ catalyst regeneration. The cycle length will affect the number of reactors employed.

Several candidate causes for deactivation were identified. The thermally cracked naphtha contained dienes<sup>13</sup>, and dienes have been implicated in fouling that takes place when processing cracked naphtha in hydrotreaters<sup>16-18</sup>. The thermally cracked naphtha also contains basic nitrogen-containing compounds<sup>14</sup>, and considering that alkene-aromatic alkylation is an acid catalyzed process, inhibition or deactivation by nitrogen bases was anticipated. Lastly, coking is a common occurrence in the conversion of hydrocarbons on acid catalysts<sup>19</sup>, and the rate at which it occurs is related to the rate of deactivation of the catalyst. All possible causes would have an impact on the formation of deposits, hence on their characteristics.

Cracked naphtha is a complex mixture, and several compounds present are expected to react under the conditions explored. Hence, although the pertinent conversion measure for the process described before would be in terms of the olefin content, this measure is not representative of all the changes occurring in the sample, and compound specific quantification in such complex liquid was impractical. In this study the causes of deactivation of the amorphous silica-alumina catalyst in the alkene-aromatic alkylation of thermally cracked naphtha were investigated by means of the characterization of the spent catalyst. The formation of carbonaceous deposit is a direct effect of the nature of the feed and of the reaction network occurring in the reactor, and the characterization of such deposits (deposition tendency and composition) could provide the information necessary to elucidate the type of reactions taking place towards their formation.

The spent catalyst samples were obtained from the alkene-aromatic alkylation of thermally cracked naphtha in a pilot scale packed bed reactor. Due to the proprietary nature of the piloting work associated with this study, some information that one would normally expect to be reported, was omitted. Data on cracked naphtha conversion are not reported. The thermally cracked naphtha employed as feed was industrially produced by visbreaking of oilsands bitumen derived vacuum residue deasphalted oil.

## **3.2. Experimental**

### **3.2.1. Materials**

Alkene-aromatic alkylation was performed using a commercial amorphous silica-alumina catalyst, Siralox 30. The catalyst used is a commercially available in the form of trilobe pellets, 1.6 mm median diameter, and was supplied by Sasol Germany. The catalyst silica-to-alumina ratio is 30:70. Characterization of the fresh and spent catalysts is reported in Section 3.3 and more detailed characterization of this type of catalyst has been reported in the literature<sup>20</sup>.

The cracked naphtha used as feed material for the alkene-aromatic alkylation was an industrially produced material that was representative of the type of cracked naphtha that is anticipated in partial upgrading processes employing visbreaking. The cracked naphtha was a distillation cut of the product from visbreaking of *n*-pentane solvent deasphalted vacuum residue in the Long Lake bitumen upgrader facility of CNOOC International (formerly Nexen) in Alberta, Canada.

The cracked naphtha was characterized previously in our laboratories <sup>13,14,21,22</sup>. For ease of reference, and due to its relevance to this investigation, some of the naphtha characterization data are listed in **Table 3.1**.

**Table 3.1.** Characterization of thermally cracked naphtha.

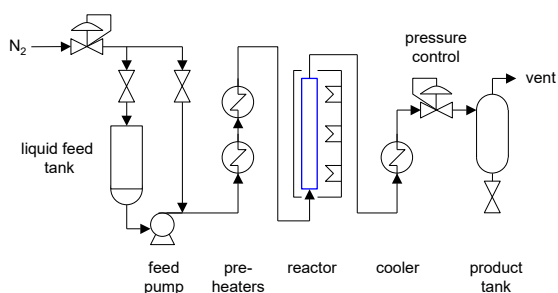
| Property                               | Cracked naphtha |
|----------------------------------------|-----------------|
| Density at 20 °C (kg/m <sup>3</sup> )  | 762.7           |
| Elemental composition (wt%)            |                 |
| carbon                                 | 84.3            |
| hydrogen                               | 13.8            |
| nitrogen                               | 0.09            |
| sulfur                                 | 0.9             |
| oxygen                                 | 0.25            |
| Alkylation reagents (wt%) <sup>a</sup> |                 |
| alkenes                                | 13              |
| aromatics                              | 4               |
| Distillation profile (°C)              |                 |
| IBP                                    | 30              |
| T10                                    | 68              |
| T30                                    | 100             |
| T50                                    | 133             |
| T70                                    | 173             |
| T90                                    | 239             |
| FBP                                    | 265             |

<sup>a</sup> These are estimates based on the detailed gas chromatographic analyses in reference <sup>22</sup>.

### 3.2.2. Equipment and procedure

The spent catalyst samples used for this study were generated from runs of alkene-aromatic alkylation in the cracked naphtha in a laboratory pilot-scale packed bed continuous flow reactor. A simplified flow diagram of the system is shown in **Figure 3.3**.

Briefly, the nitrogen supply was used to keep the cracked naphtha feed under inert atmosphere and to purge and leak test the reactor system. Nitrogen was not co-fed during operation. The only feed during operation was the cracked naphtha in the liquid feed tank. The cracked naphtha was pumped into the system. Two electric temperature-controlled preheaters were supplied to preheat the feed before it reached the reactor. The reactor was contained in a temperature-controlled three zone electric furnace. The reaction product leaving the reactor was cooled using a temperature-controlled chiller. System pressure was controlled on the mixed flow after it was cooled. The liquid product was collected in the product tank. The system was designed in such a way that it was easy to replace the reactor vessel and more than one reactor vessel was employed in the study. In all the alkene-aromatic alkylation runs a bottom-up flow configuration was employed as indicated in **Figure 3.3**.



**Figure 3.3.** Simplified flow diagram of the laboratory-scale pilot unit used for the alkene-aromatic alkylation. Instrumentation and most valves are not shown.

The first series of test runs (experiments 1–5) employed a single packed bed reactor. The objective of these test runs was to evaluate the performance of alkene-aromatic alkylation at different operating conditions. The operating conditions are given in **Table 3.2**. The packed bed reactor was 5 cm in diameter with a central thermowell. In all these test runs 111-112 g of catalyst was loaded for tests conducted at a weight hourly space velocity of  $1 \text{ h}^{-1}$ , resulting in a packed bed length of around 25 cm. For runs at different space velocity, the amount of catalyst loaded was increased or decreased, instead of changing the feed flow rate, thereby keeping the linear velocity in the catalyst bed constant. The bed length was kept constant using an inert material mixed with the catalyst. The experiments were of the same duration.

The second series of test runs (experiments RS1–RS3) employed three shorter packed bed reactors in series. The objective of these test runs was to study the coking deposition profile in the catalytic



bed. By having three reactor vessels in series, it was possible to remove the spent catalyst of the top, middle and bottom sections of the overall catalyst loading separately. Each of the reactor vessels was 2.5 cm in diameter, each packed with 16-20 g of catalyst. In this case, the flow rate was adjusted to reach the desired WHSV. These runs were done increasing the time-on-stream as the temperature was increased. By doing this, we expected to obtain a better indication of the nature of the initial deposits formed on the catalyst and their progressive change.

**Table 3.2.** Operating conditions of alkene-aromatic test runs from which the spent catalysts were obtained for this study.

| Experiment | Operating conditions <sup>a</sup> |         |                         | Reactor     |
|------------|-----------------------------------|---------|-------------------------|-------------|
|            | T (°C)                            | P (MPa) | WHSV (h <sup>-1</sup> ) |             |
| 1          | 300                               | 6       | 1                       | single      |
| 2          | 325                               | 6       | 1                       | single      |
| 3          | 350                               | 6       | 1                       | single      |
| 4          | 325                               | 6       | 0.5                     | single      |
| 5          | 325                               | 6       | 2                       | single      |
| RS1        | 250                               | 6       | 1                       | 3 in series |
| RS2        | 280                               | 6       | 1                       | 3 in series |
| RS3        | 325                               | 6       | 1                       | 3 in series |

<sup>a</sup> T = internal reactor temperature; P = pressure; WHSV = weight hourly space velocity.

In all the test work, the catalyst bed was contained between layers of glass beads to fill the void space of the reactor vessels. For each experiment, fresh Siralox 30 catalyst was loaded from the same batch of catalyst received from the supplier.

Although this study does not report on the performance of the alkene-aromatic alkylation work due to confidentiality reasons, it is worth mentioning the following for the interest of the discussions taking place:

- (i) Material balance was closed for all experiments and reaction products were characterized.
- (ii) Conversion was measured in terms of the total olefin content. Under all conditions explored, the catalyst proved to be active, with conversion following a proportional

trend with temperature and inversely proportional trend with the WHSV, as it might be expected.

- (iii) The duration of the runs is omitted due to a request from the industrial sponsor of the work.
- (iv) The time-on-stream (TOS) used in this study was representative of industrial practices. At the end of each run, the catalyst activity had decreased below the end-of-run threshold for the process although the catalyst was never fully deactivated.

### 3.2.3. Analyses

**Brunauer–Emmett–Teller (BET) surface area determination.** The surface area of the catalyst was determined using the multipoint BET model in the  $P/P_0$  range of 0.05 to 0.3, in a Quantachrome Autosorb iQ. Around 0.3 g of each sample placed in 6 mm cells and subjected to outgassing under vacuum at 250 °C for 4 h before the surface area measurement. In the case of the spent catalyst sample, the organic deposits were removed prior to the analysis by calcination under air at 500 °C for 2 h. The calcined spent catalyst sample was then analyzed following the procedure described for the fresh catalyst.

**Temperature programmed desorption of Ammonia (NH<sub>3</sub>-TPD).** Around of 250 mg of the fresh catalyst sample catalyst was introduced into a u-shaped **quartz** cell and loaded in the equipment, a Quantachrome ChemBET TPR/TPD. The sample was outgassed at 550 °C for 90 min under a helium flow, and once cooled down to 60 °C ammonia was flown through for 40 min. The physically adsorbed ammonia was flushed out of the system at 60 °C for 40 min using helium. The samples were then heated at 10 °C/min to 600 °C and the ammonia desorption was recorded. In the case of the spent catalyst sample, the organic deposits were removed prior to the analysis by calcination under air at 500 °C for 2 h. The calcined spent catalyst sample was then analyzed following the procedure described for the fresh catalyst.

**Diffuse reflectance infrared Fourier transform spectroscopy (DRIFTS) of adsorbed pyridine.** The measurement was performed using an ABB MB 3000 FTIR with a with a PIKE DiffusIR<sup>TM</sup> attachment. 5 mg of the sample was ground and mixed in equal proportion with KBr, placed in a porous ceramic crucible, and pressed until a uniform surface was obtained. The sample was outgassed 450 °C for 40 min, cooled down to 115 °C when a background was taken, and then

pyridine vapors were allowed in the chamber. After 40 min exposure to pyridine, the flow was changed to nitrogen and the IR spectra were taken every 10 min until steady state was achieved. At this point, the spectrum could be used to determine the presence of Lewis and Brønsted acid sites.

**Carbonaceous deposit content determination by thermal gravimetric analysis (TGA).** The analyses were performed in a Mettler Toledo TGA/DSC1 with LF furnace, sample robot, and MX5 internal microbalance. Around 40 mg of each catalyst sample was ground using an agate mortar and pestle and placed in a 70  $\mu$ L alumina crucible. Samples were heated to 900  $^{\circ}$ C at a rate of 10  $^{\circ}$ C/min under 100 mL/min of air. Material identified as carbonaceous deposits were material volatilized or combusted in air at temperatures above 250  $^{\circ}$ C.

**Carbonaceous deposits characterization by CHNS elemental analysis.** The analysis was performed in a Carlo Erba Model EA1108 Elemental Analyzer for CHNS and oxygen (Triad Scientific, Inc., Manasquan, NJ, USA). Around 250 mg of sample was grounded and then treated at 250  $^{\circ}$ C under a nitrogen flow to remove volatiles and water. The CHNS measurements were done in duplicate. The result was adjusted to the deposits content using the results from the TGA.

Extraction of carbonaceous deposits from the catalyst by using dichloromethane (methylene chloride). To explore the chemical composition of the soluble carbonaceous deposits, 50 mg of the spent catalyst samples were ground and subjected to extraction using 20 mL of dichloromethane. The resulting dichloromethane solution was analyzed using GC-MS, as described in previous studies <sup>23</sup>.

**Electron spin resonance (ESR) spectroscopy.** The ESR spectra were collected using an Active Spectrum extended range Electron Spin Resonance spectrometer operated at 9.7 GHz frequency. To be able to directly compare values between spent catalyst samples all measurements were performed on samples that were prepared to have the same amount of carbonaceous deposits. This was done by adding the needed amount of fresh catalyst to “dilute” the samples until the desired value of carbonaceous deposit (6 wt%) was obtained. Approximately 300 mg of each of the prepared samples were finely ground to a powder and placed in a 5 mm (OD) Wilmad-LabGlass ESR tube. The ESR spectra for the naphtha sample was obtained in the magnetic field range of

3300 to 3600 G, with a microwave power of 15 mW, 1.2 G of coil amplitude, 3 scans, and digital gain of 12 dB.

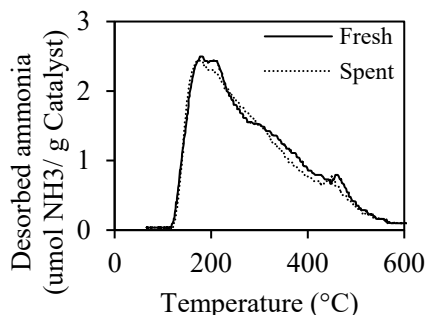
**Carbonaceous deposits characterization by FTIR.** The spent catalyst samples were treated at 250 °C under a nitrogen flow to remove volatiles. The samples were ground and analyzed for their infrared spectra, in an ABB MB3000 Fourier Transform infrared spectrometer with Horizon MB FTIR software. The spectrometer was equipped with a Pike MIRacle Reflection attenuated total reflectance (ATR) diamond crystal plate. The analysis was performed at a resolution of 8 cm<sup>-1</sup> and an average of 120 scans over the spectral region of 4000-500 cm<sup>-1</sup>.

**Thermal gravimetric analysis (TGA) coupled with FTIR.** An ABB MB 3000 FTIR coupled to a Mettler Toledo TGA/DSC1 was used to analyze the evolved gases of the combustion of the carbonaceous deposits present in each of the catalyst samples. The gases produced in the TGA traveled through a heated line (200 °C) to a PIKE heated constant path length gas flow cell (200 °C), where the gases were analyzed. The samples were prepared and treated the same way described in the **carbonaceous deposit content determination by TGA**. The spectra of the evolved gases were recorded every 1 minute at a resolution of 8 cm<sup>-1</sup> and average of 20 scans.

### 3.3. Results

#### 3.3.1. Fresh and spent catalyst characterization

The acid strength of the acid sites on the amorphous silica-alumina catalyst varied over a wide range as expressed in terms of the desorption temperature of ammonia or NH<sub>3</sub>-TPD (**Figure 3.4**).



**Figure 3.4.** Ammonia temperature programmed desorption curve of fresh (solid line) and spent and calcined (dotted line) amorphous silica-alumina catalyst.

The acid strength profile gave an indication of the amount of acid sites that would likely be inhibited or poisoned by the pyridine compounds in the cracked naphtha during operation. The acid sites were classified into three groups for quantification (**Table 3.3**).

The weak acid sites were those with an ammonia desorption temperature in the range 115–275 °C. The medium strength acid sites were those with an ammonia desorption temperature of 275–450 °C. Collectively the sites with weak and medium acid strength were the most abundant types of acidity in the catalyst, representing 87 % of the total acidity. The acid site strength distribution from NH<sub>3</sub>-TPD has been encountered in zeolites <sup>24</sup> correlating it to their activity <sup>25</sup>, and in amorphous silica-aluminas <sup>26,27</sup>. A minor variation of the acidity was seen after reactions in the spent catalyst sample.

**Table 3.3.** Characterization of the fresh and spent amorphous silica-alumina catalyst.

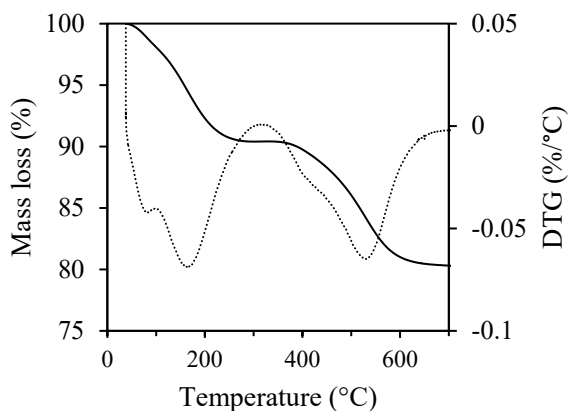
| Property                                     | Fresh | Spent <sup>a</sup> |
|----------------------------------------------|-------|--------------------|
| BET surface area (m <sup>2</sup> /g)         | 303   | 310                |
| Acid concentration (μmol NH <sub>3</sub> /g) |       |                    |
| weak                                         | 294   | 293                |
| medium                                       | 207   | 181                |
| strong                                       | 73    | 60                 |
| total                                        | 574   | 534                |

<sup>a</sup>Representative spent sample (RS3-out) after removal of deposits by calcination under air at 500 °C for 2 h.

### 3.3.2. Quantifying Carbonaceous deposits

In this study, we defined the carbonaceous deposits as the organic material volatilized or combusted at 250 °C or higher temperatures, representing the second and well-defined event in the TGA thermogram. **Figure 3.5** shows a characteristic thermogram for a representative spent catalyst sample after reaction with cracked naphtha and the corresponding DTG curve; the first event takes place from 60 °C to 250 °C approximately for all samples, and at this temperature, one can only consider desorption of volatile compounds present in the naphtha (remaining feed or product). The comparison between experiments for amount of deposits formed is based on the

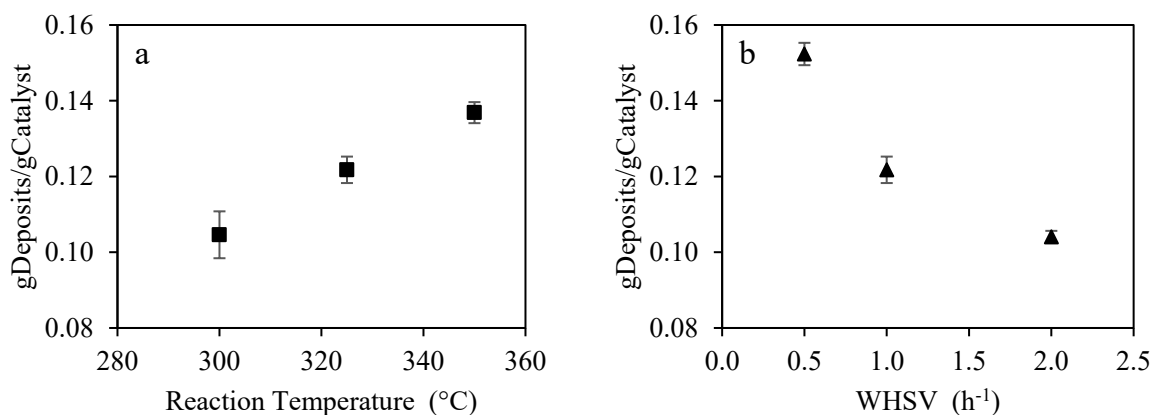
quantification of only the second event which occurs from 300 to 675 °C, as clearly shown by the DTG curve **Figure 3.5**.



**Figure 3.5.** Spent catalyst mass loss with temperature (solid line) and derivative mass loss with temperature (dotted line) to illustrate the main where regions where mass loss occurred. The data shown is for the spent catalyst sample Exp 1, performed at 325 °C and 1 h<sup>-1</sup>.

### 3.3.3. Effect of operating conditions on carbonaceous deposits

The effect of the operating temperature and the weight hourly space velocity (WHSV) on the amount of carbonaceous deposits was determined from experiments 1–5 listed in **Table 3.2**. The duration of these experiments was the same and it was therefore possible to compare directly the results that are shown in **Figure 3.6**.



**Figure 3.6.** Effect of (a) temperature at a WHSV of 1 h<sup>-1</sup>, and (b) weight hourly space velocity at a temperature of 325 °C, on the amount of carbonaceous deposits found on the spent catalysts in experiments 1–5. The error bars indicate one standard deviation of analyses in triplicate.

The amount of carbonaceous deposits increased with an increase in operating temperature when the WHSV was kept constant at  $1 \text{ h}^{-1}$  (**Figure 3.6a**). The spent catalyst from the test run performed at  $350 \text{ }^\circ\text{C}$  had the highest content of deposits.

When the temperature was kept constant at  $325 \text{ }^\circ\text{C}$  and the WHSV was varied, it was found that the amount of carbonaceous deposits on the spent catalyst decreased with an increase in WHSV (**Figure 3.6b**). The hydrodynamic conditions of these experiments were the same, because the WHSV was varied by varying the amount of catalyst loaded and not by changing the flow rate of the feed. The linear velocity of the feed in the catalyst bed was therefore the same. Differences could not be attributed to difference in mass transport. The bed volume was also kept the same by dilution.

What the results in **Figure 3.6b** show, is that the same amount of naphtha feed in contact with different amounts of catalyst for different space times (inverse of WHSV) caused the amount of carbonaceous material per unit mass of catalyst to increase with increasing loading of catalyst, i.e. with lower WHSV. In terms of space time (inverse of WHSV), the fraction of the feed converted to carbonaceous deposits increased proportionally with the time that it took to process that amount of feed, as shown in **Table 3.4**.

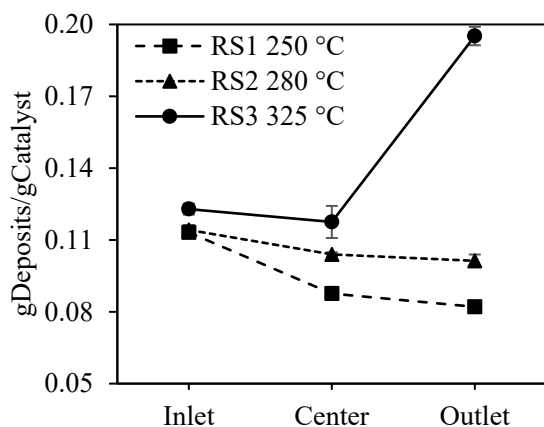
**Table 3.4.** Amount of naphtha feed material converted to carbonaceous deposits on the catalyst at  $325 \text{ }^\circ\text{C}$  in the same time period, but at different weight hourly space velocity.

| WHSV ( $\text{h}^{-1}$ ) | Carbonaceous deposit<br>(mg deposit/g naphtha) |
|--------------------------|------------------------------------------------|
| 0.5                      | 25                                             |
| 1                        | 11                                             |
| 2                        | 5                                              |

To better understand carbonaceous deposit formation, experiments were carried out using three reactors in series, experiments RS1–RS3 listed in **Table 3.2**. These experiments were of different duration and direct comparison of these runs should not be made. The amount of carbonaceous deposits found in on spent catalyst from the three different sections, are shown in **Figure 3.7**.

The intent of performing some reactions at an even lower temperature than shown in **Figure 3.6a**, was to see to reduce the formation of carbonaceous deposits. As the temperature was decreased, the time on stream was also decreased and it was hoped to obtain a better indication of the evolution of deposits due to catalyst fouling by cracked naphtha. The reason for decreasing the time on stream for **Figure 3.7** was to obtain a better indication of the nature of the initial deposits formed on the catalyst, before the deposits had time to mature on the catalyst.

It was expected that such catalyst fouling would be revealed as carbonaceous deposits concentrated at the inlet. Therefore, the results in **Figure 3.7** were surprising. For the two experiments carried out at lower temperatures, 250 °C and 280 °C, there was only a minor decrease in deposit formation moving from the inlet to the outlet. The decrease was most pronounced in experiment RS1, conducted at 250 °C, where the amount of carbonaceous deposits at the inlet was  $0.113 \pm 0.001$  g/g catalyst and  $0.082 \pm 0.001$  g/g catalyst at the outlet, less than a 30% decrease. When the reactor was operated 325 °C, which is representative of typical alkene-aromatic alkylation conditions, it was found that most of the carbonaceous deposits were at the reactor outlet (**Figure 3.7**). The amount of carbonaceous deposits increased from  $0.123 \pm 0.002$  g/g catalyst at the inlet to  $0.195 \pm 0.004$  g/g catalyst at the outlet, almost a 60% increase.



**Figure 3.7.** Carbonaceous deposit content of the spent catalyst from the different sections along the reactor bed in experiments RS1–RS3. The duration of the experiments was different. The error bars indicate one standard ion of analyses in triplicate.



### 3.3.4. Elemental analysis of carbonaceous deposits

The elemental composition of the carbonaceous deposits would provide some indication of the degree of coking, as well as of the relative enrichment of heteroatom species. When CHNS analysis was performed, it was found that the hydrogen-to-carbon ratios were unreasonable variable. This problem appeared to be a common challenge with spent catalyst analysis due to ingress of moisture from air<sup>28</sup>. Although strategies were described to account for the additional water retained in catalyst samples<sup>28</sup>, we were unsuccessful in reducing the variability.

The results are reported in **Table 3.5** are therefore limited to the nitrogen-to-carbon and sulfur-to-carbon ratios, since these ratios were not affected by variability in the moisture content.

The nitrogen-to-carbon content of the cracked naphtha feed was low, 0.001 mol/mol. It could be determined to a lower level than that of the spent catalyst samples, because it was not diluted with catalyst. The deposits on the spent catalysts from experiments 1–5 all had a nitrogen-to-carbon content of <0.02 mol/mol (**Table 3.5**). It was anticipated that the acidic catalyst would accumulate basic nitrogen containing species on the strong acid sites (**Figure 3.4**), contrary to what was observed. In all these experiments the total amount of nitrogen to which each catalyst was exposed should have caused a quantifiable increase. The total amount of nitrogen in coke was less than 0.001% of the total amount of nitrogen that passed over the catalyst during pilot testing. Thus, the observed nitrogen-to-carbon ratio indicated that only a limited amount of nitrogen containing compounds was retained on the catalyst.

In the experiments with reactors in series, experiments RS1–RS3, a measurable increase in nitrogen-to-carbon ratio was observed only for the spent catalyst at the reactor inlet (**Table 3.5**). Additionally, it was anticipated that the amount of nitrogen bases retained by the catalysts would be related to the operating temperature in relation to the acid strength, as shown by NH<sub>3</sub>-TPD (**Figure 3.4**). At reaction temperatures of 250 °C (experiment RS1), about half of the total acid sites present in the catalyst could potentially be poisoned by basic nitrogen containing compounds.

The nitrogen-to-carbon ratios of the deposits were of the same order (**Table 3.5**), but the increase in operation temperature was reflected by the nitrogen-to-carbon ratio of the catalyst at the reactor inlet. In experiment RS1 (280 °C) it was 0.034 mol/mol compared to experiment RS3 (325 °C)

that was 0.024 mol/mol. In both instances the deposits did not exclusively consist of nitrogen-containing compounds, because the nitrogen-to-carbon ratio of pyridinic compounds in the naphtha feed was of the order 0.1 mol/mol.

**Table 3.5.** Nitrogen-to-carbon and sulfur-to-carbon ratios of the carbonaceous deposits found on spent catalysts.

| Experiment                | Elemental analysis (mol/mol) <sup>a</sup> |       |
|---------------------------|-------------------------------------------|-------|
|                           | N/C                                       | S/C   |
| naphtha feed <sup>b</sup> | 0.001                                     | 0.009 |
| 1                         | <0.02                                     | 0.016 |
| 2                         | <0.02                                     | 0.010 |
| 3                         | <0.02                                     | <0.01 |
| 4                         | <0.02                                     | 0.010 |
| 5                         | <0.02                                     | 0.013 |
| RS1 inlet                 | 0.034                                     | <0.01 |
| RS1 outlet                | <0.02                                     | 0.017 |
| RS2 inlet                 | 0.033                                     | <0.01 |
| RS2 outlet                | <0.02                                     | <0.01 |
| RS3 inlet                 | 0.024                                     | <0.01 |
| RS3 outlet                | <0.02                                     | <0.01 |

<sup>a</sup> Values of <0.02 for N/C and <0.01 for S/C reflect the quantification limit on the spent catalyst, which was affected by dilution of the carbonaceous deposit with the catalyst.

<sup>b</sup> Calculated from feed characterization in Table 3.1; lower quantification limit because the feed material was not diluted with catalyst.

Sulfur appeared present in some samples with no clear trend (**Table 3.5**). Tetrahydrothiophenes and thianes are expected to be present in the naphtha <sup>14</sup>, and thiophenes/alkylthiophenes are within the boiling range of the naphtha. Although sulfur compounds are soft Lewis bases, they did not have the same adsorption behavior as the nitrogen bases. This is probably due to the reaction temperature used in this study, since adsorption of thiophene on zeolites has been observed at room temperature <sup>29,30</sup> when adsorption is favored, and found to be affected by the presence of aromatics and olefins <sup>29</sup>, because of competition for the acid sites or for addition reactions. Under fluid catalytic cracking conditions, (i.e. 500 °C and stronger acid sites) tetrahydrothiophenes easily crack

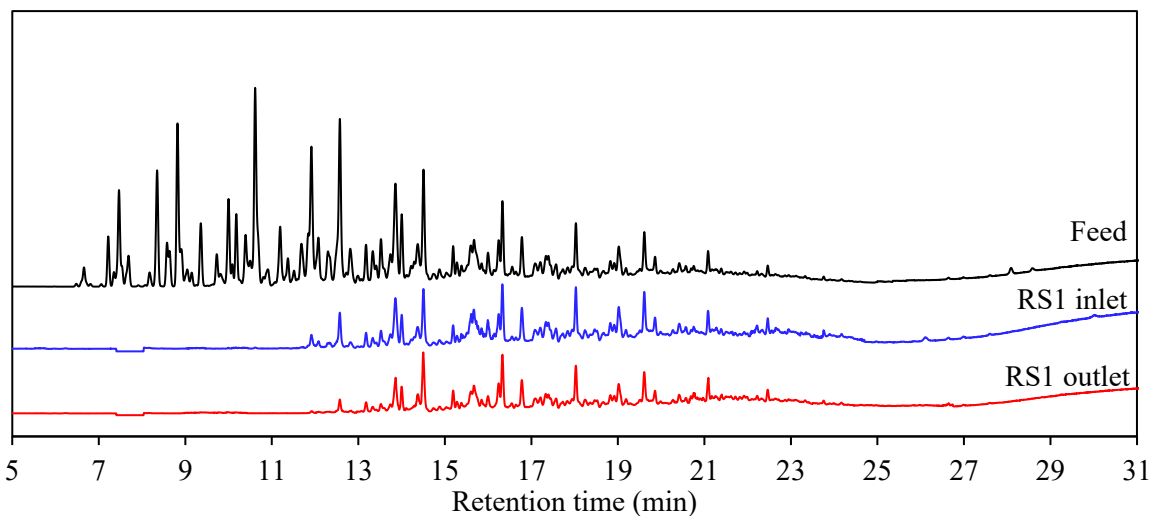
<sup>31</sup>, and thiophene and alkyl-thiophenes convert mainly into coke <sup>32</sup>. At the conditions used in this study, we can expect that olefin-aromatic alkylation take place involving thiophenic molecules, but due to the low concentration of sulfur compounds this should not be an important reaction pathway. Hence, if sulfur compounds took part on the reactions leading to coke, their contribution was probably random. The existing literature on reactions of sulfur compounds at the reaction condition and the pattern followed by the sulfur on the deposits does not clarify the role of sulfur compounds (if any) on the formation of carbonaceous deposits.

### 3.3.5. Chemical composition of carbonaceous deposits

To obtain more information about the chemical identity of the carbonaceous deposits, a solvent extraction and analysis procedure explained in Section 2.3 was followed for several samples. After extraction, there was a noticeable color change in the dichloromethane employed to extract the carbonaceous material. The amount of extracted material varied between 10-20% of the heavy deposits.

The solutions were analysed in the GC-MS obtaining similar chromatograms for all samples, where the compounds belonging to the heavier fraction of the naphtha were observed in the extract. **Figure 3.8** illustrates the findings, by showing chromatograms of the dichloromethane extracts of spent catalyst from experiment RS1 as a representative sample, and the chromatogram of the naphtha feed for comparison.

The material that eluted in the 12–24 min region of the chromatogram (**Figure 3.8**) corresponded to the material that could be volatilized at 60–250 °C during thermogravimetric analysis (**Figure 3.5**). If any new compounds were formed in this boiling range, their concentration was insufficient to cause a noticeable change in the product pattern in the chromatogram. Little heavier material was observed in the chromatograms of the extracts and when found, were present at very low concentration. It is of course possible that some material higher boiling than vacuum gas oil was extracted, which would not elute under the conditions employed for analysis.

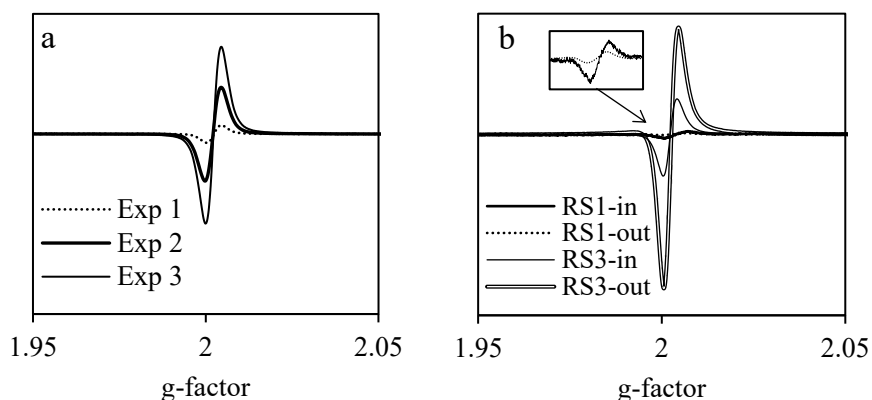


**Figure 3.8.** Chromatograms of the dichloromethane extracts of the spent catalyst samples from the top and bottom of the reactor after experiment RS1, which is compared with that of the naphtha feed material.

### 3.3.6. Electron spin resonance spectroscopy of spent catalysts

A characteristic of mixtures of polycondensed aromatic species, as those found in heavy carbon materials, is their persistent free radicals<sup>33</sup>. Persistent free radicals are possible in polyaromatic structures thanks to the stabilization that occur through resonance, and can either be present naturally or formed during thermal processes<sup>34</sup>. Several possible structures are described in<sup>34</sup>. Therefore, electron spin resonance (ESR) spectroscopy could be a useful tool in the analysis of the carbonaceous deposits on spent catalysts since the free radical content can be correlated to the aromaticity or H/C ratio of the sample. Although no reports were found on the free radical content of coke formed on an acid catalyst after conversion of cracked naphtha, several studies of acid catalyzed conversion of other materials were found. Persistent radicals were detected in the carbonaceous deposits formed in zeolites from reactions of alkene conversion<sup>35,36</sup>, and methanol/ethanol to hydrocarbon processes<sup>37-39</sup>.

The ESR spectra were taken for selected spent catalysts that were of interest. All samples were “diluted” to a carbonaceous content of 6 wt% to be able to compare the spectra obtained. The first derivative of the ESR spectrum is shown in **Figure 3.9** and the relative size gives an indication of the relative concentration of the free radicals in the carbonaceous deposits.



**Figure 3.9.** ESR spectra of the spent catalyst samples at a concentration of 6 wt% of organic deposits.

The relative areas from the double integration of the ESR first derivative signal and the g-factor are reported in **Table 3.6**. Although care was taken to have the same volume of material in the microwave cavity of the ESR spectrometer by grinding the samples to a powder, the actual volume of solid material was somewhat affected by the packing density of the solids and relating the area to an absolute free radical spin concentration was not attempted. For that reason, the areas were normalized relative to the lowest area and only a relative comparison is made.

**Table 3.6.** Relative free radical content and g-factors of the carbonaceous deposits in selected spent catalysts.

| Experiment | Relative<br>radical content <sup>a</sup> | free g-factor |
|------------|------------------------------------------|---------------|
| 1          | 15                                       | 2.0026        |
| 2          | 54                                       | 2.0024        |
| 3          | 104                                      | 2.0025        |
| RS1 inlet  | 2                                        | 2.0042        |
| RS1 outlet | 1                                        | 2.0033        |
| RS3 inlet  | 38                                       | 2.0028        |
| RS3 outlet | 104                                      | 2.0029        |

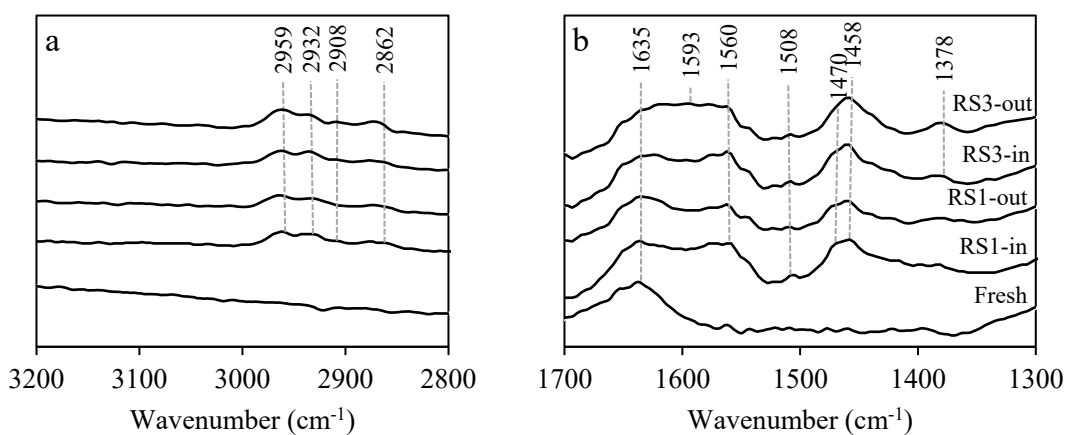
<sup>a</sup> Quantitative calibrationless measurement of free radical concentration.

A clear dependence between the free radical content and the reaction temperature of the reaction is seen in **Figure 3.9a**. Operation at the highest temperature led to the highest free radical content in the carbonaceous deposits. In order of free radical content: experiment 3 (350 °C) > experiment 2 (325 °C) > experiment 1 (300 °C). The same can be seen in **Figure 3.9b** with the free radical content in experiment RS3 (325 °C) >> experiment RS1 (250 °C).

Additionally, comparing the samples from the inlet and outlet of the reactor there is a noticeable difference for catalysts operated at the same reaction temperature. This is not as obvious from experiment RS1 (250 °C) due to the low free radical content, but in experiment RS3 (325 °C) the difference was clear (**Figure 3.9b** and **Table 3.6**). The results indicated that the free radical content of the spent catalyst at the reactor outlet was almost three times higher than that at the reactor inlet. This was consistent with the higher amount of carbonaceous deposits (**Figure 3.7**), but the higher amount of deposits at the reactor outlet compared to the inlet was insufficient to explain the magnitude of the difference in free radical content, especially considering that the analysis was performed on a same carbon basis.

### 3.3.7. Infrared spectroscopy of spent catalysts

Infrared spectroscopy was employed to comparatively look at the carbonaceous deposits on the spent catalyst at the reactor inlet and outlet after experiments RS1 and RS3. Two regions of the infrared spectra suggested by literature<sup>40</sup> are shown in **Figure 3.10** and the infrared spectrum of the fresh catalyst serves as reference.



**Figure 3.10.** Infrared spectra of the fresh catalyst and spent catalysts from the reactor inlet and outlet of experiments RS1 (250 °C) and RS3 (325 °C).

The 3200-2800  $\text{cm}^{-1}$  wavenumber region (**Figure 3.10a**) contains useful  $\text{CH}_x$  bands. The deposits in the spent catalysts displayed absorption bands at 2958, 2931, 2900, and 2864  $\text{cm}^{-1}$ . The 3200-3000  $\text{cm}^{-1}$  did not measurably show absorption.

The absorption bands with peak absorption at 2931 and 2864  $\text{cm}^{-1}$  are likely due to asymmetric and symmetric  $\text{R-CH}_2\text{-R}$  stretching, but these absorption bands overlap with those of methyl groups attached to aromatic carbons. The reason for giving preference in assignment to  $\text{CH}_2$  stretching instead of methyl groups on aromatics, is the absence of measurable absorption in the 3100-3000  $\text{cm}^{-1}$  region, where aromatic  $\text{C-H}$  stretching should have been observed. The absorption bands at 2958 and 2864  $\text{cm}^{-1}$  are indicative of the asymmetric and symmetric stretching of aliphatic methyl groups. The 2864  $\text{cm}^{-1}$  absorption could therefore be ascribed to the contributions to many different  $\text{CH}_x$  groups. The absorption at 2900  $\text{cm}^{-1}$  is due to aliphatic  $\text{CH}$  groups<sup>40</sup>.

Generally speaking, the absence of discernable absorption in the 3100-3000  $\text{cm}^{-1}$  region indicated that the deposits did not contain a large amount of aromatic  $\text{CH}$  or olefinic  $\text{CH}$  groups.

The 1700-1300  $\text{cm}^{-1}$  wavenumber region (**Figure 3.10b**) had several absorption bands. Absorption in the 1640-1540  $\text{cm}^{-1}$  of the deposits saw much overlap. Better-defined absorption bands were seen at 1510, 1470, 1458, and 1378  $\text{cm}^{-1}$ . The absorption at 1510  $\text{cm}^{-1}$  indicated that there might be aromatic species in the deposits since this is the absorption region for substituted aromatics. The increased absorption around 1600  $\text{cm}^{-1}$  supports this assignment, although the apparent lack of aromatic  $\text{C-H}$  absorption in the 3100-3000  $\text{cm}^{-1}$  region casts doubt on this assignment. The absorption bands at 1470 and 1458  $\text{cm}^{-1}$  are mainly due to deformation of  $\text{CH}_3$  and  $\text{CH}_2$  groups and support the assignments following from **Figure 3.9a** but may contain contributions from aromatic  $\text{CH}$  groups. The absorption at 1378  $\text{cm}^{-1}$  is specific to that of  $\text{C-CH}_3$ <sup>40</sup>.

The characteristic  $\text{C-H}$  stretching band for aromatics and polyaromatics should have been present in the region between 3000-3100  $\text{cm}^{-1}$  and has been reported for coke formed on acid catalysts<sup>41</sup>. However, absorption was not consistently found in all deposits on spent acid catalysts. Pinard et al.<sup>42</sup> justified the absence of absorption in this region by arguing that that deposits consisted of highly alkylated polycondensed aromatics. Although no further evidence to support or refute this interpretation follows from the infrared spectroscopy in Figure 3.10, the presence of persistent free

radicals (**Figure 3.9**) lend some support to the likely presence of polycondensed aromatics. A more direct way to determine this would be by solid state  $^{13}\text{C}$  NMR <sup>43</sup>.

### 3.3.8. FTIR analysis of evolved gases from combustion of deposits during TGA

The ESR data presented indicates that not only the aromaticity of the deposits varies with temperature, as one might expect, but also that the deposits become hydrogen-deficient towards the outlet of the reactor zone, when operated at a reaction temperature was of 325 °C. To verify these findings, the evolved gases from the thermal gravimetric analysis were analyzed in a constant path length gas flow cell using FTIR. The Gram-Schmidt curve for each one of the combustion gases was obtained using the intensity variation of the characteristic absorption wavenumber for water (1508  $\text{cm}^{-1}$ ), CO (2160  $\text{cm}^{-1}$ ), and CO<sub>2</sub> (2357  $\text{cm}^{-1}$ ). **Table 3.7** shows the integrated area for each gas.

**Table 3.7.** Area of the Gram-Schmidt curves for the evolved gases from combustion of the deposits at the inlet and out of the reactor in experiment RS3.

| Gas                               | Wavenumber used<br>( $\text{cm}^{-1}$ ) | Area of the Gram-Schmidt curve <sup>a</sup> |            |
|-----------------------------------|-----------------------------------------|---------------------------------------------|------------|
|                                   |                                         | RS3 inlet                                   | RS3 outlet |
| Water (H <sub>2</sub> O)          | 1508                                    | 0.11                                        | 0.13       |
| Carbon Monoxide (CO)              | 2160                                    | 0.11                                        | 0.15       |
| Carbon Dioxide (CO <sub>2</sub> ) | 2357                                    | 0.97                                        | 2.38       |

<sup>a</sup> Areas have been normalized to weight of the deposits.

The area for the evolved water is similar for both samples, but the evolved carbon gases (CO+CO<sub>2</sub>) are twice as high for the deposits at the outlet of the reactor. This represents strong evidence of the change of H/C ratio along the reactor for a reaction temperature of 325 °C.

## 3.4. Discussion

### 3.4.1. Nitrogen base adsorption and role in deactivation

When an acid catalyst is operated with a feed material containing nitrogen bases, it is expected that catalyst activity will be inhibited and potentially poisoned. Nitrogen bases are able to neutralize Brønsted and Lewis acid sites, because the nitrogen base can accept a proton from a



Brønsted acid and it can interact with a Lewis acid through its lone pair electrons. The inhibition and deactivation by basic nitrogen compounds of silica-alumina based monofunctional acidic catalysts was reported mainly in the context fluid catalytic cracking catalysts <sup>44-47</sup>.

The results in **Table 3.5** showed that nitrogen-enriched carbonaceous deposits were found only at the reactor inlet in the experiments RS1–RS3. The nitrogen-enrichment seen at the reactor inlet in experiments RS1–RS3 was not representative of the bulk of the carbonaceous deposits. There was no other indication that any of the carbonaceous deposits were nitrogen-enriched. Formation of the carbonaceous deposits over the amorphous silica-alumina catalyst could not be attributed to the nitrogen-containing compounds. This was consistent with evidence presented using Y-zeolite cracking catalysts <sup>45</sup>.

There were limitations imposed by the sensitivity of CHNS analysis of the spent catalyst and that was not unique to this study <sup>44</sup>. In all instances the higher nitrogen-to-carbon ratio observed at the reactor inlet was a value that was close to the quantification limit. Nevertheless, the lack of a measurable enrichment in nitrogen content of the other deposits, except at the reactor inlet, suggested two possible scenarios. (i) Coking occurs at a much faster rate than nitrogen base adsorption, and covers the acid sites irreversibly, avoiding further adsorption of nitrogen bases. (ii) Desorption of nitrogen bases was influenced by conditions other than just temperature, like competitive adsorption.

If the acid sites were covered, then access of all reactants would be limited, not just nitrogen bases. Even if one were to assume reaction by a carbon-pool on the catalyst, as is used to explain acid catalysis of methanol-to-hydrocarbon conversion <sup>48</sup>, then protonation of an alkene and protonation of a nitrogen base would still be in competition. In fact, the opposite might be a plausible explanation for nitrogen-enrichment at the reactor inlet, namely, that carbonaceous deposits formed over the adsorbed nitrogen bases limited subsequent loss by thermal desorption and competitive adsorption.

It was more likely that adsorption and desorption of nitrogen bases was a dynamic process that was influenced by temperature and other processes, such as competitive adsorption. In the absence of competitive adsorption, it was shown that a nitrogen base, such as quinoline, was equally adsorbed on an amorphous silica-alumina catalyst bed divided into three sections <sup>49</sup>. In the same

study <sup>49</sup> it was also shown that the steady state adsorption at elevated temperature (315 °C) in the presence of a continuous supply of quinoline exceeded the steady amount that remained adsorbed once continuous supply of quinoline was stopped while flow was maintained.

The displacement of nitrogen bases can take place dynamically, although the amount that is not displaced depends on the temperature. This formed the basis for suggesting an acid catalyzed process for alkene-aromatic alkylation of cracked naphtha <sup>11</sup>, despite the presence of nitrogen bases in the feed. Although the ammonia temperature programmed desorption results (**Figure 3.4** and **Table 3.3**) were used as indicators of the amount of acid sites that could be affected by nitrogen bases at different operating temperatures, the relationship between nitrogen base adsorption and ammonia adsorption on amorphous silica-alumina catalysts is not proportional <sup>50</sup>.

In conclusion, the observations in **Table 3.5** indicated that nitrogen bases had an effect on the catalyst, but that nitrogen bases were unlikely to be the main cause of catalyst deactivation and that the nitrogen bases were not the main cause for the formation of carbonaceous deposits on the catalyst.

### **3.4.2. Influence of temperature on composition of carbonaceous deposits**

The term ‘carbonaceous deposits’ rather than ‘coke’, was deliberately used to avoid creating the impression that the deposits were carbonized. The temperature range employed in the laboratory pilot runs from which the spent catalysts were obtained was 250–350 °C. These were not carbonizing temperatures.

Dichloromethane extraction recovered heavier naphtha feed components (**Figure 3.8**), but there was little evidence of heavier material in the gas oil range in the chromatograms. Within the limitations of the analysis, it was still somewhat surprising, because it indicated that there were little, if any, addition products observed in the gas oil boiling range.

It appears that the material that remained on the spent catalyst and that was not residual naphtha feed, consisted of material higher boiling than vacuum gas oil, with little material boiling in the in between range. This was consistent with thermogravimetric analysis (**Figure 3.5**) that did not show continuous devolatilization with an increase in temperature, but two distinct mass loss

events, the first representative of volatilization of residual naphtha feed and the second occurring at higher temperature.

Quantification of the carbonaceous deposits considered only mass loss above 250 °C. The higher temperatures required for mass loss, which was mainly by combustion indicated that most of the material was much heavier than the feed. So much so that it was possible to make productive use of ESR. Using the ESR results of experiments 1–3 (**Figure 3.9a** and **Table 3.6**) there is an increase in persistent free radical content with reaction temperature. This is tentatively interpreted as an indication of an increase in multinuclear aromatic formation.

Keeping the observed increase of persistent free radical content with reaction temperature in mind, the ESR results from experiment RS3 is noteworthy. There was a clear difference in free radical content of the deposits formed at the inlet and outlet of the reactor after reaction at 325 °C. This difference is not due to temperature and it is accompanied by a counterintuitive profile of deposit formation. In this case, the increase of multinuclear aromatic formation in the last zone of the reactor was supported by the lower H/C ratio inferred from the evolved gas analysis from the TGA (**Table 3.7**).

### **3.4.3. Profile of deposit formation**

If we analyse formation of carbonaceous material as a sequence of events that end up in the deposits that deactivate the catalyst, the first step would be the retention of coke precursor molecules on the surface of the catalyst<sup>51</sup>. A molecule would be considered a coke precursor if, because of its characteristics, it can get irreversible adsorbed at the reaction conditions. Cracked naphthas contain a wide variety of molecules that can potentially be irreversibly adsorbed and continue to react on the surface until carbonaceous deposits are formed. From the analysed samples we can say this is true for all conditions explored, since carbonaceous deposits were always found at the inlet of the reactor.

There is also the possibility that heavier molecules are formed upon heating of the cracked naphtha, even in the absence of an acid catalyst<sup>21</sup>. Some of these reactions may take place during preheating, but the formation of coke precursors could be favoured at reactor conditions as thermal rather than catalytic reactions.

The way coke builds up inside the reactor, as well as its composition, is related to the reactions and reaction mechanisms that lead to the formation of coke precursors in the first place. Hence, we can use the content and composition analyses of the carbonaceous products to propose pathways of formation at the conditions studied.

By quantifying the carbonaceous deposits in the first set of experiments, we came across with some observations: (i) deposition rate is proportional to the reaction temperature (**Figure 3.6a**), and (ii) deposits increased per unit mass of catalyst as space velocity is decreased (**Figure 3.6b**).

Higher temperatures and space times could account for the fact that more reactions occurred inside the reactor, that led to coke precursors, and then carbonaceous deposits. This is important because it suggested that some coke precursors were not originally in the feed as it can be expected with a feedstock like cracked naphtha, but that they were formed inside the reactor at least for some of the conditions we investigated in the range 300–350 °C and 0.5–2 h<sup>-1</sup>.

Analyzing the profile of deposit formation of experiment RS3 in **Figure 3.7** makes the previous statement more compelling. Experiment RS3, which was carried out at 325 °C, showed an ascending coking profile, having the largest amount of carbonaceous deposit at the outlet of the reactor. Although the amount of carbonaceous deposit at the inlet and in middle of the catalyst bed of the reactor was not zero, the amount of carbonaceous deposits at the outlet of the reactor was considerably higher than in the other two regions. In the case of experiments RS1 and RS2, both carried out at lower temperatures (250 and 280 °C), showed a descending profile of deposition, having the highest amount of carbonaceous deposit at the inlet of the reactor, indicating that at these conditions, formation of precursors in the reactor is not as apparent, and that deposition of carbonaceous species is only driven by the compounds present in the naphtha unable to desorb.

To explain the ascending profile deposition seen in experiment RS3, we can consider the reactions that can take place. Acid-catalyzed addition reactions like alkene oligomerization and alkene-aromatic alkylation were the focus of this process<sup>11</sup> and could be easily used to explain the findings. But intermediate boiling addition products that were derived from these reactions were not found in the analysis of the methylene chloride extract of the spent catalyst (Section 3.3.5), which means they were either not retained in the catalyst surface or not in enough concentration to be detected. If such compounds failed to be retained by the catalyst, they would not be

considered precursors for carbonaceous deposit formation. Additionally, as seen in **Figure 3.8**, the lighter fraction of the naphtha was not present in the extract from the deposits, which points at the most volatile compounds likely being in the vapor phase during reaction. This may pose the question about the role of reactions of alkenes leading to the formation of the deposits, since most of the olefinic compounds are present in that boiling range, and their concentration in the liquid phase might be limited.

Addition reactions can also occur in the liquid if free radicals are formed. At conditions where unsaturated bonds are present and hydrogen is readily transferred, free radical addition reactions can take place. Take for example the self-reaction of dihydronaphthalene (a molecule within the boiling range of the naphtha feed), which at temperatures of 250 °C underwent free radical reactions initiated by its hydrogen transfer ability<sup>52</sup>. It is worthwhile noting that alkyl aromatics, such as those produced in the process, are likely to have benzylic hydrogen. Benzylic hydrogen is more easily transferred than non-benzylic aliphatic hydrogen<sup>53</sup>. Transfer of benzylic hydrogen can be the start of a reaction sequence that leads to free radical formation and hydrogen disproportionation. For example, it was shown that molecules such as indene that have benzylic hydrogen and an unsaturated bond, readily formed heavier products by self-reaction involving molecule induced homolysis, free radical addition and hydrogen disproportion<sup>54</sup>. Other examples of hydrogen transfer as initial step for the formation of free radicals at the temperature of interest have been described in<sup>55</sup>.

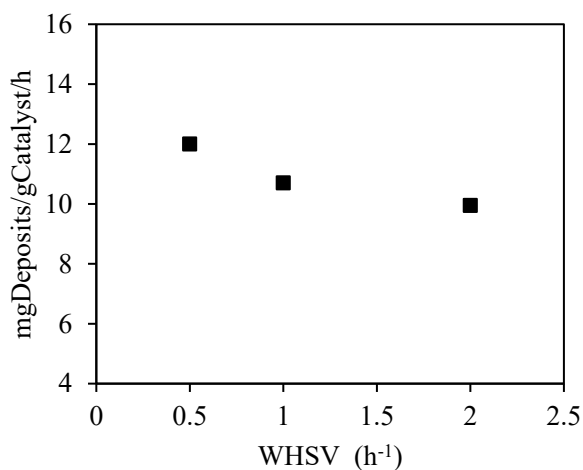
Tracking thermal reaction products in a complex mixture like cracked naphtha was impractical, especially if those changes are minor. Using a probe molecule like  $\alpha$ -methylstyrene, that could act as a hydrogen acceptor and produced easily traceable products, has proven to be helpful in understanding the nature of the thermal reaction in the cracked naphtha<sup>21</sup>, which indeed follow a free radical mechanism. This also indicated that at least some species with readily transferable hydrogen is already present in the cracked naphtha.

To clarify the role of acid catalyzed and thermal reactions on the formation of deposits we can have a closer look at the data in **Table 3.4**, the larger fraction of feed that formed carbonaceous deposits as weight hourly space velocity was decreased, indicated that the species in the feed responsible for deposit formation was sufficiently abundant not to be depleted by deposit

formation. As the weight hourly space velocity was decreased from 2 to 1 h<sup>-1</sup> and from 1 to 0.5 h<sup>-1</sup>, the amount of material deposited per mass of feed doubled each instance when the space time was doubled. Differently put, the rate of deposition appeared to be nearly constant, as shown in **Figure 3.11**. It also meant that the rate of material deposition was not much affected by differences in the amount of catalyst deposits. If anything, slightly more material was deposited from the feed at higher space time, i.e. lower weight hourly space velocity (**Table 3.4** and **Figure 3.11**).

Thus, although the contribution of acid catalysis is not ruled out, these observations indicated that the reactions leading to deposits appeared to be mainly free radical reactions.

The composition of carbonaceous deposits from reaction at 325 °C, as determined by analyses like ESR and TGA-FTIR, indicated that the organic material that accumulated in the catalyst became more aromatic towards the outlet of the reactor. Although hydrogen transfer can be performed by acid sites, amorphous silica-alumina is a poor hydrogen transfer catalyst<sup>56</sup>. It was consequently likely that free radical hydrogen transfer reactions contributed to the hydrogen disproportionation that took place to form precursor species that formed deposits with lower H/C ratio and higher persistent free radical content related to heavier aromatic material.



**Figure 3.11.** Rate of carbonaceous deposit formation calculated from Table 4 showing that there was little change with respect to weight hourly space velocity.

A more in depth and compound specific study of the reactions occurring in the naphtha is necessary to map out the reaction network leading to the formation of carbonaceous deposits. However, from the above discussion we could propose the following:

- Adsorption processes are more important at lower temperatures. We saw how nitrogen compounds adsorbed mainly in the inlet of the reactor and at higher rates at lower temperatures (Table 3.5), and the fact that a descending profile was observed across the reactor suggests that the molecules acting as coke precursors were present in the feed or formed early in the pre-heating stage. The low aromaticity evidenced by the low radical content (Figure 3.9b and Table 3.6) indicates that the deposits have undergone little hydrogen transfer reactions after being formed.
- At higher temperatures desorption readily occurs, and although molecules in the feed can act as coke precursors at these conditions, we saw evidence that there are also coke precursors forming inside the reactor. Free radical chemistry involving the compounds formed through acid-catalyzed reactions or by an increase in space time, is one plausible explanation of the trends observed in Figure 3.6 and Figure 3.7. Moreover, the clear evidence of a decrease of the H/C ratio across the reactor in the experiment RS3 suggests that hydrogen transfer reactions causing hydrogen disproportionation are part of the reaction network leading to the formation of heavy and aromatic deposits over the catalyst. At the same time, it also indicated that the hydrogen transfer was taking place prior to the deposits being formed. Deposits at the reactor inlet had a higher H/C ratio and lower persistent free radical content than at the reactor outlet. If hydrogen transfer continued after the deposits were formed the deposits at the inlet and outlet should not have differed that much.

### 3.5. Conclusions

Spent catalyst samples obtained after conversion of thermally cracked naphtha over amorphous silica-alumina provided some interesting insights about the causes of catalyst deactivation. The following main conclusions were drawn:

- (a) Although the thermally cracked naphtha contained basic nitrogen-containing compounds, nitrogen was only found in the deposits at the inlet of the reactor. The amount of nitrogen in the

deposits was less at high temperature (325 °C) than at lower temperatures (250 and 280 °C). The total amount of nitrogen accumulated in deposits on each spent catalyst was a small fraction of the total amount of nitrogen in the feed to which the catalyst was operationally exposed. This suggested that (i) nitrogen adsorption/desorption is dynamic, and that (ii) for operation at 250–325 °C nitrogen bases were not the main cause of acid catalyst deactivation.

(b) Carbonaceous deposits that restricted access of the feed material to acid sites were the main cause of acid catalyst deactivation. The concentration profile of deposits changed depending on operating temperature. At higher temperatures, such as 325 °C, the amount of material deposited on the catalyst was higher at the reactor outlet than at the reactor inlet. The deposition of organic material in the catalyst could have followed a combination of acid catalysis and free radical chemistry. The change in the nature of the deposits from the reactor inlet to outlet to become more hydrogen depleted, as well as near constant rate of deposit formation, pointed to free radical reactions being more important than acid catalysis in the formation of carbonaceous deposits.

### **Acknowledgements**

The study was funded through the through the NSERC/CNOOC Ltd. Industrial Research Chair program in Field Upgrading and Asphaltenes Processing that is financially supported by the Natural Science and Engineering Research Council (NSERC) of Canada, Alberta Innovates, and CNOOC International.

### **3.6. References**

- (1) Ali, S. A. Naphtha Hydrotreatment. In *Catalytic Naphtha Reforming*; Antos, George. J., Aitani, Abdullah. M., Eds.; CRC Press: Boca Raton, 2004; pp 105–140.
- (2) Kirsch, F. W.; Heinemann, Heinz.; Stevenson, D. H. Selective Hydrodesulfurization of Cracked Gasolines. *Ind. Eng. Chem.* **1957**, *49* (4), 646–649.
- (3) Mochizuki, T.; Itou, H.; Toba, M.; Miki, Y.; Yoshimura, Y. Effects of Acidic Properties on the Catalytic Performance of CoMo Sulfide Catalysts in Selective Hydrodesulfurization of Gasoline Fractions. *Energy Fuels* **2008**, *22* (3), 1456–1462.



- (4) Gray, M. R. *Upgrading Oilsands Bitumen and Heavy Oil*, 1st ed.; The University of Alberta Press: Edmonton, Alberta, 2015.
- (5) Gray, M. R. Fundamentals of Partial Upgrading of Bitumen. *Energy Fuels* **2019**, *33* (8), 6843–6856.
- (6) Xin, Q.; Alvarez-Majmutov, A.; Gieleciak, R.; Chen, J.; Dettman, H. Hydrotreatment of Olefins in Thermally Processed Bitumen under Mild Conditions. *Energy Fuels* **2019**, *33* (4), 3098–3107.
- (7) Rahimi, P.; Chen, J.; Brecher, L.; DeBruijn, T. Hydrotreating of Liquid Products from Cold Lake Bitumen Obtained in the WRITE Process. *Prepr. Pap.-Am. Chem. Soc., Div. Fuel Chem* **2004**, *49* (1), 75–76.
- (8) Bellussi, G.; Mizia, F.; Calemma, V.; Pollesel, P.; Millini, R. Oligomerization of Olefins from Light Cracking Naphtha over Zeolite-Based Catalyst for the Production of High Quality Diesel Fuel. *Microporous Mesoporous Mater* **2012**, *164*, 127–134.
- (9) Li, L.; Zhai, Y.; Zhang, J.; Wang, J.; Yu, T. A New Catalyst for the Non-Hydrogenation Reduction of Olefins. *Petrol. Sci. Technol.* **2007**, *25* (4), 427–441.
- (10) Fong, S. Y.; Montoya Sánchez, N.; de Klerk, A. Olefin Saturation Using Asphaltenes As a Hydrogen Source. *Energy & Fuels* **2020**, *34* (4), 4534–4543.
- (11) Zerpa, N.; de Klerk, A.; Xia, Y.; Omer, A. A. Olefins Reduction of a Hydrocarbon Feed Using Olefins Aromatics Alkylation. Patent Application WO2015000061A1, 2015.
- (12) Perego, C.; Ingallina, P. Recent Advances in the Industrial Alkylation of Aromatics: New Catalysts and New Processes. *Catal. Today* **2002**, *73* (1–2), 3–22.
- (13) Paez, N. Y.; de Klerk, A. Diolefin Characterization in a Thermally Cracked Naphtha. *Prepr. Pap.-Am. Chem. Soc., Div. Energy Fuels* **2016**, *61* (1), 12–15.
- (14) Rao, Y.; de Klerk, A. Characterization of Heteroatom-Containing Compounds in Thermally Cracked Naphtha from Oilsands Bitumen. *Energy Fuels* **2017**, *31* (9), 9247–9254.

- (15) Rezaei, M.; Gieleciak, R.; Michaelian, K. H. Determination of Olefin Contents in Liquid Hydrocarbons Using a Quantum Cascade Laser and a Photoacoustic Detector. *Energy Fuels* **2019**, *33* (4), 2859–2866.
- (16) Alzaid, A.; Wiens, J.; Adjaye, J.; Smith, K. J. Catalyst Deactivation and Reactor Fouling during Hydrogenation of Conjugated Cyclic Olefins over a Commercial Ni–Mo–S/ $\gamma$ -Al<sub>2</sub>O<sub>3</sub> Catalyst. *Energy Fuels* **2018**, *32* (5), 6213–6223.
- (17) Lengyel, A.; Magyar, S.; Hancsók, J. Catalytic Co-Processing of Delayed Coker Light Naphtha with Other Refinery Gasoline Streams. *Period. Polytech.: Chem. Eng* **2009**, *53* (1), 3–7.
- (18) Yui, S.; Chan, E. Hydrogenation of Coker Naphtha with Nimo Catalyst. *Stud. Surf. Sci. Catal* **1992**, *73*, 59–66.
- (19) Guisnet, M.; Magnoux, P. Organic Chemistry of Coke Formation. *Appl. Catal. A: General* **2001**, *212* (1–2), 83–96.
- (20) Daniell, W.; Schubert, U.; Glöckler, R.; Meyer, A.; Noweck, K.; Knözinger, H. Enhanced Surface Acidity in Mixed Alumina–Silicas: A Low-Temperature FTIR Study. *Appl. Catal. A: Gen* **2000**, *196* (2), 247–260.
- (21) Uzcátegui, G.; Fong, S. Y.; de Klerk, A. Cracked Naphtha Reactivity: Effect of Free Radical Reactions. *Energy Fuels* **2018**, *32* (5), 5812–5823.
- (22) Budnar Subramanya, A. S. Olefin Hydrotreating and Characterization of Olefins in Thermally Cracked Naphtha. MSc thesis, University of Alberta, 2020.
- (23) Guisnet, M. Characterization of Deactivating Species. In *Deactivation and regeneration of zeolite catalysts*; Imperial College Press: London, 2011; pp 51–81.
- (24) Kapustin, G. I.; Brueva, T. R.; Klyachko, A. L.; Beran, S.; Wichterlova, B. Determination of the Number and Acid Strength of Acid Sites in Zeolites by Ammonia Adsorption. *Appl. Catal.* **1988**, *42* (2), 239–246.

- (25) Mishin, I. v.; Brueva, T. R.; Kapustin, G. I. Heats of Adsorption of Ammonia and Correlation of Activity and Acidity in Heterogeneous Catalysis. *Adsorption* **2005**, *11* (3–4), 415–424.
- (26) Xia, Y. Acid Catalyzed Aromatic Alkylation in the Presence of Nitrogen Bases. MSc Thesis, University of Alberta, Edmonton, AB, Canada, University of Alberta, 2012.
- (27) Hosseinpour, N.; Mortazavi, Y.; Bazyari, A.; Khodadadi, A. A. Synergetic Effects of Y-Zeolite and Amorphous Silica-Alumina as Main FCC Catalyst Components on Triisopropylbenzene Cracking and Coke Formation. *Fuel Process. Technol.* **2009**, *90* (2), 171–179.
- (28) Karge, H. G. Coke Formation on Zeolites. In *Studies in Surface Science and Catalysis*; 2001; Vol. 137, pp 707–746.
- (29) Richardeau, D.; Joly, G.; Canaff, C.; Magnoux, P.; Guisnet, M.; Thomas, M.; Nicolaos, A. Adsorption and Reaction over HFAU Zeolites of Thiophene in Liquid Hydrocarbon Solutions. *Appl. Catal. A: Gen* **2004**, *263* (1), 49–61.
- (30) Garcia, C. L.; Lercher, J. A. Adsorption and Surface Reactions of Thiophene on ZSM 5 Zeolites. *J. Phys. Chem.* **1992**, *96* (6), 2669–2675.
- (31) Corma, A.; Gullbrand, P.; Martínez, C. Gasoline Sulfur Removal: Kinetics of s Compounds in FCC Conditions. In *Stud. Surf. Sci. Catal*; 2001; pp 153–165.
- (32) Corma, A.; Martínez, C.; Ketley, G.; Blair, G. On the Mechanism of Sulfur Removal during Catalytic Cracking. *Appl. Catal. A: Gen* **2001**, *208* (1–2), 135–152.
- (33) Chang, H.-L.; Wong, G. K.; Lin, J.-R.; Yen, T. F. Chapter 9 Electron Spin Resonance Study of Bituminous Substances and Asphaltenes. In *Asphaltenes and Asphalts*, 2; Elsevier Science B.V., 2000; pp 229–280.
- (34) Zhang, Y.; Siskin, M.; Gray, M. R.; Walters, C. C.; Rodgers, R. P. Mechanisms of Asphaltene Aggregation: Puzzles and a New Hypothesis. *Energy Fuels* **2020**, *34* (8), 9094–9107.

- (35) Lange, J.-P.; Gutsze, A.; Karge, H. G. Coke Formation through the Reaction of Olefins over Hydrogen Mordenite: I. EPR Measurements under Static Conditions. *J. Catal.* **1988**, *114* (1), 136–143.
- (36) Karge, H. G.; Lange, J.-P.; Gutsze, A.; Łaniecki, M. Coke Formation through the Reaction of Olefins over Hydrogen Mordenite: II. In Situ EPR Measurements under on-Stream Conditions. *J. Catal.* **1988**, *114* (1), 144–152.
- (37) Madeira, F. F.; Gnep, N. S.; Magnoux, P.; Vezin, H.; Maury, S.; Cadran, N. Mechanistic Insights on the Ethanol Transformation into Hydrocarbons over HZSM-5 Zeolite. *Chem. Eng. J.* **2010**, *161* (3), 403–408.
- (38) ben Tayeb, K.; Pinard, L.; Touati, N.; Vezin, H.; Maury, S.; Delpoux, O. Ethanol Transformation into Higher Hydrocarbons over HZSM-5 Zeolite: Direct Detection of Radical Species by in Situ EPR Spectroscopy. *Catal. Commun.* **2012**, *27*, 119–123.
- (39) Pinard, L.; Tayeb, K. ben; Hamieh, S.; Vezin, H.; Canaff, C.; Maury, S.; Delpoux, O.; Pouilloux, Y. On the Involvement of Radical “Coke” in Ethanol Conversion to Hydrocarbons over HZSM-5 Zeolite. *Catal. Today* **2013**, *218–219*, 57–64.
- (40) Colthup, N. B.; Daly, L. H.; Wiberley, S. E. *Introduction to Infrared and Raman Spectroscopy*, 3 rd.; Academy Press: San Diego, 1990.
- (41) Chaouati, N.; Soualah, A.; Chater, M.; Tarighi, M.; Pinard, L. Mechanisms of Coke Growth on Mordenite Zeolite. *J. Catal.* **2016**, *344*, 354–364.
- (42) Pinard, L.; Hamieh, S.; Canaff, C.; Ferreira Madeira, F.; Batonneau-Gener, I.; Maury, S.; Delpoux, O.; ben Tayeb, K.; Pouilloux, Y.; Vezin, H. Growth Mechanism of Coke on HBEA Zeolite during Ethanol Transformation. *J. Catal.* **2013**, *299*, 284–297.
- (43) Fonseca, A.; Zeuthen, P.; Nagy, J. B. <sup>13</sup>C n.m.r. Quantitative Analysis of Catalyst Carbon Deposits. *Fuel* **1996**, *75* (12), 1363–1376.

- (44) Zhang, J.; Shan, H.; Chen, X.; Liu, W.; Yang, C. Fluid Catalytic Cracking Study of Coker Gas Oil: Effects of Processing Parameters on Sulfur and Nitrogen Distributions. *Energy Fuels* **2014**, *28* (2), 1362–1371.
- (45) Caeiro, G.; Lopes, J.; Magnoux, P.; Ayrault, P.; Ramôa Ribeiro, F. A FT-IR Study of Deactivation Phenomena during Methylcyclohexane Transformation on H-USY Zeolites: Nitrogen Poisoning, Coke Formation, and Acidity–Activity Correlations. *J. Catal.* **2007**, *249* (2), 234–243.
- (46) Caeiro, G.; Magnoux, P.; Ayrault, P.; Lopes, J.; Ramôa Ribeiro, F. Deactivating Effect of Coke and Basic Nitrogen Compounds during the Methylcyclohexane Transformation over H-MFI Zeolite. *Chem. Eng. J.* **2006**, *120* (1–2), 43–54.
- (47) Barth, J.-O.; Jentys, A.; Lercher, J. A. On the Nature of Nitrogen-Containing Carbonaceous Deposits on Coked Fluid Catalytic Cracking Catalysts. *Ind. Eng. Chem. Res.* **2004**, *43* (10), 2368–2375.
- (48) Haw, J. F.; Song, W.; Marcus, D. M.; Nicholas, J. B. The Mechanism of Methanol to Hydrocarbon Catalysis. *Acc. Chem. Res.* **2003**, *36* (5), 317–326.
- (49) Mills, G. A.; Boedeker, E. R.; Oblad, A. G. Chemical Characterization of Catalysts. I. Poisoning of Cracking Catalysts by Nitrogen Compounds and Potassium Ion \*. *J Am Chem Soc* **1950**, *72* (4), 1554–1560.
- (50) Hirschler, A. E. The Effect of Ammonia Adsorption on the Acidity of Silica-Alumina and Alumina Catalysts. *J. Catal.* **1966**, *6* (1), 1–13.
- (51) Guisnet, M. Modes of Coke Formation and Deactivation. In *Deactivation and regeneration of zeolite catalysts*; 2011; pp 115–137.
- (52) Payan, F.; de Klerk, A. Hydrogen Transfer in Asphaltenes and Bitumen at 250 °C. *Energy Fuels* **2018**, *32* (9), 9340–9348.
- (53) Parsons, A. F. *Introduction to Free Radical Chemistry*; Blackwell Science: Oxford, 2000.

- (54) Tannous, J. H.; de Klerk, A. Asphaltenes Formation during Thermal Conversion of Deasphalted Oil. *Fuel* **2019**, *255*, 115786.
- (55) Rüchardt, C.; Gerst, M.; Ebenhoch, J. Uncatalyzed Transfer Hydrogenation and Transfer Hydrogenolysis: Two Novel Types of Hydrogen-Transfer Reactions. *Angew. Chem., Int. Ed. Engl.* **1997**, *36* (1314), 1406–1430.
- (56) Venuto, P. B.; Habib, E. T. *Fluid Catalytic Cracking with Zeolite Catalysts*; Marcel Dekker: New York, 1979.

## Chapter 4. Cracked naphtha reactivity: Effect of free radical reactions

### Abstract

The problems faced when dealing with thermally cracked naphtha are vast, from gum formation in storage units to fouling and deactivation of catalysts. Our interest was to gain a better understanding of the initiation of cracked naphtha fouling. The thermal reactivity of cracked naphtha from an industrial bitumen upgrading facility was investigated. The naphtha was exposed to temperatures of 200, 250 and 300 °C for a period of 1 hour. No free radicals were detected in the naphtha feed using electron spin resonance spectrometry, yet, after heating, evidence of free radical reactions was found. The influence of heating was investigated for both the naphtha on its own and the naphtha in combination with  $\alpha$ -methylstyrene (AMS). AMS was employed as a probe molecule that facilitated detection of free radical transfer reactions. The potential contribution of oxygen as free radical initiator was also investigated by heating naphtha at different oxygen partial pressures. Heating of naphtha and AMS mixtures resulted in the formation of compounds linked to free radical termination. Self-initiation by AMS was ruled out with control experiments using a mixture of AMS in n-pentane. The possible contribution of oxygen could also be ruled out in reactions performed under inert atmosphere. Reactions conducted at different partial pressures of oxygen resulted in a different product distribution than found in reactions conducted in an inert atmosphere. It appeared that the thermally cracked naphtha contained molecules capable of initiating free radical reactions at the lowest temperature studied in the absence of oxygen. An initiation pathway by molecule induced homolysis was discussed as a possible explanation of the observations.

**Keywords:** Thermally cracked naphtha, fouling, free radical initiation, free radical addition, hydrogen transfer.

## 4.1. Introduction

The naphtha fraction derived from cracking processes contains a high amount of unsaturated compounds, which contributes to the stream's characteristic instability. Cracked naphtha can cause fouling during transportation, during further processing downstream, and during storage. Fouling caused by this hydrocarbon fraction follows the same principle that describes gum formation in stored petroleum products, such as gasoline. Free radicals can be initiated by temperature in the presence or absence of oxygen, or by decomposition of peroxides,<sup>1</sup> which then react with unsaturated compounds to form high molecular weight compounds.<sup>2,3</sup> Fouling severity increases with the olefin content of the stream since olefins can easily undergo repeated addition reactions,<sup>4</sup> which end up forming heavier products, e.g. gums.

The fouling propensity of thermally cracked naphtha streams is usually ascribed to the presence of diolefins, which should preferably be removed before hydrotreating.<sup>5</sup> The formation of heavy deposits is not prevented when heating or treating cracked naphthas in the presence of hydrogen and such fouling behavior is not limited to petroleum-derived materials. When hydrotreating coal pyrolysis naphtha, even though freshly distilled, a heavy fraction forms during preheating and needs to be removed from the hot reactor feed before entering the hydrotreating reactor.<sup>6</sup>

In a study about the stability of different naphtha streams, straight run naphthas were spiked with olefins previously separated from cracked naphthas, and the gum potential was measured and compared to that of the original cracked naphtha streams.<sup>7,8</sup> The gum potential for the straight run naphthas was only half of that of the cracked naphthas, meaning that there are other compounds than olefins in the cracked naphtha that contribute to the gum formation.

This paper deals with the origin of reactions leading to heavier product formation in thermally cracked naphtha. It is studied in the context of partial upgrading of oilsands bitumen and olefins treatment of the cracked products.<sup>9</sup> The olefins treatment process is an acid catalyzed process. Even though coke formation is not a rare occurrence in acid catalysts dealing with hydrocarbon mixtures,<sup>10</sup> the deactivation behavior did not appear to be consistent with that expected from diolefin-derived gum formation. Understanding how these reactions occur and what compounds are specifically involved in the initiation step leading to high molecular weight compound



formation was of interest so that engineering strategies could be developed to deal with this behavior.

Oilsands bitumen is known to have persistent free radicals, both in its asphaltenes and maltenes fractions,<sup>11,12</sup> and thermal cracking itself is a free radical process.<sup>13</sup> Initially, it was speculated that some free radical species might remain in the cracked naphtha, or that species that are readily decomposed during preheating to form free radicals could initiate the reaction sequence leading to addition reactions.

Electron spin resonance was performed on the thermally cracked naphtha feed as part of the investigation and unpaired electrons were not detected. This means that if free radicals were present, their concentration was too low to be detected. To investigate if radical reactions were taking place in the naphtha feed on heating, use was made of  $\alpha$ -methylstyrene as a probe molecule. This compound makes a good probe molecule to determine whether free radicals are formed since it does not react by itself on heating,<sup>14</sup> and it needs to be initiated through a different mechanism. For example, the bimolecular transfer hydrogenation involving  $\alpha$ -methylstyrene has been described before,<sup>15,16</sup> as well as oxidation,<sup>17,18</sup> both forming termination products from free radical reactions. The nature of the products is indicative of the type of reactions taking place. In this work  $\alpha$ -methylstyrene spiked thermally cracked naphtha and the reaction product after heating were analyzed to gain this type of understanding. The same strategy was employed to determine whether dissolved oxygen could account for the reaction products.

## **4.2. Experimental**

### **4.2.1. Materials**

Thermally cracked naphtha was obtained directly from the sealed sample container withdrawn from the Long Lake upgrader facility of Nexen Energy ULC. Care was taken to store this reactive material properly and avoid storage degradation that is typically observed in such materials. The thermally cracked naphtha was characterized (**Table 4.1**). More detailed characterization of diolefins,<sup>19</sup> and heteroatom species,<sup>20</sup> were reported on before.

#### 4.2.2. Equipment and procedure

Reactions of naphtha and AMS to study the effect of temperature were performed for the purpose of answering the main question of this study, namely, whether heavy product formation in cracked naphtha was caused by thermally induced free radical reactions. 1 g of a solution of 12 wt% of AMS in thermally cracked naphtha feed, taken directly from the barrel, was placed in a 15 mL Swagelok reactor and pressurized to 4 MPa with N<sub>2</sub>. A glass vial was used to contain the feed, to avoid contact with the reactor walls. The pressure was chosen to ensure that the reaction mixture remained in the liquid phase. The pressurized and leak-tested reactor was placed in a sand bath heater at the desired reaction temperature. Three temperatures (200 °C, 250 °C, and 300 °C) were tested and each reaction was carried out for 1 h, after which the reactor was cooled and depressurized. The product mixture was collected for analysis.

**Table 4.1.** Characterization of thermally cracked naphtha.

| Property                    | Units             | Cracked naphtha |
|-----------------------------|-------------------|-----------------|
| Density                     | kg/m <sup>3</sup> | 762.7           |
| Carbon                      | wt%               | 84.3            |
| Hydrogen                    | wt%               | 13.8            |
| Nitrogen                    | wt%               | 0.09            |
| Sulfur                      | wt%               | 0.9             |
| Oxygen                      | wt%               | 0.25            |
| <b>Distillation profile</b> |                   |                 |
| IBT                         | °C                | 30              |
| T10                         | °C                | 68              |
| T30                         | °C                | 100             |
| T50                         | °C                | 133             |
| T70                         | °C                | 173             |
| T90                         | °C                | 239             |
| FBP                         | °C                | 265             |

Chemicals and cylinder gases that were used are listed in **Table 4.2**. These materials were used as supplied and without further purification.

Control reactions were carried under each reaction condition to test that the products seen were not being produced for the temperature effect on AMS. For the control reactions, AMS diluted in *n*-pentane to yield a 12 wt% solution was subjected to the same reaction conditions. Thermally cracked naphtha alone was also tested in the same way to see the effect of temperature on it. All

reactions were performed in triplicate. The presence of dissolved oxygen as potential free radical initiator was also investigated.

**Table 4.2.** Chemicals and cylinder gases used in the study.

| Compound              | Formula                         | CASRN <sup>a</sup> | Mass fraction purity <sup>b</sup> | Supplier          |
|-----------------------|---------------------------------|--------------------|-----------------------------------|-------------------|
| <i>Chemicals</i>      |                                 |                    |                                   |                   |
| AMS                   | C <sub>9</sub> H <sub>10</sub>  | 98-83-9            | 0.99                              | Aldrich Chemistry |
| Methylene Chloride    | CH <sub>2</sub> Cl <sub>2</sub> | 75-09-2            | 0.999                             | Fisher Chemical   |
| Pentane               | C <sub>5</sub> H <sub>12</sub>  | 109-66-0           | 0.995                             | Fisher Chemical   |
| <i>Cylinder Gases</i> |                                 |                    |                                   |                   |
| Nitrogen              | N <sub>2</sub>                  | 7727-37-9          | 0.99998 <sup>c</sup>              | Praxair           |
| Air                   | N <sub>2</sub> +O <sub>2</sub>  | 132259-10-0        | Extra dry                         | Praxair           |

<sup>a</sup> CASRN = Chemical Abstracts Services Registry Number. <sup>b</sup> This is the purity of the material guaranteed by the supplier; materials was not further purified. <sup>c</sup> Mole fraction purity.

To investigate the effect of oxygen partial pressure on the conversion of thermally cracked naphtha, the same procedure as outlined above was followed for performing and testing. The only difference was that testing was performed under different oxygen partial pressures, which were obtained mixing air and nitrogen. All reactions were carried out at 300 °C and 4 MPa total (gauge) pressure. Reactions were performed under 0, 105 and 210 kPa oxygen partial pressure. To test the reactivity of the naphtha in the complete absence of oxygen, the thermally cracked naphtha feed was degassed for 1 h using flowing nitrogen. The time period of 1 h was based on the in-situ measurement of oxygen displacement by nitrogen previously conducted in our laboratories.<sup>21</sup> Degassing with nitrogen was performed in a bath of methanol and dry ice to avoid evaporation of the lighter compounds in the naphtha. The degassed naphtha was subsequently mixed with AMS and pressurized with nitrogen to 4 MPa and subjected to reaction conditions. Control reactions of only naphtha and AMS with pentane were also carried under each oxygen partial pressure tested. All reactions were performed in triplicate.

### 4.2.3. Analyses

Gas chromatography-mass spectrometry (GC-MS) was used for product analysis. The analysis of the reaction outcome in this study relied on the separation and identification of the products using this instrument. The analyses were performed in an Agilent 7820A GC connected to a 5977E MS detector. The separation occurred in an HP5-MS UI (30m x 0.25 mm x 0.25 μm), using 1 mL/min

flow Helium as a carrier. The temperature program used started at 40 °C, a temperature that was maintained for 15 min, then ramped up at 5 °C/min to 250 °C, and finally ramped at 10 °C/min to 320 °C. The final temperature was held for 5 min.

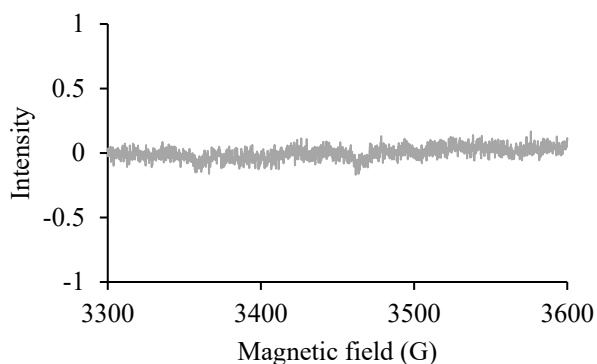
Thermal Gravimetric analysis (TGA) was employed for quantification of gum. This analysis was aimed to measure the amount of heavy compounds that do not evaporate from the naphtha at 150 °C under a relatively high nitrogen flow. This fraction of the naphtha is what we will denominate as gum content. The gum content of the feed and products were determined with a Mettler Toledo TGA/DSC1 with LF furnace, sample robot, and MX5 internal microbalance, using a STARe System software. The samples were carefully mixed to obtain a homogeneous and representative composition for analyses. Samples of around 30 mg were placed in a 70 µL alumina oxide crucible. The samples were heated from 35 °C to 150 °C at 10 °C/min under a continuous 75 mL/min flow rate of nitrogen. The 150 °C was held for 30 min. The analysis was done for each of the samples (feed and product) in triplicate.

Electron spin resonance analysis was carried in an Active Spectrum's extended range benchtop Electron Spin Resonance spectrometer, at 9.7 GHz. Approximately 1 mL of a pure sample of the thermally cracked naphtha was placed in a 5 mm (OD) Wilmad-LabGlass ESR tube. The ESR spectra for the naphtha sample was obtained in the magnetic field range of 3300 to 3600 G, with a microwave power of 15 mW, 1.2 G of coil amplitude, 10 scans, and digital gain of 0 dB.

## **4.3. Results**

### **4.3.1. Free radical content by ESR**

The thermally cracked naphtha was analyzed by electron spin resonance spectrometry to determine if any free radical species were present. The spectrum reflected noise (**Figure 4.1**). It was concluded that if free radicals were present in the thermally cracked, their concentration was too low to be detected. Quantitatively stated, if any free radical species were present in the naphtha, the signal was within the noise level of intensity, which corresponded to about  $6 \times 10^{16}$  spin/g based on calibration with 2,2-diphenyl-1-picrylhydrazyl (DPPH).



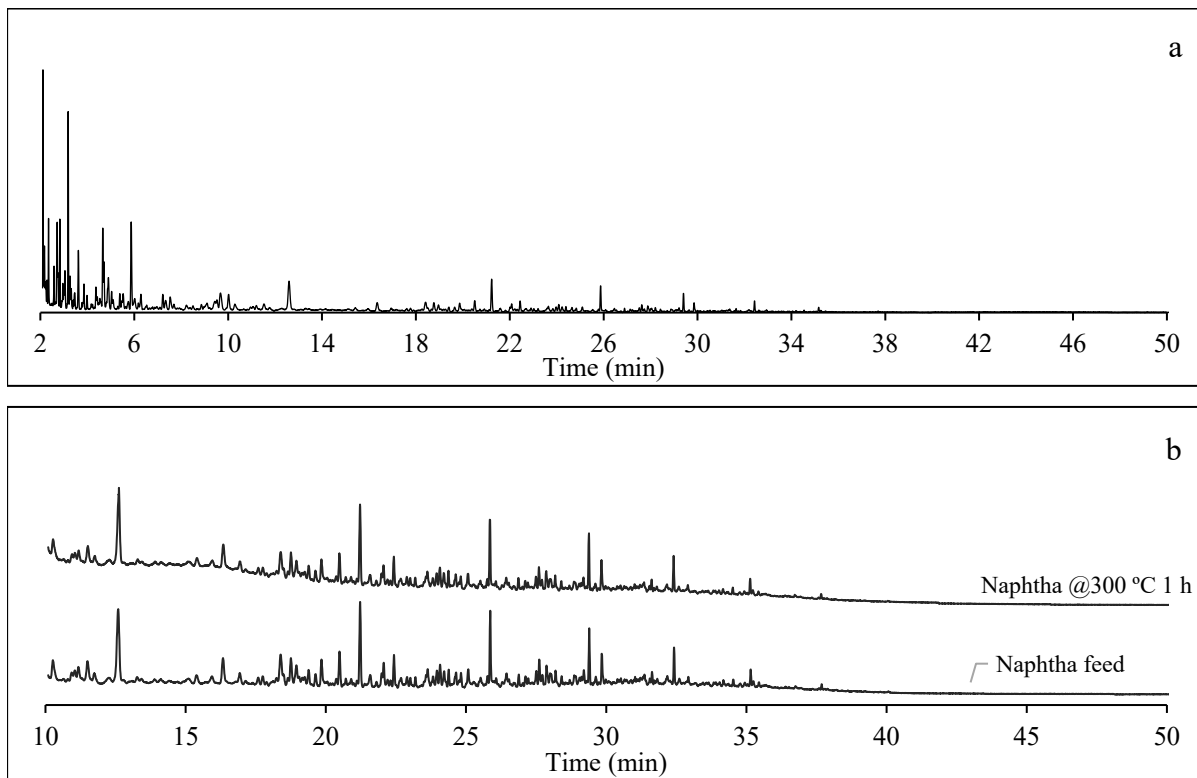
**Figure 4.1.** ESR spectra of the naphtha sample at room temperature.

#### **4.3.2. Product distribution from GC-MS chromatogram**

The effect of temperature on the reactivity of the thermally cracked naphtha was tested with AMS. In the oil industry, bond breaking reactions forming radicals, e.g. cracking, are typically expected to happen at 350 °C or higher. But, if there are compounds with weak bonds present in the thermally cracked naphtha, they could undergo homolytic bond cleavage at relatively low temperatures to initiate radical reactions. The temperature at which chemical bonds can be thermally cleaved depends on the bond dissociation energy (BDE), and since the identity of all the compounds in the thermally cracked naphtha was not known, the temperature at which free radical reactions were initiated was experimentally determined.

It was necessary to determine whether free radical reactions occurred in the thermally cracked naphtha. Considering the complexity of the chromatogram of the feed (**Figure 4.2a**), it was doubtful whether it would be possible to detect minor changes after thermal treatment by studying the chromatogram of the products. Use was therefore made of AMS as probe molecule to detect free radical reactions without simplifying the matrix. Possible changes in the naphtha upon heating were examined through control reactions containing only the thermally cracked naphtha, but no detectable changes in the composition were observed in the chromatogram (**Figure 4.2b**).

Mixtures with 12 wt% AMS in thermally cracked naphtha were exposed to three different temperatures, 200 °C, 250 °C, and 300 °C, for 1 hour to explore the reactivity of the thermally cracked naphtha. The product mixtures were analyzed using GC-MS. It was found that some products formed in very low concentration as illustrated by the chromatogram of the retention time range 41 to 46 min, as seen in **Figure 4.3**.



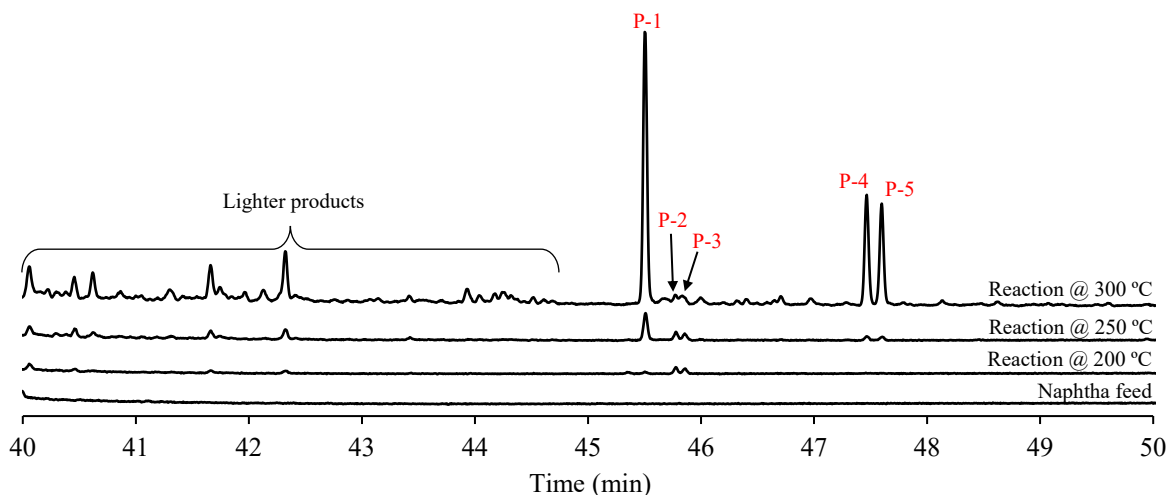
**Figure 4.2.** (a) Complete chromatogram of the thermally cracked naphtha, (b) and comparison of the section of interest of the chromatograms of the feed and product of the control reaction of the naphtha at 300 °C for 1h.

The mass spectra of the compounds with retention times higher than 40 min showed that they contained the AMS unit, indicating that they are most likely products of reactions between AMS and compounds in the naphtha. These products were labeled “lighter products” in **Figure 4.3** and the possibility of them being dimers of AMS was discarded, since their molecular weight taken from the mass spectra, was below that of AMS dimers.

The main AMS derived products after thermal conversion at 200 °C were those with retention times 45.77 min and 45.85 min, labeled as P2 and P3 in **Figure 4.3** for an easier discussion.

When AMS-containing-naphtha was subjected to 250 °C, new products appeared beside those already observed at 200 °C, as seen in **Figure 4.3**. Some new heavier compounds appeared in the chromatogram after the 40 min, the most prominent at retention times 45.50 min, 47.51 min and 47.65 min were labeled P-1, P-4, and P-5, respectively. In reactions carried at 300 °C, the formation of P-1, P-4, and P-5 (**Figure 4.3**) was favored. Other products were also formed in the retention

time range 45 to 50 min that was not studied in detail. The diversity of heavier products that formed from the thermally cracked naphtha and AMS mixture clearly increased after conversion at 300 °C.

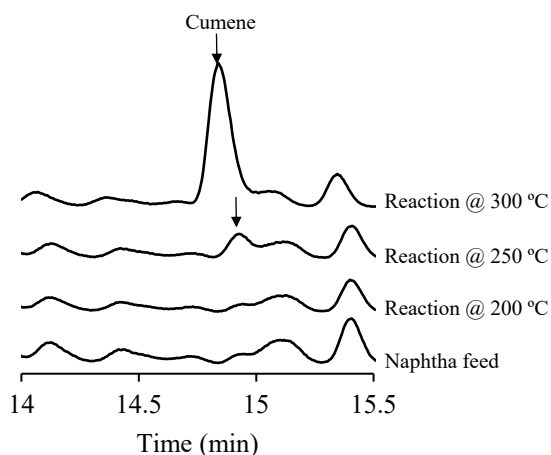


**Figure 4.3.** Product distribution from reactions of naphtha with AMS at different temperatures.

The mass spectra of the compounds labeled P-1 to P-5 indicated that they were AMS dimers, which are discussed further in the next section (Section 4.3.3). Among the lighter products, which were AMS addition products with the compound in the naphtha, higher temperature favored those at retention times of 40.06 min, 40.47 min, 40.63 min, 41.67 min, and 42.33 min.

Another region of the chromatogram that was studied, was the retention time range 14 to 15.5 min (**Figure 4.4**). This was the retention time range where cumene eluted and verification of cumene retention time was performed using a cumene standard. Cumene would provide further evidence of free radical reactions because it is the hydrogen transfer product of AMS.<sup>22</sup> In **Figure 4.4** the formation of cumene can be seen after thermal conversion at 250 °C and 300 °C.

Control reactions of a 12 wt% mixture of AMS in pentane at both 200 °C and 250 °C did not show any of the products seen in the presence of naphtha (Appendix A, Figure A1, and A2). This indicated that addition reactions at these temperatures were only initiated in the naphtha matrix. At 300 °C, the control reaction of AMS in pentane showed the formation of some product at 45.50 min in the chromatogram (Appendix A, Figure A3), but the concentration was not significant when compared with the amount of the same product formed in the reaction containing naphtha.



**Figure 4.4.** Cumene production from reactions of naphtha with AMS at different temperatures.

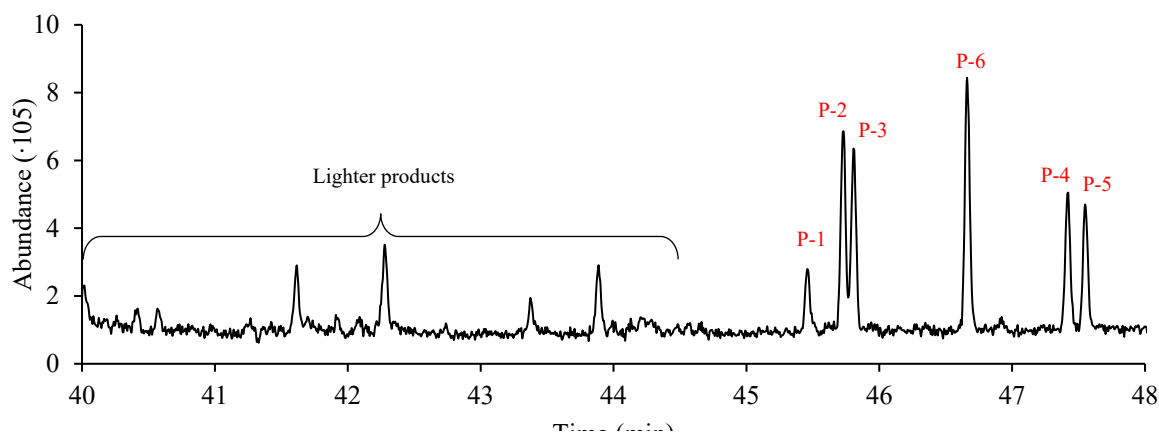
Overall, the results provided evidence that free radical chemistry took place when thermally cracked naphtha was heated to 200 °C and higher temperatures (**Figure 4.3** and **Figure 4.4**) and was not due to AMS self-initiation (Appendix A, Figures A1 and A2). Was this evidence of radical reaction caused by thermal treatment of the naphtha, or was there an external initiator involved, such as oxygen?

The effect of oxygen on the reactivity of the thermally cracked naphtha was also tested. The sample of naphtha used up to this point was taken directly from the storage barrel. The literature on naphtha stability explains the tendency of forming gum during storage as an autoxidation process driven by free radical chemistry.<sup>2,3</sup> Also, AMS has been reported to polymerize through a radical chain reaction only in the presence of oxygen.<sup>17</sup> These suggest the possibility that the products being observed could have been initiated by autoxidation. The possible contribution of oxygen to the observed thermally induced reactivity of naphtha had to be determined.

The effect of oxygen on product formation was determined by repeating the reactions of AMS spiked thermally cracked naphtha at 300 °C under different oxygen partial pressures. If the oxygen concentration was increased in a significant way, one might expect that the formation of products by an oxidative process would be increased as the oxygen partial pressure is increased. A series of reactions were performed at 0, 105, and 210 kPa O<sub>2</sub> partial pressure.



**Figure 4.5** shows the distribution of the heaviest products for the reaction at the highest oxygen partial pressure tested, but comparable products were obtained in all reactions containing oxygen. In this case, P-2 and P-3 were two of the main products and a new peak, P-6, appeared in the chromatogram around a retention time of 46.66 min. In the case of the reactions carried out with degassed naphtha (dissolved O<sub>2</sub> removed), no significant differences were observed in the products obtained with respect to those from the reactions with naphtha taken directly from the barrel (dissolved O<sub>2</sub> could be present).

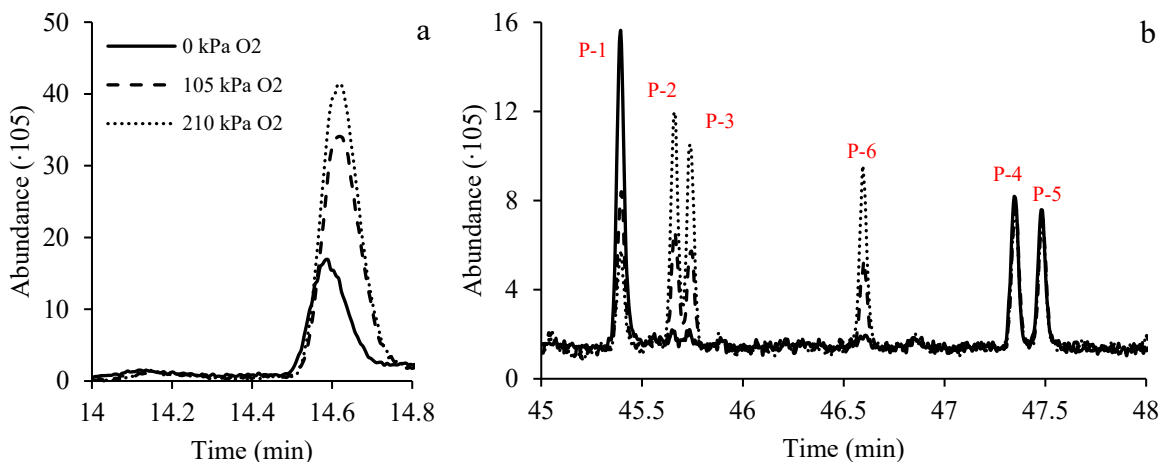


**Figure 4.5.** Product distribution from the reaction of naphtha with AMS under 210 kPa of oxygen partial pressure at 300 °C.

In the lighter products (**Figure 4.5**), four compounds were affected by the presence of oxygen, those at 41.62 min, 42.28 min, 43.39 min, and 43.88 min. Even though their concentration was too low relative to other co-eluting species to obtain a clear mass spectrum, the AMS mass fragment was present in the mass spectrum. As stated before, the molecular weight of the lighter products in this region of the chromatogram was less than that of an AMS dimer. The lighter products could be the addition products of AMS with some other compounds in the naphtha that are present in a concentration high enough to form traceable products.

The strong dependence of the product distribution on the oxygen partial pressure in the reactor is illustrated in **Figure 4.6**. Cumene was the main product formed from AMS and was greatly favored by the presence of oxygen (**Figure 4.6a**). The formation of P-1 was clearly suppressed at higher

partial pressures of oxygen, and so were products P-4 and P-5 (Figure 4.6b). On the other hand, the formation of P-2, P-3, and P-6 was favored by higher oxygen partial pressure (Figure 4.6b).



**Figure 4.6.** Effect of the oxygen partial pressure on the product distribution on the reaction of naphtha with AMS at 300 °C.

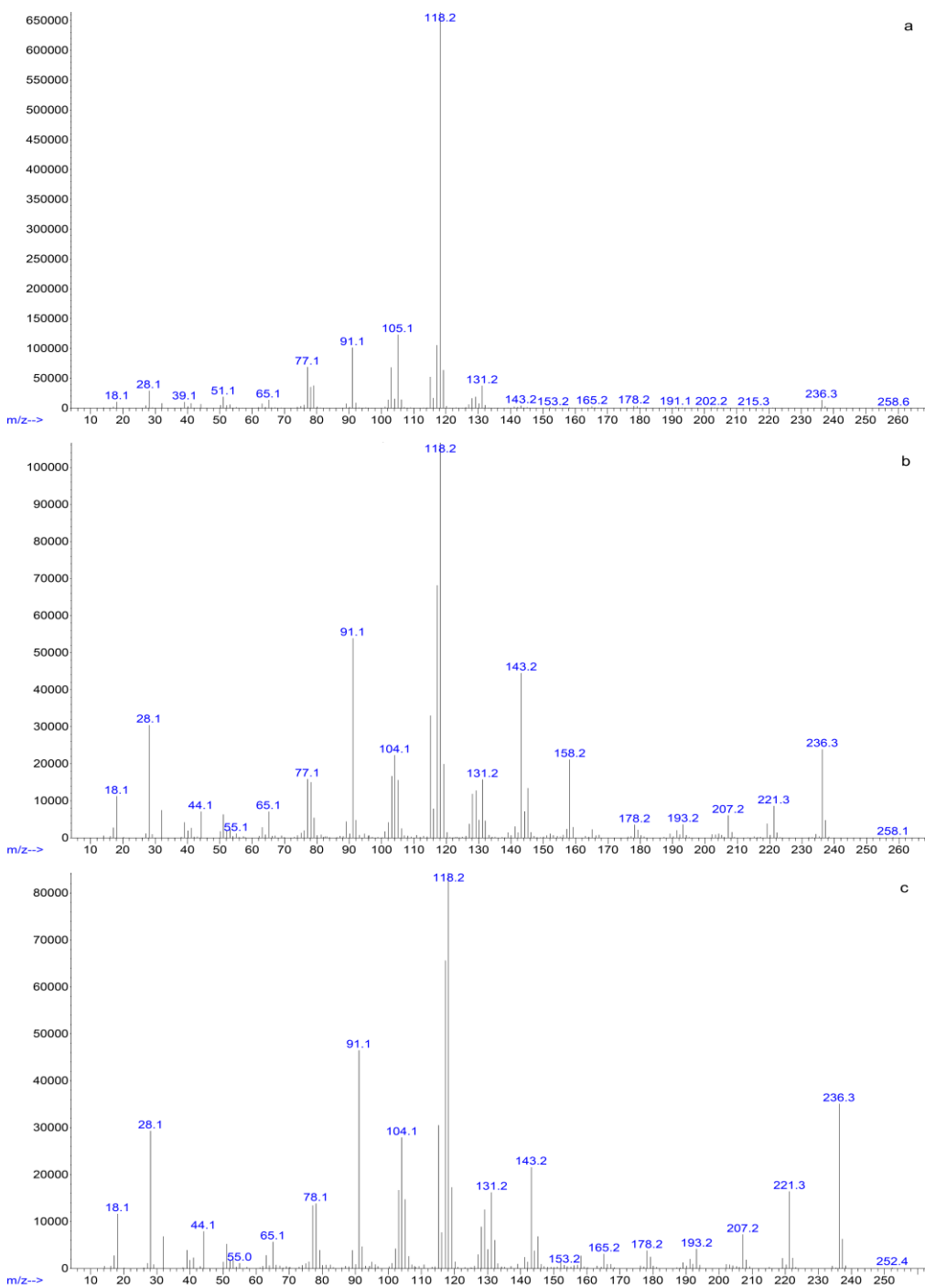
As anticipated from literature<sup>2,3</sup> an increase in oxygen partial pressure caused an increase in heavier product formation. However, it was also observed that heavier products were formed even in the absence of oxygen and that different product distributions were obtained with and without oxygen. The product distribution after removal of oxygen favored products P-1, P-4, and P-5 (Figure 4.6b), the same products that were previously favored by thermal reaction without oxygen removal (Figure 4.3). The reactivity of thermally cracked naphtha could therefore not be explained by the action of oxygen.

#### 4.3.3. Identification of products through Mass Spectra analysis

Coming from the thought that some products in the heavier end of the chromatogram (>45 min retention time) could be dimers, the mass spectra of the compounds were investigated more closely. The electron-ionization mass spectra of products P-1, P-4, and P-5 (Figure 4.7) from the thermal conversion at 300 °C had several features in common to indicate that all of these were different isomers formed by dimerization of AMS.

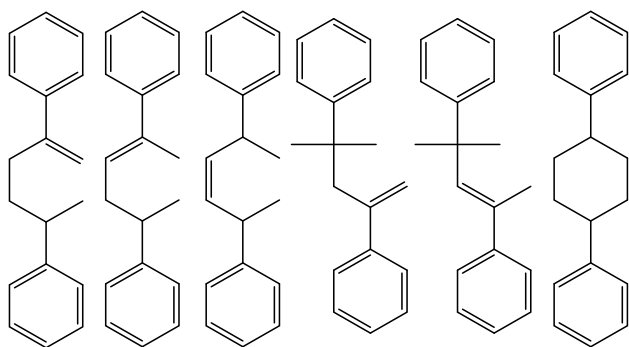
One thing that stands out in these three spectra (Figure 4.7) is the fact that their most intense peak  $m/z=118$ , which corresponds to the singly charged AMS molecular fragment. The intense  $m/z=118$  is common for the three compounds, as well as their molecular ion at  $m/z=236$  ( $2 \times 118$ ). The

highest  $m/z$  peaks recorded ( $m/z=258$  and  $m/z=252$ ) appeared to be part of the “background” as McLafferty and Tureček put it.<sup>23</sup>



**Figure 4.7.** Mass spectra of products (a) P-1, (b) P-4, and (c)P-5.

There are three structural isomers and six isomers in total that can result from the free radical dimerization of AMS (**Figure 4.8**). The last isomer is the product of a second intramolecular addition reaction after dimerization. There are few indications to support that the dimers formed through combination reactions involving at least one of the primary carbons in AMS. For instance, the absence of an  $m/z=119$  peak in the mass spectra; this peak would correspond to the cumyl cation, which would form a very stable ion on the tertiary carbon. Also, the difference between  $m/z=131$  and  $m/z=118$  gives the loss of 13 mass units, which corresponds to a CH fragment, which could not be possible if a dimer was formed through the tertiary carbons only. Lastly, the formation of an AMS dimer through both tertiary carbons would require dimerization to terminate by  $H\bullet$  acceptance (hydrogen transfer to the dimer) and not  $H\bullet$  loss (hydrogen transfer from the dimer to another species), leading to a molecular mass of 238 g/mol. This was not consistent with the observed  $m/z=236$  of the molecular ions in **Figure 4.7**.

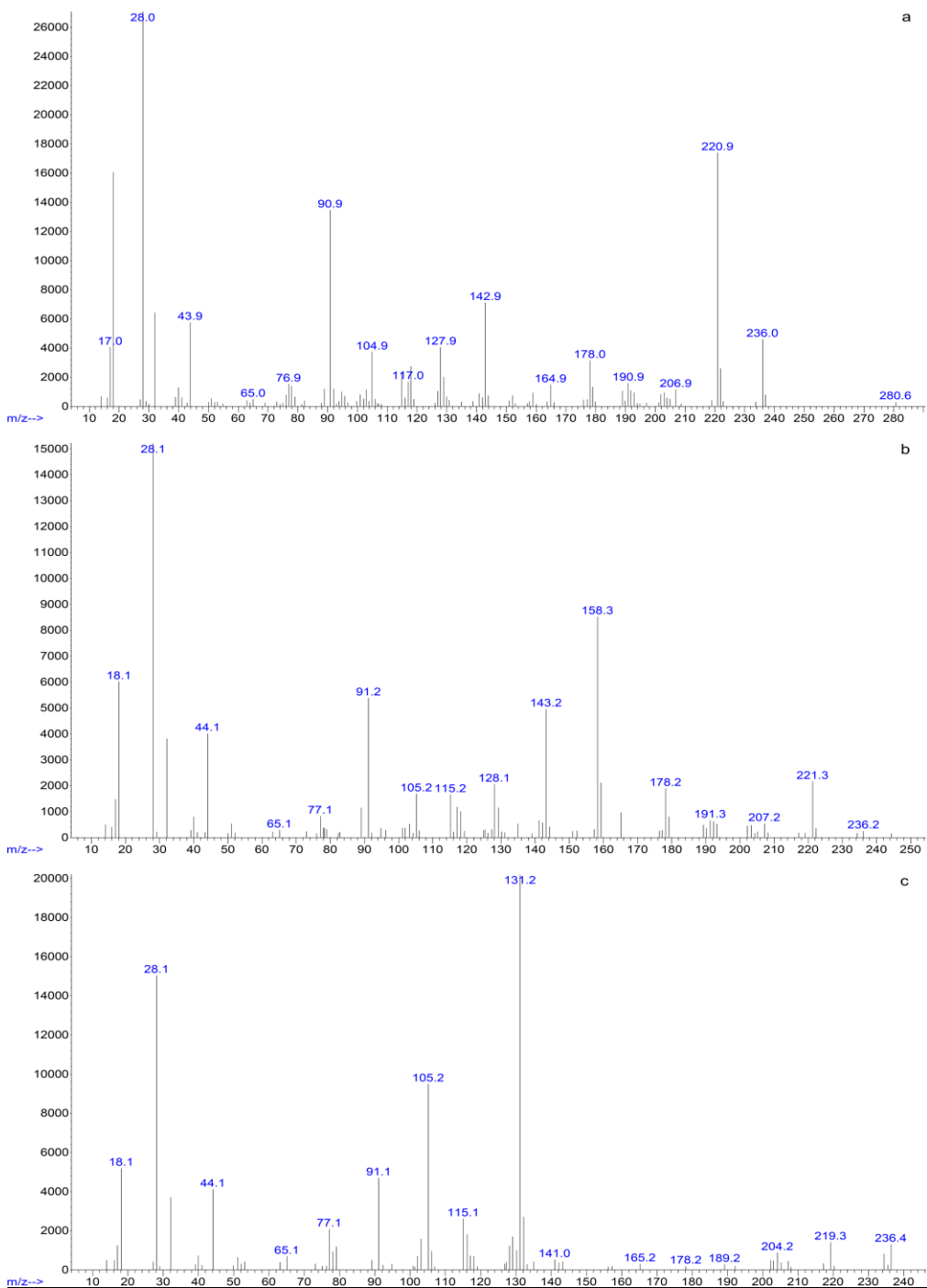


**Figure 4.8.** Possible isomers from free radical dimerization of AMS.

P-1 is different from P-4 and P-5; whatever the structures of P-4 and P-5 are, they can form a stably charged fragment by the loss of a  $CH_3$  radical, given a significant peak at  $m/z=221$ . A less abundant ion is formed by the loss of a  $\bullet CH_2-CH_3$ , which would give a peak at  $m/z=207$  that is present in the spectra as well (**Figure 4.7b** and **c**). The main difference between P-4 and P-5 structures would be the easy formation of an ion fragment with  $m/z=158$  by P-4 (**Figure 4.7b**), which matches the loss of the phenyl group as benzene. The  $m/z=158$  fragment peak is not present in the P-5 spectrum (**Figure 4.7c**), so the loss of a phenyl group is not easy for this molecule.

When the reactions were carried in the presence of oxygen, still at 300 °C, the product distribution changed; some products were significantly favored which increased their concentration, and new

products appeared. Among those products, P-2, P-3, and P-6 were produced and their mass spectra were analyzed, **Figure 4.9** shows the mass spectra of each of these three products.

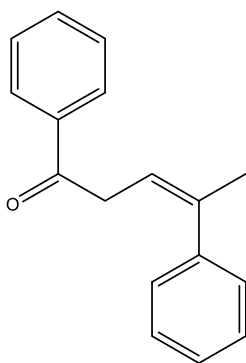


**Figure 4.9.** Mass spectra of products (a) P-2, (b) P-3, and (c) P-6.

Just as the molecules described before, P-2 and P-3 have a molecular ion of 236, which keeps supporting the hypothesis that these group of compounds are isomers of AMS dimers. Having all of them proximate retention times in the chromatogram also indicates that their boiling points are close to one another, which is also a characteristic feature of isomers.

From the mass spectra in Figures 9a and 9b, corresponding to P-2 and P-3, it is noticeable how these molecules can readily lose a methyl radical and form a stable ion of  $m/z=221$ , just as P-4 and P-5 (**Figure 4.7b** and c). The base peak for each one of these compounds is different,  $m/z=221$  is the base peak for P-2, and  $m/z=158$  is the base peak for P-3. This means that P-3 can lose 78 mass units, which corresponds to a neutral benzene molecule and form a stable ion at  $m/z=158$ .

P-6 also has a molecular ion of  $m/z=236$  (**Figure 4.9c**) and has a distinctive base peak at  $m/z=131$ . This fragment at  $m/z=131$  is observed in the mass spectra of P-1, P-4, and P-5 (**Figure 4.7**) but is not abundant. The molecular ion would have to fragment losing a styryl radical to form a stable ion with  $m/z=131$ . A peculiarity of P-6 is that it can lose 17 mass units, which corresponds to an OH fragment. This is only possible if an oxygen atom is in the molecule.<sup>24</sup> For this reason, P-6 is considered an oxygenated compound with the same molecular weight of 236, as the compounds discussed above. A possible structure for P-6 is shown in **Figure 4.10**. Note that the exact position of the double bond cannot be known from the mass spectrum.

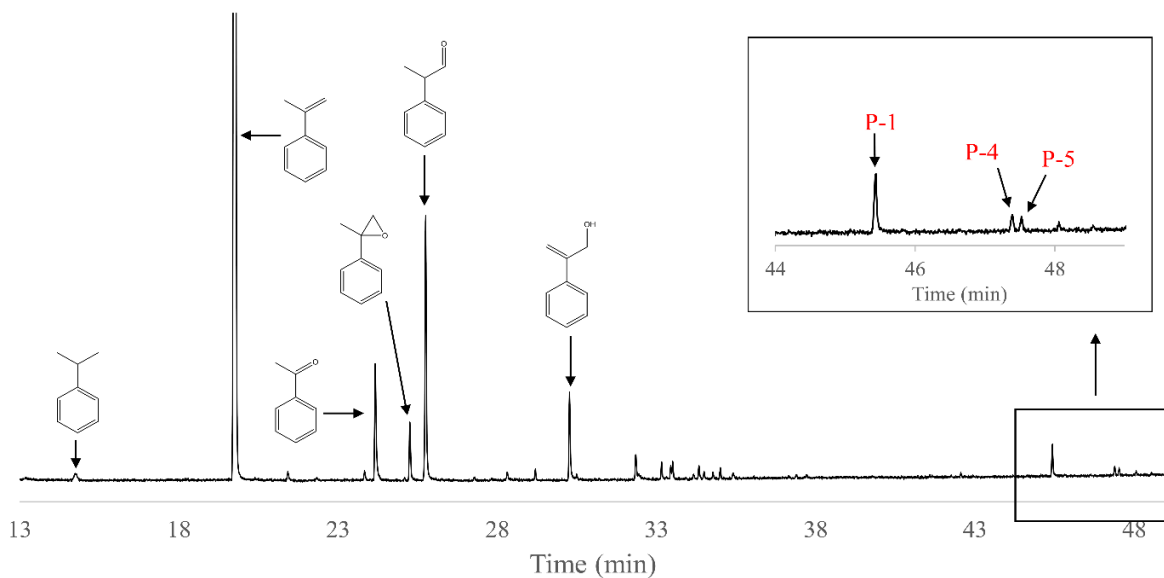


**Figure 4.10.** A possible structure for P-6.

#### 4.3.4. Oxidation products of AMS

Control reaction of AMS in pentane was also carried out in the presence of oxygen, and in the results obtained we observed clear signs of oxidation (**Figure 4.11**). At both oxygen partial

pressures tested, acetophenone was present, which is one of the principal products of oxidation of AMS.<sup>17,18</sup>



**Figure 4.11.** Chromatogram of the product from the reaction of AMS in *n*-pentane at 300 °C and 210 kPa oxygen partial pressure. The oxygenates shown (from left to right) are acetophenone, AMS oxide,  $\alpha$ -methylbenzeneacetaldehyde, and 2-phenylprop-2-en-1-ol.

The product also contained  $\alpha$ -methylbenzeneacetaldehyde, which follows from reduction or decomposition of the polyperoxide product of the oxidation of the AMS,<sup>17</sup> meaning that is an active monomer in the polymerization of AMS in the presence of oxygen, and possible residual monomer in the reactions performed with oxygen reported in Section 4.3.2.  $\alpha$ -Methylbenzeneacetaldehyde was the main product after reaction at both oxygen partial pressures studied. Addition products containing the AMS unit were observed, but their concentration was too low to properly identify them. AMS oxide was also found in one of the reactions at 210 kPa, which has been observed before in the oxidation of AMS at relatively high temperatures (170 °C).<sup>17</sup> 2-phenylprop-2-en-1-ol was also identified as part of the main products for this reaction.

After reaction of AMS in *n*-pentane at both 105 and 210 kPa of oxygen, cumene, P-1, P-4, and P-5 were also present in the reaction product, but in very low concentrations when compared with reactions carried in the presence of naphtha. Oxidation occurs through a free radical process, for which the appearance of disproportionation and combination termination products of cumyl

radicals is not strange, but should be anticipated if AMS is in high concentration. Yet, this occurrence was not previously reported in the literature on AMS oxidation.<sup>17,18</sup>

P-2, P-3, and P-6 were not formed during oxidation of AMS in *n*-pentane, despite being the main products from AMS dimerization in naphtha in the presence of oxygen (**Figure 4.6b**). The idea that P-2, P-3, and P-6 were direct products of the addition of O<sub>2</sub> to AMS must, therefore, be discarded, and a new hypothesis needs to be considered to explain their formation.

#### **4.3.5. Gum content of the feed and product**

We know that by having oxygen present in the reaction media free radical reactions can readily occur, for which we can anticipate a higher production of heavy compounds (addition reaction products). The gum formation tendency of hydrocarbons is actually tested in accelerated aging tests, under high partial pressures of oxygen and temperature.<sup>3</sup> These heavy compounds would not appear in the chromatogram because they would not vaporize and flow through the column, which makes impossible to track and correlate their production to the conditions at which the reactions were carried out. The gum content was determined for the naphtha feed and products of thermal conversion at 300 °C under different oxygen partial pressures (**Table 4.3**).

The values for gum content obtained (**Table 4.3**) showed a high standard deviation. It was visually observed that solids were formed in reactions containing oxygen, which were either suspended or at the bottom of the vial. Even though samples were strongly agitated before the portion of analysis was taken, we could not assure that the soluble and insoluble gum was equally distributed. The gum values should be considered semi-quantitative.

Despite the high deviation, reactions with similar conditions generated a gum content with the same order of magnitude, which was expected. Also, considering the high deviation, we can still observe the effect of temperature, oxygen, and the presence of AMS. Both feeds used have a very low gum content, having values very close or equal to zero. Control reactions with only naphtha in the complete absence of oxygen did not produce any gum, giving a gum content of zero in the analysis. Once the oxygen was present in these control reactions an increase on the gum content proportional to the partial pressure of oxygen was observed. The product mixture from the reaction of naphtha with AMS in the absence of oxygen has a comparable gum content to the control



reactions of only naphtha under oxygen. Finally, when naphtha + AMS + O<sub>2</sub> are subjected to reaction, the gum content values had a high standard deviation, making relative comparison untenable.

**Table 4.3.** Gum content of feed and products of conversion performed at the indicated conditions for 1 h.

| Sample                 | Reaction conditions                  |                |                                 | Gum content<br>% |         |
|------------------------|--------------------------------------|----------------|---------------------------------|------------------|---------|
|                        | Temperature                          | Total Pressure | O <sub>2</sub> Partial Pressure |                  |         |
| Naphtha <sup>a</sup>   | Not subjected to reaction conditions |                |                                 | 0                | ± 0.186 |
| Degassed Naphtha       | Not subjected to reaction conditions |                |                                 | 0                | ± 0.099 |
| Degassed Naphtha       | 300 °C                               | 4 MPa          | 0 kPa                           | 0                | ± 0.026 |
| Naphtha control        | 300 °C                               | 4 MPa          | 105 kPa                         | 0.547            | ± 0.071 |
| Naphtha control        | 300 °C                               | 4 MPa          | 210 kPa                         | 0.869            | ± 0.021 |
| Degassed Naphtha + AMS | 300 °C                               | 4 MPa          | 0 kPa                           | 0.619            | ± 0.621 |
| Naphtha + AMS          | 300 °C                               | 4 MPa          | 105 kPa                         | 1.729            | ± 0.981 |
| Naphtha + AMS          | 300 °C                               | 4 MPa          | 210 kPa                         | 1.206            | ± 0.364 |

<sup>a</sup> Naphtha refers to the feed taken directly from the barrel with no further treatment.

One important observation taken from this analysis is that temperature alone did not produce gums in naphtha, or if some gums were formed, those compounds that can activate and polymerize under these circumstances are present in very low concentrations. Naphtha feed that was not subjected to reaction conditions and degassed naphtha subjected to 300 °C for 1 hour in the absence of oxygen, had comparable gum contents (**Table 4.3**). It appeared that the ability to form dimerization-type products under thermal conditions (Section 4.3.2) did not imply that thermal conditions would lead to addition chain reactions or polymerization to form gums.

Oxygen can readily react with different molecules, activating them and promoting free radical reactions, and, on the other hand, AMS is the kind of molecule that can easily undergo free radical addition. Having one of these two reagents in the system appears to allow the formation of heavy

molecular weight compounds and having both of them appears to intensify the production of those heavy molecules.

#### 4.4. Discussion

##### 4.4.1. Free radicals present in the thermally cracked naphtha at 200–300 °C

In control reactions carried with only naphtha no new products were detected in the chromatogram for the product mixture (**Figure 4.2**), which could be because of two different possibilities:

(i) The products formed are either too light or too heavy and in too low concentrations. This would cause new products to have retention times similar to the rest of the naphtha (2-38 min) in case of light compounds and difficult to distinguish among other peaks because of their low concentration. In the case of the high molecular weight products that could be formed, they would not vaporize and would stay in the column of the GC. Ultimately new heavy products end up in what we quantified as gum, and if any new gums formed, the amount might be too low to quantify with certainty. As seen in **Table 4.3**, the gum content found for the naphtha before and after heating to 300 °C are very similar.

(ii) It could also be that there are no reactions occurring at all. It is unlikely that no reactions occurred because the chemistry observed when AMS was present in the naphtha (**Figure 4.3**) must have been promoted by a compound present in the naphtha that is reactive at the temperatures tested. The self-reactions of AMS were studied in solution with *n*-pentane and AMS gave a negative result for termination products of radical reactions like cumene and AMS dimers (Appendix A, Figures A1, and A2).

Despite the fact that no new products were detected in control reactions with the thermally cracked naphtha on its own, there was clear evidence of free radical reactions taking place at 200 to 300 °C (**Figure 4.3**) when a probe molecule, AMS, was added to facilitate identification of such reactions. Cumene and AMS dimers were the expected termination products of cumyl radicals. Cumyl radicals could be formed from AMS. Subsequent hydrogen disproportionation and combination reactions would lead to the formation of cumene and AMS dimers.

The occurrence of these reactions and selectivity towards one of the products, i.e. cumene or AMS dimers, would be governed by the entropy of the system since both are exothermic reactions.<sup>25</sup> At the reaction conditions, it is apparent that both pathways are feasible. The proven presence of cumene and AMS dimers points at a free radical mechanism occurring in the naphtha at temperatures in which they were formed. Cumene and AMS dimers were observed in all reactions carried out with naphtha and AMS at temperatures higher than 200 °C under inert atmosphere (Section 4.3.2), and in all of the reactions carried out in the presence of both oxygen and AMS in naphtha, even when the naphtha was absent. The results in the presence of oxygen corroborated the free radical pathway for the appearance of cumene, P-1, P-4, and P-5 (**Figure 4.11**), since the oxidation mechanism has been well established as a free radical process.

Another reaction pathway for the cumyl radicals would be radical chain reactions, but AMS does not polymerize at the temperatures tested, since its ceiling temperature is 61 °C, so a homopolymer of AMS is not expected. This would not mean that addition reactions producing heavy compounds did not occur; the gum content increased for the naphtha after reaction with AMS at 300 °C (**Table 4.3**), which was not observed in control reactions with only naphtha at the same temperature. Addition products between compounds present in the naphtha and few units of AMS would easily produce products that have a high boiling point and would form part of what we quantified as gum.

An often-encountered explanation of such free radical reactions is that dissolved oxygen is responsible for free radical initiation by autoxidation. This explanation could be ruled out.

Reactions of naphtha and AMS carried under oxygen can be compared with accelerated autoxidation reactions, increasing the oxygen partial pressure in the reactor and increasing the temperature would increase the overall rate of reaction of what would normally happen at ambient conditions in a long period of time. After 1 h of reaction at 300 °C, the naphtha product analyzed in the GC-MS showed that the products were similar to those seen before; cumene was present in higher concentrations than in reactions with no oxygen at the same temperature, and dimers were also formed. Also, additional products like P-2, P-3, and P-6 formed proportionally to the amount of oxygen in the system. The compound P-6 (**Figure 4.10**) was absent in the reaction products of thermal conversion of AMS in naphtha under an inert atmosphere. The presence of P-2 and P-3, that were caused by a free radical pathway initiated by oxygen also in the absence of oxygen,

corroborated the asserting that free radical species were formed in naphtha when the naphtha was subjected to temperatures between 200-300 °C.

#### 4.4.2. Comparison of product distribution from thermal and autoxidation of naphtha with AMS

In the absence of oxygen, the reaction products P-2 and P-3 were the only AMS dimerization products at 200 °C (Figure 3). Even though products P-2 and P-3 were also formed at higher temperatures, as the temperature was increased their concentration did not appear to increase. Whatever their structures are among those of the possible AMS dimers (**Figure 4.8**), temperature does not accelerate their formation. The concentration of P-2 and P-3 increased only when the reaction was carried out in the presence of oxygen. It is speculated that these isomers from AMS dimerization have a more demanding reaction intermediate that could be supplied by naphtha and that is increased by increasing the oxygen partial pressure. Whatever that intermediate is, it is not an AMS derived intermediate because P-2 and P-3 were not formed by heating AMS in *n*-pentane under an atmosphere containing oxygen (**Figure 4.11**). Based on their mass spectra, P-2 and P-3 do not contain oxygen, despite the evidence that indicates their formation is favored by increasing oxygen partial pressure.

Product P-6 only appeared after reactions in the presence of oxygen, it was identified as a compound similar to an AMS dimer, with similar boiling point and same molecular weight, but an oxygenated and was tentatively assigned the structure in **Figure 4.10**. This compound showed dependency on the oxygen partial pressure by increasing concentration as the oxygen partial pressure increased. However, P-6 does not seem to be the product of direct addition of oxygen to the AMS, since it was not formed in the control reactions of AMS in *n*-pentane; its formation is promoted by the naphtha. Although this compound was not present initially in the products from reactions using degassed naphtha in the absence of oxygen (not observed in the chromatogram), when the product mixture was re-analyzed after some time, this compound appeared for two of the three reactions carried for the degassed naphtha. This behavior can only be attributed to a slow autoxidation process of the samples after the reaction.

A possible reaction pathway for the formation of P-6 would be the combination reaction of a cumyl radical with acetophenone or an acetophenone intermediate. Acetophenone was one of the main

products in the control reaction for the oxidation of AMS. However, with this hypothesis about the formation of P-6, there is still the question of why P-6 was not formed on the control reactions of AMS in *n*-pentane in the presence of oxygen when there is a high probability that the same radical intermediates were present. There is a clear difference in the products distribution and concentrations when reactions are carried out in naphtha and when they are not. It appears that the effect of the naphtha goes beyond the production of radicals increasing the concentration of the termination products and it also affects the selectivity towards certain reactions.

Products P-1, P-4, and P-5 are present after all reactions carried at temperatures higher than 250 °C, and oxygen does not seem to increase their concentration. These products had to be initiated through another mechanism that is different than that of hydroperoxides decomposition. Their formation probably came through the breaking of bonds that need higher energy. The fact that the concentration of P-1 specifically is inversely proportional to the oxygen partial pressure, could be explained by a parallel-competitive reactions mechanism, in which P-2 and P-3, being the products of oxygen-initiated radical reaction formed in a higher rate consuming the AMS faster, suppressing the formation of P-1.

The P-4 and P-5 molecules have very similar mass spectra (Figure 7). In fact, the behavior of this “twin” pair of molecules points at the possibility of having stereoisomers, i.e. *cis* and *trans* isomers. Stereoisomers have close boiling points, which could explain the proximity of their retention times, they would also have very similar mass spectra with minor changes due to their positioning in space. In a *cis-trans* isomer pair, the *trans*-isomer would usually be thermodynamically favored, hence it would be produced in higher proportion with respect to the *cis*-isomer. Also, the *trans*-isomer has a lower boiling point (difference can be as small as 0.1 °C), what would make it have a shorter retention time. The first compound in the chromatogram, P-4, is present in a higher concentration for all reactions carried out, which is consistent with an explanation of P-4 and P-5 being *trans*- and *cis*-isomers of the same AMS dimer.

#### **4.4.3. Free radical initiation in thermally cracked naphtha**

Most of the products obtained from our reactions seem to be formed through a free radical mechanism, which is supported by the fact that there are AMS dimers present, as well as cumene. But, the initiation of this process is unclear, since free radicals can initiate through different routes.

Pryor<sup>26</sup> explains that there are three major ways of formation or initiation of radicals: thermal homolysis, irradiation, and oxidation-reduction reactions. Irradiation can be discarded because the way in which the experiments were conducted eliminated photo irradiation; experiments were performed in closed stainless steel reactors. Oxidation was controlled and the experiments included several controls that eliminated oxidation. Unless there were species present in the naphtha that were capable of oxidation-reduction reactions under an inert atmosphere, oxidation-reduction reactions can also be discarded as the origin of radical initiation. This would leave only thermal homolysis and for thermal homolysis to take place in the temperature range 200–300 °C the bonds involved in homolysis had to be weak.

Whatever caused the formation of P-2 and P-3, it is speculated that their formation was caused by species that contained a weak bond, which could be broken at low temperatures and that were present at low concentration. These products were never present in a significant amount at any temperature. Also, these initiating species had to be present in the naphtha and had to easily react with oxygen. This inference is made based on the fact that AMS in *n*-pentane did not produce P-2 and P-3 on heating. So, P-2 and P-3 did not come from the direct addition of oxygen to the AMS double bond, and were formed in high concentration only when naphtha, AMS, and oxygen were present; P-2 and P-3 formed in low concentration during the reaction of naphtha and AMS in the absence of oxygen.

The presence of oxygen in the naphtha, either as diluted gas or as an oxygenated reactive compound, would not be a surprise and is the reason for the hypothesis that motivated this study. Peroxides are commonly used as initiators when free radical chain reactions are desired to happen at low temperatures, because of the nature of their weak peroxide (O-O) bond, temperatures of 50 to 150 °C are necessary to achieve the energy necessary and break the bond and initiate free radical reactions.<sup>25</sup> Also, peroxides are intermediates in the autoxidation of hydrocarbons,<sup>1</sup> the oxygen molecule easily reacts with unsaturated compounds, forming peroxides which decompose increasing the number of radicals in the system. What was observed with products P-2 and P-3, points at the presence of peroxides or similarly weak bonds, which could have been present in low concentration in the thermally cracked naphtha feed.

Products P-1, P-4, and P-5 formed in reactions of naphtha and AMS in the absence of oxygen only when the temperature reached 250 °C, they were also formed in all partial pressures of oxygen in reactions of naphtha with AMS and in control reactions of AMS on pentane. They did not form in control reaction of AMS on pentane in the absence of oxygen. It is clear that their formation is directly linked to a free radical process. The question that arises is if peroxides were responsible for the initiation of these reactions, would not 200 °C be enough to break this kind of bonds? Initiation reactions that lead to the formation of P-1, P-4, and P-5 in reactions of naphtha and AMS in the absence of oxygen is obviously a thermal process, but the bonds that broke and initiated the reactions are stronger than those found in peroxides and in any case weaker than a C–C bond.

Thermal homolysis of a covalent bond can occur within a single molecule (unimolecular) or by the synergistic interaction of two non-radical molecules, what was described by Pryor<sup>26</sup> as molecule induced homolysis. In this process, two radicals are formed from two non-radicals. The driving force for the cleavage of the bond is the formation of a stronger bond, and the reaction rate is first order in both molecules involved.<sup>26</sup>

If the bond to be cleaved were a bond with hydrogen and in a compound R-H (donor), the reaction in this molecule by induced homolysis would follow a reverse disproportionation pathway if a proper molecule (acceptor) were available to form the new and stronger bond. Different studies have been done on describing this reaction for molecules like dihydroanthracene and AMS, as donor and acceptor molecules respectively.<sup>15,16,27</sup> If there are compounds in the naphtha with an R-H bond weak enough it will readily react when AMS is present, especially if it is present in high concentrations. This does not mean that the reaction observed only occurred because AMS was present. Other compounds can also work as acceptors promoting molecule induced reactions. Röchardt et al.<sup>28</sup> listed some donors and acceptor compounds that can undergo this reaction when paired. Among the compounds listed are olefins of the styrene type (e.g. AMS) and diolefins. Some diolefins were proven to be present in the thermally cracked naphtha used in this research,<sup>19</sup> and it is likely that other similarly reactive compounds are present.

Free radical initiation by molecule induced homolysis is possible when the naphtha is under the right conditions. This type of radical formation has been described as the initiation step for the thermal polymerization of styrene<sup>29–32</sup> and in the addition of alkane to alkenes through a free

radical chain reaction.<sup>33,34</sup> Possible acceptors are known to be present in the naphtha. The question that remains is: what kind of compounds present could donate a hydrogen through this pathway, producing free radical in an already reactive and complex mixture to increase the chances of producing high molecular weight compounds? This question is of industrial relevance because the formation of high molecular weight compounds can end up causing problems in downstream processes and/or accelerating the deactivation process of catalysts.

#### 4.5. Conclusions

No free radicals were detected by electron spin resonance spectroscopy in thermally cracked naphtha, but when the temperature was increased to 200–300 °C evidence of free radical reactions was found. Use was made of  $\alpha$ -methylstyrene (AMS) as probe molecule to improve the sensitivity of detecting free radical reactions. Using this approach, the following could be concluded:

(a) The formation of dimerization products between material in the naphtha and AMS, as well as dimerization of AMS, became noticeable at 200 °C within 1 hour under an inert atmosphere. At 300 °C after 1 hour both dimers and hydrogen transfer to AMS to form cumene was clearly evident. These are products of free radical reactions.

(b) The potential contribution of dissolved oxygen as initiator could be ruled out. Experiments with extensively degassed naphtha and under different partial pressures of oxygen were performed. The results indicated that free radical reactions following on autoxidation had different product selectivity. The thermal conversion of the extensively degassed naphtha under inert atmosphere resulted in similar products and product selectivity as the naphtha that was not degassed but also thermally converted under an inert atmosphere.

(c) The potential contribution of self-initiation of free radical reactions by AMS could be ruled out. No evidence of self-initiation was seen in experiments conducted under an inert atmosphere with AMS in *n*-pentane instead of naphtha. In the presence of oxygen, the free radical dimerization selectivity from the reaction of AMS in *n*-pentane was different to that of AMS in naphtha.

(d) A minor amount of free radical addition products could potentially be explained by the presence of species with weak, thermally labile bonds, which could account for specific products observed at 200 °C and that did not increase with an increase in temperature. The majority of the addition



products could be explained in terms of molecule induced homolysis. Although no direct proof is provided, the explanation is forwarded because: (i) AMS is known to form cumyl radicals that end up in cumene, when initiated through molecule induced homolysis, and (ii) the wide diversity of compounds present in the naphtha that could take part in molecule induced homolysis, also independently of AMS.

### **Acknowledgement**

The study was funded through the through the NSERC/CNOOC Ltd. Industrial Research Chair program in Field Upgrading and Asphaltenes Processing that is financially supported by the Natural Science and Engineering Research Council (NSERC) of Canada, Alberta Innovates, and CNOOC International.

### **4.6. References**

- (1) Mayo, F. R. Some New Ideas on Oxidation. *Ind. Eng. Chem.* **1960**, 52 (7), 614–618.
- (2) Kawahara, F. K. Composition of Gum in Cracked Naphtha. *Ind. Eng. Chem. Prod. Res. Dev.* **1965**, 4 (1), 7–9.
- (3) Nagpal, J. M.; Joshi, G. C.; Singh, I. D.; Kumar, K. Studies on the Nature of Gum Formed in Cracked Naphthas. In *6th International Conference on Stability and Handling of Liquid Fuels*; Vancouver, Canada, 1997; pp 543–550.
- (4) Stark, C. M. *Free Radical Telomerization*; New York: Academic Press, 1974.
- (5) Yui, S. Removing Diolefins from Coker Naphtha Necessary before Hydrotreating. *Oil Gas J.* **1999**, 97 (36), 64–69.
- (6) de Klerk, A. Sasol 2 and 3 Facilities. In *Fischer-Tropsch Refining*; Wiley-VCH: Weinheim, Germany, 2011; pp 181–216.
- (7) Nagpal, J. M.; Joshi, G. C.; Rastogi, S. N. Stability of Cracked Naphthas from Thermal and Catalytic Processes and Their Additive Response. Part I. Evaluation of Stability and Additive Response. *Fuel* **1995**, 74 (5), 714–719.

- (8) Nagpal, J. M.; Joshi, G. C.; Rastogi, S. N. Stability of Cracked Naphthas from Thermal and Catalytic Processes and Their Additive Response. Part II. Composition and Effect of Olefinic Structures. *Fuel* **1995**, *74* (5), 720–724.
- (9) Zerpa, N.; de Klerk, A.; Xia, Y.; Omer, A. A. Olefins Reduction of a Hydrocarbon Feed Using Olefins Aromatics Alkylation. Patent Application WO2015000061A1, 2015.
- (10) Guisnet, M.; Magnoux, P. Organic Chemistry of Coke Formation. *Appl. Catal. A: General* **2001**, *212* (1–2), 83–96.
- (11) Niizuma, S.; Steele, C. T.; Gunning, H. E.; Strausz, O. P. Electron Spin Resonance Study of Free Radicals in Athabasca Asphaltene. *Fuel* **1977**, *56* (3), 249–256.
- (12) Schultz, F.; Seluckyts, L. E.s.r. Measurements on Asphaltene and Resin Fractions from Various Separation Methods\*. **1981**, *60*, 951–956.
- (13) Gray, M. R.; McCaffrey, W. C. Role of Chain Reactions and Olefin Formation in Cracking, Hydroconversion, and Coking of Petroleum and Bitumen Fractions. *Energy Fuels* **2002**, *16* (3), 756–766.
- (14) Hersberger, A. B.; Reid, J. C.; Heiligmann, R. G. Polymerization of Alpha-Methylstyrene. *Industrial and Engineering Chemistry* **1945**, *37* (11), 1073–1078.
- (15) Röchardt, C.; Gerst, M.; Nölke, M. The Uncatalyzed Transfer Hydrogenation of  $\alpha$ -Methylstyrene by Dihydroanthracene or Xanthene—a Radical Reaction. *Angew. Chem., Int. Ed. Engl.* **1992**, *31* (11), 1523–1525.
- (16) Keller, F.; Röchardt, C. Bimolecular Formation of Radicals by Hydrogen Transfer. 14. The Uncatalyzed Transfer Hydrogenation of  $\alpha$ -Methylstyrene by 2,6-Disubstituted 9,10-Dihydroanthracenes. *Journal für Praktische Chemie/Chemiker-Zeitung* **1998**, *340* (7), 642–648.
- (17) Mayo, F. R.; Miller, A. A. The Oxidation of Unsaturated Compounds. VI. The Effect of Oxygen Pressure on the Oxidation of  $\alpha$ -Methylstyrene. *J Am Chem Soc* **1958**, *80* (10), 2480–2493.

- (18) Jayaseharan, J.; Kishore, K. Mechanism of “Autoacceleration” in the Thermal Oxidative Polymerization of  $\alpha$ -Methylstyrene. *Macromolecules* **1997**, *30* (14), 3958–3964.
- (19) Paez, N. Y.; de Klerk, A. Diolefin Characterization in a Thermally Cracked Naphtha. *Prepr. Pap.-Am. Chem. Soc., Div. Energy Fuels* **2016**, *61* (1), 12–15.
- (20) Rao, Y.; de Klerk, A. Characterization of Heteroatom-Containing Compounds in Thermally Cracked Naphtha from Oilsands Bitumen. *Energy Fuels* **2017**, *31* (9), 9247–9254.
- (21) Siddiquee, M. N.; de Klerk, A. In Situ Measurement of Liquid Phase Oxygen during Oxidation. *Ind. Eng. Chem. Res.* **2016**, *55* (23), 6607–6618.
- (22) Naghizada, N.; Prado, G. H. C.; de Klerk, A. Uncatalyzed Hydrogen Transfer during 100–250 °C Conversion of Asphaltenes. *Energy Fuels* **2017**, *31* (7), 6800–6811.
- (23) McLafferty, F. W.; Tureček, František. *Interpretation of Mass Spectra*, 4 ed.; University Science Books: Mill Valley, CA, 1993.
- (24) Silverstein, R. M.; Webster Francis X. Mass Spectrometry. In *Spectrometric Identification of Organic Compounds*; John Wiley & Sons, Inc.: New York, 1998; pp 2–70.
- (25) Parsons, A. F. *Introduction to Free Radical Chemistry*; Blackwell Science: Oxford, 2000.
- (26) Pryor, W. A. Part II The Production of Radicals. In *Free radicals*; McGraw-Hill: New York, 1966; pp 57–145.
- (27) Billmers, R.; Griffith, L. L.; Stein, S. E. Hydrogen Transfer between Anthracene Structures. *Am. J. Phys. Chem.* **1986**, *90* (3), 517–523.
- (28) Rüchardt, C.; Gerst, M.; Ebenhoch, J. Uncatalyzed Transfer Hydrogenation and Transfer Hydrogenolysis: Two Novel Types of Hydrogen-Transfer Reactions. *Angew. Chem., Int. Ed. Engl.* **1997**, *36* (1314), 1406–1430.
- (29) Pryor, W. A.; David, G.; Green, J. G. Radical Production from the Interaction of Closed-Shell Molecules. 5. The Chemistry of Methylene cyclohexadiene<sup>1</sup>. *Journal of Organic Chemistry* **1978**, *43* (3), 526–528.

- (30) Kopecky, K. R.; Lau, M.-P. Thermal Reaction between 5-Methylene-1,3-Cyclohexadiene and Styrene. *The Journal of Organic Chemistry* **1978**, *43* (3), 525–526.
- (31) Mayo, F. R. The Dimerization of Styrene. *J Am Chem Soc* **1968**, *90* (5), 1289–1295.
- (32) Chong, Y. K.; Rizzardo, E.; Solomon, D. H. Confirmation of the Mayo Mechanism for the Initiation of the Thermal Polymerization of Styrene. *J Am Chem Soc* **1983**, *105* (26), 7761–7762.
- (33) Metzger, J. O.; Bangert, F. Thermally Initiated Free-Radical Chain Addition of Alkanes to Alkynes, II. Kinetics of the Addition of Cyclohexane to Phenylethyne under Supercritical Fluid Conditions. *Chem Ber* **1994**, *127* (4), 673–675.
- (34) Metzger, J. O. Formation of Alkyl Radicals by Thermal Bimolecular Reaction of Alkanes and Alkenes. *Angewandte Chemie International Edition in English* **1983**, *22* (11), 889–889.

## **Chapter 5. Acid catalyzed reactions of cyclopentene in cracked naphtha and their role on catalyst deactivation**

### **Abstract**

The conversion of cracked naphtha over an amorphous silica alumina (ASA) catalyst, which is a process used in partial upgrading of bitumen to decrease the olefin content without the use of hydrogen, lead the formation of deposits on the catalyst with time on stream. It was of interest to explore whether cyclopentene substructures would be more likely to lead to formation of deposits than linear olefinic substructures. There have been a few indications that 5-member ring olefins can undergo reactions that accelerate the formation of carbonaceous deposits. As part of this investigation we aim to determine if such species are present in the naphtha and if they could react towards the formation of heavy aromatic deposits formed on the surface of the ASA catalyst. It was found that cyclopentene species were indeed present in the cracked naphtha, and they were reacting in the presence of the ASA catalyst at 300 °C. During reactions of model compounds, it was seen as bicyclic compounds like decalin and octalin were being formed from reactions of cyclopentene at 300 °C on the ASA catalyst. It was determined that hydrogen transfer was part of the reaction network, since decalin had to be the result of hydrogen transfer to an octalin molecule. The impact of reactions of cyclopentene on the formation of deposits on the catalyst was tracked using electron spin resonance spectroscopy (ESR), taking advantage of the relation between the free radical content and the amount of condensed polyaromatic species in the deposits. It was found that after reactions with cyclopentene, the free radical content on the spent catalyst tripled that of the catalyst after reaction with 1-hexene. The relation between the formation of intermediary radical cation bicyclic compounds and the formation of deposits is discussed. Additionally, fluorescence spectroscopy proved instrumental to expose the thermal nature of part of the reactions occurring during conversion of he cracked naphtha at 300 °C.

### **Key Words**

Cracked naphtha, cyclopentene, deposit formation, ESR, fluorescence spectroscopy.

## 5.1. Introduction

Cracking processes are central to the upgrading and refining of heavy oils and are used to convert the residua to lighter boiling fractions for the production of transport fuels. When cracking is performed in the absence of hydrogen, such as by visbreaking, delayed coking, or fluid catalytic cracking, the lighter products are olefinic. Light olefins, normally gaseous and in the naphtha boiling range, are useful for motor-gasoline refining and petrochemical production. If the refinery is not situated close to petrochemical facilities, the lighter olefins can be oligomerized to naphtha and distillate range products.<sup>1,2</sup>

In the Canadian bitumen upgrading context, relevant to this study, reducing the olefin content in the final upgraded product is desirable due to limitations in their concentration during pipeline transportation of bitumen. Pipeline specifications cap the allowable olefin content in the transportable product to 1 wt% 1-decene equivalent.<sup>3</sup> In bitumen upgraders the olefins are usually converted during hydroprocessing. However, due to the high capital and operational costs associated with hydrogen production,<sup>4</sup> it is desirable in the development of technologies like partial upgrading to avoid hydroprocessing.

Looking for alternatives to hydrogen-based processes, it was considered that the use of an acid catalyst to perform olefin-aromatic alkylation could reduce the olefin content without the use of hydrogen. Olefin-aromatic alkylation in the cracked naphtha stream is possible over acid catalysts, like amorphous silica-alumina (ASA).<sup>5,6</sup> In early observations, it was found that catalyst deactivation with time-on-stream took place in a short time. Since frequent oxidative catalyst regeneration cycles would be needed, there was economic incentive to increase the catalyst cycle life, and study how the deactivation was occurring.

In a previous study,<sup>7</sup> covered in Chapter 3, it was described how the deactivation of the ASA catalyst is caused by the deposition of organic material on the catalyst surface during the treatment of cracked naphtha. Additionally, it was seen that at temperatures of 325 °C the deposition was mainly in the outlet of the reactor, which indicated that it might be (at least in part) caused by molecules formed in the reactor, during reaction, instead of molecules already present in the cracked naphtha. According to the observations made, the reactions leading to the formation of

deposits on the catalyst were of thermal nature, but there was also a catalytic component to the reaction network that produce the deposits.

In a different study,<sup>8</sup> captured in Chapter 4, changes in the cracked naphtha were investigated through use of a probe molecule ( $\alpha$ -methylstyrene) that participated in free radical reactions. In the cracked naphtha changes were detected with the probe molecule upon heating, while no observable changes were detected in the cracked naphtha after thermal reactions without the aid of the probe molecule, likely due to the inherent complexity of the mixture. This indicated that the possible initiation of the free radical chain reactions leading to catalyst coking was a molecule induced radical formation step, like hydrogen transfer. Species capable of such free radical initiation can be formed at reaction conditions and they might be produced through acid catalyzed reactions.

A wide variety of olefinic compounds are present in the cracked naphtha, with concentrations going as high as 54 vol%, as in the case of fluid catalytic cracking (FCC) naphthas.<sup>9,10</sup> Olefins can react over acid catalysts and are known to contribute to the formation of carbonaceous deposits in acid catalysts.<sup>11</sup>

One aspect that received comparatively little attention is the reactions of 5-membered cyclic olefins in cracked products, either as cyclopentene derivatives, or cyclopentene substructures of larger molecules. The cracked products from Canadian bitumen are naturally rich in cyclic species due to the naphthenic nature of the bitumen and it was found that cyclopentene and alkylated cyclopentenes are present in the cracked naphtha,<sup>12,13</sup> even in a higher proportion when compared to other cyclic olefins like cyclohexene.

It was reported that cyclopentane, cyclopentene, and cyclopentadiene contributed to the formation of coke during naphtha reforming,<sup>14</sup> which was explained in terms of the formation of indene. Indene is an especially reactive molecule, that can lead to and promote free radical addition reactions in a hydrocarbon mixture.<sup>15,16</sup> It was of interest to understand better the role of cyclopentenes in reactions that could lead to the formation of carbonaceous deposits on acid catalysts, and ASA in particular.

In this study, we identified cyclopentene-type molecules in an industrial thermally cracked naphtha feed, using GC-MS. After thermal and catalytic reactions of the cracked naphtha, the reactivity of the identified cyclopentene species was assessed.

To improve understanding further, the study of the acid catalyzed products of the reactions of cyclopentene over ASA was performed using model compounds. Reactions of the olefin in the presence of an aromatic were also investigated. The contribution to the formation of deposits by cyclopentene was evaluated using electron spin resonance (ESR) spectroscopy and was compared to the deposits formed after reaction of a linear olefin, 1-hexene, as control.

## 5.2. Experimental

### 5.2.1. Materials

The chemicals and cylinder gases that were used are listed in **Table 5.1**. These materials were used as supplied and without further purification.

**Table 5.1.** Chemicals and cylinder gases used in the study.

| <b>Compound</b>         | <b>Formula</b>                 | <b>CASRN <sup>a</sup></b> | <b>Mass fraction purity <sup>b</sup></b> | <b>Supplier</b> |
|-------------------------|--------------------------------|---------------------------|------------------------------------------|-----------------|
| <i>Chemicals</i>        |                                |                           |                                          |                 |
| <b><i>n</i>-Heptane</b> | C <sub>7</sub> H <sub>16</sub> | 142-82-5                  | >99%                                     | Sigma-Aldrich   |
| <b>1-Hexene</b>         | C <sub>6</sub> H <sub>12</sub> | 592-41-6                  | >99%                                     | Sigma-Aldrich   |
| <b>Cyclopentene</b>     | C <sub>5</sub> H <sub>8</sub>  | 142-29-0                  | 96%                                      | Sigma-Aldrich   |
| <b>Ethylbenzene</b>     | C <sub>8</sub> H <sub>10</sub> | 100-41-4                  | 99.8%                                    | Sigma-Aldrich   |
| <i>Cylinder gases</i>   |                                |                           |                                          |                 |
| <b>Nitrogen</b>         | N <sub>2</sub>                 | 7727-37-9                 | 0.99998 <sup>c</sup>                     | Praxair         |
| <b>Helium</b>           | He                             | 7440-59-7                 | 0.99999 <sup>c</sup>                     | Praxair         |

<sup>a</sup> CASRN = Chemical Abstracts Services Registry Number. <sup>b</sup> This is the purity of the material guaranteed by the supplier; materials was not further purified. <sup>c</sup> Mole fraction purity.

The catalysts used in this study are a series of commercially available silica-alumina/alumina hydrates. Siral10, Siral30, and Pural SB were obtained from Sasol Germany and were calcined to obtain the amorphous silica-aluminas (ASA) and  $\gamma$ -alumina catalysts used in this study. The



calcination took place in a Carbolite Laboratory Furnace with temperature control. The temperature program used for calcination started at room temperature, heating at a rate of 10 °C/min until reaching 550 °C, temperature that was held for 4 h. After cooling, the samples were stored in a sealed container placed in a desiccator, to avoid adsorption of ambient moisture. Characterization of these catalysts has been done, also after treatment at 550 °C,<sup>17</sup> and a summary of their textural properties can be found in **Table 5.2**.

The relative amount of silica and alumina present in each catalyst type determines its acidity. Siral 30, with 30% silica, has a higher acidity, as seen in **Table 5.2**, followed by Siral 10, with 10%. Pural SB, has 0% silica. The acidity sequence is explained by the higher concentration of bridged Bronsted acid sites (Al(OH)Si), like those in zeolites.<sup>18</sup> The mean particle diameter for the silica-aluminas (Siral 10 and 30) and the  $\gamma$ -alumina (Pural SB) was 35  $\mu\text{m}$  and 45  $\mu\text{m}$ , respectively.

**Table 5.2.** Catalysts textural properties after treatment at 550 °C.

| Catalyst        | BET                                            | Acid site concentration ( $\mu\text{mol/g}$ ) <sup>e</sup> |                   |                     |                     | Bronsted acidity ( $\mu\text{mol/g}$ ) <sup>e</sup> |                   |                     |                     |
|-----------------|------------------------------------------------|------------------------------------------------------------|-------------------|---------------------|---------------------|-----------------------------------------------------|-------------------|---------------------|---------------------|
|                 | S.A. <sup>a</sup><br>( $\text{m}^2/\text{g}$ ) | Total                                                      | Weak <sup>b</sup> | Medium <sup>c</sup> | Strong <sup>d</sup> | Total                                               | Weak <sup>b</sup> | Medium <sup>c</sup> | Strong <sup>d</sup> |
| <b>Pural SB</b> | 238                                            | 719                                                        | 337               | 124                 | 258                 | 0                                                   | 0                 | 0                   | 0                   |
| <b>Siral10</b>  | 391                                            | 938                                                        | 493               | 353                 | 92                  | 60                                                  | 25                | 14                  | 21                  |
| <b>Siral30</b>  | 483                                            | 1127                                                       | 452               | 489                 | 186                 | 274                                                 | 92                | 139                 | 43                  |

<sup>a</sup>S.A=surface area. <sup>b</sup>Defined by the ammonia desorbed from 150-300°C. <sup>c</sup>Defined by the ammonia desorbed from 300-400°C. <sup>d</sup>Defined by the ammonia desorbed from 400-500°C. <sup>e</sup>Catalyst treatment was done under helium.

The thermally cracked naphtha used in the reactions was obtained from the Long Lake upgrader of CNOOC Intl. and was characterized previously.<sup>8,13,19,20</sup> For ease of reference and due to its relevance to this investigation, some of the naphtha characterization data are listed in **Table 5.3**.

## 5.2.2. Equipment and procedure

### 5.2.2.1.Reaction setup

Reactions were carried out in 10 mL stainless steel Swagelok batch reactors, 1.3 cm outer diameter (OD) and 7.6 cm long. A volume of 4 mL of the liquid feed was placed in a vial inserted into the

reactor, to limit any catalytic interference of the reactor wall, as shown in **Figure 5.1**. In the case of reactions with a catalyst, 250 mg of each one of the catalysts listed in **Table 5.2** was also placed in the vial, which was then placed in the reactor, for each reaction. After including a magnetic stirrer, the reactor was closed, flushed with nitrogen, and pressurized to 4 MPa with nitrogen.

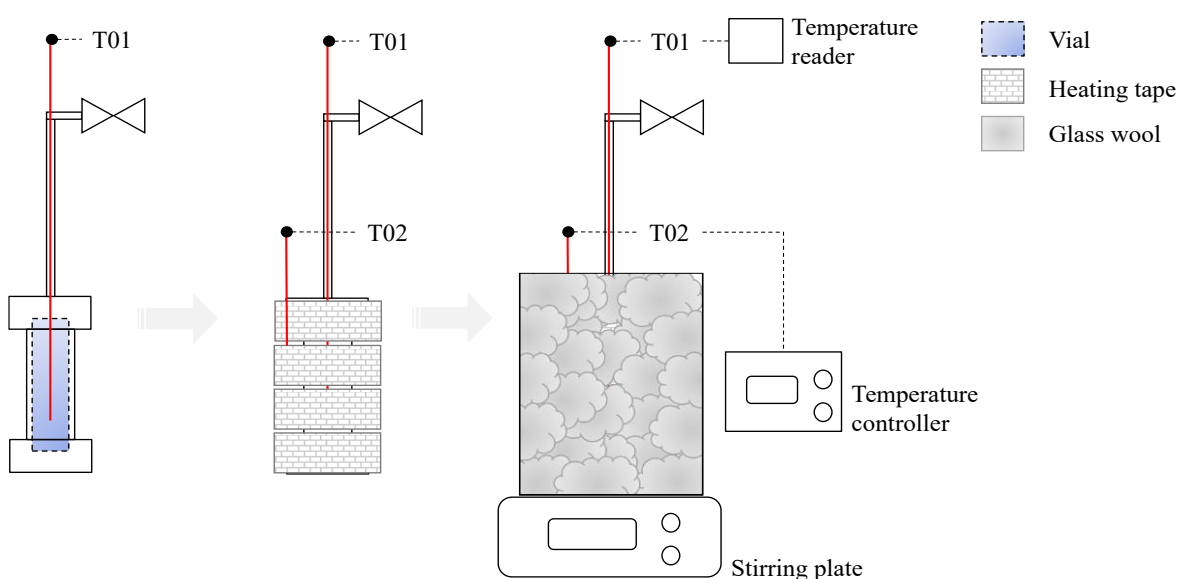
**Table 5.3.** Characterization of thermally cracked naphtha.

| <b>Property</b>             | <b>Units</b>      | <b>Value</b> |
|-----------------------------|-------------------|--------------|
| <b>Density</b>              | kg/m <sup>3</sup> | 762.7        |
| <b>Carbon</b>               | wt%               | 84.3         |
| <b>Hydrogen</b>             | wt%               | 13.8         |
| <b>Nitrogen</b>             | wt%               | 0.09         |
| <b>Sulfur</b>               | wt%               | 0.9          |
| <b>Oxygen</b>               | wt%               | 0.25         |
| <b>Olefin Content</b>       | wt%               | 13           |
| <b>Aromatic Content</b>     | wt%               | 4            |
| <b>Distillation profile</b> |                   |              |
| IBP                         | °C                | 30           |
| T10                         | °C                | 68           |
| T30                         | °C                | 100          |
| T50                         | °C                | 133          |
| T70                         | °C                | 173          |
| T90                         | °C                | 239          |
| FBP                         | °C                | 265          |

To agitate the liquid+catalyst mixture effectively the reaction was performed on a stirring plate at a stirring speed 500 rpm. At this speed, the suspension of the catalyst throughout the liquid was confirmed by a prior observation. Stirring was done in all reactions, including that with no catalyst.

The heating of the reactor was accomplished using a fiberglass insulated heating tape. Glass wool was used for extra insulation, to avoid excessive heat loss (See **Figure 5.1**). The reaction temperature of 300 °C was controlled by two thermocouples: the first was placed inside of the

reactor (T01 in **Figure 5.1**), and it was considered the real reaction temperature, targeted at 300 °C. The second thermocouple was placed directly in contact with the heating tape (T02 in **Figure 5.1**), and it was used to tune the heat output of the heating tape manually. Once the determined reaction time was reached, the heating tape was turned off and removed along with the insulation. The reactor was cooled using an air flow at room temperature. Heat-up times vary in the range of 30-40 min, while complete cool-down was achieved in 10-15 min.



**Figure 5.1.** Reaction setup. Thermocouple T01 measured the temperature in the reaction mixture and thermocouple T02 measured the temperature outside of the reactor for control of the heater.

After the reactor was cooled, the pressure was slowly released, and the reactor was opened. Material balance was done by weighing the internal vial with the naphtha+catalyst mixture before and after reaction. In all cases the recovery was 97-99%.

After the reaction was finished, the liquid was separated from the catalyst, using a syringe and syringe filter of 0.2  $\mu\text{m}$  pores. The resulting liquid was taken for analysis with GC-MS and fluorescence spectroscopy. The catalyst samples were left to “dry”, so that the remaining organic liquid evaporated. Once dry, the catalyst sample was analyzed by FTIR and ESR.

### 5.2.2.2. Reactions of cracked naphtha

Four reactions were performed with the thermally cracked naphtha: one reaction with no catalyst with a residence time of 1 h, and three catalyzed reactions using the catalysts from **Table 5.2** with a residence time of 30 min. The increase of residence time for the non-catalyzed reaction was done to magnify any possible changes that could occur in the cracked naphtha, since it was previously found that it was difficult to observe changes in the cracked naphtha after thermal reactions due to the complexity of the mixture.<sup>8</sup> Catalysts with different acidity were used to provide an indication of the impact of acidity on the reactions observed. For example, if the concentration of a compound changes proportionally to the Brønsted acidity of the catalyst, it would indicate that it is likely that the molecule is undergoing a Brønsted acid catalyzed reaction.

### 5.2.2.3. Reactions of model compounds with Siral 30

Reactions of cyclopentene were done with Siral 30. Since olefins can react through olefin oligomerization and olefin-aromatic alkylation, reactions were carried out in the absence and presence of ethylbenzene. Additionally, a linear olefin (1-hexene) was used as control to compare the reaction pathways and effect on the deposits formed on the catalyst.

The solutions listed in **Table 5.4** were prepared using heptane as solvent and were subjected to reactions in the same manner described for reactions of naphtha with the different catalysts in Section 5.2.2.2. The residence time was 30 min. Material balance was done by weighing the internal vial with the naphtha+catalyst mixture before and after reaction. In all cases the recovery was 97-99%.

**Table 5.4.** Solutions for reaction with model compounds.

| <b>Solution</b> | <b>Reactant 1</b> | <b>wt%</b> | <b>Reactant 2</b> | <b>wt%</b> | <b>Heptane (wt%)</b> |
|-----------------|-------------------|------------|-------------------|------------|----------------------|
| <b>1</b>        | 1-Hexene          | 10%        |                   | 0%         | 90%                  |
| <b>2</b>        | Cyclopentene      | 10%        |                   | 0%         | 90%                  |
| <b>3</b>        | Ethylbenzene      | 10%        | 1-Hexene          | 10%        | 80%                  |
| <b>4</b>        | Ethylbenzene      | 10%        | Cyclopentene      | 10%        | 80%                  |

### **5.2.3. Analyses**

#### **5.2.3.1. Gas chromatography-mass spectrometry (GC-MS) for product analysis**

The analysis of the liquid after reaction in this study relied on the separation and identification of the products using the GC-MS. The analyses were performed in an Agilent 7820A GC connected to a 5977E MS detector. The separation occurred in an Agilent HP-PONA capillary column (50 m × 0.20 mm × 0.50 μm), using 1 mL/min flow helium as a carrier. The temperature program used started at 40 °C, a temperature that was maintained for 15 min, then ramped up at 5 °C/min to 315 °C. A volume of 0.1 μL of the samples were injected with no prior dilution. The mass spectra search library software used for the mass spectra analysis for compound identification was NIST/EPA/NIH mass spectral library version 2.0., based on the NIST Mass Spectrometry Data Center library.

#### **5.2.3.2. Fluorescence spectroscopy for product analysis**

To analyze the liquid product by fluorescence spectroscopy, the sample was diluted in cyclohexane to a concentration of 525 ppm (μg/g) to avoid saturation of the detector. The solution was placed in a 1 cm path length quartz cell, and then placed in the sample cell holder of the equipment. The fluorescence spectra were measured in a Horiba Scientific Aqualog fluorescence spectrometer. The spectra were collected in an excitation wavelength range of 240-800 nm. All measurements were done with an increment of 3 nm, and the integration time was kept at 0.1s. The emission range measured covered the wavelengths 250-800 nm. The spectra were therefore two-dimensional maps of excitation wavelength versus fluorescence emission over the wavelength range.

#### **5.2.3.3. Electron spin resonance (ESR) spectroscopy**

The ESR spectra were collected using an Active Spectrum extended range benchtop Electron Spin Resonance spectrometer operated at 9.7 GHz frequency. Approximately 300 mg of each of the samples were placed in a 5 mm Norell NMR tubes, which was sufficient to fill the resonance cavity volume. The ESR spectra was obtained in the magnetic field range of 3400 to 3500 G, with a microwave power of 15 mW, 1.2 G of coil amplitude, 10 scans, and digital gain of 12 dB. These analyses were only semi-quantitative.

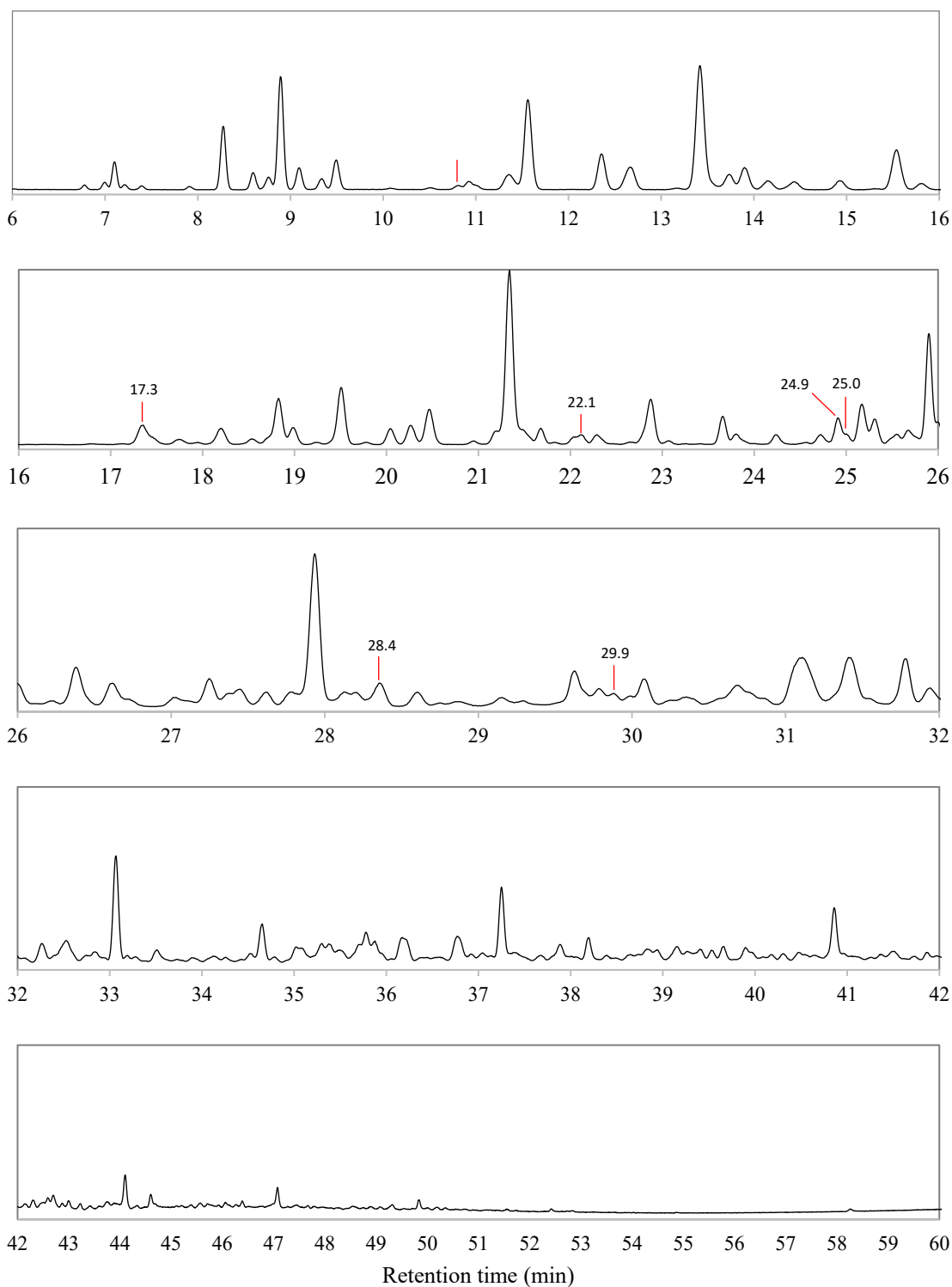
## 5.3. Results

### 5.3.1. Identification of cyclopentene species

The cracked naphtha feed sample was analyzed using GC-MS, and the resulting chromatogram is plotted in **Figure 5.2**. Among the compounds in the mixture, 7 peaks were identified as possible 5-member rings olefinic compounds. These compounds are highlighted with their retention time in **Figure 5.2**.

The initial identification relied on the mass spectra of the compounds analyzed through the search library software using the NIST Mass Spectrometry Data Center. The mass spectra are also discussed in the cases where uncertainty was the highest. Below, each one of the highlighted peaks are discussed:

- The compound with a retention time of 10.8 min was identified as cyclopentene, with a probability of 39%, according to the search library software. The next two most likely compounds were 2,3-diazobicyclohept-2-ene and 1,3-pentadiene, with 12 and 10% probability. The suggested nitrogen compound is unlikely since no diazo compound were detected during a study of the nitrogen containing compounds in this cracked naphtha sample.<sup>19</sup> The cracked naphtha is expected to contain diolefins, and some were identified in a past study, but all in very low concentrations, which also points that it is unlikely that this compound is a diolefin.<sup>12</sup> Since cyclopentene is a commercially available compound, its retention time was verified with the authentic chemical, and it was confirmed that the peak at 10.8 min belonged to cyclopentene.
- The three most likely compounds suggested by the MS search library software for the peak at 17.3 min are 1-methylcyclopentene, 3-methylcyclopentene, and 4-methylcyclopentene, with 18.3 %, 16.2%, and 7.86% of respective probability. In a past study in this naphtha sample,<sup>12</sup> the presence of 1-methylcyclopentene was confirmed using a model compound, and its concentration was determined to be 0.67 wt%. We did not confirm with a model compound in this study, since there is a high level of certainty that the compound is a cyclopentene with a methyl functionality.



**Figure 5.2.** Chromatogram of the cracked naphtha feed.

- The compound suggestions for the peak at 22.1 min include 1,4-dimethyl 2,3-diazabicyclohept-2-ene, 4,4-dimethylcyclopentene, and 3,5-dimethylcyclopentene with 31%, 7%, and 6.8% probability respectively. As argued before, the presence of compounds with a N=N functionality in this sample of naphtha is unlikely.<sup>19</sup> Although the probability given by the MS search library software is lower, the likelihood of having a dimethyl cyclopentene specie is higher when compared to that kind of nitrogen compound, hence we have a medium level on certainty that this compound is a dimethyl cyclopentene isomer.
- For the compound with a retention time 24.9 min the three most likely compounds were (1-methylethylidene)-cyclobutane, 4,4-dimethyl-cyclopentene, and 2,3-diazabicyclohept-2-ene, with probabilities of 15.3%, 11.4%, and 8.8% respectively. As mentioned before, the diazo compound is not likely. But the possibility of the compound being a cyclobutane cannot be discarded. Thus, the certainty of this compound being a cyclopentene is low.
- The three most likely compounds for the peak with a retention time of 25.0 were ethylidenecyclopentane, 1-ethylcyclopentene, and 3-ethylcyclopentene, with probabilities of 49.8%, 35.1%, and 7.6%. Hence, there is a high certainty that this compound is a 5-member ring olefin with an ethyl functionality, but the position of the double bond is not known.
- The compound suggestions for the peak at 28.4 min 1,5-dimethyl-bicyclohexane, 1,2,3-trimethylcyclopentene, 2,5-dimethyl-2,4-hexadiene. The probability given by the MS search software is 9.4%, 9.0%, and 8.3% respectively. Since the suggested compound are all likely to be present in the cracked naphtha, the certainty that this compound is a cyclopentene is low.
- The peak with a retention time of 29.9 had the following suggestions from the MS library: 1-ethyl-5-methylcyclopentene, methylethylcyclopentene, ethylidenecyclohexane, with probabilities of 26.2%, 10.3%, and 5.6%, respectively. All these compounds are likely to be present in the naphtha, hence, the level of certainty that the compound is an isomer of a cyclopentene specie having methyl and ethyl functionalities is medium.

A summary of what has been discussed above is contained in **Table 5.5**. Although there is uncertainty about the identity of some of the cyclopentene compounds, we assess their reactivity to thermal and acid catalyzed reactions in the next section.



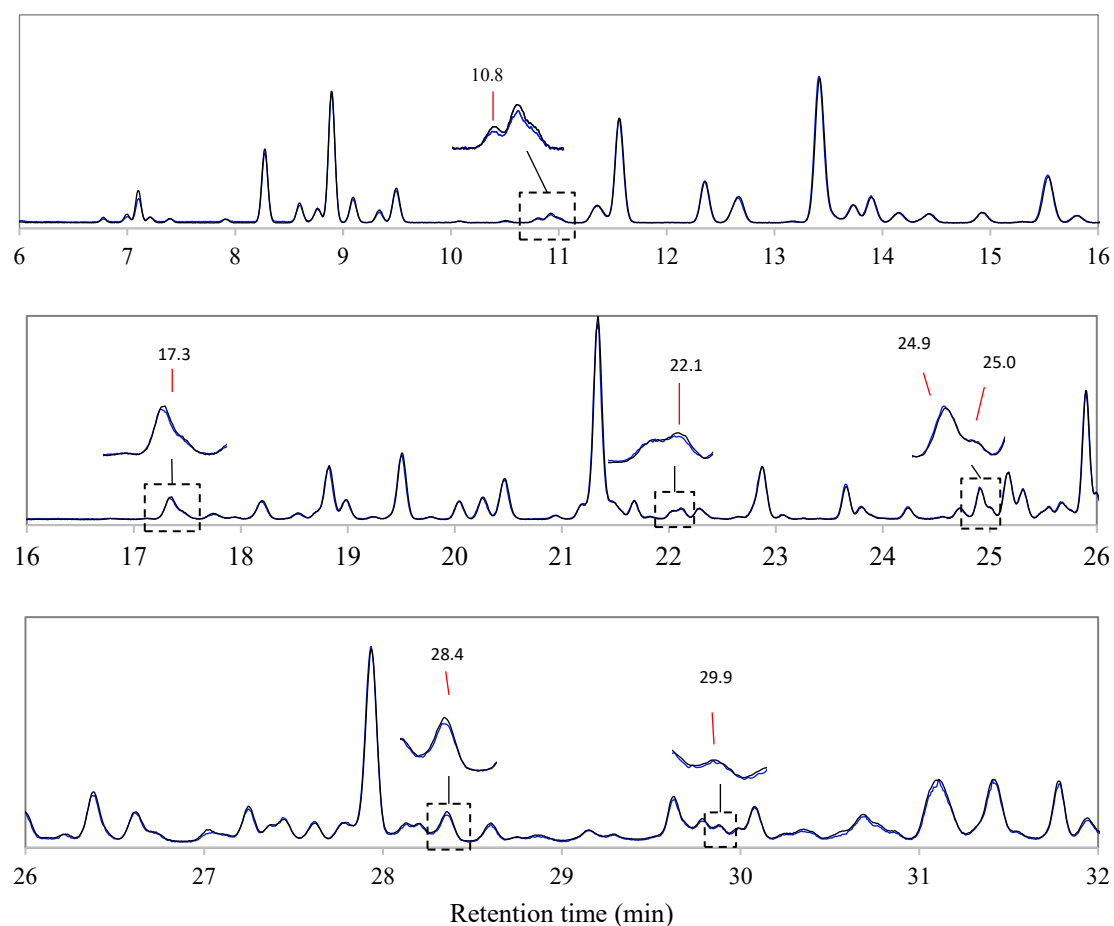
**Table 5.5.** Summary identified cyclopentenes

| Retention time (min) | Compound                                   | Level of certainty | Comments                                                                                |
|----------------------|--------------------------------------------|--------------------|-----------------------------------------------------------------------------------------|
| 10.8                 | Cyclopentene                               | Certain            | Confirmed with model compound.                                                          |
| 17.3                 | Methyl cyclopentene isomer                 | high               | The three most likely compounds were methylcyclopentene isomers.                        |
| 22.1                 | Dimethyl cyclopentene isomer               | medium             | Other possible compound included a N=N functionality, unlikely in this cracked naphtha. |
| 24.9                 | Dimethyl cyclopentene isomer               | low                | There is the possibility that the compound is a cyclobutane.                            |
| 25.0                 | Ethylidenecyclopentane / ethylcyclopentene | high               | Position of double bond uncertain.                                                      |
| 28.4                 | Trimethylcyclopentene isomer               | low                | Other 2 possible compounds are likely to be found in naphtha.                           |
| 29.9                 | Methylethylcyclopentene isomer             | medium             | The only other possibility is a compound likely to be found in naphtha.                 |

### 5.3.2. Thermal and catalytic reactivity of cyclopentenes in cracked naphtha

The reactivity of the identified cyclopentenes in the cracked naphtha was evaluated by subjecting the liquid mixture to reaction at 300 °C for 1 hour. The resulting chromatogram was overlapped with the original chromatogram of the feed, in **Figure 5.3**, to assess any change visually.

Changes could be observed in several peaks in **Figure 5.3**, including some of the peaks previously identified as cyclopentenes. Changes were observed in peaks at 10.8, 17.3, 22.1, and 28.4 after reaction at 300 °C, indicating that some of these species were consumed. The rest of the compounds in question, with retention times of 24.9, 25.0, and 29.9 min displayed no observable difference in the chromatogram. It should be noted that conversion is not necessarily limited to those compounds where the chromatogram visibly changed, it just means that conversion is below the detection limit of the analysis.

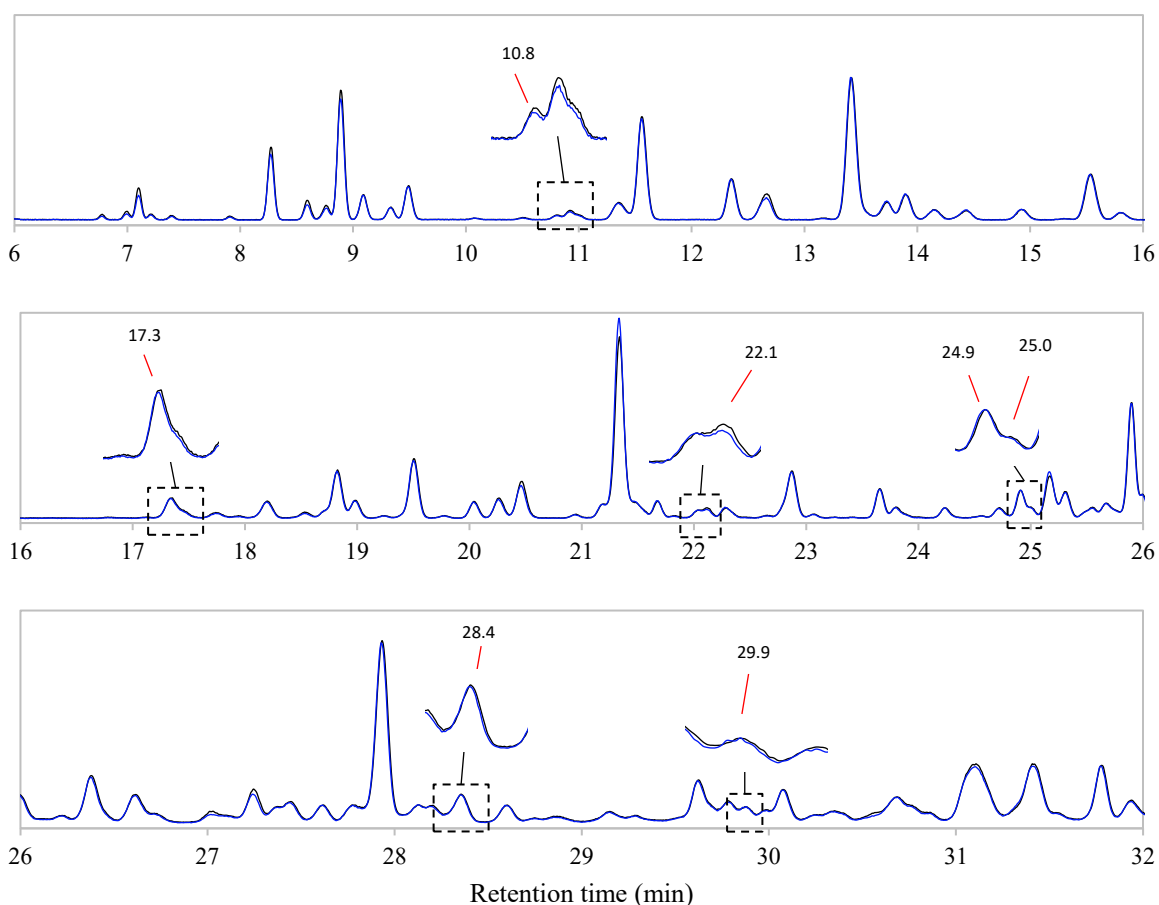


**Figure 5.3.** Chromatogram of cracked naphtha feed (black line) and after reaction at 300 °C (blue line).

To evaluate the reactivity of these compounds to acid catalysis, reactions of the cracked naphtha at 300 °C were carried out in the presence of the catalysts listed in **Table 5.2**.

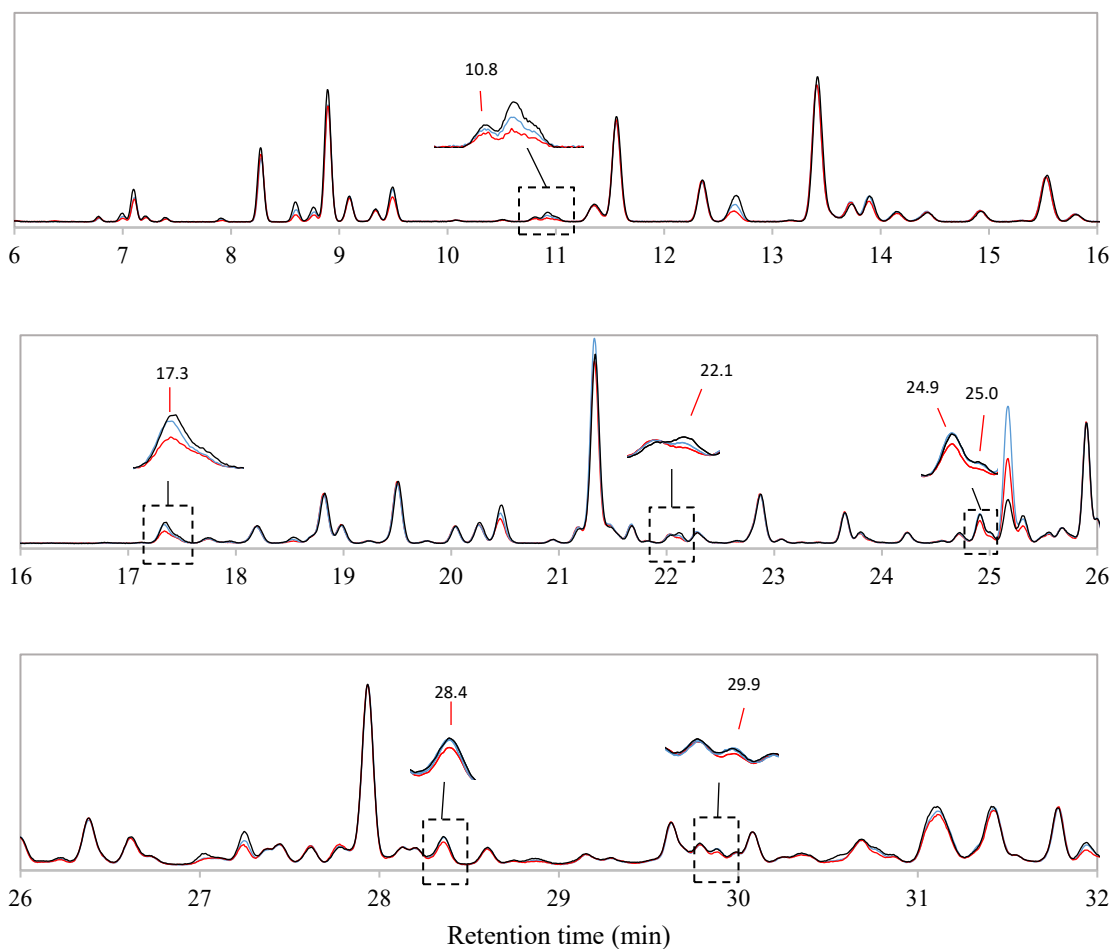
The chromatogram of the product of the reaction with Pural SB is overlapped with the naphtha feed chromatogram in **Figure 5.4**. This catalyst is a  $\gamma$ -alumina material, with only Lewis acid and base sites. When analyzing the chromatograms in **Figure 5.4**, a visible change was detected in peaks at 10.8, 17.3, and 22.1 min. The rest of compounds, including some that had been seen to react thermally over a 1 h period, as opposed to 30 minutes, did not show any changes. Again, it is worthwhile pointing out that the absence of changes did not imply absence of conversion, only that conversion that may have taken place, caused a change that is below the detection limit of the analytical technique used.

The reactivity of the compounds of interest to Brønsted acidity was evaluated using Siral 10 and Siral 30, catalysts listed on **Table 5.2**. The overlapping chromatograms of the feed and reaction products are contained in **Figure 5.5**. It was expected to see a change in the peaks that was proportional to acidity of the catalyst, i.e., a more pronounced change in the peak area when Siral 30 is used, being a catalyst containing more 30% silica and hence more Brønsted acid sites (see **Table 5.2**).



**Figure 5.4.** Chromatogram of cracked naphtha feed (black line) and after reaction with Pural SB at 300 °C (blue line).

As observed in **Figure 5.5**, all compounds of interest reacted over Siral 30, whereas only the peaks at 10.8, 17.3, and 22.1 min decreased after reaction over Siral 10. For those compounds where reaction caused a detectable change with both catalysts, the change observed appeared to be proportional to the acidity of the catalyst used, as expected.



**Figure 5.5.** Chromatogram of the cracked naphtha feed (black line) and product of the reactions with Siral10 (blue line), and Siral30 (red line).

A summary of the compounds reacting at each of the conditions studied is presented in **Table 5.6**. Comparing the outcome of the thermal reaction and the reaction with Pural SB, we could detect more compounds reacting when there is no catalyst present, albeit at double the reaction time. It appears that the Pural SB did not accelerate the rate of the olefin reactions and that the difference in conversion observed between **Figure 5.3** and **Figure 5.4** can be ascribed to the longer reaction time used for the thermal reaction.

In the case of the catalytic reactions, the results indicate that all 7 species studied reacted in 30 minutes at 300 °C in the presence of Siral 30, and only 3 observably reacted over Siral 10.

**Table 5.6.** Summary of reactivity of cyclopentene compounds.

| Retention time (min) | Compound                                   | Reactivity* |          |          |          |
|----------------------|--------------------------------------------|-------------|----------|----------|----------|
|                      |                                            | Thermal     | Pural SB | Siral 10 | Siral 30 |
| 10.8                 | Cyclopentene                               | x           | x        | x        | x        |
| 17.3                 | Methyl cyclopentene isomer                 | x           | x        | x        | x        |
| 22.1                 | Dimethyl cyclopentene isomer               | x           | x        | x        | x        |
| 24.9                 | Dimethyl cyclopentene isomer               |             |          |          | x        |
| 25.0                 | Ethylidenecyclopentane / ethylcyclopentene |             |          |          | x        |
| 28.4                 | Trimethylcyclopentene isomer               | x           |          |          | x        |
| 29.9                 | Methylethylcyclopentene isomer             |             |          |          | x        |

\*Reactivity measured by the visual comparison of the chromatograms before and after reaction.

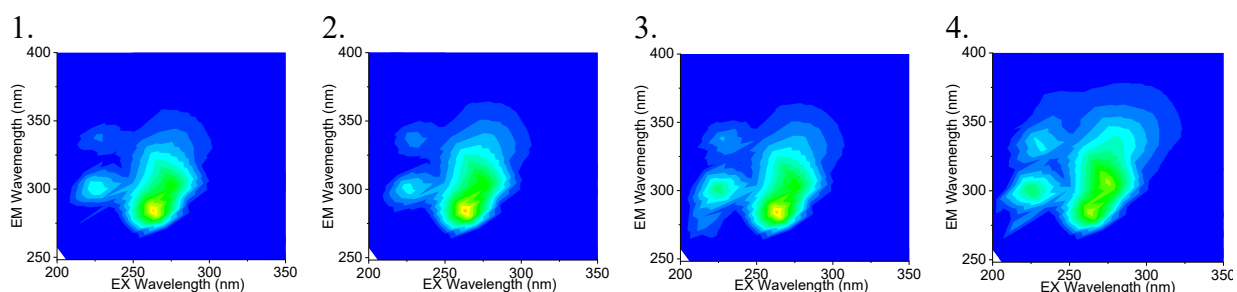
This study highlighted several analytical challenges when working with cracked naphtha. Identification of species by GC-MS analysis was tentative (**Table 5.5**) and discerning conversion based on a comparison of chromatograms (**Figure 5.3 - Figure 5.5**) was difficult. Observable changes presented evidence of conversion, but absence of observable changes did not present evidence of the absence of reaction. Nevertheless, the study showed that at 300 °C cyclopentenenes, and other species, were converted thermally and by acid catalysis.

### 5.3.3. Fluorescence spectroscopy of feed and reaction products

Since gas chromatography is limited when detecting changes that cannot be observed in the chromatograms of the sample mixtures, fluorescence spectroscopy was employed to verify if there were changes after reaction and how such changes compared to each other.

Fluorescence spectroscopy has been long used to track traces of fluorophore molecules in water and soil. Although its use on crude oil-related studies is limited, it has been used to characterized differences in composition.<sup>21</sup>

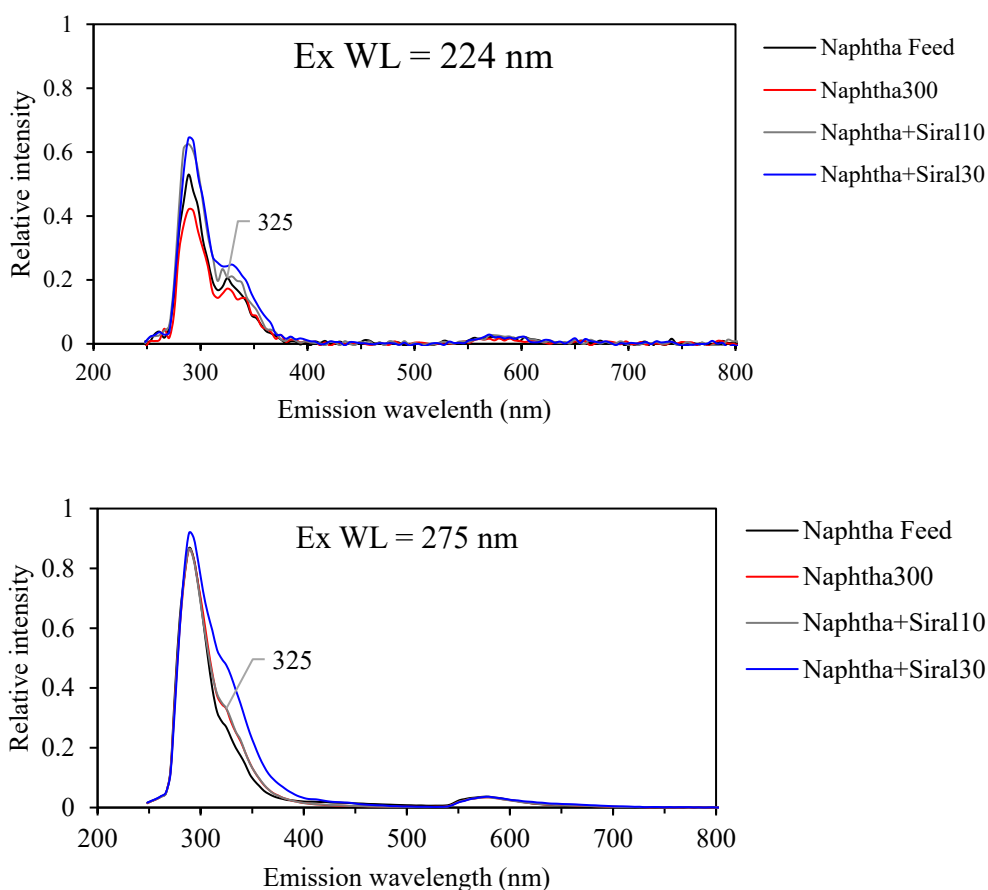
If the compounds present in the cracked naphtha undergo reactions producing heavy conjugated compounds, or consuming fluorophores, the fluorescence spectra should show such changes. The fluorescence spectra were measured for the cracked naphtha feed, as well as for the product of the non-catalyzed reaction, and the product from the reaction with Siral10 and Siral30. The solvent chosen and the high dilution ensures that quenching of the emitted light is avoided. The resulting contour plots are shown in **Figure 5.6**.



**Figure 5.6.** Fluorescence contour plots for (1) cracked naphtha feed, (2) cracked naphtha after 1h at 300 °C with stirring, and cracked naphtha after reaction with (3) Siral10 and (4) Siral30 at 300 °C for 30 min. EX = 200-350 nm. EM = 250-400 nm.

It is known that cracked naphtha is reactive, and that free radical reactions occur in the liquid bulk,<sup>8</sup> for this reason it was expected that changes upon heating could be traced with this technique. But little change was seen on the contour plot of the cracked naphtha subjected to the reaction with no catalyst when compared to the feed, **Figure 5.6**. Based on this qualitative observation, this could mean that the reactive compounds are not in enough concentration, or fluorophores are not part of this reaction, either as reactants or products. It is difficult to imagine that no change in fluorophore composition would take place as result of reaction, since the reaction products of free radical reactions in a mixture containing olefins are expected to be heavy conjugated molecules. On the other hand, qualitatively clear differences are seen with cracked naphtha samples after reaction with Siral10 and Siral30.

The highest intensities are obtained with excitation wavelengths of 224 and 275 nm, as seen in **Figure 5.6**. Fluorescence spectroscopy is a quantitative technique, and it was not necessary to rely only on the qualitative assessment based on the contour plots. The emission spectra at the 224 and 275 nm excitation wavelengths were normalized to the maximum intensity in the contour plots for each sample and plotted in **Figure 5.7** for comparison. Normalization to the highest intensity point allows one to compare the differences in the samples based on the emitting species present, removing instrumental or sampling effects.<sup>21</sup>



**Figure 5.7.** Emission spectra of different samples at excitation wavelength (Ex WL) of 224 and 275 nm.

When analyzing the curves shown in **Figure 5.7**, it is seen that the emitting spectra for an excitation wavelength of 224 nm decreases after reaction with no catalyst (red line), evidencing the

conversion of emitting species under this excitation wavelength. Also, in the same plot, a new peak appears at around 340 nm in the cracked naphtha after thermal reaction. After excitation at a wavelength of 275 nm, there is an increase of the emission spectra specifically at 325 nm. The observed increase in emission in both plots might indicate that some species emitting at such wavelength are formed during uncatalyzed reactions at 300 °C.

After catalyzed reactions, there was a visible increase in intensity at both excitation wavelengths (**Figure 5.7**), the sample after reaction with Siral 30 the one with most change. This could be interpreted as having the most emitting species after reaction with the most acidic catalyst, which is expected.

In the case of the reaction product of the cracked naphtha with Siral10 and Siral30, similar responses are obtained at an excitation wavelength of 224 nm, having an increase in the overall emission compared to the feed. While a significant change was seen in the emission spectrum with an excitation wavelength of 275 nm, after reaction with Siral30. The maximum intensity increased, as well as the intensity in the shoulder at 325 nm. After reaction with Siral10, only an increase at 325 nm is observed.

#### **5.3.4. Reactions of cyclopentene with Siral30**

Due to the complexities of working with cracked naphtha that were noted in Section 5.3.2, it was decided to use model compounds to improve interpretability of the experiments.

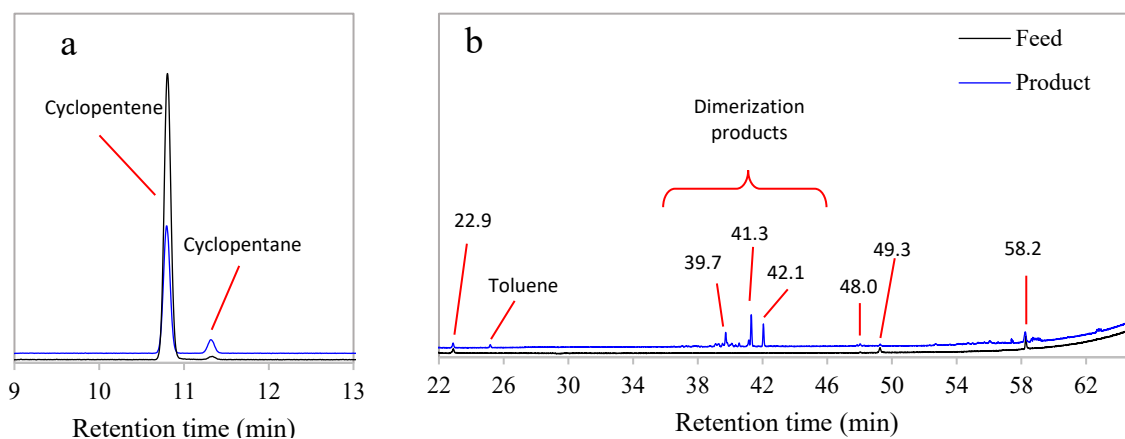
Since the cyclopentene species reacted in the presence of Siral 30, the reaction pathway was followed using model compounds. Cyclopentene was used as representative of the studied species, and 1-hexene was also used for comparison.

**Figure 5.8** shows the chromatograms of the feed and products of the reactions of cyclopentene over Siral 30 at 300 °C. The main products were cyclopentane and dimerization products.

Some impurities can be seen in the chromatograms at retention times 22.9, 49.3, 58.2 min. The compound at 22.9 min is a heptane isomer, present in the solvent as an impurity. The remaining compounds with retention times of 49.3, and 58.2 min also seemed to be solvent impurities, but when a second solvent was analyzed in the gas chromatograph, they were also present. This



suggests that such compounds are trapped species in the gas chromatograph's column. The mass spectrum of the compounds at 49.3 and 58.2 min show that they have molecular weights of 154 and 180 g/mol respectively. The suggestions of the MS search library for these compounds are biphenyl and a benzo-cinnoline isomers respectively.



**Figure 5.8.** Chromatograms of the reaction products of cyclopentene and Siral30.

While a quantitative analysis was not done, we can rely on the relative areas of the chromatogram peaks to give an idea on the consumption of the reactant and relative formation of the products. The peak at 22.9 min, a solvent impurity constantly present in the chromatograms, served as a convenient internal standard for semiquantitative comparisons. With this approach, we can refer to semiquantitative values of conversion and selectivity.

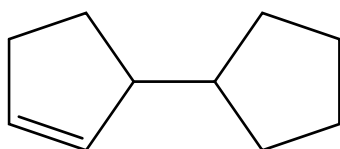
In the products chromatogram in **Figure 5.8a** (blue line), there was a decrease of 53% on the peak area of cyclopentene, which can be interpreted as a conversion of 53%. The peak corresponding to cyclopentane increased in area, indicating that some of the cyclopentene was converted to cyclopentane.

Toluene also appears present in traces in the product chromatogram, which might indicate its presence during reaction as a contaminant. This is a solvent commonly used for cleaning purposes in the laboratory and contamination could have occurred. Alkyl aromatic products were not detected, although the peak at 48.0 min could be within the range of elution of a mono-alkylated

aromatic compound. The identity of such compound was not determined due to its low concentration.

Heavier compounds were also formed eluting at retention times higher than 52 min. These compounds were not identified and had a low concentration.

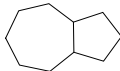
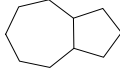
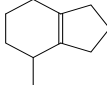
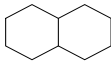
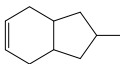
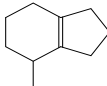
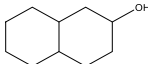
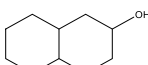

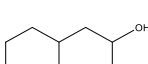
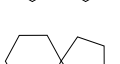
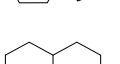
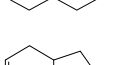
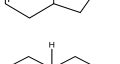
The addition products of cyclopentene, seen in the chromatogram retention time range of 38-43 min, do not seem to be simple cyclopentene dimers. Among the suggestions of the MS search library there are bicyclic compounds that might be produced from the addition and rearrangement of cyclopentene dimers. In fact, dimerized cyclopentene have only four possible double bond isomers and there are more than four peaks in the indicated retention time range. This means that at least some of those products had to be products from skeletal rearrangement. The mass spectra of the bicyclic compounds were analyzed to determine their identity. **Table 5.7** contains the suggestions of the MS search library for the most likely identity for the main products. The expected dimer from the dimerization of cyclopentene would be cyclopentyl-cyclopentene (**Figure 5.9**), which has indeed been reported as one of the reactions products of cyclopentene in zeolites.<sup>22</sup> But ring-fusion products, like the compounds listed in **Table 5.7**, are also possible. For example, octahydronaphthalene (possible product with a retention time of 42.1 min) was seen to formed in the reactions of cyclopentene on H-mordenite at low temperatures.<sup>23</sup>



**Figure 5.9.** Cyclopentene dimer, 2-cyclopentyl-cyclopentene.

Ring-fusion products could be diverse, but we could verify the presence of some of these by using the authentic compound. Decahydronaphthalene, or decalin, is commercially available as a *cis* and *trans* mixture. The retention time was determined for these compounds and coincided with the compounds at 39.7 and 41.3 min, as shown in **Figure 5.10**. According to the MS search library software, the *trans* isomer is that eluting at 39.7 min and the *cis* isomer is the one eluting at 41.3 min, this is logical since the boiling point of the *trans* isomer is lower than that of the *cis* isomer.

**Table 5.7.** Suggested compounds for the main products from reactions of cyclopentene on Siral30.

| Retention time (min) | Suggestions                               | Structure                                                                            | Probability* |
|----------------------|-------------------------------------------|--------------------------------------------------------------------------------------|--------------|
| 39.1                 | Bicyclo[5.3.0]decane (cis)                |     | 30.4%        |
| 39.3                 | Bicyclo[5.3.0]decane (cis)                |     | 12.5%        |
| 39.5                 | 2-Methylbicyclonon-1(6)-ene               |     | 36.2%        |
| 39.7                 | Decahydronaphthalene                      |     | 18.4%        |
| 39.8                 | 2-Methyl-cis-3a,4,7,7a-tetrahydroindan    |     | 12.7%        |
| 40.0                 | 2-Methylbicyclo[4.3.0]non-1(6)-ene        |     | 16.1%        |
| 40.1                 | Decahydro-2-naphthalenol                  |    | 34.1%        |
| 40.3                 | Decahydro-2-naphthalenol                  |    | 28.6%        |
| 40.6                 | Spirodecane                               |   | 14.9%        |
| 41.2                 | Decahydro-2-naphthalenol                  |  | 9.2%         |
| 41.3                 | Spirodecane                               |   | 26.8%        |
|                      | Decahydronaphthalene                      |   | 21.6%        |
| 42.1                 | 2-Methyl-trans-3a,4,7,7a-tetrahydroindane |   | 10.4%        |
|                      | Octahydronaphthalene                      |   | 8.5%         |

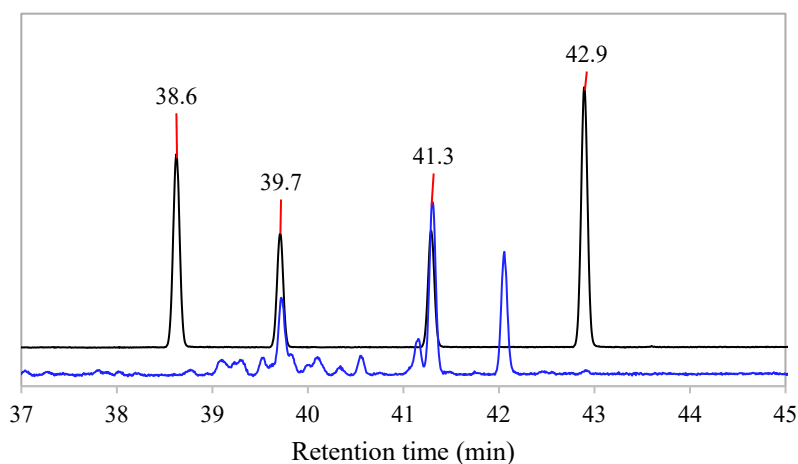
\*Probability given by the MS search library.

Although not suggested by the MS search library, the retention times for possible products like indene and tetrahydronaphthalene (tetralin) was determined. Indene and tetrahydronaphthalene eluted at 38.7 and 42.9 min, respectively, as shown in **Figure 5.10**. Among the reaction products

(blue line), there is a compound eluting at 42.9 min, that would correspond to tetralin, but it is present at very small amounts.

Indene is not present in the product mixture, but the likely product would be methyindene because it is a C<sub>10</sub> molecule, as the rest of the products from the cyclopentene dimerization, whereas indene has only 9 carbons. There are 3 possible isomers for methyindene, but verification of the retention times was not done since not all the authentic compounds are commercially available. The additional -CH<sub>3</sub> of the methyindene could place the molecule in the retention time range observed for dimerization products of cyclopentene (higher boiling point), but the mass spectra of the main reaction products do not point to indene, as explained in Appendix B.

Three of the products were tentatively labeled as decahydro-naphthanols (C<sub>10</sub>H<sub>18</sub>O). Whatever the identity of those compounds, the presence of oxygen suggests that olefin hydration took place, with the catalyst being the likely source of the water.

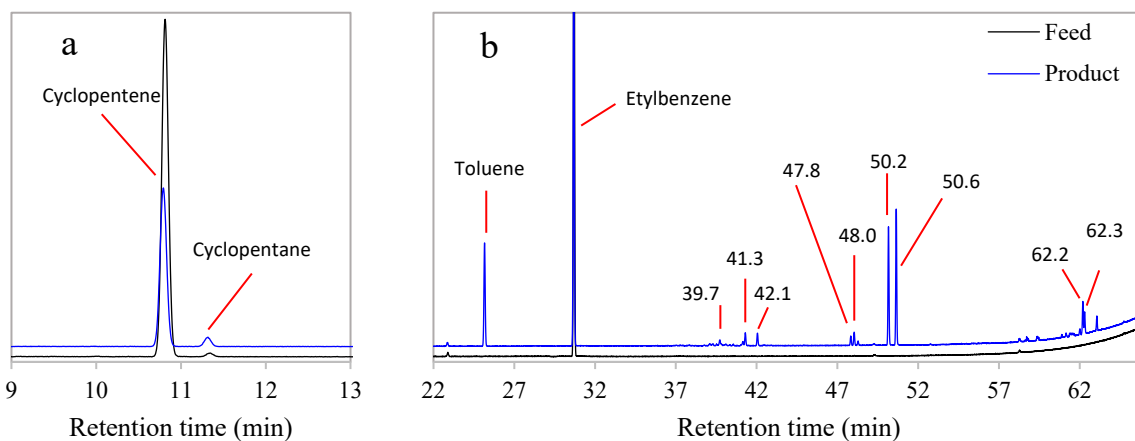


**Figure 5.10.** Chromatogram of model compounds (black line) and dimerization products of cyclopentene (blue line).

### Reactions of cyclopentene in the presence of ethylbenzene

Since olefins can react with aromatics through olefin-aromatic alkylation, the reaction was also carried out in the presence of these molecules. The chosen compound to represent the aromatics was ethylbenzene, since it is a compound found in the naphtha.

The reaction product of cyclopentene and ethylbenzene on Siral 30 can be observed in **Figure 5.11**. The same product distribution of bicyclic compounds (38-43 min) was obtained as in reactions of cyclopentene on Siral 30. A semiquantitative approach was taken to compare the formation of cyclopentene dimers in the presence and absence of ethylbenzene, and the results are in **Table 5.8**. The relative areas were obtained normalizing the area of each peak to that of the peak at 22.9 min, which is constant throughout the chromatograms since it is an impurity in the solvent. The relative areas are lower in the case of the reaction of cyclopentene in the presence of ethylbenzene, which indicates that the selectivity of the reaction was shifted. The consumption of cyclopentene (retention time 10.8 min) as a reactant also varied in both reactions, as seen in **Table 5.8**. These values represent a conversion of 28% in the presence of ethylbenzene, versus 53% in the case of the reaction of cyclopentene alone.



**Figure 5.11.** Chromatograms of the reaction products of cyclopentene and ethylbenzene with Siral30.

Most of the products from this reaction were from the olefin-aromatic reaction pathway. Two ethylbenzene-cyclopentene single alkylation products were formed in a high proportion, with

retention times of 50.2 and 50.6 min (**Figure 5.11b**). Toluene was again present in the reaction and in a higher proportion. In this case some toluene alkylates were detected, with retention times of 47.8 and 48.0 min. Polyalkylation products also formed; the mass spectrum of the compound eluting at 62.2 min indicates that there is a high chance of it being a dicyclopentyl ethylbenzene type molecule. The compound eluting at 62.3 min has a molecular mass of 281 g/mol, according to the molecular ion in its mass spectrum, that would correspond to 1,3,5-tricyclopentylbenzene – suggested compound of the MS search library. This last compound does not have an ethyl or methyl functionality, which makes difficult to know if it is a product of toluene or ethylbenzene reactions with cyclopentene.

**Table 5.8.** Relative areas of cyclopentene dimers formed after reaction with Siral 30.

| Retention time (min) | Relative areas        |                                      |
|----------------------|-----------------------|--------------------------------------|
|                      | Reaction Cyclopentene | Reaction Cyclopentene + Ethylbenzene |
| 10.8                 | 25.44                 | 38.85                                |
| 39.7                 | 3.38                  | 1.74                                 |
| 41.3                 | 5.89                  | 2.61                                 |
| 42.1                 | 3.76                  | 2.53                                 |

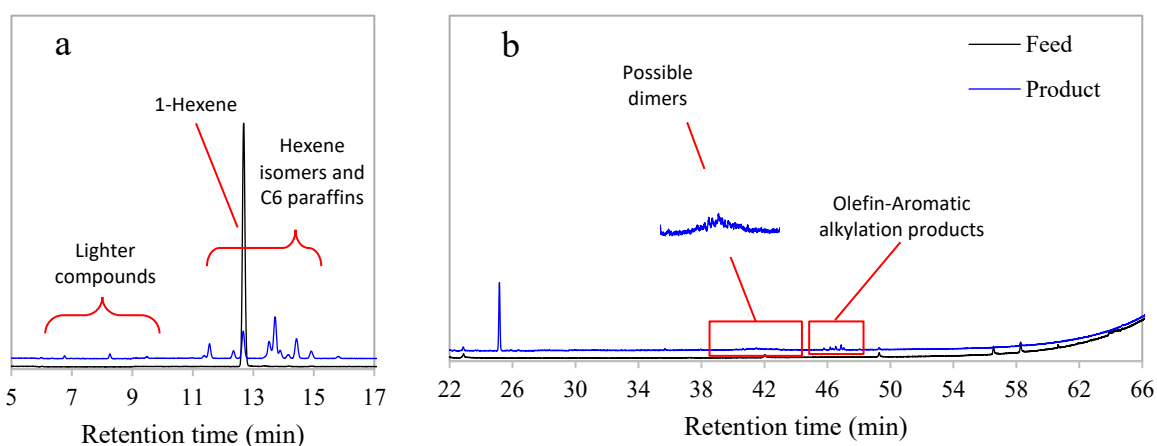
Note: Relative areas obtained normalizing the area of each peak to that of the peak at 22.9 min.

### 5.3.5. Reactions of 1-hexene with Siral30

Reactions of 1-hexene were also carried out to compare the products obtained from reactions of the cycloolefin with a linear olefin. The resulting chromatogram is in **Figure 5.12**.

Besides the impurities identified before (Section 5.3.3), the chromatogram of the feed on **Figure 5.12** has a couple more of species eluting at 42.0, and 56.5 min. These compounds did not appear on other chromatograms involving the same chemicals, so they are not contaminants in the reaction. However, the mass spectrum of each compound indicate they might be respective isomers of the compounds eluting at 49.3 and 58.2 min since they have the same molecular weight, i.e., 154 and 180 g/mol. This could indicate that they were also species trapped in the column.

The 1-hexene reacted substantially, with a conversion of 86%, as seen in **Figure 5.12a**. This may create the impression that 1-hexene is much more reactive than cyclopentene, but there are two important reaction pathways that are available to 1-hexene, but that are not likely to lead to observable conversion of cyclopentene. Double bond isomerization of 1-hexene leads to different products (2- and 3-hexenes), but double bond isomerization does not lead to a distinguishable difference in cyclopentene the absence of carbon-labelling. Skeletal isomerization of 1-hexene leads to different products (branched C<sub>6</sub> olefins), but skeletal isomerization of cyclopentene to methylcyclobutene isomers is not a favorable reaction pathway due to higher ring strain energy of the 4-membered ring.



**Figure 5.12.** Chromatograms of the reaction products of 1-hexene and Siral30.

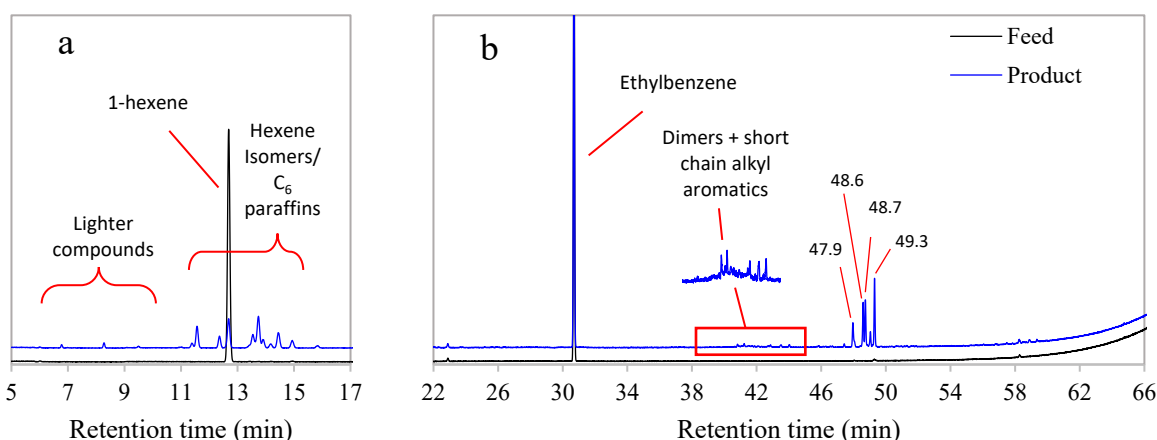
A big portion of the products of the reactions of 1-hexene with Siral30 were the result of double bond/skeletal isomerization of 1-hexene, as suggested by the presence of hexene isomers (from double bond and skeletal isomerization) in the retention time range of the chromatogram of 11-16 min, in **Figure 5.12a**. The increase in area in this region of the chromatogram represented 79% of the area reduction of the 1-hexene peak. In other words, it can be considered that the selectivity of 1-hexene conversion to double bond and skeletal isomerization reactions was 79%. The high conversion of 1-hexene compared to cyclopentene should therefore be seen in this context. Of the 86% conversion noted, only 18% conversion was by product forming pathways to heavier products that could be compared to that of cyclopentene. C<sub>6</sub> paraffins were also detected in small

concentration in the same 11-16 min retention time region, but does not affect the conclusion that cyclopentene was more reactive for reactions that could lead to deposit formation.

Dimers of 1-hexene were not detected. Although there are some changes in the chromatogram in the region of 39-44.5 min (**Figure 5.12b**), which would be the retention time range expected for hexene dimers, the identity of the peaks was not confirmed. Due to the increased likelihood of dimerization of branched C<sub>6</sub>-isomers, it is speculated that skeletal isomerization may have contributed to the formation of heavier products, which would also explain some of the cracking products, since longer chain olefins can adopt more structures containing secondary and tertiary carbocations that can be cracked more easily.<sup>24</sup> The presence of lighter products like isobutane (6.8 min), 2-methylbutane (8.3 min), and pentene (9.5 min), detected in small concentrations (**Figure 5.12a**), could be evidence of addition + cracking reactions during this experiment. Olefin-aromatic alkylation products were the result of the presence of toluene as a contaminant, and they are seen in the range 45-48 min in the chromatogram.

#### *Reaction of 1-hexene with Siral 30 in the presence of ethylbenzene*

In the case of the reaction of 1-hexene with the aromatic, the peak area was reduced by 85% (**Figure 5.13a**), a similar conversion to that seen without the aromatic (86%). The same distribution of lighter compounds than in the case of the reaction of the olefin alone with the catalyst is observed (**Figure 5.13**).



**Figure 5.13.** Portion of the chromatograms of the reaction products of 1-hexene + ethylbenzene and Siral30.



To better compare the impact of having ethylbenzene in the reaction mixture, the relative areas of the products, grouped in reaction classes, are summarized in **Table 5.9**.

**Table 5.9.** Relative areas of 1-hexene products after reaction on Siral 30 at 300 °C.

| Retention time (min) | Products        | Relative areas    |                                  |
|----------------------|-----------------|-------------------|----------------------------------|
|                      |                 | Reaction 1-hexene | Reaction 1-hexene + Ethylbenzene |
| 11-16 <sup>a</sup>   | Isomerization   | 36.58             | 36.66                            |
| 39-44.5              | Dimers          | 8.76              | 9.66                             |
| 44.5-50              | Alkyl aromatics | 3.27              | 44.58                            |

<sup>a</sup>Area of 1-hexene peak (at 12.7 min) was subtracted.

Note: Relative areas obtained normalizing the area of each peak to that of the peak at 22.9 min.

Double bond and skeletal isomerization products, eluting in the retention time range of 11-16 min, were present in nearly equal concentrations that in reactions without the aromatic. Since these are intramolecular reactions, the inclusion of a second reactant might not have affected them.

The agglomeration of peaks seen for 1-hexene with retention times 39-44.5 min (**Figure 5.12**), was also observed in the reactions with the aromatic. Due to their retention time, there is the suspicion that they might be dimers. Their identity was not confirmed with the mass spectra since their low concentration and potential overlapping elution of more than one species did not result in well-defined spectra to interpret. But this time there were also some peaks of larger area, and identification of those species was possible. Short chain alkyl aromatics like 1-ethyl-3-isopropylbenzene, 1-(1,1-dimethylethyl)-3-ethyl-benzene, and 1-methyl-2-(1-ethylpropyl)-benzene were formed, which can be the product of alkylation reactions of ethylbenzene with shorter chain olefins from oligomers cracking reactions. The elution of these short chain alkyl aromatics in this retention time range could have been the reason for the slight increase of the relative area seen in **Table 5.9**.

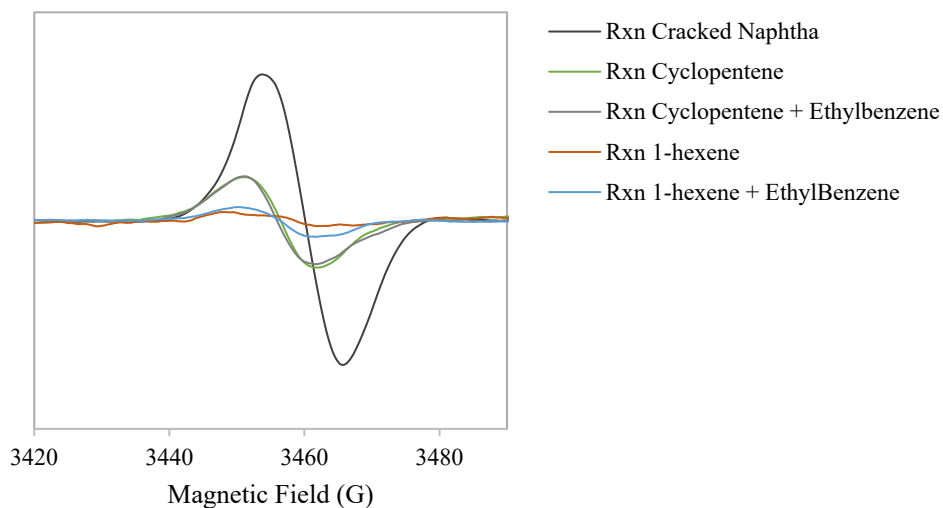
Alkyl aromatics of longer chain are the main products formed, in the residence time range of 47-50 min of the chromatogram in **Figure 5.13b**. According to their mass spectra, all these compounds have a molecular weight of 190 g/mol, which corresponds to monoalkylated products of 1-hexene

and ethylbenzene. In the portion of the chromatogram of 57-60 min some heavy compounds are seen, and they are believed to be dialkylated aromatics based on their retention times. There is the possibility that the alkylated ethylbenzene formed tetralin-like structures upon ring closure reactions, but among the products identified there is no indication of ring closure products.

### 5.3.6. Electron Spin Resonance (ESR) of the spent catalyst.

We can proportionally correlate the free radical content of the spent catalysts to the amount of condensed polyaromatics present on the catalyst surface. This inferred relationship is based on the fact that the coke formed on the acid catalyst surface has persistent free radicals, as many other polyaromatic mixtures.<sup>7,25,26</sup> A similar approach was taken in Chapter 3, where the free radical content of spent catalyst samples was correlated with the aromaticity of the carbonaceous deposits.

Using ESR we can assess the effect of each reactant on the catalyst deactivation, since the formation of deposits containing heavy polyaromatics is the main cause of deactivation, as found in Chapter 3. The spent Siral 30 catalysts samples from reactions with the cracked naphtha and the olefinic model compounds were subjected to this analysis. The resulting first derivative of the ESR spectra can be observed in **Figure 5.14**.



**Figure 5.14.** ESR spectra of the spent Siral30 after reaction with cracked naphtha and model compounds.

The highest intensity signal was obtained for the spent Sira130 after reaction with cracked naphtha, and its double integral was used to normalize the rest of the values in **Table 5.10**.

**Table 5.10.** Free radical content relative to that of the spent catalyst from the reaction with cracked naphtha.

| <b>Experiment</b>                           | <b>Relative free radical content</b> |
|---------------------------------------------|--------------------------------------|
| <b>Reaction 1-hexene</b>                    | 0.08                                 |
| <b>Reaction 1-hexene + Ethylbenzene</b>     | 0.11                                 |
| <b>Reaction Cyclopentene</b>                | 0.36                                 |
| <b>Reaction Cyclopentene + Ethylbenzene</b> | 0.33                                 |
| <b>Reaction Cracked Naphtha</b>             | 1.00                                 |

Comparing the spent catalysts after reaction with cyclopentene and 1-hexene, the free radical content after reaction with the cyclic olefin is about 4 times higher (0.36 vs. 0.08). In the case of the reactions with the aromatic present, the free radical content is about 3 times higher for the reaction of cyclopentene (0.33 vs. 0.11).

The presence of ethylbenzene in the reaction changed the free radical content in the spent catalyst sample with respect to that of the reaction with the olefin alone, but such change is only of 3% when compared to the radical content of the sample after reaction with cracked naphtha. Also, the change observed in the presence of ethylbenzene represented an increase in the free radical content in the case of 1-hexene, and a decrease in the case of cyclopentene.

## **5.4. Discussion**

### **5.4.1. Thermal compared to catalytic conversion of cracked naphtha**

There is no doubt that species in the cracked naphtha can be converted using an acid catalyst. If we consider an olefinic feed reacting on an acid catalyst, we can expect to see products from intramolecular reactions like *cis/trans*, double bond, and skeletal isomerization, as well as intermolecular reactions like oligomerization and olefin-aromatic alkylation if aromatics are

present – as is the case of cracked naphtha. The reaction temperature, acid site strength, and acid site concentration of the catalyst dictate possible reaction pathways and the product distribution.

Double bond isomerization of olefins can take place over a wide range of temperatures. It has been observed to occur with 1-hexene on solid acids with strong acid sites even at room temperature,<sup>27</sup> and over a silica-alumina catalyst with significant conversion for double bond and *cis/trans* isomerization reactions at 150 °C.<sup>28</sup> If the catalyst contains medium/strong strength acid sites, it can catalyze oligomerization of olefins at 150-250 °C,<sup>29</sup> and aromatic alkylation at 220-350 °C.<sup>5</sup> At temperatures above 300 °C cracking reactions progressively become important,<sup>30</sup> especially if the olefins have 7 carbons or more.<sup>31</sup> At high temperatures, acid-catalyzed hydrogen transfer and cyclization reactions are also favored, a reason why coke formation on the catalyst is enhanced at higher temperatures.<sup>11</sup>

In the case of the olefinic material in the cracked naphtha, thermal reactions are not as straightforward as catalyzed reactions. Thermal reactions proceed via a free radical mechanism. Once radicals are formed, olefins can be involved in the reaction network, such as undergoing radical-olefins addition reactions.

Free radical chain reactions start by the cleavage of a covalent bond. The energy needed for a bond to break varies depending on the molecule. For the most abundant carbon-carbon bond in the skeletal structure, aliphatic C-C, the bond dissociation requires thermal cracking temperatures usually above 420 °C.<sup>32</sup> But, there are certain molecules that by comparison contain a weak C-H bond, which need temperatures as low 280-320 °C to break.<sup>33</sup> These molecules are capable of donating the hydrogen via molecule induced radical formation, if a hydrogen acceptor molecule is present.<sup>33-35</sup>

It could be the case that the extent of thermal reactions in the cracked naphtha at the temperature studied (300 °C) are constrained by the concentration of those species that are able to undergo molecule induced radical formation. It appears logical that such reactions are slower or not significant when compared to acid catalyzed reactions. Nevertheless, whether thermal reactions have a role during the catalytic conversion of cracked naphtha, and whether thermal reactions contribute to deposit formation, have been two unanswered questions that we wanted to answer.

There is evidence of the thermal reactivity of cracked naphtha. In Chapter 3, the carbonaceous deposits in a catalytic bed were higher and more hydrogen depleted in the outlet of the packed bed reactor after reaction with cracked naphtha at a temperature of 325 °C, suggesting that free radical reactions took part in the reaction network that yielded such deposits. In Chapter 4, free radical reaction products were observed after adding a probe molecule to thermal reactions of cracked naphtha. But there has not been a direct observation of species in the cracked naphtha being consumed or formed upon heating, without involving additional reactants or catalysts.

In this study, after close observation of the chromatograms plotted in **Figure 5.3**, there was evidence that some of the monitored molecules (cyclopentenes) were being consumed during thermal reactions of cracked naphtha, although in lower amount than during catalytic reactions with Siral 30 (**Table 5.6**). Although the emphasis in this investigation was placed on cyclopentenes, the conversion of material in the cracked naphtha was by no means limited to the cyclopentenes (for example, see **Figure 5.5**). Changes due to thermal conversion (**Figure 5.3**) were less obvious in the chromatograms and appeared to be slower than changes due to acid catalyzed conversion (**Figure 5.5**). The study showed that there was a contribution of thermal reactions to the conversion of cracked naphtha at 300 °C. However, the extent of conversion is not necessarily a measure of the selectivity to products that are coke precursors. Evidence of thermal conversion could not be extended to be evidence of contribution to deposit formation without additional evidence.

Additionally, the results from fluorescence spectroscopy suggested that the concentrations and/or nature of fluorophores were being affected by thermal reactions, but again in a lesser proportion when compared to the catalytic effect, as seen in **Figure 5.7**.

Fluorophores tend to be molecules with conjugated double bonds and planar structures,<sup>36</sup> so although this does not include cyclopentenes (it has only one double bond), it could describe many other molecules present in the cracked naphtha feed, including some that have a cyclopentene substructure.

A shift in the fluorescence emission spectra at a specific excitation wavelength can indicate a change in concentration of a group of conjugated molecules. In **Figure 5.7** at an excitation wavelength of 224 nm, there was a decrease in the overall intensity of the peaks at 300 and 330

nm in the sample of cracked naphtha subjected to thermal reaction. On the other hand, at an excitation wavelength of 275 nm, there was an additional peak at 325 nm in the emission curve.

These observations can be interpreted as evidence of thermal conversion of molecules in the cracked naphtha able to absorb light at 224 nm and emitting at 300 and 330 nm, and of the formation of conjugated species able to absorb light at 275 nm and emitting 325 nm.

Since thermal conversion proceeds by a free radical mechanism, it involves radical propagation and hydrogen disproportionation steps. This reaction network could contribute to the formation of heavy unsaturated species with conjugated double bonds. Hence, the increase of the intensity in the fluorescence spectra shown in **Figure 5.7** (with an excitation wavelength of 275 nm) of the cracked naphtha after thermal reaction, is likely due to the formation of conjugated species through a free radical mechanism.

Thermal conversion relative to catalytic conversion contributed less to the formation for additional fluorophores. If we assume that the formation of fluorophores is indicative of the formation of larger species that could adsorb on the catalyst contributing to the formation of deposits, for which no direct evidence is presented, then it can be concluded that catalytic reactions of the cracked naphtha are the major contributor to the formation of coke precursors at 300 °C, although there is a clear contribution of thermal conversion too.

The question of whether thermal conversion contributes to deposit formation is therefore not fully answered. The answer is contingent on the assumption that an increase in fluorophores in a naphtha boiling range material is indicative of the formation of larger molecules and deposits.

#### **5.4.2. Reactivity of different olefinic compounds on an ASA catalyst.**

The ease with which olefins react on an acid catalyst, compared to saturated molecules, have earned them the general classification of being reactive. The reactivity of olefins is explained by the presence of a  $\pi$ -bond, which is a nucleophilic center, and it can act as a weak Brønsted-Lowry base reacting with strong acids.<sup>37</sup> When an olefin interacts with the Brønsted acid sites of a zeolite or ASA catalyst, it accepts a proton and forms a carbocation.

The reactivity of an olefin on an acid catalyst is directly related to the stability of the adsorbed carbocation in the absence of steric effects that hinder adsorption. The structure of the adsorbing olefin determines such stability. For this reason, the reactivity of olefins can be considered a spectrum, that is as broad as the existing structures of olefins.

The stability of a carbocation increases with increasing substitution and additional neighboring double bonds.<sup>38</sup> If we consider the molecules in question in this study, cyclopentene having a disubstituted double bond would form a more stable carbocation (secondary carbocation) than 1-hexene (primary or secondary carbocation depending on the carbon that is protonated), which has a monosubstituted double bond. Double bond isomerization proceeds easily, which would take the primary olefin to an internal olefin that would form a secondary carbocation regardless of the position of the protonation. It appears that the stability of the carbocation is not a differentiating feature for the two model compounds used in this study, since both olefins can form secondary carbocations.

For a more quantitative approach, we can rely on the heat of hydrogenation of an olefin as an indication of the stability of its carbocation. This is possible because the heat of hydrogenation of an olefin also follows a trend with the number of substituents of the double bond, decreasing with substitution of the double bond.<sup>39</sup> More stable olefins have a lower (absolute value) heat of hydrogenation.<sup>40</sup> Hence, we can expect that olefins with a lower heat of hydrogenation would form a more stable carbocation, reacting more easily. Taking the two model compounds used in this study, 1-hexene and cyclopentene, with heat of hydrogenation of -125 kJ/mol and -111.6 kJ/mol,<sup>41</sup> we see that cyclopentene would form a more stable carbocation. If we consider the internal olefins, *trans*-2-hexene and *trans*-3-hexene, products of the double bond isomerization of 1-hexene, they have a heat of hydrogenation of 116 and 117 kJ/mol. These olefins would still form a less stable carbocation than cyclopentene. Note, this does not imply anything with respect to the kinetics, and heat of hydrogenation is used only as an indirect measure of the relative stability of the carbocation on the catalyst surface.

Even though cyclopentene carbocation is more stable, 1-hexene seems to have been consumed in a higher proportion; 86% of 1-hexene reacted (**Figure 5.12**), versus only 53% of cyclopentene

(**Figure 5.8**). However, conversion on its own is not useful to determine the reactivity for heavier product formation that could potentially lead to deposits.

As observed in Section 5.3.5, the main reaction pathway for 1-hexene are isomerization reactions, with 79% of the converted 1-hexene forming double bond and skeletal isomerization products (main product form seen in the retention times 11-16 min in **Figure 5.12**). Upon adsorption of 1-hexene on the acid catalyst and formation of the carbocation, the double bond shifts towards the most thermodynamically favored position, forming a mixture of 2- and 3-hexenes in their *trans* or *cis* configurations.<sup>28,30</sup> A portion of the 1-hexene adsorbed in the catalyst will also reconfigure their skeletal structure, producing branched C<sub>6</sub> molecules.<sup>30</sup> The observations about isomerization in this study are therefore congruent with the literature.

Isomerization reaction pathways are in principle also available to cyclopentene, but double bond isomerization would not lead to identifiably different products, i.e., isotopically unlabeled cyclopentene would be isomerized to cyclopentene. Skeletal isomerization cyclopentene to methylcyclobutene isomers is not a favorable reaction pathway due to higher ring strain energy of the 4-membered ring. Thus, the noted conversion of cyclopentene excludes isomerization reactions. The conversion of cyclopentene to non-isomerization products is higher than that of 1-hexene.

Both olefins seemed to be able to undergo addition reactions. Addition reactions of olefins are relevant from a catalyst deactivation perspective, since heavier compounds are required to act as coke precursors. Once the heavier molecules are retained on the surface, subsequent reactions like cyclization and hydrogen transfer can convert the deposits into coke.<sup>11</sup>

Although 1-hexene dimers were not individually identified, there is the possibility that they were present in as products in the 38-45 min retention time region, as highlighted in **Figure 5.12** and explained in Section 5.3.5. The selectivity of 1-hexene to the dimers (area percentage of products) was 18%. 1-hexene would form dodecene upon dimerization, and as seen with 1-hexene itself double bond and skeletal isomerization are possible on this catalyst. The number of possible isomers of dodecene is vast, which would explain why many dimers would form but none at high concentration. There are many peaks in the chromatogram at 38-45 min retention time and due to



the proximity, elution of some could be overlapping. This hindered identification beyond compound class and molecular mass.

In the case of cyclopentene, dimers were the clear main product from the reaction. The identified dimers seem to be the products of several reactions in series, for example, leading to products like decalin. Although decalin has not been reported as a product of cyclopentene dimerization, octalin has.<sup>23,42</sup> The formation of octalin from cyclopentene proceeds via the formation of an octalin radical cation thought to be the result from transannular ring closure of a 1,6-cyclodecadiene molecule. Hydrogen migration to the radical cation would yield octalin.<sup>23</sup> The rapid formation of bicyclic compounds from radical cations has not been reported for linear mono-olefins, at least not at the rate seen for cyclopentene.

The implications of the formation of bicyclic compounds as main products can be seen in the ESR spectra of the spent catalysts (Section 5.3.6). The spent catalyst after reaction with cyclopentene has 4 times the free radical content as that of 1-hexene, as seen in **Table 5.10**. As explained in Section 5.3.6, we can relate the free radical content of the spent catalysts to the amount of condensed polynuclear aromatics, since coke formed on the acid catalyst surface has persistent free radicals, as reported for many other polyaromatic mixtures.<sup>7,25,26,43</sup>

In principle, 1-hexene can also form heavy deposits. In fact the formation of such deposits has been explained to occur through acid catalyzed reactions of 1-hexene that yield cyclopentadiene as an intermediary, which continues to react towards aromatics and alkylated indanes and indenenes, as well as higher aromatics.<sup>44</sup> This reactions of 1-hexene were not seen to occur in the ASA catalyst, probably because the reaction step from 1-hexene to cyclopentadienes require strong acid sites, as those found in zeolites.<sup>45</sup>

Although the implied causal link between the formation of bicyclic compounds and the persistent free radical content related to polynuclear aromatics in the deposits has not been demonstrated, there is a correlation. The contribution of the formation of addition products to a higher rate of polyaromatic deposit formation could potentially be linked to the inability of the product formed to readily desorb from the catalyst surface, or the ability of the desorbed products to undergo subsequent reactions leading to deposits.

Product desorption could also be affected by the low solubility of the new product in the liquid bulk, the ability of the product to diffuse out of the pores,<sup>46</sup> or a higher stability of the new carbocation. Desorption is an endothermic process, which needs the input of energy to dissociate the surface specie. If the carbocation specie is stabilized, by resonance effects for example, the energy needed for it to desorb would be higher.

The products from dimerization of cyclopentene are bulkier molecules than 1-hexene dimers. If those bulky molecules could form more stable carbocations it would favor more acid catalyzed reactions like addition or hydrogen transfer. These reactions would increase the product molecular size and unsaturation, which would lead to conjugated systems that would potentially lead to even more stable carbocations due to the resonance stabilization possible in these structures.

Desorbed products can also undergo addition and hydrogen transfer reactions in the liquid, if they are able to start free radical reactions by reactions like molecule induced homolysis.<sup>8</sup> Decalin, which is the main product from the reaction of cyclopentene, is not a good hydrogen donor/acceptor and it is unlikely that it would start this kind of reactions at 300 °C. But unsaturated analogs of decalin (like dihydronaphthalene) could act as hydrogen donors,<sup>47</sup> and could have been present at some point and end up as the condensed species present in the spent catalyst.

Directionally there is therefore evidence to support the claim that there is a causal link between the increase in number of condensed rings, as exemplified by the formation of condensed bicyclic products, and the pathways leading to deposits.

Cracking products were present only on reactions of 1-hexene. Proof for this are the lighter compounds in chromatograms in **Figure 5.12a** and **Figure 5.13a**, and the formation of short chain alkyl aromatics seen in reactions of 1-hexene and ethylbenzene. No evidence of cracking was seen in reactions of cyclopentene. Cracking of C<sub>6</sub> olefins at 300 °C is difficult due to nature of the carbocation intermediates of the reactants and products. It is more likely that the sequence of steps is skeletal isomerization of the C<sub>6</sub>, dimerization, and then cracking.<sup>24</sup>

Cracking reactions have been suggested as an indication of a faster rate of deposit formation,<sup>11</sup> but the occurrence of these reactions did not correlate with the amount of condensed polyaromatics detected in the catalyst samples in this study. The addition products of cyclopentene conversion,

unlike those from 1-hexene conversion, were not prone to cracking and resulted in a higher amount of heavier material (**Table 5.10**).

It is clear that cyclopentene has a significant effect on the formation of deposits on an acid catalyst, but such effect cannot account for all the deposits formed during the reaction of cracked naphtha. The free radical content of the spent catalyst after reactions with the cracked naphtha is 3 times higher than that recorded for the spent catalyst after reaction with cyclopentene. Additionally, cyclopentene and cyclopentene-containing species are present only in low concentrations in the cracked naphtha. This indicates that there is a large concentration of molecules able to contribute to the formation of deposits other than species with a cyclopentene substructure. Such molecules could be present in the cracked naphtha or are being formed during reactions, having a similar effect as the bicyclic compounds formed during reactions of cyclopentene. This was already speculated in Chapter 3, when it was observed that the concentration of deposits in the catalytic bed increased towards the outlet of the reactor.<sup>7</sup>

Even though the olefinic content of cracked naphtha is regarded as a measure of its potential reactivity or its deposit forming tendencies, we have seen here that it is affected by the specific nature of the olefin in question. Although most olefins would be reactive on the acid sites, not all unsaturated molecules would yield condensed molecules that would easily be retained by the catalyst surface. Although cracking occurs in reactions of 1-hexene on the acid catalyst, the formation of condensed bicyclic compounds, such as octalin, as intermediates in reactions of cyclopentene, seems to be a key step for the accelerated formation of polyaromatic condensed deposits detected with ESR.

In conclusion, it was found that cyclopentene was more reactive than 1-hexene for deposit formation over the acid catalyst at 300 °C, but that cracked naphtha contained species even more reactive for deposit formation.

### **5.4.3. Modification of olefin reactivity by aromatics**

Including an aromatic molecule in the reaction could limit olefins intramolecular reactions and olefin-olefin reactions by diluting both the catalyst surface concentration and concentration of olefins in the bulk fluid. One reason for this is that the formation of a carbocation, which is a key

step for olefin reaction, is limited through competitive adsorption. Aromatics can adsorb on the catalyst, occupying the acid sites and decreasing their availability for olefin protonation. This affects both intra- and intermolecular reactions by reducing the number of available acid sites for olefin adsorption.

The reactions follow a Eley-Rideal mechanism, which describes the reaction of an adsorbed molecule (carbocation) with a non-adsorbed molecule. If olefins are the only reactant, one would only observe dimerization products (or larger oligomers). In a mixture containing olefins and aromatics, we can expect to see a decrease in dimerization products since part of the adsorbed olefins are reacting with the aromatics forming alkylaromatics.

Both acid site availability and dilution of the olefins in the liquid can explain what was seen with cyclopentene. Cyclopentene's conversion nearly halved after reaction with ethylbenzene (28%) compared to the reaction in the absence of the aromatic (53%). This shift was also observed in the concentration of dimerization products, which decreased when the aromatic was present (**Table 5.8**). This suggested that ethylbenzene competed with cyclopentene for adsorption and that the surface coverages of the species were near equal. Since adsorbed ethylbenzene does not measurably participate in surface reactions at 300 °C, but occupies acid sites, conversion is decreased in proportion to the fraction of acid sites that are occupied by ethylbenzene as opposed to cyclopentene.<sup>48</sup>

In the case of 1-hexene, the presence of ethylbenzene did not seem to affect the conversion (86% and 85%), or the product distribution of the reaction in the absence of the aromatic beyond the generation of alkyl aromatics. The concentration of double bond and skeletal isomers was not affected (**Table 5.9**). While there was a slight increase in the relative area in the retention time range assigned to the dimerization products, this is likely due to the elution of short chain alkyl aromatics in this region of the chromatogram (**Figure 5.13**). Hence, the concentration of dimers can also be considered practically unchanged. On the other hand, the alkylated ethylbenzenes were also present and were the main product.

This indicates that ethylbenzene did not observably hinder the adsorption of the linear olefin, and that 1-hexene adsorbed preferably on the active sites being able to react on monomolecular reactions. Moreover, the little effect on the concentration of the dimers despite of the formation of

alkylaromatics could point to the fact that different olefinic species are reactive to specific addition reactions. This was observed by Nel and de Klerk,<sup>49</sup> during the alkylation of benzene with hexene dimers over solid phosphoric acid. They found that branched olefins would preferably dimerize, whereas linear olefins preferred the alkylation pathway.

Since the presence of the aromatic limits olefin-olefin addition reactions of cyclopentene, as seen in **Table 5.8**, we can expect a decrease in the formation of heavy oligomers. In fact, commercial olefin-aromatic alkylation units operate at a high aromatic content to limit the formation of oligomers and multiple alkylation.<sup>50</sup> However, it does not preclude the formation of alkylated aromatics, and even multiply alkylated aromatics.

Hence, the implication of the presence of aromatic during reactions of a mixture containing olefins on an acid catalyst would be a reduction of the deposits caused by the formation of oligomers. This was not exactly seen in the ESR spectra (**Figure 5.14** and **Table 5.10**), which, as mentioned before, can offer an indication of the amount of condensed polyaromatics by correlating it to the free radicals content of the spent catalyst (Section 5.3.6). For the spent catalyst sample after reaction with cyclopentene, the free radical content decreased slightly when ethylbenzene was present. This was expected due to the above mentioned. But this slight decrease in radical content does not match the reduction in conversion or the reduction in concentration of dimerization product when the aromatic was present, which were nearly half of the values after reaction of cyclopentene alone (**Table 5.8**). If dimerization products are an indication of the formation of heavier addition products, we could expect to see reduction of the deposits equivalent to that seen based on the concentration of dimerization products. The minor decrease seen in the free radical content compared to the expectation, could be due to the possible involvement of ethylbenzene, or alkylated ethylbenzene in the formation of deposits, but no direct evidence is provided to support this speculation.

For 1-hexene there was a slight increase in the free radical content after reaction with the aromatic. An increase in the polyaromatic deposits can indicate that alkylation might be part of the reactions leading to the deposits. Instead of oligomerization and olefin-aromatic alkylation occurring in parallel, there could be alkylation reactions following oligomerization reactions. In other words, alkyl aromatics with long chain alkyl functionalities could be formed and could be retained in the

surface of the catalyst. Reactions like ring-closure and hydrogen transfer could follow,<sup>11</sup> and it would explain the increase in the radical content.

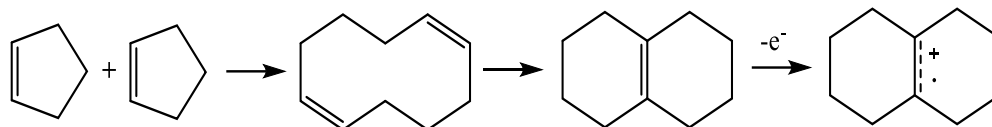
At the conditions studied, the presence of the aromatic slightly modified the deposit forming tendencies of the olefins studied. The results suggest that at the conditions studied olefin-aromatic alkylation products might take part in the reactions leading to the formation of deposits, although no direct evidence for this is provided.

#### **5.4.4. Formation of bicyclic compounds from acid catalyzed reactions of cyclopentene.**

The expected product from cyclopentene dimerization is cyclopentyl-cyclopentene isomers, as mentioned in Section 5.3.4. But the main products observed after reaction were decalin *cis* and *trans* isomers, confirmed through use of authentic compounds as *trans*- and *cis*-decalin with retention times 39.7 and 41.3 min respectively in **Figure 5.10**. Additionally, there is what is believed to be an octalin isomer, with retention time of 42.1 min in the same Figure. The reason for this tentative assignment is as follows. Decalin has a molecular weight (MW) of 138 g/mol, when a cyclopentene dimer's molecular weight should be 136 g/mol. This indicates that there was a hydrogen transfer step along the way, and therefore the likelihood that the compound present at 42.1 min is octalin (MW 136 g/mol) is high.

The formation of octalin from reactions of cyclopentene on H-mordenite has been reported before.<sup>23,42</sup> In these studies, the formation of octalin was detected using electron spin resonance (ESR), since a radical cation octalin specie was formed upon adsorption of cyclopentene on the acid catalyst. The formation of octalin from cyclopentene was explained in terms of the initial formation of 1,6-cyclodecadiene by metathesis, as is shown in **Figure 5.15**.<sup>23</sup> The 1,6-cyclodecadiene proceeds to react through intramolecular ring closure to form octalin. The reaction yielding the octalin radical cation is believed to occur on the Lewis acid sites (Al centers), since radical cations are not seen on Al-free zeolites.<sup>51</sup> The generation of radical cations on Lewis acid sites is thought to occur with molecules with sufficiently low ionization potentials.<sup>23</sup>

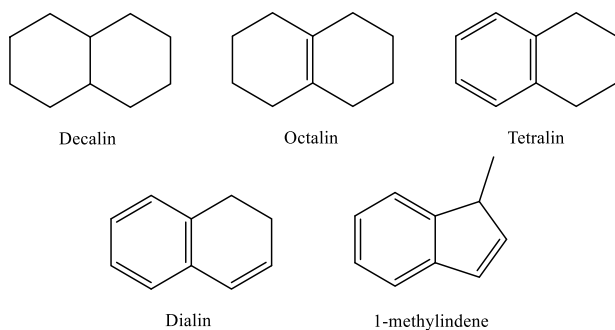
Decalin has been proposed as part of the mechanism leading to octalin radical cation,<sup>23</sup> but while in the literature about radical cation formation has not been reported<sup>23,42,51,52</sup> it has been seen to be formed on reactions of cyclopentene at catalytic cracking conditions.<sup>53</sup>



**Figure 5.15.** Possible reaction pathway for the formation of octalin from cyclopentene.

Subsequent reactions of the octalin radical cation are unclear. Proton transfer and electron transfer are possible reactions leading to the neutral decalin and octalin observed in the liquid product (**Figure 5.10**), and to unsaturated species that could have desorbed or stayed in the catalyst surface. After all, acid catalyzed hydrogen transfer has been widely accepted as the explanation for the high aromaticity of coke in zeolites.<sup>11</sup>

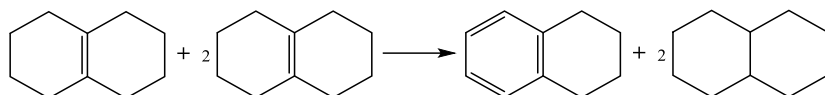
If decalin was formed by hydrogen transfer from the octalin neutral or ionic molecule, then unsaturated bicyclic compounds, like those in **Figure 5.16**, could be present as hydrogen disproportionation products. These compounds have been seen to be formed on reactions of cyclopentene at catalytic cracking conditions.<sup>53</sup> This piece of the puzzle is relevant to assess the complete role of cyclopentene on the formation of deposits on the catalyst. If partially unsaturated molecules reach the liquid, free radical hydrogen transfer and hydrogen disproportionation reactions can take place, due to the ability of partially unsaturated molecules to accept or donate hydrogen. These species can also be skeletally isomerized to form alkyl 5-membered rings, such as the 1-methylindene shown in **Figure 5.16**.



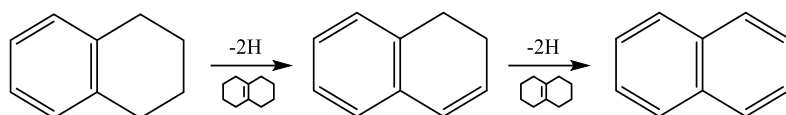
**Figure 5.16.** Possible bicyclic compounds present after reaction of cyclopentene with Siral 30.

Although it was not possible to determine its presence, there is a small peak at 42.9 min in the chromatogram of the reaction products of cyclopentene (**Figure 5.10**) that coincided with the retention time of tetralin. Tetralin is often used as a hydrogen donor solvent during cracking or

processing of heavy hydrocarbon mixtures,<sup>54,55</sup> The formation of tetralin is possible upon successive hydrogen transfer from an octalin molecule to other 2 octalin molecules, producing 2 moles of decalin and 1 of tetralin (**Figure 5.17**). Since tetralin can be further dehydrogenated producing dihydronaphthalene or naphthalene (**Figure 5.18**), which is more stable, is possible that it was consumed by the same types of hydrogen transfer reactions that caused it to be formed as an intermediate product.



**Figure 5.17.** Octalin-octalin hydrogen transfer.



**Figure 5.18.** Production of decahydronaphthalene and naphthalene from tetralin.

Other possible compounds that make good hydrogen donors and could have been formed due to hydrogen transfer reactions (catalyzed or uncatalyzed) are methylindane/methylindene and dihydronaphthalene (dialin) (**Figure 5.16**). As described in Appendix B, the presence of methylindene in the liquid product is unlikely. As for dihydronaphthalene there is no proof that this molecule is present in the liquid product. Naphthalene, being the completely dehydrogenated version of the bicyclic compounds was not detected on the chromatogram, making Figure 5.18 an unlikely reaction at the conditions studied.

Another possibility is that such unsaturated species remained retained on the catalyst surface. Although literature on cyclopentene adsorption on zeolites only confirmed the presence of the octalin radical cation on the surface, it is unlikely that it is the only surface specie in the reactions carried out during this study. Rhodes et al.<sup>42</sup> were the first to identify the octalin radical cation on H-mordenite upon adsorption of cyclopentene and they described the ESR spectra of octalin radical cation in the zeolite as a quintet of quintets. Such spectrum differs greatly from the well-defined first derivative curve we have observed in the present study (**Figure 5.14**). The spectrum we obtained is likely due to the overlapping of the spectra of different radical species present on



the catalyst surface. Our experiments were carried out at 300 °C, compared to the below zero temperatures used by Rhodes<sup>42</sup> and Crockett<sup>23</sup>, hence we can expect products from diverse acid catalyzed reactions to be present in the surface of the catalyst. Similar ESR spectra to ours were obtained in the spent catalyst samples after reactions of olefins on H-mordenite at high temperatures (>220 °C).<sup>43,56</sup> This could indicate that the unsaturated bicyclic compounds and various other species did not desorb, and hence could not be individually detected in the liquid. Furthermore, gas chromatography is limited in the boiling range of material that can be volatilized at column conditions.

Addition reactions of cyclopentene yielding bicyclic compounds is the preferred reaction pathway on Siral 30, and the probability of such reactions occurring through a surface octalin radical cation appears to be high. Moreover, the presence of desorbed decalin in the liquid product is an indirect proof of the formation of unsaturated species through hydrogen transfer, since decalin could only be formed upon saturation of the initial octalin, yielding more unsaturated products together with the formation of decalin. There is a possibility that the more unsaturated species were retained on the surface of the catalyst, which would explain the lack of such products in the bulk liquid and may indicate that these species contributed to the formation of deposits. This is the topic discussed next.

#### **5.4.5. Role of bicyclic compounds on the formation of deposits on the catalyst surface.**

Although there is no direct proof that unsaturated bicyclic compounds (other than octalin) were formed, the formation of decalin from octalin indicates that hydrogen transfer reactions occurred and that more unsaturated compounds, including more unsaturated bicyclic compounds are likely byproducts. The role of these unsaturated compounds could be relevant to the formation of deposits, and the mode in which they could contribute would be determined by where their reactions are taking place.

It was of interest to find out if unsaturated species like tetralin, dialin, and methyldiene were desorbed to the liquid, because their hydrogen transfer ability could promote molecule induce radical formation reactions, which would lead to free radicals in the liquid. This type of contribution towards the formation of deposits could help explain the observations made in Chapter 3, where it was hypothesized that some of the molecules leading to the deposits were being

formed in the reactor at the conditions studied. Although there is the possibility that tetralin was present at 42.9 min (**Figure 5.10**) in very small concentrations, there are no indications of the presence of other unsaturated bicyclic molecules in the liquid.

If these unsaturated species were not present in the liquid, it means that they were consumed by reactions leading to heavy molecules that could not elute, or that they could have stayed adsorbed in the catalyst surface. In both instances they could have an impact on deposit formation. If multiply unsaturated species remained on the catalyst surface, subsequent addition and hydrogen transfer reactions involving these species could easily happen, leading to heavier polyaromatics.

This is a plausible explanation if we consider the ESR spectrum of the spent catalyst, which indicated that radical species were present on the surface. The presence of radical species is an indirect measure of the amount condensed polyaromatics deposits on the surface since some such structures have persistent unpaired electrons.<sup>7,25,26</sup> Similar ESR spectra as found in this study were obtained in the spent catalyst samples after reactions of olefins on H-mordenite at high temperatures (>220 °C), and it was assigned to organic deposits.<sup>43,56</sup>

The formation of bicyclic radical cation compounds is not unique to reactions of cyclopentene. The same surface specie has been reported by Rhodes and Standing<sup>52</sup> after adsorption of C<sub>5</sub> and C<sub>6</sub> dienes (conjugated and isolated) on an acid catalyst. They refer to an acid mechanism for the formation of the bicyclic compound, which then converts to the radical cation. If we consider the fact that dienes are known to be enhancers of deposit formation in acid catalysts,<sup>11</sup> it makes us wonder if cyclopentenes should be regarded as species that are as problematic as dienes. Dienes have long been considered as source of catalyst deposits. Since acid catalysed reactions of cyclopentenes and dienes share the same radical cation bicyclic intermediate, it is plausible that the cyclopentenes and dienes share a pathway leading to the formation of deposits on the catalyst.

We can consider the formation of organic deposits in a catalyst as a series of reactions that end up in condensed polyaromatic structures. For linear olefins, for example, such reactions can occur in the order of isomerization, addition, cyclization, and hydrogen transfer. While in the presence of aromatics, alkylation and ring closure reactions are expected before hydrogen transfer. We have seen here that reactions involving cyclopentene have been demonstrated to rapidly yield bicyclic compounds, bypassing several reaction steps linear olefins would need to take. Bicyclic

compounds could contribute to the formation of deposits by being retained on the surface and further reacting through acid catalyzed addition and hydrogen transfer. Bicyclic molecules could also potentially react through free radical reactions.

While there is proof of the contribution of the surface reactions of the bicyclic compound, whether some of these desorbed and reacted further in the liquid, or if surface radical cations can interact with desorbed species in free radical reactions are questions that remain unanswered.

## 5.5. Conclusions

It was determined that the cyclopentenenes in the cracked naphtha are reactive species during acid-catalyzed reactions. Their contribution to the formation of deposits was evaluated using model compounds, and the following conclusions were drawn:

- Cyclopentene has a higher impact on the formation of condensed aromatic deposits on the catalyst when compared to 1-hexene. The contribution of the two studied olefinic species to the formation of organic deposits was evaluated in terms of the free radical content on the catalyst samples, since we can correlate the free radical content on the catalyst to the presence of condensed polyaromatic species. Even though 1-hexene's conversion was higher, the effect of the reactions of cyclopentene on the catalysts deposits was more significant, having 3 times the radical content compared to the catalyst after reaction with 1-hexene. The linear olefin reacted to form cracking, isomerization, and dimerization products, with special emphasis in the monomolecular reactions. While the only products detected for cyclopentene were dimers. The cyclopentene dimers detected are the product of reaction in series, that have an octalin radical cation as intermediary and could take part on hydrogen transfer reactions leading to decalin, which was detected on the liquid. These results highlight the impact of the type of olefin present versus the total concentration of olefinic compounds, when assessing the possible contribution of a feed to the formation of deposits on an acid catalyst.
- Olefin aromatic alkylation products seem to be part of the reactions leading to the formation of deposits. Although the presence of ethylbenzene only caused a slight change on the free radical content on the catalyst samples, on reactions with 1-hexene such change represented a slight increased of the total radical content. This can be explained by the possible retention of alkyl aromatics with long chain alkyl functionalities on the surface of the catalyst that could further react

through ring-closure reactions. On the other hand, the slight decrease in the radical content on the catalyst after reaction with cyclopentene, does not correspond to the high decrease in conversion of the cyclic olefin. Hence, there should also be a contribution of the olefin-aromatic alkylation products to the formation of deposits.

- Indene or methylindene isomers were not present among the products detected in the liquid after reactions with cyclopentene. But the presence of decalin in the liquid product of reactions of cyclopentene with the ASA is proof of the formation of more unsaturated compounds during reaction. Decalin is the product of hydrogen transfer reactions that involved octalin, a product of dimerization + arrangement reactions of cyclopentene. The relevance of the formation of more unsaturated compound, including more unsaturated bicyclic compounds like tetralin and dihydronaphthalene, is in their ability to start free radical chain reactions by hydrogen transfer, or when adsorbed in the catalyst, to contribute to the formation and growth of deposits.
- It was noteworthy that according to the literature and evidence from this study, cyclopentenes and dienes are both capable of forming octalin-type intermediate over acid catalysts. If octalin is an intermediate that could lead to deposit formation, as evidence of hydrogen disproportionation suggests, then it is plausible that the cyclopentenes and dienes share a pathway leading to the formation of deposits on the catalyst surface.
- During the study of the reactivity of cyclopentenes in cracked naphtha, there were indications of uncatalyzed reactions in the naphtha in the GC-MS chromatograms. With the help of fluorescence spectroscopy, it was determined that during the conversion of cracked naphtha on an acid catalyst both uncatalyzed and acid-catalyzed reactions take place. We were able to corroborate that the concentration of molecules able to emit fluorescence light (i.e., fluorophores) was being affected on uncatalyzed reactions of cracked naphtha at 300 °C. Since thermal conversion is a free radical mechanism, we can expect radical propagation and hydrogen disproportionation steps to produce heavy unsaturated species with conjugated double bonds that can act as fluorophores. Hence, the increase on the concentration of these species could shift the fluorescence spectra. However, when compared to the thermal effect, it was evident that acid catalyzed reactions have a higher impact on the conversion of species in the cracked naphtha, which was seen both in the GC-MS chromatograms and on the fluorescence spectra.

## **Acknowledgement**

The study was funded through the through the NSERC/CNOOC Ltd. Industrial Research Chair program in Field Upgrading and Asphaltenes Processing that is financially supported by the Natural Science and Engineering Research Council (NSERC) of Canada, Alberta Innovates, and CNOOC International.

## 5.6. References

- (1) Ipatieff, V. N.; Corson, B. B.; Egloff, G. Polymerization, a New Source of Gasoline. *Ind. Eng. Chem.* **1935**, *27* (9), 1077–1081.
- (2) Knottenbelt, C. Moss gas “Gas-to-Liquid” Diesel Fuels—an Environmentally Friendly Option. *Catal. Today* **2002**, *71* (3–4), 437–445.
- (3) Gray, M. R. Fundamentals of Partial Upgrading of Bitumen. *Energy Fuels* **2019**, *33* (8), 6843–6856.
- (4) de Klerk, A. Processing Unconventional Oil: Partial Upgrading of Oilsands Bitumen. *Energy Fuels* **2021**, *35* (18), 14343–14360.
- (5) Xia, Y. Acid Catalyzed Aromatic Alkylation in the Presence of Nitrogen Bases. MSc Thesis, University of Alberta, Edmonton, AB, Canada, University of Alberta, 2012.
- (6) Zerpa, N.; de Klerk, A.; Xia, Y.; Omer, A. A. Olefins Reduction of a Hydrocarbon Feed Using Olefins Aromatics Alkylation. Patent Application WO2015000061A1, 2015.
- (7) Uzcátegui, G.; de Klerk, A. Causes of Deactivation of an Amorphous Silica-Alumina Catalyst Used for Processing of Thermally Cracked Naphtha in a Bitumen Partial Upgrading Process. *Fuel* **2021**, *293*, 120479.
- (8) Uzcátegui, G.; Fong, S. Y.; de Klerk, A. Cracked Naphtha Reactivity: Effect of Free Radical Reactions. *Energy Fuels* **2018**, *32* (5), 5812–5823.
- (9) Nagpal, J. M.; Joshi, G. C.; Rastogi, S. N. Stability of Cracked Naphtas from Thermal and Catalytic Processes and Their Additive Response. Part I. Evaluation of Stability and Additive Response. *Fuel* **1995**, *74* (5), 720–724.

- (10) Nagpal, J. M.; Joshi, G. C.; Singh, I. D.; Kumar, K. Studies on the Nature of Gum Formed in Cracked Naphthas. In *6th International Conference on Stability and Handling of Liquid Fuels*; Vancouver, Canada, 1997; pp 543–550.
- (11) Guisnet, M.; Magnoux, P. Organic Chemistry of Coke Formation. *Appl. Catal. A: General* **2001**, *212* (1–2), 83–96.
- (12) Paez, N. Identification, Conversion and Reactivity of Diolefins in Thermally Cracked Naphtha. MSc. Thesis, University of Alberta, 2016.
- (13) Budnar Subramanya, A. S. Olefin Hydrotreating and Characterization of Olefins in Thermally Cracked Naphtha. MSc thesis, University of Alberta, 2020.
- (14) Beltramini, J. N.; Cabrol, R. A.; Churin, E. J.; Figoli, N. S.; Martinelli, E. E.; Parera, J. M. Catalyst Deactivation by Naphthas Doped with Hydrocarbons. *Appl. Catal.* **1985**, *17* (1), 65–74.
- (15) Tannous, J. H.; de Klerk, A. Asphaltenes Formation during Thermal Conversion of Deasphalted Oil. *Fuel* **2019**, *255*, 115786.
- (16) Siddiquee, M. N.; de Klerk, A. Hydrocarbon Addition Reactions during Low-Temperature Autoxidation of Oilsands Bitumen. *Energy Fuels* **2014**, *28* (11), 6848–6859.
- (17) Xia, Y. Acid Catalyzed Aromatic Alkylation in the Presence of Nitrogen Bases, University of Alberta, 2012.
- (18) Caillot, M.; Chaumonnot, A.; Digne, M.; van Bokhoven, J. A. The Variety of Brønsted Acid Sites in Amorphous Aluminosilicates and Zeolites. *J. Catal.* **2014**, *316*, 47–56.
- (19) Rao, Y.; de Klerk, A. Characterization of Heteroatom-Containing Compounds in Thermally Cracked Naphtha from Oilsands Bitumen. *Energy Fuels* **2017**, *31* (9), 9247–9254.
- (20) Paez, N. Y.; de Klerk, A. Diolefin Characterization in a Thermally Cracked Naphtha. *Prepr. Pap.-Am. Chem. Soc., Div. Energy Fuels* **2016**, *61* (1), 12–15.

- (21) Ryder, A. G. Analysis of Crude Petroleum Oils Using Fluorescence Spectroscopy. In *Reviews in Fluorescence 2005 Volume 2*; Geddes, C. D., Lakowicz, J. R., Eds.; Springer International Publishing, 2005; pp 169–194.
- (22) Nuntasri, D. High Selectivity of MCM-22 for Cyclopentanol Formation in Liquid-Phase Cyclopentene Hydration. *J. Catal.* **2003**, *213* (2), 272–280.
- (23) Crockett, R.; Roduner, E. Dimerisation and Transannular Reactions of Cycloalkenes on H-Mordenite. *J. Chem. Soc., Perkin Trans. 2* **1993**, No. 8, 1503.
- (24) Buchanan, J. S.; Santiesteban, J. G.; Haag, W. O. Mechanistic Considerations in Acid-Catalyzed Cracking of Olefins. *J. Catal.* **1996**, *158* (1), 279–287.
- (25) Chang, H.-L.; Wong, G. K.; Lin, J.-R.; Yen, T. F. Chapter 9 Electron Spin Resonance Study of Bituminous Substances and Asphaltenes. In *Asphaltenes and Asphalts, 2*; Elsevier Science B.V., 2000; pp 229–280.
- (26) Zhang, Y.; Siskin, M.; Gray, M. R.; Walters, C. C.; Rodgers, R. P. Mechanisms of Asphaltene Aggregation: Puzzles and a New Hypothesis. *Energy Fuels* **2020**, *34* (8), 9094–9107.
- (27) Lynch, D. T.; Wanke, S. E. Isomerization of Alkenes during Drying over Zeolites. *React. Kinet. Catal. Lett.* **1994**, *52* (2), 241–247.
- (28) BROUWER, D. The Mechanism of Double-Bond Isomerization of Olefins on Solid Acids. *J. Catal.* **1962**, *1* (1), 22–31.
- (29) Nicholas, C. P. Applications of Light Olefin Oligomerization to the Production of Fuels and Chemicals. *Appl. Catal. A: Gen* **2017**, *543* (March), 82–97.
- (30) Naragon, E. A. Catalytic Isomerization of 1-Hexene. *Ind. Eng. Chem.* **1950**, *42* (12), 2490–2493.
- (31) Sie, S. T. Acid-Catalyzed Cracking of Paraffinic Hydrocarbons. 1. Discussion of Existing Mechanisms and Proposal of a New Mechanism. *Ind. Eng. Chem. Res.* **1992**, *31* (8), 1881–1889.

- (32) Gray, M. R. Upgrading Reactions and Kinetics. In *Upgrading Oilsands Bitumen and Heavy Oil*; Gray, M. R., Ed.; The University of Alberta Press: Edmonton, Alberta, 2015; pp 151–209.
- (33) Rüdhardt, C.; Gerst, M.; Ebenhoch, J. Uncatalyzed Transfer Hydrogenation and Transfer Hydrogenolysis: Two Novel Types of Hydrogen-Transfer Reactions. *Angew. Chem., Int. Ed. Engl.* **1997**, *36* (1314), 1406–1430.
- (34) Sandhiya, L.; Jangra, H.; Zipse, H. Molecule-Induced Radical Formation (MIRF) Reactions—A Reappraisal. *Angew. Chem. Int. Ed.* **2020**, *59* (16), 6318–6329.
- (35) Pryor, W. A. Part II The Production of Radicals. In *Free radicals*; McGraw-Hill: New York, 1966; pp 57–145.
- (36) Stockert, J. C.; Blazquez-Castro, A. *Fluorescence Microscopy in Life Sciences*; Stockert, J. C., Blazquez-Castro, A., Eds.; BENTHAM SCIENCE PUBLISHERS: Sharjah, 2017.
- (37) Smith, M. B. Acids, Bases, Nucleophiles, and Electrophiles. In *Organic Chemistry: An Acid-Base Approach*; Smith, M. B., Ed.; CRC Press, 2016; pp 163–205.
- (38) Arnett, E. M.; Hofelich, T. C. Stabilities of Carbocations in Solution. 14. An Extended Thermochemical Scale of Carbocation Stabilities in a Common Superacid. *J. Am. Chem. Soc.* **1983**, *105* (9), 2889–2895.
- (39) Kistiakowsky, G. B.; Ruhoff, J. R.; Smith, H. A.; Vaughan, W. E. Heats of Organic Reactions III. Hydrogenation of Some Higher Olefins. *J. Am. Chem. Soc.* **1936**, *58* (1), 137–145.
- (40) Ouellette, R. J.; Rawn, J. D. Alkenes: Structures and Properties. In *Organic Chemistry*; Elsevier, 2018; pp 135–165.
- (41) Afeefy, H. Y.; Liebman, J. F.; Stein, S. E. Neutral Thermochemical Data. In *NIST Chemistry WebBook, NIST Standard Reference Database*; Linstrom, P. J., Mallard, W. G., Eds.; National Institute of Standards and Technology: Gaithersburg MD, 2022.



- (42) Rhodes, C. J. Electron Paramagnetic Resonance Study of Radical Formation from Cyclopentene and Dimethylacetylene Following Adsorption onto H-Mordenite. *J. Chem. Soc. Faraday Trans.* **1991**, *87* (19), 3179–3184.
- (43) Karge, H. G.; Lange, J.-P.; Gutsze, A.; Łaniecki, M. Coke Formation through the Reaction of Olefins over Hydrogen Mordenite: II. In Situ EPR Measurements under on-Stream Conditions. *J. Catal.* **1988**, *114* (1), 144–152.
- (44) Anderson, J. R.; Chang, Y. F.; Western, R. J. Retained and Desorbed Products from Reaction of 1-Hexene over H-ZSM5 Zeolite: Routes to Coke Precursors. *J. Catal.* **1989**, *118* (2), 466–482.
- (45) Anderson, J. R.; Chang, Y.-F.; Western, R. J. The Effect of Acidity on the Formation of Retained Residue From-1-Hexene over Usy Zeolite Catalysts. In *Catalyst Deactivation*; Elsevier, 1991; pp 745–751.
- (46) Guisnet, M. Modes of Coke Formation and Deactivation. In *Deactivation and regeneration of zeolite catalysts*; 2011; pp 115–137.
- (47) Payan, F.; de Klerk, A. Hydrogen Transfer in Asphaltenes and Bitumen at 250 °c. *Energy Fuels* **2018**, *32* (9), 9340–9348.
- (48) Sakuneka, T. M.; de Klerk, A.; Nel, R. J. J.; Pienaar, A. D. Synthetic Jet Fuel Production by Combined Propene Oligomerization and Aromatic Alkylation over Solid Phosphoric Acid. *Ind. Eng. Chem. Res.* **2008**, *47* (6), 1828–1834.
- (49) Nel, R. J. J.; de Klerk, A. Selectivity Differences of Hexene Isomers in the Alkylation of Benzene over Solid Phosphoric Acid. *Ind. Eng. Chem. Res.* **2007**, *46* (9), 2902–2906.
- (50) de Klerk, A. Aromatic Alkylation. In *Fischer-Tropsch Refining*; Wiley-VCH Verlag GmbH & Co. KGaA: Weinheim, Germany, 2011; pp 393–406.
- (51) García, H.; Roth, H. D. Generation and Reactions of Organic Radical Cations in Zeolites. *Chem. Rev.* **2002**, *102* (11), 3947–4008.

- (52) Rhodes, C. J.; Standing, M. Formation of 9-Octalin (1,2,3,4,5,6,7,8-Octahydronaphthalene) Radical Cations on Adsorption of Acyclic Dienes onto H-Mordenite. *J. Chem. Soc., Perkin Trans. 2* **1992**, No. 9, 1455.
- (53) Mercier Des Rochettes, B.; Marcilly, C.; Gueguen, C.; Bousquet, J. Coke Formation Mechanism from Olefins or Diolefins under Catalytic Cracking Conditions. *Studies in Surface Science and Catalysis* **1987**, 34 (C), 589–603.
- (54) Carlson, C. S.; Langer, A. W.; Stewart, J.; Hill, R. M. Thermal Hydrogenation. Transfer of Hydrogen from Tetralin to Cracked Residua. *Ind. Eng. Chem.* **1958**, 50 (7), 1067–1070.
- (55) Li, L.; Hou, Y.; Wu, W.; Liang, S.; Ren, S. Behaviors of Tetralin and 9,10-Dihydroanthracene as Hydrogen Donor Solvents in the Hydrogenolysis of Coal-Related Model Compounds. *Fuel Process. Technol.* **2019**, 191 (April), 202–210.
- (56) Lange, J.-P.; Gutsze, A.; Karge, H. G. Coke Formation through the Reaction of Olefins over Hydrogen Mordenite: I. EPR Measurements under Static Conditions. *J. Catal.* **1988**, 114 (1), 136–143.

## **Chapter 6. Desorption of organic nitrogen bases from an amorphous silica-alumina catalyst used for treating cracked naphtha**

### **Abstract**

A limitation when contemplating the use of an acid catalyst to convert cracked naphthas is the vulnerability of their active sites to poisoning by organic nitrogen bases. Although poisoning is regarded as an irreversible process, observations made during the study of deactivation of an acid catalyst treating cracked naphtha hinted that poisoning by nitrogen bases was not the main contributor to the deactivation of the catalyst. Compounds in the cracked naphtha could be competitively adsorbing on the acid sites to displace adsorbed nitrogen bases. To test this, a pyridine-saturated amorphous silica-alumina catalyst was subject to temperatures ranging from 100 to 250 °C in the presence of the cracked naphtha and heptane respectively. Using gas chromatography coupled with a nitrogen phosphorus detector (GC-NPD) it was found that at the temperature range studied (100-250 °C), a higher concentration of pyridine was detected in the cracked naphtha compared to the heptane, after the experiments with previously pyridine saturated catalyst, at all temperatures studied. It was concluded that these observations indicated that while the process is only driven by equilibrium (solid and liquid phase partitioning) in the case of desorption in heptane, competitive adsorption also plays a role when the desorption of pyridine takes place in the presence of cracked naphtha.

**Keywords:**Pyridine adsorption, acid catalyst, competitive adsorption, phase partitioning.

## 6.1. Introduction

Acid catalysts are used for the conversion of petroleum feeds in units like catalytic cracking or oligomerization.<sup>1-3</sup> The acid catalysts in these processes are subjected to deactivation, but these units have been designed to deal with such deactivation, either by prolonging catalyst life, or by incorporating catalyst regeneration as part of the technology.

The acid catalyzed olefin-aromatic alkylation unit developed for partial upgrading is aimed to treat naphtha derived from bitumen thermal cracking without hydrogen.<sup>4</sup> In this process, the deactivation of the acid catalyst with time on stream is a relevant topic for the technology development.

The deactivation of the acid catalyst can occur by deposition of organic matter on the surface of the catalyst, which obstructs the active sites.<sup>5</sup> Also, some petroleum feeds have heteroatom containing compounds,<sup>6</sup> which could include nitrogen bases. Nitrogen bases present a problem for acid catalysts, which due to their strong affinity to the acid sites could inhibit or poison the catalyst surface and hinder the reaction.<sup>7</sup> Cracked naphthas are expected to contain nitrogen bases of the pyridine kind, especially when the cracked naphtha is derived from high nitrogen-content feeds like bitumen.<sup>6</sup>

Poisoning of a catalyst refers to the irreversible chemisorption of a molecule to the active sites.<sup>7</sup> Although reactants chemically adsorb on the active sites during a catalyzed reaction, their adsorption is reversible, and we can expect a desorption step. In the case of a nitrogen base like pyridine, which is a stronger base than hydrocarbon species in the same boiling range, it binds to the acid sites forming an acid-base pair as product. The resulting acid-base pair may require a higher energy to dissociate and desorb than is provided at the reaction conditions. For this reason, the reaction conditions matter in terms of the poisoning ability of nitrogen bases like pyridine.

Removal of nitrogen-containing species prior to cracked naphtha treatment, although possible,<sup>8</sup> would require an additional step. The additional step adds cost and complexity to the partial upgrading process, which is contrary to the low-cost objective of partial upgrading.

Specific studies on the deactivation of acid catalysts treating cracked naphthas are scarce, and more so are the studies of the presence of nitrogen bases on this process.

In a study on the olefin-aromatic alkylation reaction of phenol with 1-hexene in the presence of pyridine,<sup>9</sup> using an amorphous silica-alumina (ASA) catalyst, it was found that when operating at a temperature of 315 °C the alkylation reaction can proceed in the presence of nitrogen bases, although at a lower rate. Treating the catalyst with a higher temperature, restored the original rates. This means that there is the possibility that nitrogen bases, although they inhibit the reaction, do not irreversibly poison the catalyst.

During experiments for the olefin-aromatic alkylation of olefins in cracked naphtha using an ASA catalyst, it was determined that nitrogen bases did not interfere with the main reaction, and that their contribution to the catalyst deactivation was limited.<sup>10</sup> This study, covered in Chapter 3, was based on the analysis of the spent catalyst samples, from which it was observed that nitrogen was only present in the deposits formed in the inlet of the reactor, and at low concentrations compared to the amount of nitrogen that passed through the catalyst during the time on stream. This generated the question of how the adsorption/desorption of pyridine type molecules was affected when in the presence of the rest of the compounds in the cracked naphtha. More specifically, to determine what is the role of competitive adsorption in relation to thermal desorption to displace adsorbed nitrogen bases on the acid catalyst.

The hypothesis formulated at this point was that pyridine adsorption/desorption on acid sites is a dynamic process, affected by temperature and the compounds in cracked naphtha that can compete for the acid sites. To test this, a pyridine-saturated ASA catalyst was subject to heat (temperature ranging from 100 to 250 °C) in the presence of either the cracked naphtha or heptane. If the permanent desorption is driven by competition for the acid sites caused by the compounds in the cracked naphtha, a higher amount of pyridine should desorb in this case and remain in the liquid, compared to heptane. Using gas chromatography coupled with a nitrogen phosphorous detector (GC-NPD), the amount of pyridine desorbed from the catalyst was quantified and compared to that desorbed in the presence of heptane only, at the same temperatures.

## 6.2. Experimental

### 6.2.1. Materials

The cracked naphtha was a distillation cut of the product from visbreaking of *n*-pentane solvent deasphalted vacuum residue in the Long Lake bitumen upgrader facility of CNOOC International (formerly Nexen) in Alberta, Canada. The cracked naphtha was characterized previously in our laboratories,<sup>6,11,12</sup> and for ease of reference some of the naphtha characterization data are listed in **Table 6.1**.

**Table 6.1.** Characterization of thermally cracked naphtha.

| Property                    | Units             | Cracked naphtha |
|-----------------------------|-------------------|-----------------|
| Density                     | kg/m <sup>3</sup> | 762.7           |
| Carbon                      | wt%               | 84.3            |
| Hydrogen                    | wt%               | 13.8            |
| Nitrogen                    | wt%               | 0.09            |
| Sulfur                      | wt%               | 0.9             |
| Oxygen                      | wt%               | 0.25            |
| <b>Distillation profile</b> |                   |                 |
| IBT                         | °C                | 30              |
| T10                         | °C                | 68              |
| T30                         | °C                | 100             |
| T50                         | °C                | 133             |
| T70                         | °C                | 173             |
| T90                         | °C                | 239             |
| FBP                         | °C                | 265             |

The amorphous silica-alumina (ASA) catalyst used in this study, Siral 40, was obtained through the calcination of a commercially available silica-alumina material from Sasol Germany. The characterization relevant to this study was performed as part of the study and reported as results. The catalyst calcination before use was done in a Carbolite Laboratory Furnace in air atmosphere, using a temperature program that started at room temperature and reaching 550 °C with a heating

ramp of 10 °C/min and held for 4 h at 550 °C. After cooling down, the samples were carefully stored in a sealed container placed in a desiccator, to avoid adsorption of ambient moisture. Some other chemicals used in this study are listed in **Table 6.2**.

## 6.2.2. Equipment and procedure

### 6.2.2.1. Pyridine saturated catalyst preparation

Siral 40, a commercially obtained silica-alumina catalyst, was calcined as explained in Section 6.2.1. The ASA catalyst was later saturated with pyridine, by mixing the powdered catalyst with the pure basic organic compound, in a catalyst:pyridine volume ratio of approximately 1:4, and agitated for 1 h at ambient temperature, in a closed container under the fumehood. The now saturated catalyst was “washed” with pentane, following the same procedure as for the saturation step. The washing step was repeated 3 times. By exposing the catalyst to pyridine, the acid sites would be neutralized. This process was aimed to titrate the acid sites of the catalyst, leaving the chemisorbed pyridine, and removing physically absorbed pyridine in the washing step. This procedure was not quantitative, although the absence of physisorbed pyridine was confirmed by infrared spectrometry.

**Table 6.2.** Chemicals and cylinder gases used in the study.

| Compound          | Formula                         | CASRN <sup>a</sup> | Mass fraction purity <sup>b</sup> | Supplier          |
|-------------------|---------------------------------|--------------------|-----------------------------------|-------------------|
| Chemicals         |                                 |                    |                                   |                   |
| Heptane           | C <sub>7</sub> H <sub>16</sub>  | 142-82-5           | >99 %                             | Sigma Aldrich     |
| Pyridine          | C <sub>5</sub> H <sub>5</sub> N | 110-86-1           | >99 %                             | Sigma-Aldrich     |
| 2-methylpyridine  | C <sub>6</sub> H <sub>7</sub> N | 109-06-8           | 98 %                              | Sigma-Aldrich     |
| Pentane           | C <sub>5</sub> H <sub>12</sub>  | 109-66-0           | >98%                              | Fisher Scientific |
| Potassium Bromide | KBr                             | 7758-02-3          | -                                 | PIKE technologies |
| Cobalt hydroxide  | Co(OH) <sub>2</sub>             | 21041-93-0         | 95%                               | Aldrich           |
| Cylinder gases    |                                 |                    |                                   |                   |
| Nitrogen          | N <sub>2</sub>                  | 7727-37-9          | 0.99998 <sup>c</sup>              | Praxair           |

<sup>a</sup> CASRN = Chemical Abstracts Services Registry Number. <sup>b</sup> This is the purity of the material guaranteed by the supplier; materials was not further purified. <sup>c</sup> Mole fraction purity.

### **6.2.2.2.Desorption process in batch micro reactors**

To study the desorption of pyridine from the acid catalyst and the effect of having the cracked naphtha compounds present, two types of experiments were performed. (i) The pyridine saturated catalyst was heated in the presence of cracked naphtha, and (ii) the pyridine saturated catalyst was heated in the presence of heptane. The resulting liquid products were later analyzed, and the pyridine present in each liquid product was quantified.

The experiments were done in a batch micro reactor with stirring. 2.5 g of the liquid, cracked naphtha or heptane, were placed in a glass vial along with 0.25 g of the saturated catalyst and a magnetic stirrer. The vial was placed in the batch micro reactor and the reactor was flushed with nitrogen, sealed, and pressurized to 4 MPa using nitrogen. The heating was achieved by placing the batch reactor in an oil bath, on top of a heating plate with stirring. The mixture was stirred at 500 rpm for 1 h. The temperature was controlled inside of the reactor using a thermocouple. Experiments with cracked naphtha were carried out in triplicate, and only once in the case of the heptane. All material was collected after reaction.

The temperatures studied were 100, 150, 200, and 250 °C. The temperatures chosen were aimed to cover a wide range to allow for different amounts of pyridine to be desorbed. But the maximum temperature of the reaction setup was limited by the need for agitation that is possible on a heating plate with stirrer, and the maximum temperature allowed by the oil bath in an open system.

The liquid product was analyzed by gas chromatography (GC) equipped with both a flame ionization detector (FID) and a nitrogen phosphorus detector (NPD). The spent catalyst was analyzed by Diffuse reflectance infrared Fourier transform spectroscopy (DRIFTS).

### **6.2.2.3.Quantification of desorbed pyridine.**

Quantification of nitrogen-containing compounds was performed on an Agilent 7890A gas chromatograph (GC) equipped with both a flame ionization detector (FID) and a nitrogen phosphorus detector (NPD). The sample separation was achieved with Agilent 19091S-001HP-PONA column (50 m × 200 μm × 0.5 μm, max temperature 325 °C). Split ratio was 1:100. The oven initial temperature was 35 °C, which was maintained for 30 min, then increased to 200 °C at 2 °C/min, and finally increased to 300 °C at 10 °C/min and held at 300 °C for 7.5 min. The



quantification of the amount of pyridine desorbed was achieved through an internal standard calibration, using pyridine as analyte and 2-methylpyridine as internal standard. The calibration curve covered the concentration range of 0.1 to 1.6 mg/mL of pyridine. The relative NPD response factor for pyridine and 2-methylpyridine was determined to be 1.02, and it was considered when determining the concentration of pyridine in the liquid resulting from the experiments.

#### **6.2.2.4. Fresh and recovered catalyst characterization**

The freshly calcined catalyst was characterized for its acid site strength and concentration using temperature programmed desorption (TPD) of ammonia in a Quantachrome ChemBET TPR/TPD. Around of 180 mg of the sample catalyst was introduced in a u-shaped quartz cell and loaded into the equipment. The sample was outgassed at 550 °C for 4 h under a helium flow, and once cooled down to 60 °C it was subjected to an ammonia flow for 40 min. The physically adsorbed ammonia was flushed out of the system at 60 °C for 40 min using helium. The samples were then heated at 10 °C/min to 600 °C to determine the ammonia desorption as function of temperature.

Diffuse reflectance infrared Fourier transform spectroscopy (DRIFTS) of adsorbed pyridine was measured using fresh calcined Siral 40. The measurement was performed using an ABB MB 3000 FTIR with a with a PIKE DiffusIR™ attachment. The spectra were collected under absorbance mode, with a resolution of 8, 120 scans, and a detector gain of 729. About 5 mg of the sample was mixed in equal proportion with KBr, placed in a porous ceramic crucible, and pressed until a uniform surface was obtained. The sample was outgassed 450 °C for 40 min using a nitrogen flow. As the sample was cooling down, background was taken at 375, 275, and 115 °C. Once the sample reached 115 °C pyridine vapors were allowed in the chamber. After 40 min exposure to pyridine, the flow was changed to only nitrogen and the IR spectra were taken every 10 min until steady state was achieved (i.e. physisorbed pyridine was removed). The temperature was increased to 275 °C and then to 375 °C, maintaining each temperature for 20 min, and a spectrum was collected at each condition. The temperatures were chosen based on the results from the TPD of ammonia.

The catalyst recovered after the experiments with naphtha and heptane (Section 6.2.2.2) was washed with pentane and left to dry before being analyzed by DRIFTS. The measurement was performed using an ABB MB 3000 FTIR with a with a PIKE DiffusIR™ attachment. Around 4 mg of the sample was mixed with 5 mg of KBr, and 1 mg of Co(OH)<sub>2</sub>. The mixture was placed in

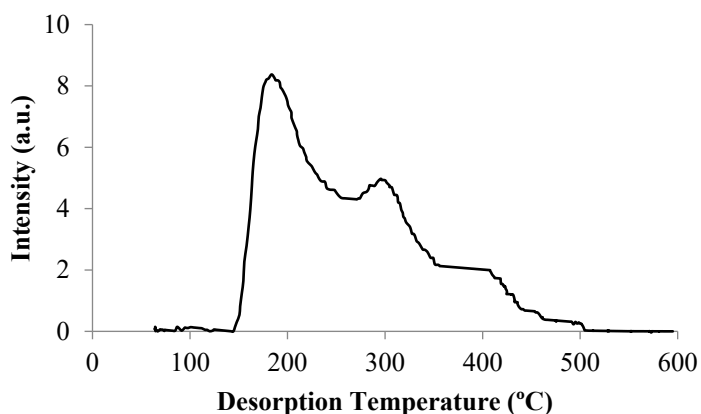
a porous ceramic crucible and pressed until a uniform surface was obtained. The spectra were taken after outgassing the sample at 60 °C for 1 h under a nitrogen flow. As background a sample of 4 mg of freshly calcined catalyst (not saturated with pyridine), 5 mg of KBr, and 1 mg of Co(OH)<sub>2</sub> was used. The spectra were collected under absorbance mode, with a resolution of 8, 120 scans, and a detector gain of 729. Pyridine vapours were not introduced in the chamber for this analysis.

The Co(OH)<sub>2</sub> was included as a potential internal standard for the quantification of desorbed pyridine from the catalyst using DRIFTS, since its adsorption bands did not interfere with the spectra of interest. Since the amount of pyridine desorbed was small and changes were not significant within the spectra, this approach was found to be redundant. The procedure could be simplified by just employing KBr without Co(OH)<sub>2</sub>.

### 6.3. Results and discussion

#### 6.3.1. Fresh catalyst characterization

The acid strength and concentration of acid sites in calcined Siral 40 is given by the Ammonia-TPD curve in **Figure 6.1**. Ammonia, being a relatively strong base ( $pK_b=4.75$ ),<sup>13</sup> can interact and bind with the acid sites of the catalyst. The three ammonia desorption peaks, observed at 185, 300 and 405 °C, indicate that three types of acid sites with different strength are present.



**Figure 6.1.** NH<sub>3</sub>-TPD curve of Siral 40.

Different acid site strengths have been determined in zeolites and ASAs before,<sup>14,15</sup> using this technique. Ammonia binds to all three types of acid sites at low temperature but requires different temperatures to desorb from them. The distribution of acid sites can be correlated to the activity of a catalyst for a given reaction,<sup>16</sup> but in our case as the TPD curve can be used as an indication of the temperatures at which a base like pyridine can desorb.

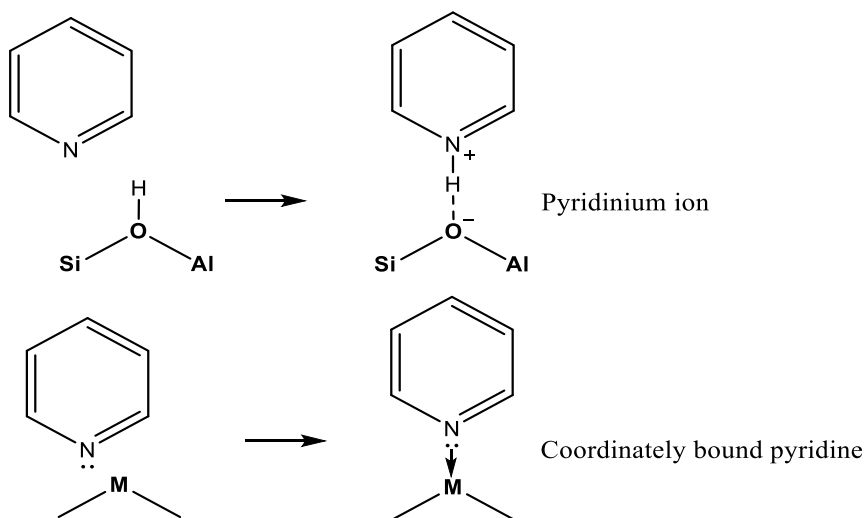
Each peak was integrated, and its area correlated with the amount of ammonia desorbed using a calibration curve. These values are shown in **Table 6.3**. The sites that require the least amount of energy to desorb are the weak acid sites, with a peak temperature of 185 °C, and these represent 53% of the acid sites. They are followed by the medium strength sites (300 °C), and strong acid sites (405 °C), representing 35 and 13% of acid sites, respectively.

**Table 6.3.** Acid site strength and distribution in Siral 40 from NH<sub>3</sub>-TPD data.

| <b>Acid site type</b>  | <b>Peak desorption temperature (°C)</b> | <b>Temperature range (°C)</b> | <b>Acid site concentration (μmol NH<sub>3</sub>/ g Catalyst)</b> | <b>Relative amount of each site</b> |
|------------------------|-----------------------------------------|-------------------------------|------------------------------------------------------------------|-------------------------------------|
| <b>Weak</b>            | 185                                     | 140-275                       | 183                                                              | 53%                                 |
| <b>Medium strength</b> | 300                                     | 275-375                       | 120                                                              | 35%                                 |
| <b>Strong</b>          | 405                                     | 375-507                       | 45                                                               | 13%                                 |

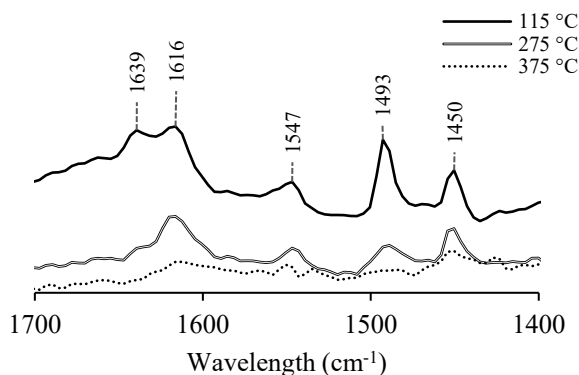
As reported before,<sup>9</sup> the acid sites in the Siral 40 catalyst can be either Lewis or Brønsted acids. The ammonia TPD results shown in **Figure 6.1** and **Table 6.3** do not distinguish between these two types of acid sites. For the olefin-aromatic alkylation process, only the Brønsted acid sites are relevant for the alkylation of aromatics with olefins. The sites can be differentiated using infrared spectrometry, since the nitrogen base reacts differently with these two sites.

A molecule like pyridine will bind to both types of acid sites by forming two different adsorbed species (**Figure 6.2**). On Brønsted acid sites, the pyridine will accept the proton and form the pyridinium ion, whereas on Lewis acid sites it will coordinately bind to the Lewis acid in an acid-base complex.



**Figure 6.2.** Pyridine adsorption in Bronsted and Lewis acid sites.

When the fresh ASA catalyst is in contact with pyridine vapours and analyzed with DRIFTS, typical adsorption bands of adsorbed pyridine appear in the IR spectrum of the catalyst surface, as shown in **Figure 6.3**. The presence of the pyridinium ion in Siral 40 is characterized by the bands at  $1639\text{ cm}^{-1}$  and  $1547\text{ cm}^{-1}$ . While the acid-base complex absorption bands are present in  $1450\text{ cm}^{-1}$  and  $1616\text{ cm}^{-1}$ . The band at  $1493\text{ cm}^{-1}$  is a contribution of both species present on the surface. Similar bands have been reported for other silica-alumina materials.<sup>17</sup>



**Figure 6.3.** Diffuse Reflectance Infrared Fourier Transform Spectroscopy (DRIFTS) of pyridine desorption from Siral 40. Pyridine-free Siral 40 was used as background.

The peak height for the pyridine absorption bands at each temperature are listed in **Table 6.4**. The percentage reduction for each peak after increasing the temperature was also included for the ease of discussion.

The assumption that was made in the quantification was that the pathlength remained constant, although the actual pathlength was not known, since the sample remained undisturbed during the analysis. Using this assumption, the adsorption at each band follows the Beer-Lambert Law (Equation 1), the absorbance ( $A$ ) is proportional to the concentration of the specie ( $C$ ) adsorbing at that specific wavelength, the path length ( $l$ ), and the molar attenuation coefficient ( $\epsilon$ ). The molar attenuation coefficient is specific of the adsorbed molecule, and it is a function of the wavenumber. Because of this, a change in the peak height can be ascribed to the change in concentration of that specie when comparing changes at the same wavenumber.

$$A = \epsilon l C \quad \text{Equation 1}$$

**Table 6.4.** Peak height of infrared absorption bands corresponding to adsorbed pyridine over Siral 40 at different temperatures.

| Desorption<br>Temperature (°C) | Peak height at each band         |                       |                       |                       |                       |
|--------------------------------|----------------------------------|-----------------------|-----------------------|-----------------------|-----------------------|
|                                | 1639 cm <sup>-1</sup>            | 1616 cm <sup>-1</sup> | 1547 cm <sup>-1</sup> | 1493 cm <sup>-1</sup> | 1450 cm <sup>-1</sup> |
| <b>115</b>                     | 0.2683                           | 0.2731                | 0.1988                | 0.2554                | 0.2143                |
| <b>275</b>                     | 0.1097                           | 0.1524                | 0.1099                | 0.1114                | 0.1361                |
| <b>375</b>                     | 0.0672                           | 0.0915                | 0.0844                | 0.0800                | 0.1060                |
|                                | Percentage peak height reduction |                       |                       |                       |                       |
| <b>115</b>                     | 0%                               | 0%                    | 0%                    | 0%                    | 0%                    |
| <b>275</b>                     | 59%                              | 44%                   | 45%                   | 56%                   | 36%                   |
| <b>375</b>                     | 75%                              | 66%                   | 58%                   | 69%                   | 51%                   |

At 115 °C, both protonated pyridine and coordinately bound pyridine are present in the surface, indicating that the ASA catalyst contains both types of acid sites, strong enough to retain the pyridine at this temperature. As the temperature increases to 275 °C, we see that the bands that are primarily affected are those corresponding to the protonated pyridine (1639 and 1547 cm<sup>-1</sup>) with a peak height reduction of 59 and 45% (**Table 6.4**). Also considerably affected was the band 1493 cm<sup>-1</sup>, which has a contribution of the two types of adsorbed pyridine. Relatively speaking, the bands corresponding to the pyridine coordinated in Lewis acid sites, especially that at 1450 cm<sup>-1</sup>,

were not as affected. These numbers potentially show that mostly Brønsted-adsorbed pyridine desorbed at this temperature, compared to the Lewis adsorbed pyridine.

At 375 °C, the surface coverage of pyridine drastically decreased, with some of the adsorption bands practically disappearing from the spectrum (**Figure 6.3**). According to the values shown on **Table 6.4**, the band with the greatest reduction was that at 1639 cm<sup>-1</sup>, which belongs to the protonated pyridine specie.

In overall, after subsequently heating the sample at 275 and 375 °C, the least affected absorption band was that at 1450 cm<sup>-1</sup>, with a total reduction of 51 % (**Table 6.4**). This band belongs to pyridine coordinately bound to a Lewis acid site. This indicates that the strong acid sites are mostly Lewis acid sites. This is in accordance with what was determined in previous characterization of the material.<sup>9</sup>

The peak at 1493 cm<sup>-1</sup>, which is a contribution of both Brønsted and Lewis adsorbed pyridine, saw its height decreased to 31% of the value at 115 °C (**Table 6.4**). In principle, this should correspond to the amount of acid sites seen with the ammonia-TPD analysis in the region of 375-507 °C, but this was not the case. According to the TPD, only 13% of the total acid sites are strong enough to retain ammonia at temperatures higher than 375 °C. Although only a semi-quantitative analysis can be achieved with the DRIFTS technique, the possible difference can be explained by the fact that pyridine binds more strongly to the acid sites.

This could be counterintuitive given that ammonia is a stronger base than pyridine, with pK<sub>b</sub> of 4.75 and 8.77 respectively.<sup>13</sup> But since most of the acid sites appear to be Lewis acid sites, the base dissociation constant is not a universal indicator that can be used for both types of acid sites. Pyridine might be a stronger Lewis base, forming a more stable acid-base Lewis complex than ammonia. Comparative evaluation of the same material using ammonia and pyridine indicate that there are differences, although this has been observed before,<sup>18,19</sup> since the methodology of pairing ammonia TPD with pyridine DRIFTS is well-established in the catalysis literature.

Brønsted sites are related to the activity of the acid catalyst for the olefin-aromatic alkylation process. Very strong Brønsted acid sites are present in crystalline silica-alumina materials, such as zeolites, where bridge hydroxyl groups are formed.<sup>20</sup> The strength of the Brønsted acid sites in

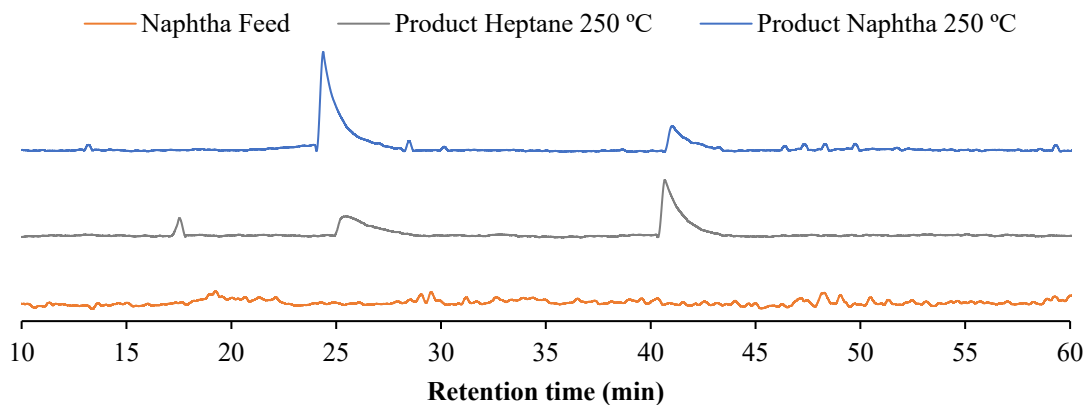
ASAs can vary depending on the configuration of neighboring atoms, being the stronger protonic sites only present in lower amount.<sup>17</sup> In the case of Siral 40, the concentration of strong Brønsted acid sites is expected to be low, which agrees with the results in this section, and agrees with previous quantitative determination of the Lewis and Brønsted acid sites in the Siral 40 catalyst.<sup>9</sup>

### 6.3.2. Desorbed pyridine at different temperatures in cracked naphtha and heptane

#### 6.3.2.1. Desorption measurements in the liquid

The desorption of pyridine from the saturated ASA catalyst to cracked naphtha and heptane was followed and quantified by GC-NPD. Typical chromatograms for the liquids resulting from the experiments can be observed in **Figure 6.4**. The eluted nitrogen bases show an atypical peak shape for chromatography, different from the usual Gaussian shaped. The tailing of the peak is due to a strong interaction of the basic compounds with the chromatography column.

Numerous small peaks were detected by the GC-NPD in the naphtha sample (orange line in **Figure 6.4**), to which no internal standard was added. The same naphtha sample has been characterized before and it was determined that nitrogen containing compounds were present at a concentration of 126 mg/L.<sup>6</sup> With such concentration one might expect to see more pronounced peaks, but the nitrogen containing compounds can be diverse, and each is present in concentrations too low to generate a significant signal. Also, it is worth mentioning, that in the cited study,<sup>6</sup> the naphtha was separated in fractions to decrease its complexity before analysis. In our case, the naphtha was analyzed without prior treatment.



**Figure 6.4.** Chromatogram signal of the GC-NPD, with pyridine eluting at 25 min and internal standard 2-methyl pyridine eluting at 40 min.

The pyridine desorbed from the catalyst to the liquid product naphtha (blue line) and the product heptane (grey line) can be seen in the chromatograms in **Figure 6.4**, at an elution time of around 24.5 min. 2-methylpyridine, the internal standard, elutes at around 41 min.

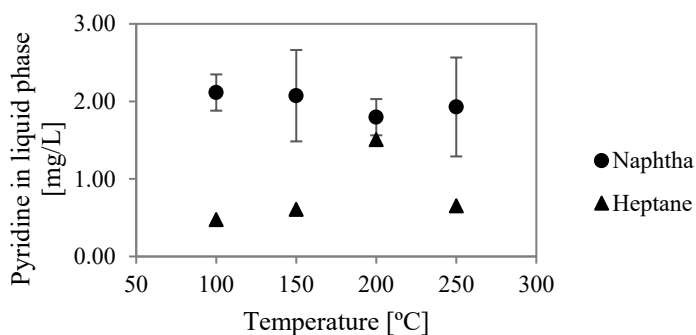
In the product naphtha chromatogram (blue line in **Figure 6.4**), a few additional unidentified compounds eluted at around 28 min and between 45-50 min. This could be compounds present in the cracked naphtha feed, since some compounds seem to generate a signal at similar retention times (orange line in **Figure 6.4**). Although an NPD detector was used, which is highly sensitive to nitrogen and phosphorous compounds, carbon rich compounds can generate a signal if their concentration is high enough. For instance, the peak showing at around 17 min in the chromatogram of the heptane product (grey line in **Figure 6.4**) corresponds to the heptane itself. This explains why the chromatograms for the naphtha samples (blue and orange) show a series of small peaks at different retention times, when the chromatogram for heptane does not.

The desorbed pyridine from the different experiments was quantified in the cracked naphtha and heptane and the resulting values are presented in **Figure 6.5**. The quantification was done using the GC-NPD chromatograms, following an internal standard method, which allowed to correct any signal variation between chromatograms.

As observed in **Figure 6.5**, the amount of pyridine detected in both cracked naphtha and heptane resulting liquids did not vary with temperature, but in every case the amount of pyridine in cracked naphtha exceeded that found in heptane.

The one exception was the experiment carried out with heptane at 200 °C, which had a concentration of pyridine comparable to that obtained with naphtha at the same temperature. This data point was initially considered as a true measurement that had to be explained. Some of the thoughts to explain this “jump” was the solubility of pyridine in heptane at that specific temperature, although solubility at this temperature was not found in the literature reviewed.<sup>21–23</sup> No credible explanations could be devised. An alternative is that this measurement is the result of contamination, which is the more likely explanation.





**Figure 6.5.** Desorbed pyridine in reactions with naphtha and heptane. Analysis in the liquid product.

The lack of variation of the amount of pyridine with temperatures 100-250 °C could be explained by the fact that at 250 °C only the weak acid sites are affected (see **Figure 6.1** and **Figure 6.3**), hence the same amount of pyridine can be considered to be desorbed. But this does not explain why the concentration of pyridine after heating at 100-150 °C is not lower, since a temperature of 185 °C is needed for a base molecule like ammonia to desorb from weak acid sites, according to **Figure 6.1**, and significant desorption of pyridine was achieved when heated from 115 to 275 °C, as seen in **Figure 6.3**. This could indicate two things:

- (i) Due to the nature of the experimental set, that involved the cooling down of a pressurized batch reactor before opening, the liquid analyzed was in contact with the catalyst during the cool down period. During this time, the re-adsorption of pyridine to the solid is a possibility. In such a case the concentration in the liquid phase would be determined by partitioning of pyridine between the liquid and solid phase at the temperature before the liquid phase is sampled. Although, it is worth mentioning that as soon as the cooling down period started, stirring stopped as well, and the catalyst fell to the bottom of the reactor. Therefore, mass transfer was lower during the cooling down period. Depending on the rate of diffusion in relation to the time spent during the cooling down period, the re-adsorption may or may not have equilibrated.
- (ii) The desorption of pyridine in the liquid phase during the conditions explored does not follow the same behavior observed in gas phase desorption of basic molecules, as with

TPD and DRIFTS. Desorption, being an endothermic process, is driven by the temperature of the system. But the desorbed molecule needs to diffuse out of the ASA catalyst particle and reach the liquid bulk to be able to be detected as desorbed. During analyses like DRIFTS and TPD there is a continuous operation, in which a carrier gas is constantly passing through. The concentration of the nitrogen compound in the bulk fluid is 0. In the case of the experimental conditions explored, there is a liquid in which the concentration of pyridine is increasing over time, due to the nature of batch operation, and where the pyridine that is desorbed is not removed from the system. This would slow down the desorption of the pyridine over time.

In all temperatures studied, the desorption of pyridine was higher in the cracked naphtha compared to that in the presence of heptane. This could be explained either by the relative solubility of pyridine in each one of the liquids used, or by considering the competition of pyridine for adsorption in the ASA catalyst surface with other compounds.

Pyridine is a polar molecule. Although it is completely soluble in heptane, since its critical solution temperature is  $-22\text{ }^{\circ}\text{C}$ ,<sup>23</sup> the wide variety of compounds in the cracked naphtha, including some polar compounds, might offer a more suitable media for pyridine dissolution. If solubility is playing a role in this process, it should be possible to determine by using liquids with different polarity and different pyridine solubility in the same experiments. This experimental work was not pursued in this study.

On the other hand, picturing the desorption of pyridine as a dynamic process in which a pyridine molecule can adsorb and desorb with temperature in different acid sites, the presence of another molecule with similar or stronger affinity to the acid sites can influence this dynamic process. After pyridine desorbed from the saturated ASA catalyst, re-adsorption could have been hindered by another molecule. This does not happen to the same extent in the case of heptane. If there are compounds in the cracked naphtha competing and adsorbing in the catalyst, then the recovered catalyst should give an indication of the adsorption of such molecules. To test this, the recovered catalyst after experiments with naphtha and heptane was also characterized with DRIFTS, to determine if there were bands corresponding to other hydrocarbons besides pyridine. In this case

pyridine gas was not used in the DRIFTS chamber. This investigation is covered in the next section.

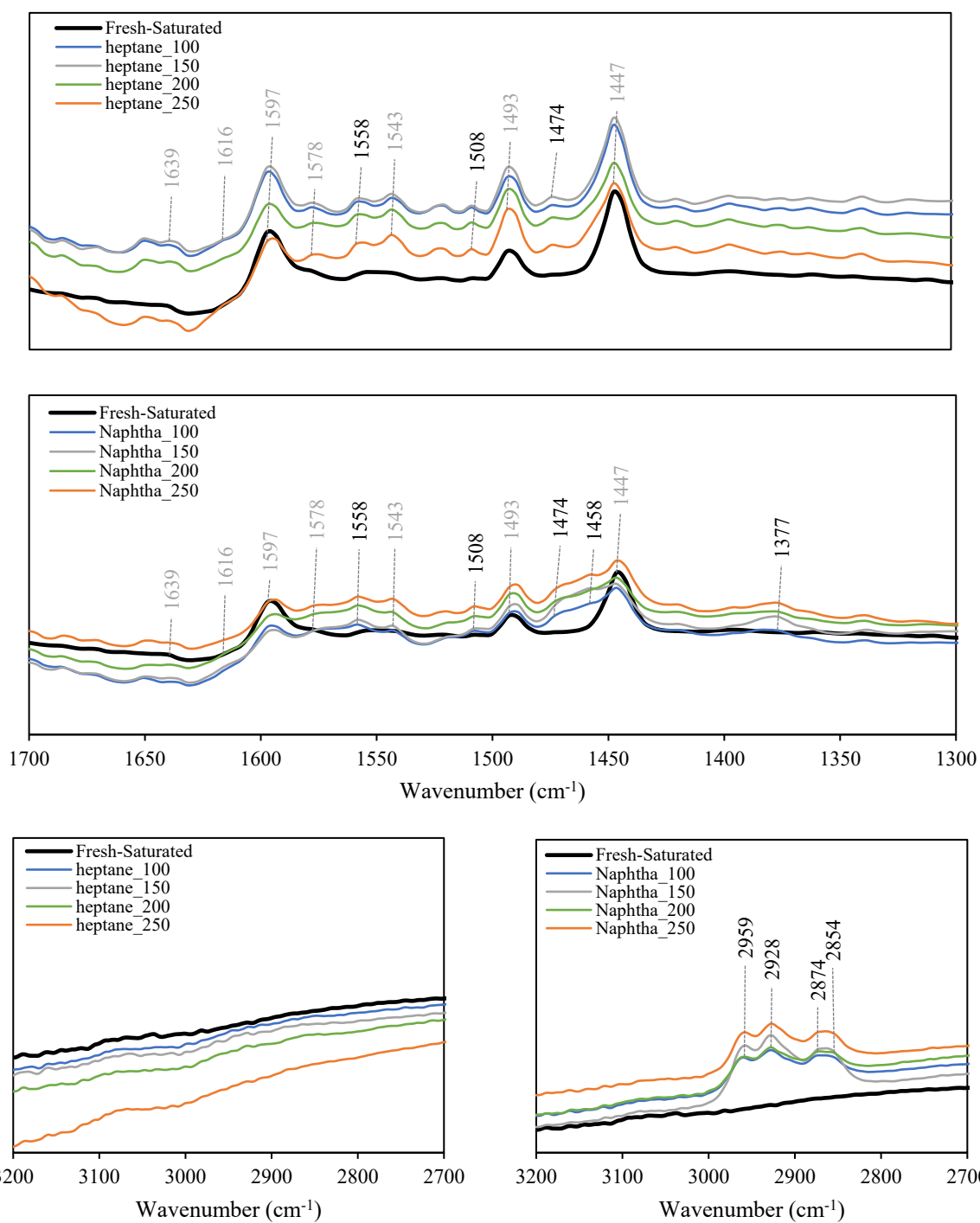
### 6.3.2.2. Infrared analysis of the recovered catalyst

The resulting IR spectra from the recovered ASA catalysts is shown in **Figure 6.6**. The bands corresponding to the adsorbed pyridine can be seen in the pyridine-saturated catalyst, which was not subjected to heating with naphtha or heptane. The bands in this spectrum (labeled in grey) differ from those seen in the pyridine DRIFTS analysis (**Figure 6.3**). In here, the characteristic bands for the pyridinium ion show a weak absorption at 1639 and 1543  $\text{cm}^{-1}$ . The band at 1616  $\text{cm}^{-1}$ , corresponding to the pyridine coordinately bound to Lewis acid sites, do not seem to be present in the pyridine-saturated catalyst. But the absorption band at 1447  $\text{cm}^{-1}$  could be a contribution of hydrogen-bonded pyridine, as well as pyridine adsorbed in Lewis acid sites.<sup>24</sup> Also, absorption at the wavelength 1578  $\text{cm}^{-1}$ , assigned to Lewis bonded pyridine, suggest the adsorption of pyridine to such acid sites.<sup>17,24</sup>

Physisorbed pyridine would absorb in the wavelengths 1585 and 1445-1435  $\text{cm}^{-1}$ ,<sup>24</sup> but these bands were not present in the spectrum of the pyridine-saturated catalyst. The absorption bands 1597 and 1447  $\text{cm}^{-1}$  indicate the presence of a hydrogen bonded pyridine.<sup>24</sup> The band at 1493  $\text{cm}^{-1}$ , is a contribution of Brønsted and Lewis acid site bound pyridine, but also of the hydrogen bonded pyridine. This surface specie is weakly adsorbed, and it is expected to be desorbed at 100 °C.<sup>17</sup>

The desorption of this surface pyridine specie could account for the detected pyridine in the liquid heptane and naphtha at the temperatures studied. If the hydrogen bonded pyridine represents most of the desorbed pyridine, then it would explain the lack of change upon heating (**Figure 6.5**). Since the minimum temperature used during the DRIFTS analysis of adsorbed pyridine was 115 °C, this specie was not seen in the spectrum in **Figure 6.3**.

In the recovered catalyst (after heating), infrared absorption bands corresponding to protonated pyridine at 1639 and 1543  $\text{cm}^{-1}$  and bands corresponding to coordinately bound pyridine at 1616 and 1578  $\text{cm}^{-1}$ , seem to be better defined. This could be because the desorption of the hydrogen bonded pyridine slightly shifted the surface concentration of species.



**Figure 6.6.** DRIFTS of pyridine-saturated ASA catalyst after exposure to heptane and cracked naphtha.

Besides the bands corresponding to the adsorbed pyridine, the recovered catalyst after heating in the presence of naphtha and heptane showed new bands corresponding to the presence of

hydrocarbons (labeled in black in **Figure 6.6**). Since different groups can be contributing to the peak observed at the same wavelength, **Table 6.5** was built to facilitate the analysis of the spectra.

**Table 6.5.** Contributing groups for observed absorption bands in each catalyst sample.

| Wavenumber<br>(cm <sup>-1</sup> ) | Possible contributing groups for<br>observed absorption bands      | Bands in sample's DRIFTS |                      |                      |
|-----------------------------------|--------------------------------------------------------------------|--------------------------|----------------------|----------------------|
|                                   |                                                                    | Saturated<br>catalyst    | Heptane<br>recovered | Naphtha<br>Recovered |
| <b>2959</b>                       | Aliphatic CH <sub>3</sub> <sup>25,26</sup>                         |                          |                      | x                    |
| <b>2928</b>                       | Aliphatic (paraffins and olefins) CH <sub>2</sub> <sup>25,26</sup> |                          |                      | x                    |
|                                   | Aromatic CH <sub>3</sub> <sup>25,26</sup>                          |                          |                      |                      |
| <b>Broad band<br/>2874-2854</b>   | Aliphatic CH <sub>3</sub> <sup>25,26</sup>                         |                          |                      |                      |
|                                   | Aliphatic (paraffins and olefins) CH <sub>2</sub> <sup>25,26</sup> |                          |                      | x                    |
|                                   | Aromatic CH <sub>3</sub> <sup>25,26</sup>                          |                          |                      |                      |
| <b>1639</b>                       | Bronsted-bonded pyridine <sup>24</sup>                             | x                        | x                    | x                    |
|                                   | Olefinic C=C <sup>26</sup>                                         |                          |                      |                      |
| <b>1616</b>                       | Lewis-bonded pyridine <sup>24</sup>                                |                          | x                    | x                    |
|                                   | Olefinic C=C <sup>26</sup>                                         |                          |                      |                      |
| <b>1597</b>                       | Hydrogen-bonded pyridine <sup>17,24</sup>                          | x                        | x                    | x                    |
|                                   | Aromatic C=C <sup>26,28</sup>                                      |                          |                      |                      |
| <b>1578</b>                       | Lewis-bonded pyridine <sup>17,24</sup>                             | x                        | x                    | x                    |
| <b>1558</b>                       | Aromatic C=C <sup>26,28</sup>                                      | x (broad                 | x                    | x                    |
| <b>1543</b>                       | Bronsted-bonded pyridine <sup>17,24</sup>                          | peak)                    | x                    | x                    |
| <b>1508</b>                       | Substituted aromatics <sup>25</sup>                                |                          | x                    | x                    |
| <b>1493</b>                       | Bronsted-bonded pyridine <sup>17</sup>                             |                          |                      |                      |
|                                   | Lewis-bonded pyridine <sup>17</sup>                                | x                        | x                    | x                    |
|                                   | Hydrogen-bonded pyridine <sup>17</sup>                             |                          |                      |                      |
| <b>1474</b>                       | Aliphatic CH <sub>3</sub> <sup>25,26</sup>                         |                          |                      |                      |
|                                   | Aliphatic CH <sub>2</sub> <sup>25,26</sup>                         |                          | x                    | x                    |
| <b>1458</b>                       | Aliphatic CH <sub>3</sub> <sup>25</sup>                            |                          |                      |                      |
|                                   | Aliphatic (paraffins and olefins) CH <sub>2</sub> <sup>25,26</sup> |                          | x                    | x                    |
|                                   | Substituted aromatics <sup>25</sup>                                |                          |                      |                      |
| <b>1447</b>                       | Lewis-bonded pyridine <sup>17,24</sup>                             |                          |                      |                      |
|                                   | Hydrogen-bonded pyridine <sup>17,24</sup>                          | x                        | x                    | x                    |
| <b>1377</b>                       | Aliphatic CH <sub>3</sub> <sup>25,26</sup>                         |                          | x                    | x                    |

In the recovered catalyst after heating in the presence of heptane, new bands are observed in the region 1400-1600<sup>-1</sup>, but the lack of absorption in the 2800-3100 cm<sup>-1</sup> region rules out the assignment of possible hydrocarbon species and indicates that little heptane was adsorbed. In fact,

the analysis indicated that the pyridine was not displaced by competitive adsorption, but that the pyridine in the heptane was more likely to be the consequence of thermodynamically driven partitioning of heptane between the liquid and solid phases.

In the case of the recovered catalyst subjected to heating with naphtha, new absorption bands corresponding to hydrocarbons emerged. According to literature,<sup>25,26</sup> absorption at the wavenumbers 2959, 2874, 1474 and 1377  $\text{cm}^{-1}$  represent asymmetric and symmetric stretch, and asymmetric and symmetric deformation vibration of the aliphatic  $\text{CH}_3$  group, respectively. All these absorptions were found in the experiments using cracked naphtha (**Figure 6.6**), although the absorptions at 1474 and 1377  $\text{cm}^{-1}$  were comparatively weak compared to those at 2959 and 2874  $\text{cm}^{-1}$ .

The absorption at 2928, 2854  $\text{cm}^{-1}$  are probably due to asymmetric and symmetric  $\text{CH}_2$  stretching, while the bands at 1474 and 1458  $\text{cm}^{-1}$  could be deformations of  $\text{CH}_2$ . Methylene groups in an olefinic structure could also contribute to the absorption at bands 2928, 2854, and 1458  $\text{cm}^{-1}$ .<sup>25</sup> The C=C bond in olefins usually absorbs in the region 1680-1600  $\text{cm}^{-1}$ , which makes us wonder if those bands could be overlapping with those already assigned to pyridine at 1639 and 1616  $\text{cm}^{-1}$ . Characteristic bands for olefins in the region 3100-3000  $\text{cm}^{-1}$  were not present, and those expected at 1000-600  $\text{cm}^{-1}$  could not be verified due to a poor signal to noise ratio in this region. The likelihood that olefins are part of the hydrocarbons present in the surface of the recovered catalyst after heating with naphtha is high, since olefins represent approximately 10wt% of the cracked naphtha<sup>12</sup> and due to their basic nature<sup>27</sup> they can readily interact with the acid sites that become available after the pyridine desorption.

Substituted aromatics absorb in the regions 1510 and 1460  $\text{cm}^{-1}$ , hence the bands at 1508 and 1458  $\text{cm}^{-1}$  suggest the presence of such compounds. The increase in absorption around 1460  $\text{cm}^{-1}$  is particularly evident in ASA catalyst samples exposed to cracked naphtha (**Figure 6.6**). Additionally, the absorption at 2928  $\text{cm}^{-1}$  and a possible overlapped peak in the region 2870-2860  $\text{cm}^{-1}$  could evidence the presence of aromatic  $\text{CH}_3$ . In coked catalysts, the bands at 1597 and 1558 have been assigned to aromatics.<sup>28</sup> No bands were observed in the region of 3000-3200  $\text{cm}^{-1}$  corresponding to aromatic CH stretching modes. Although the formation of heavy condensed polyaromatic species is not anticipated at the conditions studied, the lack of absorbance in the

3000-3200  $\text{cm}^{-1}$  region for spent catalyst samples has not been unique to this study,<sup>10,28</sup> and has been explained by the possibility of having very alkylated aromatics.<sup>28</sup>

These observations evidence the adsorption of hydrocarbons on the ASA catalyst surface upon heating in the presence cracked naphtha, and the chances that such compounds are alkylated aromatics is high. The presence of aliphatic chains is obvious, the bands in the region 2960-2850  $\text{cm}^{-1}$  are specific to  $\text{CH}_x$  groups that can be found in linear hydrocarbons, and the absorption at 1378  $\text{cm}^{-1}$  unquestionably belongs to  $\text{CH}_3$ . Also, there are clear signs of the presence of aromatics: there is a high chance of the presence of aromatic methyl, absorbing in 2928 and  $\sim 2870$   $\text{cm}^{-1}$ , and there are distinctive absorptions of substituted aromatics like 1508 and 1458  $\text{cm}^{-1}$ . As for olefins, their presence is not so obvious, since their characteristic bands either coincide with the absorption of other compounds (regions 1680-1600  $\text{cm}^{-1}$ ), are found on a region with poor resolution (1000-650  $\text{cm}^{-1}$ ) or are just not present (3100-3000  $\text{cm}^{-1}$ ). Although olefins have a strong affinity to the acid sites, there was not measurable evidence of their presence in the surface. If olefins did in fact adsorb to the acid sites, they could have reacted, losing their olefinic markers.

### 6.3.3. Causes of pyridine desorption

In principle, the amount of pyridine that can desorb and is eventually measured in the liquid bulk of the desorbing media (naphtha or heptane) is going to depend on two factors: temperature and time to reach adsorption/desorption equilibrium.

When a compound adsorbs chemically on an acid site, it forms a new bond. For desorption to occur, enough energy needs to be supplied for that new bond to break, and for the adsorbate to return to its original form – if unreacted. Since the adsorbate can bond in different sites on the catalyst we can expect the formation of different surface species, which decompose at different temperatures. This was seen during the analysis of the fresh ASA catalyst, using ammonia and pyridine, in **Figure 6.1** and **Figure 6.2**, where the progressive increase of temperature caused the desorption of an increasingly larger portion of the adsorbed pyridine.

The same process failed to be observed during the experiments in the presence of naphtha and heptane described in Section 6.3.2.1. At every temperature explored we would expect that a portion of the pyridine to be desorbed. This portion would correspond to those molecules forming a bond

to the acid sites that is weak enough to decompose at the target temperature. In these tests, there same amount of pyridine was measured regardless of the temperature.

The spectra of the pyridine-saturated ASA catalyst indicated that a portion of the adsorbed pyridine was a hydrogen bonded specie. This surface compound can decompose at temperatures of 100 °C and could account for most of the measured pyridine. Additional pyridine desorbed from Lewis and Bronsted acid sites might not have been significant enough to cause a shift on the measured pyridine at different temperatures.

Moreover, another thing to consider is the reaction system configuration, which is a batch operation. In this system, adsorption/desorption equilibrium could also play a role in the final concentration of pyridine in the liquid.

At a given temperature the catalyst surface coverage ( $\theta_A$ ) is going to be given by the concentration of the adsorbate in the media ( $C_A$ ) and the equilibrium constant ( $K$ ), as described by Langmuir isotherms (Equation 2).<sup>29</sup>

$$\theta_A = \frac{KC_A}{(1 + KC_A)} \quad \text{Equation 2}$$

In our case,  $C_A$  and  $\theta_A$  are going to be limited to the amount of pyridine that can desorb at the target temperature, and the sites that become available upon pyridine desorption. If this is a dynamic process, we can expect some re-adsorption of pyridine at the target temperature as the system is equilibrated. As the system was cooled before separation of the liquid from the catalyst, some re-adsorption of pyridine at lower temperatures is also expected. If equilibration occurred during the cooling period preceding the opening of the reactor (see (i) in Section 6.3.2.1), then this would explain the lack of variation of the amount of desorbed pyridine.

Since heptane has a low affinity to the acid sites, we do not foresee that the pyridine re-adsorption is hindered by heptane interactions. This is further backed by the IR spectra of the recovered catalyst after heating up in the presence of heptane, where the lack of absorption in the region 3000-2800  $\text{cm}^{-1}$  evidences the lack of aliphatic chains. In this case, partitioning between liquid and solid appeared to be the only driving force for pyridine displacement.



By heating the pyridine-saturated catalyst in the presence of cracked naphtha, competition for the acid sites becomes important since cracked naphtha contains species able to strongly interact with the acid sites. While the amount of desorbed pyridine might be limited by the temperature at which the catalyst is exposed to, the re-adsorption process will differ from that in the presence of only heptane. Other adsorbates will play a role on the adsorption equilibrium, and the surface coverage is going to be determined by:<sup>29</sup>

$$\theta_i = \frac{K_i C_i}{1 + \sum_{j=1}^N K_j C_j} \quad \text{Equation 3}$$

The amount of desorbed pyridine in the cracked naphtha was 4 times higher than that desorbed in heptane, as displayed in **Figure 6.5**. This could indicate that, in principle, that much pyridine can be desorbed due to the temperature of the system. Also, it evidences that absorption/desorption processes of pyridine at these conditions is a dynamic process, and that this re-adsorption of pyridine is hindered by the adsorption of competing species. In Section 6.3.2.2, this was proven true by the clear presence of hydrocarbons in the recovered catalyst surface after heating with cracked naphtha was evidenced through the infrared spectrum from the DRIFTS analysis. That analysis pointed at the presence of alkylated aromatics as the main compound class that could be identified with the infrared technique.

Pyridine interacts with the acid sites as shown in **Figure 6.2**. Being a basic molecule, is expected to adsorb strongly in these sites. But other molecules, even some not as basic, can also adsorb and restrict the access of pyridine.

Olefins for example, which are weak bases,<sup>27</sup> can adsorb in the surface of the catalyst forming a carbocation intermediate. This carbocation can react with different molecules in the cracked naphtha mixture, including other olefins and aromatics. At the temperature studied addition reactions are possible in an ASA catalyst. Oligomerization is possible at 150-250 °C,<sup>3</sup> and olefin-aromatic alkylation can occur at 250 °C.<sup>9</sup>

Reaction of olefins on the surface would decrease the concentration of the double bonds, which can explain why olefinic structures were not seen in the deposits from the recovered catalyst

(**Figure 6.6**) in spite of their strong affinity to the acid sites and their considerable concentration in the cracked naphtha (10 wt%<sup>12</sup>).

In the case of heptane, retention of hydrocarbons was minimum (**Figure 6.6**), hence re-adsorption of pyridine was possible, and equilibrium might have been achieved. But the cracked naphtha used in this study has been seen to form deposits in an ASA catalyst at 250 °C.<sup>10</sup> If deposits develop or coke precursors are formed once the pyridine desorbs, then the sites affected would not be available for pyridine re-adsorption.

The availability of the acid sites could be hindered by the formation of large molecules or deposits is the blockage of the catalyst pores. The access of pyridine to the acid sites would be limited. This was observed in a study about the thiophene adsorption capacity on zeolites in the presence of different molecules.<sup>30</sup> In the presence of 1-hexene the total adsorption of thiophene dropped. They explained that although 1-hexene does not directly compete with thiophene for the acid sites, because the sulfur compound is more basic, 1-hexene reacts with thiophene forming bulky alkylthiophenes which block pores and limit the adsorption of thiophene. This effect was more pronounced when toluene was included in the mixture, because of the formation of alkylated toluenes. Due to the contact times used in our studies, pore blockage is not anticipated, but formation of “coke precursors” or early formation of deposits is a possibility.

Cerqueira et al.<sup>31</sup> studied the adsorption of pyridine on coked catalysts from reactions of *m*-xylene at 247 and 447 °C. They found that re-adsorption of pyridine was limited on Brønsted acid sites of the coked catalyst but was not significantly affected on Lewis sites. This is due to the preferential interaction of coke molecules with strong Brønsted sites, besides the fact that such molecules are possibly formed on those same sites. If this is occurring in our case, and the pyridine that remained in the liquid desorbed from Brønsted acid sites of enough strength to catalyze the formation and to retain coke precursor molecules, then this is an indirect proof of the existence and possible concentration of strong Brønsted acid sites in the ASA catalyst.

Additionally, in the same study,<sup>31</sup> they found that upon adsorption of pyridine on the coked catalyst followed by evacuation, 45% and 35% of the coke was removed from each spent catalyst sample. They concluded that at low deposit content, the competition for the acid sites between pyridine and coke molecules (or coke precursors) favors pyridine, and that this molecule displaces the less

basic coke molecules facilitating their diffusion. This is not directly comparable to our study, but there is certainty that there are molecules in the cracked naphtha capable of displacing pyridine, either by their strong affinity to the acid sites or their ease to react towards the formation of molecules that are unable to desorb. This can be seen from the appearance of infrared bands of species other than pyridine on the catalyst.

If reactions occurred and irreversibly adsorbed species formed, then adsorption/desorption equilibrium might not have played an important role in the final amount of desorbed pyridine during the experiments in the presence of cracked naphtha. The observations of Adkins et al.<sup>32</sup> on the adsorption of nitrogen bases and sodium during hydrotreating of coal liquids can be extended to support this claim. They observed that when sodium was not present in the feed, the deposition of nitrogen on the catalyst was constant through time on stream. Once sodium was present on the feed, the content of nitrogen on the catalyst declined with time on stream. They explained this by the fact that although the adsorption of nitrogen bases is preferred, sodium adsorbs irreversibly, and eventually displaces the nitrogen bases. Moreover, the reversibility of the adsorption of nitrogen on the catalyst was proven when its displacement took place upon exposure of a nitrogen free feed.

In our case, cracked naphtha does not contain sodium, but there are species able to adsorb irreversibly, or adsorb and react to form retained compounds. Then, in this case the re-adsorption of pyridine would be limited by the rate of adsorption or formation of such compounds.

Although the re-adsorption of pyridine would be determined by the temperature and the time to reach an equilibrium, one needs to consider other molecules present in the system and their interactions with the acid sites. The re-adsorption of pyridine could be hindered by less basic compounds if these would react on the acid site and get retained. Hence the dynamic process would be governed by the relative rates of adsorption and desorption, but also the rate of reaction of the adsorbed compounds. In our case, it could occur that the reaction rate of adsorbed cracked naphtha compounds is higher than the desorption rate of the same compound. This would yield an increasing formation of deposits, as pyridine desorbs, and cracked naphtha compounds adsorb and react. This would explain what was observed on the study covered in Chapter 3,<sup>10</sup> where nitrogen

was only found in very small concentrations in the inlet of the reactor, and carbonaceous deposit formation was the main cause of the ASA catalyst deactivation.

The experiments with heptane showed that partitioning of pyridine between the liquid and solid phase also takes place. In that case partitioning between liquid and solid appeared to be the only driving force for pyridine displacement, where as partition and competitive adsorption contributed to the displacement of pyridine by cracked naphtha.

#### **6.4. Conclusions**

The desorption of pyridine from the ASA catalyst was studied on the temperature range 100-250 °C, in the presence of cracked naphtha and heptane. The observations support the fact that pyridine adsorbs dynamically on the catalyst surface, and desorption is possible.

Moreover, while the re-adsorption of pyridine might be driven by equilibrium in the case of the experiments with heptane, there is also a contribution of irreversibly adsorbed species when the experiment was carried out in the presence of cracked naphtha. This is evidenced by the fact that pyridine desorbs to a higher extent from the ASA catalyst when heated in the presence of the cracked naphtha compared to when it is heated in the presence of heptane. Also, it is supported by the infrared analysis of the recovered catalyst that indicated the presence of alkylated aromatics in the surface of the catalyst after the experiment with cracked naphtha.

An increasing desorption of pyridine with increasing temperature was not observed. Although the TPD of ammonia and DRIFTS or pyridine vapor analyses indicated the progressive desorption of the nitrogen compounds with temperature, a single concentration of pyridine was found throughout the studied temperatures. This could either be explained by the fact that a large portion of the pyridine desorbed was initially present in the catalyst weakly bonded to hydrogen and could desorb at a temperature of around 100 °C, or because the system equilibrated during the cooling down period.

#### **Acknowledgement**

The study was funded through the through the NSERC/CNOOC Ltd. Industrial Research Chair program in Field Upgrading and Asphaltenes Processing that is financially supported by the

Natural Science and Engineering Research Council (NSERC) of Canada, Alberta Innovates, and CNOOC International.

The assistance of Cloribel Santiago (University of Alberta) with her technical knowledge on gas-chromatography is gratefully acknowledged.

## 6.5. References

- (1) Gary, J. H.; Handwerk, G. E.; Kaiser, M. J. Chapter 6. Catalytic Cracking. In *Petroleum Refining*; CRC Press: Boca Raton, FL, 2007.
- (2) de Klerk, A. Chapter 5. Catalysis in the Upgrading of Fischer-Tropsch Syncrude. In *Catalysis in the Refining of Fischer-Tropsch Syncrude*; Royal Society of Chemistry: Cambridge, 2010; pp 40–164.
- (3) Nicholas, C. P. Applications of Light Olefin Oligomerization to the Production of Fuels and Chemicals. *Appl. Catal. A: Gen* **2017**, *543* (March), 82–97.
- (4) Zerpa, N.; de Klerk, A.; Xia, Y.; Omer, A. A. Olefins Reduction of a Hydrocarbon Feed Using Olefins Aromatics Alkylation. Patent Application WO2015000061A1, 2015.
- (5) Guisnet, M. Modes of Coke Formation and Deactivation. In *Deactivation and regeneration of zeolite catalysts*; 2011; pp 115–137.
- (6) Rao, Y.; de Klerk, A. Characterization of Heteroatom-Containing Compounds in Thermally Cracked Naphtha from Oilsands Bitumen. *Energy Fuels* **2017**, *31* (9), 9247–9254.
- (7) Guisnet, M. Poisoning of Zeolite Catalysts. In *Deactivation and regeneration of zeolite catalysts*; Guisnet, M., Ribeiro, F. R., Eds.; Imperial College Press: London, 2011; pp 101–114.
- (8) Prado, G. H. C.; Rao, Y.; de Klerk, A. Nitrogen Removal from Oil: A Review. *Energy Fuels* **2017**, *31* (1), 14–36.
- (9) Xia, Y. Acid Catalyzed Aromatic Alkylation in the Presence of Nitrogen Bases. MSc Thesis, University of Alberta, Edmonton, AB, Canada, University of Alberta, 2012.

- (10) Uzcátegui, G.; de Klerk, A. Causes of Deactivation of an Amorphous Silica-Alumina Catalyst Used for Processing of Thermally Cracked Naphtha in a Bitumen Partial Upgrading Process. *Fuel* **2021**, *293*, 120479.
- (11) Paez, N. Y.; de Klerk, A. Diolefin Characterization in a Thermally Cracked Naphtha. *Prepr. Pap.-Am. Chem. Soc., Div. Energy Fuels* **2016**, *61* (1), 12–15.
- (12) Budnar Subramanya, A. S. Olefin Hydrotreating and Characterization of Olefins in Thermally Cracked Naphtha. MSc thesis, University of Alberta, 2020.
- (13) Lide, D. R. *CRC Handbook of Chemistry and Physics*, 84th ed.; CRC Press: New York, 2003.
- (14) Kapustin, G. I.; Brueva, T. R.; Klyachko, A. L.; Beran, S.; Wichterlova, B. Determination of the Number and Acid Strength of Acid Sites in Zeolites by Ammonia Adsorption. *Appl. Catal.* **1988**, *42* (2), 239–246.
- (15) Hosseinpour, N.; Mortazavi, Y.; Bazyari, A.; Khodadadi, A. A. Synergetic Effects of Y-Zeolite and Amorphous Silica-Alumina as Main FCC Catalyst Components on Triisopropylbenzene Cracking and Coke Formation. *Fuel Process. Technol.* **2009**, *90* (2), 171–179.
- (16) Mishin, I. v.; Brueva, T. R.; Kapustin, G. I. Heats of Adsorption of Ammonia and Correlation of Activity and Acidity in Heterogeneous Catalysis. *Adsorption* **2005**, *11* (3–4), 415–424.
- (17) Crépeau, G.; Montouillout, V.; Vimont, A.; Mariey, L.; Cseri, T.; Maugé, F. Nature, Structure and Strength of the Acidic Sites of Amorphous Silica Alumina: An IR and NMR Study. *J. Phys. Chem. B* **2006**, *110* (31), 15172–15185.
- (18) Corma, A.; Fornés, V.; Melo, F. V.; Herrero, J. Comparison of the Information given by Ammonia t.p.d. and Pyridine Adsorption—Desorption on the Acidity of Dealuminated HY and LaHY Zeolite Cracking Catalysts. *Zeolites* **1987**, *7* (6), 559–563.

- (19) Loveless, B. T.; Gyanani, A.; Muggli, D. S. Discrepancy between TPD- and FTIR-Based Measurements of Brønsted and Lewis Acidity for Sulfated Zirconia. *Appl. Catal. B: Environ* **2008**, *84* (3–4), 591–597.
- (20) Caillot, M.; Chaumonnot, A.; Digne, M.; van Bokhoven, J. A. The Variety of Brønsted Acid Sites in Amorphous Aluminosilicates and Zeolites. *J. Catal.* **2014**, *316*, 47–56.
- (21) Cornish, R. E.; Archibald, R. C.; Murphy, E. A.; Evans, H. M. Purification of Vitamins - Fractional Distribution between Immiscible Solvents. *Ind. Eng. Chem.* **1934**, *26* (4), 397–406.
- (22) Francis, A. W. Solvent Selectivity for Hydrocarbons. *Ind. Eng. Chem.* **1944**, *36* (8), 764–771.
- (23) Francis, A. W. *Critical Solution Temperatures*; FRANCIS, A. W., Ed.; Advances in Chemistry; American Chemical Society: Washington, D. C., 1961; Vol. 31.
- (24) Zaki, M. I.; Hasan, M. a; Al-sagheer, F. a. In Situ FTIR Spectra of Pyridine Adsorbed on  $\text{SiO}_2 - \text{Al}_2\text{O}_3$ ,  $\text{TiO}_2$ ,  $\text{ZrO}_2$  and  $\text{CeO}_2$ : General Considerations for the Identification of Acid Sites on Surfaces of Finely Divided Metal Oxides. *Colloids and Surfaces A*. 2001, pp 261–274.
- (25) Colthup, N. B.; Daly, L. H.; Wiberley, S. E. *Introduction to Infrared and Raman Spectroscopy*, 3 rd.; Academy Press: San Diego, 1990.
- (26) Stuart, B. H. *Infrared Spectroscopy: Fundamentals and Applications*; Analytical Techniques in the Sciences; John Wiley & Sons, Ltd: Chichester, UK, 2004.
- (27) Pinard, L.; Hamieh, S.; Canaff, C.; Tarighi, M.; Maury, S.; Tayeb, K. ben; Pouilloux, Y.; Vezin, H. Growth Mechanism of Coke on Outside and inside HBEA Zeolite Pore during Ethanol Transformation. **2013**, *3*, 4–5.
- (28) Smith, M. B. Acids, Bases, Nucleophiles, and Electrophiles. In *Organic Chemistry: An Acid-Base Approach*; Smith, M. B., Ed.; CRC Press, 2016; pp 163–205.
- (29) Bartholomew, C. H.; Farrauto, R. J. Introduction and Fundamentals. In *Fundamentals of Industrial Catalytic Processes*; John Wiley & Sons, Inc.: Hoboken, NJ, USA, 2010; pp 3–59.

- (30) Richardeau, D.; Joly, G.; Canaff, C.; Magnoux, P.; Guisnet, M.; Thomas, M.; Nicolaos, A. Adsorption and Reaction over HFAU Zeolites of Thiophene in Liquid Hydrocarbon Solutions. *Appl. Catal. A: Gen* **2004**, *263* (1), 49–61.
- (31) Cerqueira, H. S.; Ayrault, P.; Datka, J.; Guisnet, M. Influence of Coke on the Acid Properties of a USHY Zeolite. *Microporous Mesoporous Mater.* **2000**, *38* (2–3), 197–205.
- (32) Adkins, B. D.; Milburn, D. R.; Goodman, J. P.; Davis, B. H. Mechanism for Coking of Coal Liquefaction Catalysts Involving Basic Nitrogen Compounds, Sodium and Catalyst Acid Sites. *Appl. Catal.* **1988**, *44*, 199–222.



## **Chapter 7. Conclusions**

### **7.1. Introduction**

The thesis dealt with different aspects related to the catalysis and catalyst deactivation of a process for the conversion of olefins in cracked naphtha without hydrogen by olefin-aromatic alkylation. This olefin-aromatic alkylation process is part of the BituMax™ partial upgrading technology developed for converting oilsands bitumen to a pipeline transportable oil product.

The olefin-aromatic alkylation process employs an amorphous silica-alumina acid catalyst in a packed bed reactor. The deactivation of this acid catalyst during treatment of cracked naphtha is one of the main technological risks of the process unit aimed to reduce the olefin content of the final product through olefin-aromatic alkylation. Although cracked naphtha is common in industry, the conversion of cracked naphtha by acid catalysis in the absence of hydrogen is not common. Cracked naphthas are more likely to participate in reactions leading to heavy compounds and deposits when compared to other light feeds. Because of this, it was of interest to study of the specific role of the components of cracked naphtha on the formation of organic deposits and how it led to catalyst deactivation with time on stream.

The objective of this study was to understand what compounds in cracked naphtha could react and contribute to the formation of deposits and through what reaction pathways. The investigation spanned topics ranging from the analysis of the characteristic deposits of spent catalyst samples derived from a unit treating cracked naphtha, to the study of reactions in the bulk liquid and the reactions and interactions of different molecules with the amorphous silica-alumina catalyst. The main observations and findings derived from this work are presented in the following section.

### **7.2. Major Conclusions and Insights**

The association of cracked naphtha with the formation of heavy compounds and deposits is well known. A commonly held perception was that reactions causing deactivation were due to the presence of di-olefins in the cracked naphtha, but in this study, it was soon realized that the observed deactivation behavior could not be fully explained so simplistically. Various attempts at cracked naphtha pretreatment were not successful in reducing catalyst deactivation by much. These

observations are mentioned anecdotally to provide additional context for what was found; the present study was part of a larger process development effort led by industry.

It was acknowledged that an insight into the cause of the challenges associated with cracked naphtha and its processing was needed. For this, the instances in which cracked naphtha causes issues in an industrial setting needed to be reviewed to gain an understanding of the conditions that could trigger the unwanted behavior. Two main types of instability of cracked naphtha were identified after the review: (i) oxidative instability during storage, caused by the contact with air over long periods of time, and (ii) thermal instability during processing, caused by the thermal reactions occurring upon heating of the cracked naphtha. Both processes occur through a free radical reaction mechanism initiated by the abstraction or donation of a hydrogen. The compound classes in cracked naphtha were assessed in their ability to take part in the free radical reactions that promote both oxidative and thermal instability, narrowing down a list of possible contributing species. While olefins can participate in propagation steps of free radical reactions, compounds like alkylaromatics with a double bond in the alkyl chain, or compounds that have a carbon that is simultaneously in the allylic and benzylic position can in fact initiate free radical reactions through hydrogen abstraction. It was also demonstrated that instability due to oxygen and oxidation resulted in chemically distinguishable products from instability in the absence of oxygen, although both were free radical processes.

It was expected that the instability of the feed that was shown to be unrelated to oxidation, could be detrimental for the catalyst time on stream life before that catalyst had to be regenerated. This was confirmed in early observations and motivated the study of the causes of deactivation of the acid catalyst. We took on the task of extensively characterizing the spent catalyst samples generated in runs of an olefin-alkylation pilot plant unit (kg/day capacity), at different conditions in the range 250–350 °C, 6 MPa and WHSV of 0.5–2 h<sup>-1</sup>. Information about catalyst deposit content, composition, and location gave important insights about the reactions leading to deposits. It was determined that deposition of carbonaceous material was the main cause of catalyst deactivation, and while the mechanism of deposit formation is in part catalytic, many observations in the study indicated that free radical chemistry also took part. For instance, the change in the nature of the deposits from the reactor inlet to outlet to become more hydrogen depleted, as well as the near constant rate of deposit formation, pointed at a free radical mechanism. It was also

found that the role of nitrogen bases on catalyst deactivation was limited. The nitrogen present in the deposits was concentrated in the inlet of the reactor, and it represented only a minor fraction of the total amount of basic nitrogen to which the catalyst was exposed. Although deactivation by deposit formation (colloquially referred to as coking) was expected, the limited presence of nitrogen bases in the deposits and the profile of deposits over the length of the catalyst bed that changed with operating temperature were unanticipated. In particular, finding that at some conditions, the amount of deposits was highest at the reactor outlet and not the inlet, highlighted that the deactivation process was more complex than could be attributed to di-olefins in the feed.

The review on the challenges while treating cracked naphtha indicated that there are cases in which cracked naphtha can become unstable due to heating to temperatures below those needed for thermal cracking initiated by thermolysis. Moreover, the analysis of the spent catalyst samples gave indications that free radical chemistry was taking place in the reactor at 250–350 °C and contributing to the deposition of carbonaceous material in the catalyst.

A study of the reactivity of cracked naphtha corroborated these observations. In this study,  $\alpha$ -methylstyrene (AMS) was used as a probe molecule to study the free radical chemistry occurring in the cracked naphtha, to facilitate the detection of free radical transfer reactions. Heating of naphtha and AMS mixtures resulted in the formation of compounds linked to free radical termination, like cumene and AMS dimers. Control reactions of AMS ruled out the possibility of self-initiation reactions. To dissipate the doubts around the initiation of such free radical reactions, the experiments were done in the presence or absence of oxygen. The results suggested that compounds in the cracked naphtha, that are not necessarily peroxides, could be initiating the reaction network leading to the observed products, partly because AMS act as a hydrogen acceptor and participate in molecule induced radical formation. Although the complexity of the cracked naphtha precluded positive identification of the species responsible for initiation, the work nevertheless provided evidence to show that free radical reactions took place in the operating temperature range of the olefin-aromatic alkylation process, 250–350 °C.

Besides free radical chemistry, it is well known that acid catalyzed reactions can also contribute to deposit formation. Among the compounds in the cracked naphtha that have a higher reactivity during carbocation chemistry are the compounds in the olefinic group. A structural motif that was

found by several studies in the research group to cause heavy product formation during free radical conversion, was the cyclopentene substructure. It was speculated that the same might hold true during acid catalyzed conversion. While the literature on the role of olefins on acid catalyzed reactions and deposit formation is vast, cyclopentene chemistry has received rather less attention, although reports on its ability to form coke precursors exist. After verifying the presence of such structures in the cracked naphtha and their reactivity to acid catalysis, it was postulated that the reaction pathways and contribution to deposit formation from different olefinic compounds could be different. This was investigated using cyclopentene and 1-hexene as model compounds, which confirmed that cyclopentene was about three times as reactive as 1-hexene for deposit formation.

Detailed characterization of the product distribution revealed that bicyclic compounds were major products from the acid catalyzed conversion of cyclopentenes. The bicyclic compounds were formed through dimerization reactions of cyclopentene through an octalin radical cation. Decalin and octalin were confirmed as the part of the products, which was an indirect proof that unsaturated compounds like tetralin and tetrahydronaphthalene might have been present at some point although not detected. The presence of such compounds is important since they are expected to donate hydrogen and initiate free radical reactions in the liquid. Interestingly, the same octalin radical cation has been observed on dimerization of conjugated dienes, indicating that cyclopentenes and dienes share a pathway leading to the formation of deposits on the catalyst surface. This is not a link that was previously established.

In this same study, the extent of the catalytic and thermal reactions was measured with fluorescence spectroscopy. It was found, that uncatalyzed thermal reactions at 300 °C affected the concentration of fluorophore molecules in cracked naphtha, although not in the same magnitude as catalytic reactions. We could explain this by the fact that thermal conversion is a free radical mechanism, and steps like radical addition and hydrogen disproportionation produce heavy unsaturated species with conjugated double bonds that can act as fluorophores. It independently corroborated the earlier work in this study, namely, that thermal reactions occurred in the cracked naphtha in the absence of a catalyst.

One of the major outcomes from the analysis of the spent catalyst samples from the pilot plant operation was the observations related to the deposition of nitrogen along the catalyst bed in the packed bed reactor. Nitrogen was only found in the inlet of the reactor and at very low concentrations given the amount of nitrogen bases that passed through the catalyst during its time on stream. It was hypothesized that the adsorption of pyridine bases is a dynamic process and that there are compounds in the cracked naphtha that can compete with pyridine bases for the acid sites. This was tested using a pyridine-saturated catalyst and subjecting it to heat in the presence of cracked naphtha and heptane, as control. It was found that in the temperature range studied, more pyridine desorbs when cracked naphtha is the desorbing media. This was partly explained by the competitive adsorption of molecules in the cracked naphtha capable of reacting and remain retained by the catalyst. Infrared spectra of the recovered catalyst confirmed that alkyl aromatics were retained in the surface. There was also a contribution of partitioning of the previously adsorbed pyridine between the solid and liquid. It meant that even in the absence of competitive adsorption, pyridine was an inhibitor, but not a permanent catalyst poison for the amorphous silica-alumina catalyst used in the olefin-aromatic alkylation process.

### **7.3. Recommended future work**

#### **7.3.1. Contribution of thermal reactions of olefin-alkylation products to deposit formation**

In the study on the analysis of spent catalyst samples from the pilot scale olefin-alkylation process dealing with cracked naphtha (Chapter 3), there were strong indications that part of the mechanisms leading to the deposition of carbonaceous material were of thermal nature. However, during the exploration of thermal reactions of cracked naphtha in Chapter 4, we did not observe changes in the complex chromatograms of cracked naphtha upon heating in the absence of AMS. Although using a more sensitive technique like fluorescence spectroscopy (Chapter 5), changes upon heating could be measured, but they were minor compared to those observed after catalytic reactions.

The difference between the laboratory studies and pilot scale operation could be that the compounds reacting on free radical reactions were formed in the reactor and were not initially present in the cracked naphtha.

The study of cyclopentene supports this hypothesis (Chapter 5). We saw how bicyclic compounds were formed which indicated the presence of partially unsaturated products able to initiate free radical reactions. Moreover, when reviewing the literature about the challenges while processing cracked naphtha in Chapter 2, alkylated aromatics with a double bond in the alkyl chain were identified as compounds able to donate a hydrogen and increase the instability of the cracked naphtha when present.

Experiments where the cracked naphtha is spiked with different species within that compound class ( $\alpha$ -methylstyrene,  $\beta$ -methylstyrene, 4-phenyl-1-butene, indene) could be carried out in the presence and absence of an amorphous silica-alumina catalyst. Analyses like GC-MS and fluorescence spectroscopy of the liquid products, coupled with ESR spectroscopy of the spent catalyst could provide the evidence of whether this type of compounds undergo free radical reactions and promote the formation of deposits in the catalyst. Control reactions can be done using reactive molecules from different compound classes, like 1-hexene and ethylbenzene.

### **7.3.2. Plug flow reactions of cracked naphtha spiked with cyclopentene and 1-hexene.**

During the study on reactions of cyclopentene over amorphous silica-alumina covered in Chapter 5, we observed the formation of decalin and octalin. Although the presence of decalin offers evidence of the formation of bicyclic unsaturated compounds, a direct observation of such compound was not achieved. Desorption of bicyclic unsaturated compounds of the kind of tetralin, methylindene, and dihydronaphthalene, from the amorphous silica-alumina catalyst would be a key step for them to further react in the liquid. Whether this occurs in the catalyst of interest is a question that could not be answered.

To test this, reactions would need to be carried in a flow reactor. Maintaining the conversion low might limit reactions leading the unsaturated bicyclic compounds to convert to decalin.

### **7.3.3. Pyridine cyclopentene competitive adsorption**

In Chapter 6 it was found that pyridine competes with compounds in cracked naphtha for the acid sites, resulting in its permanent displacement. If molecules in cracked naphtha adsorb and immediately react forming species that remain retained in the surface, it could explain why the re-adsorption of pyridine was hindered. In Chapter 5, cyclopentene was found to be a molecule that

had a significant impact on the formation of deposits of aromatic nature. By evaluating the desorption of pyridine in the presence of cyclopentene, we could evaluate this hypothesis. We could take advantage of the clear absorption infrared bands of pyridine and monitor the desorption of pyridine through time using DRIFTS. After the initial adsorption of the nitrogen base, a flow of cyclopentene vapors could be allowed in and the desorption rate of nitrogen could be recorded. A control experiment could be done using a linear olefin molecule like 1-hexene or 1-pentene.

## References

- Adkins, B. D.; Milburn, D. R.; Goodman, J. P.; Davis, B. H. Mechanism for Coking of Coal Liquefaction Catalysts Involving Basic Nitrogen Compounds, Sodium and Catalyst Acid Sites. *Appl. Catal.* **1988**, *44*, 199–222.
- Afeefy, H. Y.; Liebman, J. F.; Stein, S. E. Neutral Thermochemical Data. In *NIST Chemistry WebBook, NIST Standard Reference Database*; Linstrom, P. J., Mallard, W. G., Eds.; National Institute of Standards and Technology: Gaithersburg MD, 2022.
- Aksoy, P.; Gül, Ö.; Cetiner, R.; Fonseca, D. A.; Sobkowiak, M.; Falcone-Miller, S.; Miller, B. G.; Beaver, B. Insight into the Mechanisms of Middle Distillate Fuel Oxidative Degradation. Part 2: On the Relationship between Jet Fuel Thermal Oxidative Deposit, Soluble Macromolecular Oxidatively Reactive Species, and Smoke Point. *Energy Fuels* **2009**, *23* (4), 2047–2051.
- Ali, S. A. Naphtha Hydrotreatment. In *Catalytic Naphtha Reforming*; Antos, George. J., Aitani, Abdullah. M., Eds.; CRC Press: Boca Raton, 2004; pp 105–140.
- Alili, A. S.; Siddiquee, M. N.; de Klerk, A. Origin of Free Radical Persistence in Asphaltenes: Cage Effect and Steric Protection. *Energy Fuels* **2020**, *34* (1), 348–359.
- Al-Malaika, S. Chapter 2. Autoxidation. In *Atmospheric Oxidation and Antioxidants. Volume I*; Scott, G., Ed.; Elsevier, 1993; pp 45–82.
- Altgelt, K. H.; Boduszynski, M. M. *Composition and Analysis of Heavy Petroleum Fractions*; CRC Press: Boca Raton, FL, 1994.
- Alzaid, A.; Wiens, J.; Adjaye, J.; Smith, K. J. Catalyst Deactivation and Reactor Fouling during Hydrogenation of Conjugated Cyclic Olefins over a Commercial Ni–Mo–S/ $\gamma$ -Al<sub>2</sub>O<sub>3</sub> Catalyst. *Energy Fuels* **2018**, *32* (5), 6213–6223.
- Alzaid, A.; Wiens, J.; Adjaye, J.; Smith, K. J. Impact of Molecular Structure on the Hydrogenation and Oligomerization of Diolefins over a Ni-Mo-S/ $\gamma$ -Al<sub>2</sub>O<sub>3</sub> Catalyst. *Fuel* **2018**, *221*, 206–215.



Anderson, J. R.; Chang, Y. F.; Western, R. J. Retained and Desorbed Products from Reaction of 1-Hexene over H-ZSM5 Zeolite: Routes to Coke Precursors. *J. Catal.* **1989**, *118* (2), 466–482.

Anderson, J. R.; Chang, Y.-F.; Western, R. J. The Effect of Acidity on the Formation of Retained Residue From-1-Hexene over Usy Zeolite Catalysts. In *Catalyst Deactivation*; Elsevier, 1991; pp 745–751.

Arnett, E. M.; Hofelich, T. C. Stabilities of Carbocations in Solution. 14. An Extended Thermochemical Scale of Carbocation Stabilities in a Common Superacid. *J. Am. Chem. Soc.* **1983**, *105* (9), 2889–2895.

Asomaning, S.; Watkinson, A. P. Heat Exchanger Fouling by Olefin-Kerosene Mixtures. *Can. J. Chem. Eng.* **1992**, *70* (3), 444–451.

Balster, L. M.; Zabarnick, S.; Striebich, R. C.; Shafer, L. M.; West, Z. J. Analysis of Polar Species in Jet Fuel and Determination of Their Role in Autoxidative Deposit Formation. *Energy Fuels* **2006**, *20* (6), 2564–2571.

Barth, J.-O.; Jentys, A.; Lercher, J. A. On the Nature of Nitrogen-Containing Carbonaceous Deposits on Coked Fluid Catalytic Cracking Catalysts. *Ind. Eng. Chem. Res.* **2004**, *43* (10), 2368–2375.

Bartholomew, C. H.; Farrauto, R. J. Introduction and Fundamentals. In *Fundamentals of Industrial Catalytic Processes*; John Wiley & Sons, Inc.: Hoboken, NJ, USA, 2010; pp 3–59.

Bartholomew, C. H.; Farrauto, R. J. Petroleum Refining and Processing. In *Fundamentals of Industrial Catalytic Processes*; John Wiley & Sons, Inc.: Hoboken, NJ, USA, 2010; pp 635–704.

Batts, B. D.; Fathoni, A. Z. A Literature Review on Fuel Stability Studies with Particular Emphasis on Diesel Oil. *Energy Fuels* **1991**, *5* (1), 2–21.

Bellussi, G.; Mizia, F.; Calemma, V.; Pollesel, P.; Millini, R. Oligomerization of Olefins from Light Cracking Naphtha over Zeolite-Based Catalyst for the Production of High Quality Diesel Fuel. *Microporous Mesoporous Mater* **2012**, *164*, 127–134.

Beltramini, J. N.; Cabrol, R. A.; Churin, E. J.; Figoli, N. S.; Martinelli, E. E.; Parera, J. M. Catalyst Deactivation by Naphthas Doped with Hydrocarbons. *Appl. Catal.* **1985**, *17* (1), 65–74.

ben Tayeb, K.; Pinard, L.; Touati, N.; Vezin, H.; Maury, S.; Delpoux, O. Ethanol Transformation into Higher Hydrocarbons over HZSM-5 Zeolite: Direct Detection of Radical Species by in Situ EPR Spectroscopy. *Catal. Commun.* **2012**, *27*, 119–123.

Billmers, R.; Griffith, L. L.; Stein, S. E. Hydrogen Transfer between Anthracene Structures. *Am. J. Phys. Chem.* **1986**, *90* (3), 517–523.

Blanksby, S. J.; Ellison, G. B. Bond Dissociation Energies of Organic Molecules. *Acc. Chem. Res.* **2003**, *36* (4), 255–263.

Brooks, B. T. The Chemistry of Gasolines 1: Particularly with Respect to Gum Formation and Discoloration. *Ind. Eng. Chem.* **1926**, *18* (11), 1198–1203.

Brouwer, D. The Mechanism of Double-Bond Isomerization of Olefins on Solid Acids. *J. Catal.* **1962**, *1* (1), 22–31.

Buchanan, J. S.; Santiesteban, J. G.; Haag, W. O. Mechanistic Considerations in Acid-Catalyzed Cracking of Olefins. *J. Catal.* **1996**, *158* (1), 279–287.

Buckley, R. P.; Szwarc, M. The Addition of Methyl Radicals to Ethylene, Propylene, the Butenes and Higher 1-Olefines. *Proceedings of the Royal Society of London. Series A. Mathematical and Physical Sciences* **1957**, *240* (1222), 396–407.

Budnar Subramanya, A. S. Olefin Hydrotreating and Characterization of Olefins in Thermally Cracked Naphtha. MSc thesis, University of Alberta, 2020.

Caeiro, G.; Lopes, J.; Magnoux, P.; Ayrault, P.; Ramôa Ribeiro, F. A FT-IR Study of Deactivation Phenomena during Methylcyclohexane Transformation on H-USY Zeolites: Nitrogen Poisoning, Coke Formation, and Acidity–Activity Correlations. *J. Catal.* **2007**, *249* (2), 234–243.

Caeiro, G.; Magnoux, P.; Ayrault, P.; Lopes, J.; Ramôa Ribeiro, F. Deactivating Effect of Coke and Basic Nitrogen Compounds during the Methylcyclohexane Transformation over H-MFI Zeolite. *Chem. Eng. J.* **2006**, *120* (1–2), 43–54.

Caillot, M.; Chaumonnot, A.; Digne, M.; van Bokhoven, J. A. The Variety of Brønsted Acid Sites in Amorphous Aluminosilicates and Zeolites. *J. Catal.* **2014**, *316*, 47–56.

Carlson, C. S.; Langer, A. W.; Stewart, J.; Hill, R. M. Thermal Hydrogenation. Transfer of Hydrogen from Tetralin to Cracked Residua. *Ind. Eng. Chem.* **1958**, *50* (7), 1067–1070.

Cerqueira, H. S.; Ayrault, P.; Datka, J.; Guisnet, M. Influence of Coke on the Acid Properties of a USHY Zeolite. *Microporous Mesoporous Mater.* **2000**, *38* (2–3), 197–205.

Chang, H.-L.; Wong, G. K.; Lin, J.-R.; Yen, T. F. Chapter 9 Electron Spin Resonance Study of Bituminous Substances and Asphaltenes. In *Asphaltenes and Asphalts*, 2; Elsevier Science B.V., 2000; pp 229–280.

Chaouati, N.; Soualah, A.; Chater, M.; Tarighi, M.; Pinard, L. Mechanisms of Coke Growth on Mordenite Zeolite. *J. Catal.* **2016**, *344*, 354–364.

Chatelain, K.; Nicolle, A.; ben Amara, A.; Starck, L.; Catoire, L. Structure–Reactivity Relationships in Fuel Stability: Experimental and Kinetic Modeling Study of Isoparaffin Autoxidation. *Energy Fuels* **2018**, *32* (9), 9415–9426.

Chertkov, Ya. B.; Zrelov, V. N. The Oxidation of Hydrocarbon Fuels under Storage Conditions. In *The Oxidation of Hydrocarbons in the Liquid Phase*; Emanuel, N. M., Ed.; Elsevier, 1965; pp 351–361.

Cheshkova, T. v.; Sergun, V. P.; Kovalenko, E. Y.; Gerasimova, N. N.; Sagachenko, T. A.; Min, R. S. Resins and Asphaltenes of Light and Heavy Oils: Their Composition and Structure. *Energy Fuels* **2019**, *33* (9), 7971–7982.

Chong, Y. K.; Rizzardo, E.; Solomon, D. H. Confirmation of the Mayo Mechanism for the Initiation of the Thermal Polymerization of Styrene. *J Am Chem Soc* **1983**, *105* (26), 7761–7762.

Clark, D. E. Peroxides and Peroxide-Forming Compounds. *Chemical Health and Safety* **2001**, 8 (5), 12–22.

Colthup, N. B.; Daly, L. H.; Wiberley, S. E. *Introduction to Infrared and Raman Spectroscopy*, 3rd.; Academy Press: San Diego, 1990.

Corma, A.; Fornés, V.; Melo, F. V.; Herrero, J. Comparison of the Information given by Ammonia t.p.d. and Pyridine Adsorption—Desorption on the Acidity of Dealuminated HY and LaHY Zeolite Cracking Catalysts. *Zeolites* **1987**, 7 (6), 559–563.

Corma, A.; Gullbrand, P.; Martínez, C. Gasoline Sulfur Removal: Kinetics of s Compounds in FCC Conditions. In *Stud. Surf. Sci. Catal*; 2001; pp 153–165.

Corma, A.; Martínez, C.; Ketley, G.; Blair, G. On the Mechanism of Sulfur Removal during Catalytic Cracking. *Appl. Catal. A: Gen* **2001**, 208 (1–2), 135–152.

Corma, A.; Orchillés, A. V. Current Views on the Mechanism of Catalytic Cracking. *Microporous Mesoporous Mater.* **2000**, 35–36 (3 (76)), 21–30.

Cornish, R. E.; Archibald, R. C.; Murphy, E. A.; Evans, H. M. Purification of Vitamins - Fractional Distribution between Immiscible Solvents. *Ind. Eng. Chem.* **1934**, 26 (4), 397–406.

Crépeau, G.; Montouillout, V.; Vimont, A.; Mariey, L.; Cseri, T.; Maugé, F. Nature, Structure and Strength of the Acidic Sites of Amorphous Silica Alumina: An IR and NMR Study. *J. Phys. Chem. B* **2006**, 110 (31), 15172–15185.

Crockett, R.; Roduner, E. Dimerisation and Transannular Reactions of Cycloalkenes on H-Mordenite. *J. Chem. Soc., Perkin Trans. 2* **1993**, No. 8, 1503.

Curiale, J. A.; Frolov, E. B. Occurrence and Origin of Olefins in Crude Oils. A Critical Review. *Org. Geochem.* **1998**, 29 (1–3), 397–408.

Cvetanović, R. J.; Irwin, R. S. Rates of Addition of Methyl Radicals to Olefins in the Gas Phase. *J. Chem. Phys* **1967**, 46 (5), 1694–1702.

Daniell, W.; Schubert, U.; Glöckler, R.; Meyer, A.; Noweck, K.; Knözinger, H. Enhanced Surface Acidity in Mixed Alumina–Silicas: A Low-Temperature FTIR Study. *Appl. Catal. A: Gen* **2000**, *196* (2), 247–260.

Dappe, V.; ben Tayeb, K.; Vezin, H.; Mariette, S.; Serve, O.; Livadaris, V. Effect of Thermal Treatment of Different Petroleum Fractions: Characterization by In Situ EPR Spectroscopy. *Energy Fuels* **2020**, *34* (10), 12026–12032.

de Klerk, A. Aromatic Alkylation. In *Fischer-Tropsch Refining*; Wiley-VCH Verlag GmbH & Co. KGaA: Weinheim, Germany, 2011; pp 393–406.

de Klerk, A. Chapter 5. Catalysis in the Upgrading of Fischer-Tropsch Syncrude. In *Catalysis in the Refining of Fischer-Tropsch Syncrude*; Royal Society of Chemistry: Cambridge, 2010; pp 40–164.

de Klerk, A. Processing Unconventional Oil: Partial Upgrading of Oilsands Bitumen. *Energy Fuels* **2021**, *35* (18), 14343–14360.

de Klerk, A. Sasol 2 and 3 Facilities. In *Fischer-Tropsch Refining*; Wiley-VCH: Weinheim, Germany, 2011; pp 181–216.

de Klerk, A. Thermal Conversion Modeling of Visbreaking at Temperatures below 400 °C. *Energy Fuels* **2020**, *34* (12), 15285–15298.

de Klerk, A.; Gray, M. R.; Zerpa, N. Unconventional Oil and Gas. In *Future Energy: Improved, sustainable and clean options for our planet*; Elsevier, 2014; pp 95–116.

de Klerk, A.; Zerpa, N.; Xia, Y.; Abduljawad, O. A. Integrated Central Processing Facility (CPF) in Oil Field Upgrading (OFU). Pat. Appl. US 2014/0138287 A1, 2014.

Dryer, C. G.; Lowry, C. D.; Morrell, J. C.; Egloff, Gustav. Mechanism of Gum Formation in Cracked Gasoline - Formation of Peroxide, Aldehyde, and Acid in Storage. *Ind. Eng. Chem.* **1934**, *26* (8), 885–888.

Dupain, X.; Krul, R. A.; Makkee, M.; Moulijn, J. A. Are Fischer–Tropsch Waxes Good Feedstocks for Fluid Catalytic Cracking Units? *Catal. Today* **2005**, *106* (1–4), 288–292.

Dupain, X.; Makee, M.; Moulijn, J. Optimal Conditions in Fluid Catalytic Cracking: A Mechanistic Approach. *Appl. Catal. A: Gen* **2006**, *297* (2), 198–219.

Emanuel, N. M.; Denisov, E. T.; Maizus, Z. K. *Liquid-Phase Oxidation of Hydrocarbons*; Plenum Press: New York, 1967.

Epping, R.; Kerkering, S.; Andersson, J. T. Influence of Different Compound Classes on the Formation of Sediments in Fossil Fuels During Aging. *Energy Fuels* **2014**, *28* (9), 5649–5656.

Fong, S. Y.; Montoya Sánchez, N.; de Klerk, A. Olefin Saturation Using Asphaltenes As a Hydrogen Source. *Energy Fuels* **2020**, *34* (4), 4534–4543.

Fonseca, A.; Zeuthen, P.; Nagy, J. B. <sup>13</sup>C n.m.r. Quantitative Analysis of Catalyst Carbon Deposits. *Fuel* **1996**, *75* (12), 1363–1376.

Francis, A. W. *Critical Solution Temperatures*; FRANCIS, A. W., Ed.; Advances in Chemistry; American Chemical Society: Washington, D. C., 1961; Vol. 31.

Francis, A. W. Solvent Selectivity for Hydrocarbons. *Ind. Eng. Chem.* **1944**, *36* (8), 764–771.

Galya, L. G.; Cronauer, D. C.; Painter, P. C.; Li, N. C. Thermal Instability of Coal-Derived Naphtha. *Ind. Eng. Chem. Fundam.* **1986**, *25* (1), 129–135.

Garcia, C. L.; Lercher, J. A. Adsorption and Surface Reactions of Thiophene on ZSM 5 Zeolites. *J. Phys. Chem.* **1992**, *96* (6), 2669–2675.

García, H.; Roth, H. D. Generation and Reactions of Organic Radical Cations in Zeolites. *Chem. Rev.* **2002**, *102* (11), 3947–4008.

Gary, J. H.; Handwerk, G. E.; Kaiser, M. J. Chapter 5. Coking and Thermal Processes. In *Petroleum Refining*; CRC Press, 2007.

Gary, J. H.; Handwerk, G. E.; Kaiser, M. J. Chapter 6. Catalytic Cracking. In *Petroleum Refining*; CRC Press: Boca Raton, FL, 2007.

Gary, J. H.; Handwerk, G. E.; Kaiser, M. J. *Petroleum Refining*, Fifth.; CRC Press: Boca Raton, FL, 2007.

Gray, M. R. Chemical Composition. In *Upgrading Oilsands Bitumen and Heavy Oil*; The University of Alberta Press: Edmonton, Alberta, 2015; pp 93–142.

Gray, M. R. Fundamentals of Partial Upgrading of Bitumen. *Energy Fuels* **2019**, *33* (8), 6843–6856.

Gray, M. R. Hydrotreating Processes. In *Upgrading Oilsands Bitumen and Heavy Oil*; Gray, M. R., Ed.; The University of Alberta Press: Edmonton, Alberta, 2015; pp 405–438.

Gray, M. R. Marketing of Bitumen Products. In *Upgrading Oilsands Bitumen and Heavy Oil*; Gray, M. R., Ed.; The University of Alberta Press: Edmonton, Alberta, 2015; pp 209–230.

Gray, M. R. Thermal Cracking and Coking Processes. In *Upgrading Oilsands Bitumen and Heavy Oil*; Gray, M. R., Ed.; The University of Alberta Press: Edmonton, Alberta, 2015; pp 295–346.

Gray, M. R. *Upgrading Oilsands Bitumen and Heavy Oil*, 1st ed.; The University of Alberta Press: Edmonton, Alberta, 2015.

Gray, M. R. Upgrading Reactions and Kinetics. In *Upgrading Oilsands Bitumen and Heavy Oil*; Gray, M. R., Ed.; The University of Alberta Press: Edmonton, Alberta, 2015; pp 151–209.

Gray, M. R.; McCaffrey, W. C. Role of Chain Reactions and Olefin Formation in Cracking, Hydroconversion, and Coking of Petroleum and Bitumen Fractions. *Energy Fuels* **2002**, *16* (3), 756–766.

Gresser, J.; Rajbenbach, A.; Szwarc, M. Methyl Affinities of Some Cyclic Olefins and Polyenes. *J. Am. Chem. Soc.* **1961**, *83* (14), 3005–3008.

Gritter, R. J.; Chriss, R. J. Free-Radical Reactions of Pyrroles. *J. Org. Chem.* **1964**, *29* (5), 1163–1167.

Guisnet, M. Characterization of Deactivating Species. In *Deactivation and regeneration of zeolite catalysts*; Imperial College Press: London, 2011; pp 51–81.

Guisnet, M. Modes of Coke Formation and Deactivation. In *Deactivation and regeneration of zeolite catalysts*; 2011; pp 115–137.

Guisnet, M. Poisoning of Zeolite Catalysts. In *Deactivation and regeneration of zeolite catalysts*; Guisnet, M., Ribeiro, F. R., Eds.; Imperial College Press: London, 2011; pp 101–114.

Guisnet, M.; Magnoux, P. Organic Chemistry of Coke Formation. *Appl. Catal. A: General* **2001**, *212* (1–2), 83–96.

Hardy, D. R.; Wechter, M. A. Characterization of Soluble Macromolecular Oxidatively Reactive Species (SMORS) from Middle Distillate Diesel Fuels: Their Origin and Role in Instability. *Energy Fuels* **1994**, *8* (3), 782–787.

Havran-Mueller, V.; Blommel, J.; Nedohin, G. J. Selective Hydrogenation Processes. In *Handbook of petroleum refining processes*; Meyers, R. A., Ed.; McGraw-Hill: New York, 2016; pp 365–373.

Haw, J. F.; Song, W.; Marcus, D. M.; Nicholas, J. B. The Mechanism of Methanol to Hydrocarbon Catalysis. *Acc. Chem. Res.* **2003**, *36* (5), 317–326.

Heinrich, G.; Kasztelan, S. Hydrotreating. In *Petroleum Refining. Vol. 3. Conversion processes*; Leprince, P., Ed.; Editions Technip: Paris, 2001; pp 533–573.

Hendry, D. G.; Gould, C. W.; Schuetzle, D.; Syz, M. G.; Mayo, F. R. Autoxidations of Cyclohexane and Its Autoxidation Products. *J. Org. Chem.* **1976**, *41* (1), 1–10.

Hersberger, A. B.; Reid, J. C.; Heiligmann, R. G. Polymerization of Alpha-Methylstyrene. *Industrial and Engineering Chemistry* **1945**, *37* (11), 1073–1078.

Hirschler, A. E. The Effect of Ammonia Adsorption on the Acidity of Silica-Alumina and Alumina Catalysts. *J. Catal.* **1966**, *6* (1), 1–13.



Hosseinpour, N.; Mortazavi, Y.; Bazyari, A.; Khodadadi, A. A. Synergetic Effects of Y-Zeolite and Amorphous Silica-Alumina as Main FCC Catalyst Components on Triisopropylbenzene Cracking and Coke Formation. *Fuel Process. Technol.* **2009**, *90* (2), 171–179.

Howard, J. A.; Ingold, K. U. Absolute Rate Constants for Hydrocarbon Autoxidation. VI. Alkyl Aromatic and Olefinic Hydrocarbons. *Can. J. Chem.* **1967**, *45* (8), 793–802.

Howard, J. A.; Ingold, K. U. Absolute Rate Constants for Hydrocarbon Autoxidation. XVII. The Oxidation of Some Cyclic Ethers. *Can. J. Chem.* **1969**, *47* (20), 3809–3815.

Ipatieff, V. N.; Corson, B. B.; Egloff, G. Polymerization, a New Source of Gasoline. *Ind. Eng. Chem.* **1935**, *27* (9), 1077–1081.

Jackson, H. L.; McCormack, W. B.; Rondestvedt, C. S.; Smeltz, K. C.; Viele, I. E. Control of Peroxidizable Compounds. *J. Chem. Educ.* **1970**, *47* (3), A175.

Jayaseharan, J.; Kishore, K. Mechanism of “Autoacceleration” in the Thermal Oxidative Polymerization of  $\alpha$ -Methylstyrene. *Macromolecules* **1997**, *30* (14), 3958–3964.

Jin, Y.; Liu, T.; Ma, J.; Wang, H. Selective Hydrogenation Catalyst of Ni-Mg/Al<sub>2</sub>O<sub>3</sub> for FCC Light Gasoline. *Petrol. Sci. Technol.* **2005**, *23* (2), 109–117.

Jones, D. S. J. Upgrading the Bottom of the Barrel. In *Handbook of Petroleum Processing*; Treese, S. A., Pujado, P. R., Jones, D. S. J., Eds.; Springer International Publishing: Cham, 2015; pp 531–564.

Joshi, J. B.; Pandit, A. B.; Kataria, K. L.; Kulkarni, R. P.; Sawarkar, A. N.; Tandon, D.; Ram, Y.; Kumar, M. M. Petroleum Residue Upgradation via Visbreaking: A Review. *Ind. Eng. Chem. Res.* **2008**, *47* (23), 8960–8988.

Kaiser, M. J.; de Klerk, A.; Gary, J. H.; Handwerk, G. E. *Petroleum Refining: Technology, Economics, and Markets*, Sixth Edit.; CRC Press: Boca Raton, FL, 2020.

Kapustin, G. I.; Brueva, T. R.; Klyachko, A. L.; Beran, S.; Wichterlova, B. Determination of the Number and Acid Strength of Acid Sites in Zeolites by Ammonia Adsorption. *Appl. Catal.* **1988**, *42* (2), 239–246.

Karge, H. G. Coke Formation on Zeolites. In *Studies in Surface Science and Catalysis*; 2001; Vol. 137, pp 707–746.

Karge, H. G.; Lange, J.-P.; Gutsze, A.; Łaniecki, M. Coke Formation through the Reaction of Olefins over Hydrogen Mordenite: II. In Situ EPR Measurements under on-Stream Conditions. *J. Catal.* **1988**, *114* (1), 144–152.

Kawahara, F. K. Composition of Gum in Cracked Naphtha. *Ind. Eng. Chem. Prod. Res. Dev.* **1965**, *4* (1), 7–9.

Keller, F.; Röchardt, C. Bimolecular Formation of Radicals by Hydrogen Transfer. 14. The Uncatalyzed Transfer Hydrogenation of  $\alpha$ -Methylstyrene by 2,6-Disubstituted 9,10-Dihydroanthracenes. *Journal für Praktische Chemie/Chemiker-Zeitung* **1998**, *340* (7), 642–648.

Khorasheh, F.; Gray, M. R. High-Pressure Thermal Cracking of n-Hexadecane. *Ind. Eng. Chem. Res.* **1993**, *32* (9), 1853–1863.

Kirsch, F. W.; Heinemann, Heinz.; Stevenson, D. H. Selective Hydrodesulfurization of Cracked Gasolines. *Ind. Eng. Chem.* **1957**, *49* (4), 646–649.

Kistiakowsky, G. B.; Ruhoff, J. R.; Smith, H. A.; Vaughan, W. E. Heats of Organic Reactions III. Hydrogenation of Some Higher Olefins. *J. Am. Chem. Soc.* **1936**, *58* (1), 137–145.

Knottenbelt, C. Moss gas “Gas-to-Liquid” Diesel Fuels—an Environmentally Friendly Option. *Catal. Today* **2002**, *71* (3–4), 437–445.

Kokayeff, P.; Zink, S.; Roxas, P. Hydrotreating in Petroleum Processing. In *Handbook of Petroleum Processing*; Treese, S. A., Pujado, P. R., Jones, D. S. J., Eds.; Springer International Publishing: Cham, 2015; pp 361–434.

Kopecky, K. R.; Lau, M.-P. Thermal Reaction between 5-Methylene-1,3-Cyclohexadiene and Styrene. *The Journal of Organic Chemistry* **1978**, *43* (3), 525–526.

Lange, J.-P.; Gutsze, A.; Karge, H. G. Coke Formation through the Reaction of Olefins over Hydrogen Mordenite: I. EPR Measurements under Static Conditions. *J. Catal.* **1988**, *114* (1), 136–143.

Lengyel, A.; Magyar, S.; Hancsók, J. Catalytic Co-Processing of Delayed Coker Light Naphtha with Other Refinery Gasoline Streams. *Period. Polytech.: Chem. Eng* **2009**, *53* (1), 3–7.

Letzsch, W. Fluid Catalytic Cracking (FCC) in Petroleum Refining. In *Handbook of Petroleum Processing*; Treese, S. A., Pujadó, P. R., Jones, D. S. J., Eds.; Springer International Publishing: Cham, 2015; pp 261–316.

Li, J. Storage Stability of Jet Fuels. *Fuel* **1985**, *64* (8), 1041–1046.

Li, L.; Hou, Y.; Wu, W.; Liang, S.; Ren, S. Behaviors of Tetralin and 9,10-Dihydroanthracene as Hydrogen Donor Solvents in the Hydrogenolysis of Coal-Related Model Compounds. *Fuel Process. Technol.* **2019**, *191* (April), 202–210.

Li, L.; Zhai, Y.; Zhang, J.; Wang, J.; Yu, T. A New Catalyst for the Non-Hydrogenation Reduction of Olefins. *Petrol. Sci. Technol.* **2007**, *25* (4), 427–441.

Lide, D. R. *CRC Handbook of Chemistry and Physics*, 84th ed.; CRC Press: New York, 2003.

Loison, R.; Foch, P.; Boyer, A. *Coke. Quality and Production*; Butterworth: London, 1989.

Loveless, B. T.; Gyanani, A.; Muggli, D. S. Discrepancy between TPD- and FTIR-Based Measurements of Brønsted and Lewis Acidity for Sulfated Zirconia. *Appl. Catal. B: Environ* **2008**, *84* (3–4), 591–597.

Lynch, D. T.; Wanke, S. E. Isomerization of Alkenes during Drying over Zeolites. *React. Kinet. Catal. Lett.* **1994**, *52* (2), 241–247.

Madeira, F. F.; Gnep, N. S.; Magnoux, P.; Vezin, H.; Maury, S.; Cadran, N. Mechanistic Insights on the Ethanol Transformation into Hydrocarbons over HZSM-5 Zeolite. *Chem. Eng. J.* **2010**, *161* (3), 403–408.

Martin, P.; McCarty, F.; Ehrmann, U.; Lima, L. de; Carvajal, N.; Rojas, A. Characterization and Deposit Forming Tendency of Polar Compounds in Cracked Components of Gasoline. Identification of Phenols and Aromatic Sulfur Compounds. *Fuel Science and Technology International* **1994**, *12* (2), 267–280.

Mayo, F. R. Some New Ideas on Oxidation. *Ind. Eng. Chem.* **1960**, *52* (7), 614–618.

Mayo, F. R. The Dimerization of Styrene. *J Am Chem Soc* **1968**, *90* (5), 1289–1295.

Mayo, F. R.; Miller, A. A. The Oxidation of Unsaturated Compounds. VI. The Effect of Oxygen Pressure on the Oxidation of  $\alpha$ -Methylstyrene. *J Am Chem Soc* **1958**, *80* (10), 2480–2493.

McLafferty, F. W.; Tureček, František. *Interpretation of Mass Spectra*, 4 ed.; University Science Books: Mill Valley, CA, 1993.

Melpolder, F. W.; Brown, R. A.; Young, W. S.; Headington, C. E. Composition of Naphtha from Fluid Catalytic Cracking. *Ind. Eng. Chem.* **1952**, *44* (5), 1142–1146.

Mercier Des Rochettes, B.; Marcilly, C.; Gueguen, C.; Bousquet, J. Coke Formation Mechanism from Olefins or Diolefins under Catalytic Cracking Conditions. *Studies in Surface Science and Catalysis* **1987**, *34* (C), 589–603.

Metzger, J. O. Formation of Alkyl Radicals by Thermal Bimolecular Reaction of Alkanes and Alkenes. *Angewandte Chemie International Edition in English* **1983**, *22* (11), 889–889.

Metzger, J. O.; Bangert, F. Thermally Initiated Free-Radical Chain Addition of Alkanes to Alkynes, II. Kinetics of the Addition of Cyclohexane to Phenylethyne under Supercritical Fluid Conditions. *Chem Ber* **1994**, *127* (4), 673–675.

Mills, G. A.; Boedeker, E. R.; Oblad, A. G. Chemical Characterization of Catalysts. I. Poisoning of Cracking Catalysts by Nitrogen Compounds and Potassium Ion \*. *J Am Chem Soc* **1950**, *72* (4), 1554–1560.

Mirzoeva, L. M. Low-Temperature Hydrofining of Catalytically Cracked Light Gasoline Fraction. *Chem. Technol. Fuels Oils* **2014**, *50* (3), 225–229.

Mishin, I. v.; Brueva, T. R.; Kapustin, G. I. Heats of Adsorption of Ammonia and Correlation of Activity and Acidity in Heterogeneous Catalysis. *Adsorption* **2005**, *11* (3–4), 415–424.

Mochizuki, T.; Itou, H.; Toba, M.; Miki, Y.; Yoshimura, Y. Effects of Acidic Properties on the Catalytic Performance of CoMo Sulfide Catalysts in Selective Hydrodesulfurization of Gasoline Fractions. *Energy Fuels* **2008**, *22* (3), 1456–1462.

Montoya Sánchez, N.; de Klerk, A. Autoxidation of Aromatics. *Appl. Petrochem. Res* **2018**, *8* (2), 55–78.

Morgenthaler, J.; Rüchardt, C. Bimolecular Formation of Radicals by Hydrogen Transfer, 11. Transfer Hydrogenation of Conjugated Cyclic Dienes and Trienes. *Liebigs Annalen* **1996**, *1996* (10), 1529–1532.

Naghizada, N.; Prado, G. H. C.; de Klerk, A. Uncatalyzed Hydrogen Transfer during 100–250 °C Conversion of Asphaltenes. *Energy Fuels* **2017**, *31* (7), 6800–6811.

Nagpal, J. M.; Joshi, G. C.; Rastogi, S. N. Stability of Cracked Naphthas from Thermal and Catalytic Processes and Their Additive Response. Part I. Evaluation of Stability and Additive Response. *Fuel* **1995**, *74* (5), 714–719.

Nagpal, J. M.; Joshi, G. C.; Rastogi, S. N. Stability of Cracked Naphthas from Thermal and Catalytic Processes and Their Additive Response. Part II. Composition and Effect of Olefinic Structures. *Fuel* **1995**, *74* (5), 720–724.

Nagpal, J. M.; Joshi, G. C.; Rastogi, S. N. Stability of Cracked Naphthas from Thermal and Catalytic Processes and Their Additive Response. Part I. Evaluation of Stability and Additive Response. *Fuel* **1995**, *74* (5), 714–719.

Nagpal, J. M.; Joshi, G. C.; Singh, I. D.; Kumar, K. Studies on the Nature of Gum Formed in Cracked Naphthas. In *6th International Conference on Stability and Handling of Liquid Fuels*; Vancouver, Canada, 1997; pp 543–550.

Nagpal, J. M.; Joshi, G. C.; Singh, J.; Rastogi, S. N. Gum Forming Olefinic Precursors in Motor Gasoline, a Model Compound Study. *Fuel Science and Technology International* **1994**, *12* (6), 873–894.

Naragon, E. A. Catalytic Isomerization of 1-Hexene. *Ind. Eng. Chem.* **1950**, *42* (12), 2490–2493.

Nel, R. J. J.; de Klerk, A. Selectivity Differences of Hexene Isomers in the Alkylation of Benzene over Solid Phosphoric Acid. *Ind. Eng. Chem. Res.* **2007**, *46* (9), 2902–2906.

Nicholas, C. P. Applications of Light Olefin Oligomerization to the Production of Fuels and Chemicals. *Appl. Catal. A: Gen* **2017**, *543* (March), 82–97.

Niizuma, S.; Steele, C. T.; Gunning, H. E.; Strausz, O. P. Electron Spin Resonance Study of Free Radicals in Athabasca Asphaltene. *Fuel* **1977**, *56* (3), 249–256.

Nuntasri, D. High Selectivity of MCM-22 for Cyclopentanol Formation in Liquid-Phase Cyclopentene Hydration. *J. Catal.* **2003**, *213* (2), 272–280.

Oswald, A. A.; Noel, F. Role of Pyrroles in Fuel Instability. *J. Chem. Eng. Data* **1961**, *6* (2), 294–301.

Ouellette, R. J.; Rawn, J. D. Alkenes: Structures and Properties. In *Organic Chemistry*; Elsevier, 2018; pp 135–165.

Ouellette, R. J.; Rawn, J. D. Conjugated Alkenes and Allylic Systems. In *Organic Chemistry*; Ouellette, R. J., Rawn, J. D., Eds.; Elsevier, 2018; pp 321–351.

Paez, N. Identification, Conversion and Reactivity of Diolefins in Thermally Cracked Naphtha. MSc. Thesis, University of Alberta, 2016.

Paez, N. Y.; de Klerk, A. Diolefin Characterization in a Thermally Cracked Naphtha. *Prepr. Pap.-Am. Chem. Soc., Div. Energy Fuels* **2016**, *61* (1), 12–15.

Parsons, A. F. *Introduction to Free Radical Chemistry*; Blackwell Science: Oxford, 2000.

Payan, F.; de Klerk, A. Hydrogen Transfer in Asphaltenes and Bitumen at 250 °C. *Energy Fuels* **2018**, *32* (9), 9340–9348.

Perego, C.; Ingallina, P. Recent Advances in the Industrial Alkylation of Aromatics: New Catalysts and New Processes. *Catal. Today* **2002**, *73* (1–2), 3–22.

Pereira, R. C. C.; Pasa, V. M. D. Effect of Mono-Olefins and Diolefins on the Stability of Automotive Gasoline. *Fuel* **2006**, *85* (12–13), 1860–1865.

Pinard, L.; Hamieh, S.; Canaff, C.; Ferreira Madeira, F.; Batonneau-Gener, I.; Maury, S.; Delpoux, O.; ben Tayeb, K.; Pouilloux, Y.; Vezin, H. Growth Mechanism of Coke on HBEA Zeolite during Ethanol Transformation. *J. Catal.* **2013**, *299*, 284–297.

Pinard, L.; Hamieh, S.; Canaff, C.; Tarighi, M.; Maury, S.; Tayeb, K. ben; Pouilloux, Y.; Vezin, H. Growth Mechanism of Coke on Outside and inside HBEA Zeolite Pore during Ethanol Transformation. **2013**, *3*, 4–5.

Pinard, L.; Tayeb, K. ben; Hamieh, S.; Vezin, H.; Canaff, C.; Maury, S.; Delpoux, O.; Pouilloux, Y. On the Involvement of Radical “Coke” in Ethanol Conversion to Hydrocarbons over HZSM-5 Zeolite. *Catal. Today* **2013**, *218–219*, 57–64.

Pradelle, F.; Braga, S. L.; Martins, A. R. F. A.; Turkovics, F.; Pradelle, R. N. C. Gum Formation in Gasoline and Its Blends: A Review. *Energy Fuels* **2015**, *29* (12), 7753–7770.

Prado, G. H. C.; Rao, Y.; de Klerk, A. Nitrogen Removal from Oil: A Review. *Energy Fuels* **2017**, *31* (1), 14–36.

Pryor, W. A. Part II The Production of Radicals. In *Free radicals*; McGraw-Hill: New York, 1966; pp 57–145.

Pryor, W. A.; David, G.; Green, J. G. Radical Production from the Interaction of Closed-Shell Molecules. 5. The Chemistry of Methylene cyclohexadiene<sup>1</sup>. *Journal of Organic Chemistry* **1978**, *43* (3), 526–528.

Rahimi, P.; Chen, J.; Brecher, L.; DeBruijn, T. Hydrotreating of Liquid Products from Cold Lake Bitumen Obtained in the WRITE Process. *Prepr. Pap.-Am. Chem. Soc., Div. Fuel Chem* **2004**, *49* (1), 75–76.

Rajbenbach, A.; Szwarc, M. Addition of Methyl Radicals to Isolated, Conjugated and Cumulated Dienes. *Proceedings of the Royal Society of London. Series A. Mathematical and Physical Sciences* **1959**, *251* (1266), 394–406.

Rajbenbach, A.; Szwarc, M. Methyl Affinities of Dienes. *J. Am. Chem. Soc.* **1957**, *79* (23), 6343–6344.

Rao, Y.; de Klerk, A. Characterization of Heteroatom-Containing Compounds in Thermally Cracked Naphtha from Oilsands Bitumen. *Energy Fuels* **2017**, *31* (9), 9247–9254.

Rezaei, M.; Gieleciak, R.; Michaelian, K. H. Determination of Olefin Contents in Liquid Hydrocarbons Using a Quantum Cascade Laser and a Photoacoustic Detector. *Energy Fuels* **2019**, *33* (4), 2859–2866.

Rhodes, C. J. Electron Paramagnetic Resonance Study of Radical Formation from Cyclopentene and Dimethylacetylene Following Adsorption onto H-Mordenite. *J. Chem. Soc. Faraday Trans.* **1991**, *87* (19), 3179–3184.

Rhodes, C. J.; Standing, M. Formation of 9-Octalin (1,2,3,4,5,6,7,8-Octahydronaphthalene) Radical Cations on Adsorption of Acyclic Dienes onto H-Mordenite. *J. Chem. Soc., Perkin Trans. 2 Society, Perkin Transactions 2* **1992**, No. 9, 1455.

Richardeau, D.; Joly, G.; Canaff, C.; Magnoux, P.; Guisnet, M.; Thomas, M.; Nicolaos, A. Adsorption and Reaction over HFAU Zeolites of Thiophene in Liquid Hydrocarbon Solutions. *Appl. Catal. A: Gen* **2004**, *263* (1), 49–61.

Rogel, E. Theoretical Approach to the Stability of Visbroken Residues. *Energy Fuels* **1998**, *12* (5), 875–880.



Rüchardt, C.; Gerst, M.; Ebenhoch, J. Uncatalyzed Transfer Hydrogenation and Transfer Hydrogenolysis: Two Novel Types of Hydrogen-Transfer Reactions. *Angew. Chem., Int. Ed. Engl.* **1997**, *36* (1314), 1406–1430.

Rüchardt, C.; Gerst, M.; Nölke, M. The Uncatalyzed Transfer Hydrogenation of  $\alpha$ -Methylstyrene by Dihydroanthracene or Xanthene—a Radical Reaction. *Angew. Chem., Int. Ed. Engl.* **1992**, *31* (11), 1523–1525.

Ryder, A. G. Analysis of Crude Petroleum Oils Using Fluorescence Spectroscopy. In *Reviews in Fluorescence 2005 Volume 2*; Geddes, C. D., Lakowicz, J. R., Eds.; Springer International Publishing, 2005; pp 169–194.

Sadeghbeigi, R. Process Description. In *Fluid Catalytic Cracking Handbook*; Sadeghbeigi, R., Ed.; Elsevier, 2012; pp 1–42.

Sakuneka, T. M.; de Klerk, A.; Nel, R. J. J.; Pienaar, A. D. Synthetic Jet Fuel Production by Combined Propene Oligomerization and Aromatic Alkylation over Solid Phosphoric Acid. *Ind. Eng. Chem. Res.* **2008**, *47* (6), 1828–1834.

Sandhiya, L.; Jangra, H.; Zipse, H. Molecule-Induced Radical Formation (MIRF) Reactions—A Reappraisal. *Angew. Chem. Int. Ed.* **2020**, *59* (16), 6318–6329.

Schultz, F.; Seluckyts, L. E.s.r. Measurements on Asphaltene and Resin Fractions from Various Separation Methods. *Fuel.* **1981**, *60*, 951–956.

Sergeyev, P. G.; Ivanova, L. A. The Oxidation of Hexenes. In *The Oxidation of Hydrocarbons in the Liquid Phase*; Emanuel, N. M., Ed.; Elsevier, 1965; pp 211–218.

Shaban, H. I.; Khan, A. R. Pressure-Related Operational Problems and Their Remedies in Hydrotreating Reactors in Petroleum Refineries. *J. Pet. Sci. Eng* **1995**, *14* (1–2), 79–88.

Shan Ahamed, T.; Anto, S.; Mathimani, T.; Brindhadevi, K.; Pugazhendhi, A. Upgrading of Bio-Oil from Thermochemical Conversion of Various Biomass – Mechanism, Challenges and Opportunities. *Fuel* **2021**, *287*, 119329.

Siddiquee, M. N.; de Klerk, A. Hydrocarbon Addition Reactions during Low-Temperature Autoxidation of Oilsands Bitumen. *Energy Fuels* **2014**, *28* (11), 6848–6859.

Siddiquee, M. N.; de Klerk, A. In Situ Measurement of Liquid Phase Oxygen during Oxidation. *Ind. Eng. Chem. Res.* **2016**, *55* (23), 6607–6618.

Siddiquee, M. N.; de Klerk, A. Reaction Engineering Related to Initiation in Liquid Phase Hydrocarbon Autoxidation. *Unpublished*.

Siddiquee, M. N.; Wu, Y.; de Klerk, A.; Nazemifard, N. The Impact of Microfluidic Reactor Configuration on Hydrodynamics, Conversion and Selectivity during Indan Oxidation. *J. Flow Chem* **2020**, *10* (4), 647–660.

Sie, S. T. Acid-Catalyzed Cracking of Paraffinic Hydrocarbons. 1. Discussion of Existing Mechanisms and Proposal of a New Mechanism. *Ind. Eng. Chem. Res.* **1992**, *31* (8), 1881–1889.

Silverstein, R. M.; Webster Francis X. Mass Spectrometry. In *Spectrometric Identification of Organic Compounds*; John Wiley & Sons, Inc.: New York, 1998; pp 2–70.

Smith, M. B. Acids, Bases, Nucleophiles, and Electrophiles. In *Organic Chemistry: An Acid-Base Approach*; Smith, M. B., Ed.; CRC Press, 2016; pp 163–205.

Speight, J. G. Thermal Cracking. In *The Refinery of the Future*; Speight, J. G., Ed.; Elsevier, 2020; pp 161–195.

Stark, C. M. *Free Radical Telomerization*; New York: Academic Press, 1974.

Stiegel, G. J.; Shah, Y. T.; Krishnamurthy, S.; Panvelker, S. v. Refining of Coal Liquids. In *Reaction engineering in direct coal liquefaction*; Shah, Y. T., Ed.; Addison-Wesley: Reading, MA, 1981; pp 285–381.

Stockert, J. C.; Blazquez-Castro, A. *Fluorescence Microscopy in Life Sciences*; Stockert, J. C., Blazquez-Castro, A., Eds.; BENTHAM SCIENCE PUBLISHERS: Sharjah, 2017.

Stuart, B. H. *Infrared Spectroscopy: Fundamentals and Applications*; Analytical Techniques in the Sciences; John Wiley & Sons, Ltd: Chichester, UK, 2004.

Tannous, J. H.; de Klerk, A. Asphaltenes Formation during Thermal Conversion of Deasphalted Oil. *Fuel* **2019**, *255*, 115786.

Tannous, J. H.; de Klerk, A. Quantification of the Free Radical Content of Oilsands Bitumen Fractions. *Energy Fuels* **2019**, *33* (8), 7083–7093.

Taylor, W. F. Kinetics of Deposit Formation from Hydrocarbons. Fuel Composition Studies. *Ind. Eng. Chem. Prod. Res. Dev.* **1969**, *8* (4), 375–380.

Taylor, W. F.; Wallace, T. J. Kinetics of Deposit Formation from Hydrocarbons. Effect of Trace Sulfur Compounds. *Ind. Eng. Chem. Prod. Res. Dev.* **1968**, *7* (3), 198–202.

Thompson, R. B.; Chenicek, J. A.; Druge, L. W.; Symon, T. Stability of Fuel Oils in Storage - Effect of Some Nitrogen Compounds. *Ind. Eng. Chem.* **1951**, *43* (4), 935–939.

Thompson, R. B.; Druge, L. W.; Chenicek, J. A. Stability of Fuel Oils in Storage: Effect of Sulfur Compounds. *Ind. Eng. Chem.* **1949**, *41* (12), 2715–2721.

Usmanov, M. R.; Batyrov, N. A.; Galimov, Z. F.; Khairullin, R. N.; Bilalov, R. T. Treatment of Visbreaker Naphtha Fraction by Oligomerization. *Chem. Technol. Fuels Oils* **1999**, *35* (1), 4–6.

Uzcátegui, G.; de Klerk, A. Causes of Deactivation of an Amorphous Silica-Alumina Catalyst Used for Processing of Thermally Cracked Naphtha in a Bitumen Partial Upgrading Process. *Fuel* **2021**, *293*, 120479.

Uzcátegui, G.; Fong, S. Y.; de Klerk, A. Cracked Naphtha Reactivity: Effect of Free Radical Reactions. *Energy Fuels* **2018**, *32* (5), 5812–5823.

Venuto, P. B.; Habib, E. T. *Fluid Catalytic Cracking with Zeolite Catalysts*; Marcel Dekker: New York, 1979.

Vogt, E. T. C.; Weckhuysen, B. M. Fluid Catalytic Cracking: Recent Developments on the Grand Old Lady of Zeolite Catalysis. *Chem. Soc. Rev.* **2015**, *44* (20), 7342–7370.

Walters, E. L.; Minor, H. B.; Yabroff, D. L. Chemistry of Gum Formation in Cracked Gasoline. *Ind. Eng. Chem.* **1949**, *41* (8), 1723–1729.

Watkinson, A. P.; Wilson, D. I. Chemical Reaction Fouling: A Review. *Exp. Therm. Fluid Sci.* **1997**, *14* (4), 361–374.

Wiehe, I. A. Self-Incompatible Crude Oils and Converted Petroleum Resids. *J Dispers Sci Technol* **2004**, *25* (3), 333–339.

Wright, B.; Hughes, B. Mitigation of Heat Exchanger Fouling. *Digital refining* **2012**, 1–5.

Wu, G.; Katsumura, Y.; Matsuura, C.; Ishigure, K.; Kubo, J. Comparison of Liquid-Phase and Gas-Phase Pure Thermal Cracking of n -Hexadecane. *Ind. Eng. Chem. Res.* **1996**, *35* (12), 4747–4754.

Xia, Y. Acid Catalyzed Aromatic Alkylation in the Presence of Nitrogen Bases. MSc Thesis, University of Alberta, Edmonton, AB, Canada, University of Alberta, 2012.

Xin, Q.; Alvarez-Majmutov, A.; Gieleciak, R.; Chen, J.; Dettman, H. Hydrotreatment of Olefins in Thermally Processed Bitumen under Mild Conditions. *Energy Fuels* **2019**, *33* (4), 3098–3107.

Xing, T.; Ali, M.; Alem, T.; Gieleciak, R.; Chen, J. Fouling Tendency of Bitumen Visbreaking Products. *Fuel* **2021**, *289*, 119735.

Yan, Y.; C. Prado, G. H.; de Klerk, A. Storage Stability of Products from Visbreaking of Oilsands Bitumen. *Energy Fuels* **2020**, *34* (8), 9585–9598.

Yui, S. Removing Diolefins from Coker Naphtha Necessary before Hydrotreating. *Oil Gas J.* **1999**, *97* (36), 64–69.

Yui, S.; Chan, E. Hydrogenation of Coker Naphtha with Nimo Catalyst. *Stud. Surf. Sci. Catal* **1992**, *73*, 59–66.

Zaikov, G. E.; Howard, J. A.; Ingold, K. U. Absolute Rate Constants for Hydrocarbon Autoxidation. XIII. Aldehydes: Photo-Oxidation, Co-Oxidation, and Inhibition. *Can. J. Chem.* **1969**, *47* (16), 3017–3029.

Zaki, M. I.; Hasan, M. a; Al-sagheer, F. a. In Situ FTIR Spectra of Pyridine Adsorbed on SiO<sub>2</sub> – Al<sub>2</sub>O<sub>3</sub>, TiO<sub>2</sub>, ZrO<sub>2</sub> and CeO<sub>2</sub>: General Considerations for the Identification of Acid Sites on Surfaces of Finely Divided Metal Oxides. *Colloids and Surfaces A*. 2001, pp 261–274.

Zerpa, N. G.; de Klerk, A.; Xia, Y.; Omer, A. A. Olefins Reduction of a Hydrocarbon Feed Using Olefins- Aromatics Alkylation. Canadian Patent application 2916767, 2015.

Zhang, J.; Shan, H.; Chen, X.; Liu, W.; Yang, C. Fluid Catalytic Cracking Study of Coker Gas Oil: Effects of Processing Parameters on Sulfur and Nitrogen Distributions. *Energy Fuels* **2014**, 28 (2), 1362–1371.

Zhang, N.; Zhao, S.; Sun, X.; Xu, Z.; Xu, C. Storage Stability of the Visbreaking Product from Venezuela Heavy Oil. *Energy Fuels* **2010**, 24 (7), 3970–3976.

Zhang, Y.; Siskin, M.; Gray, M. R.; Walters, C. C.; Rodgers, R. P. Mechanisms of Asphaltene Aggregation: Puzzles and a New Hypothesis. *Energy Fuels* **2020**, 34 (8), 9094–9107.

## Appendixes

### Appendix A. Support information for Chapter 4.

#### A.1. Chromatograms of control reactions.

The following figures show the chromatograms of the products from the reactions of the thermally cracked naphtha with AMS (Naphtha + AMS) compared to the same section of the chromatograms corresponding to the two control reactions carried: (i) Naphtha alone, to check for possible thermal reactions occurring in the naphtha, and (ii) Pentane with AMS on the same concentration as reactions carried with naphtha, to discard AMS self-initiation. Figure A1, A2, and A3, shows the results for 200 °C, 250 °C, and 300 °C, respectively.

#### 7.4. A.1. Chromatograms of control reactions.

The following figures show the chromatograms of the products from the reactions of the thermally cracked naphtha with AMS (Naphtha + AMS) compared to the same section of the chromatograms corresponding to the two control reactions carried: (i) Naphtha alone, to check for possible thermal reactions occurring in the naphtha, and (ii) Pentane with AMS on the same concentration as reactions carried with naphtha, to discard AMS self-initiation. Figure A1, A2, and A3, shows the results for 200 °C, 250 °C, and 300 °C, respectively.

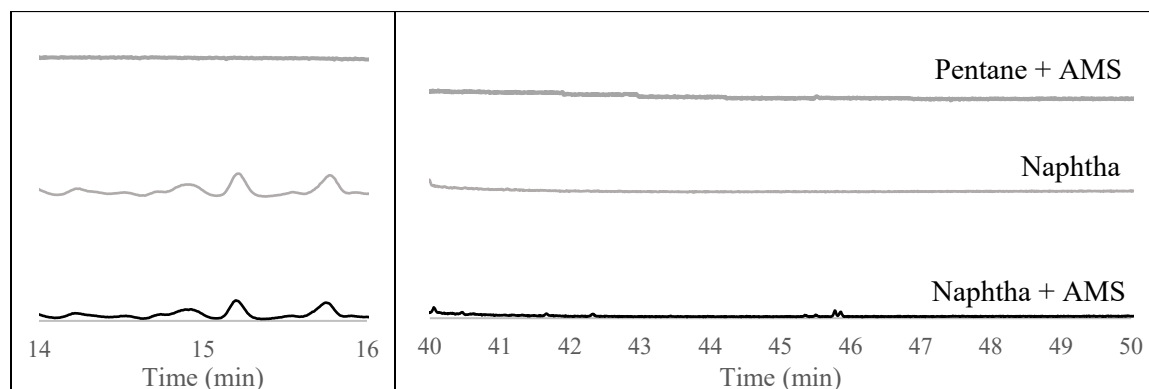


Figure A7. Reactions at 200 °C

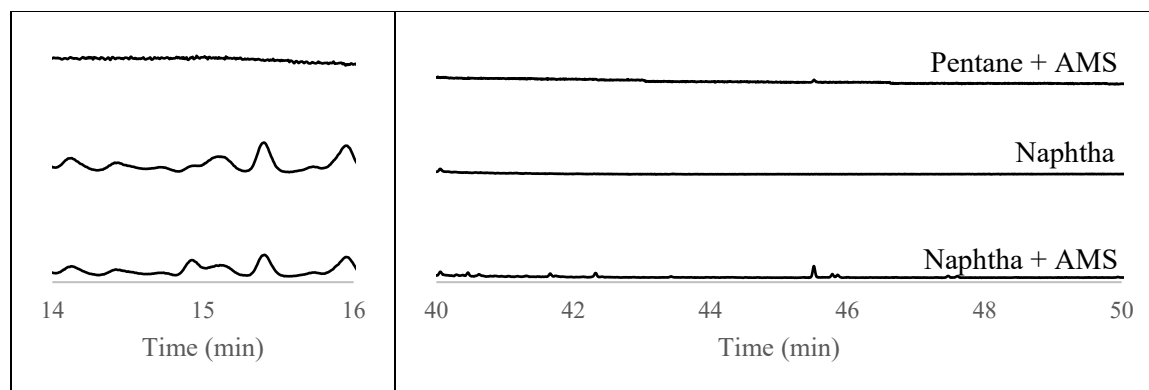


Figure A8. Reactions at 250 °C

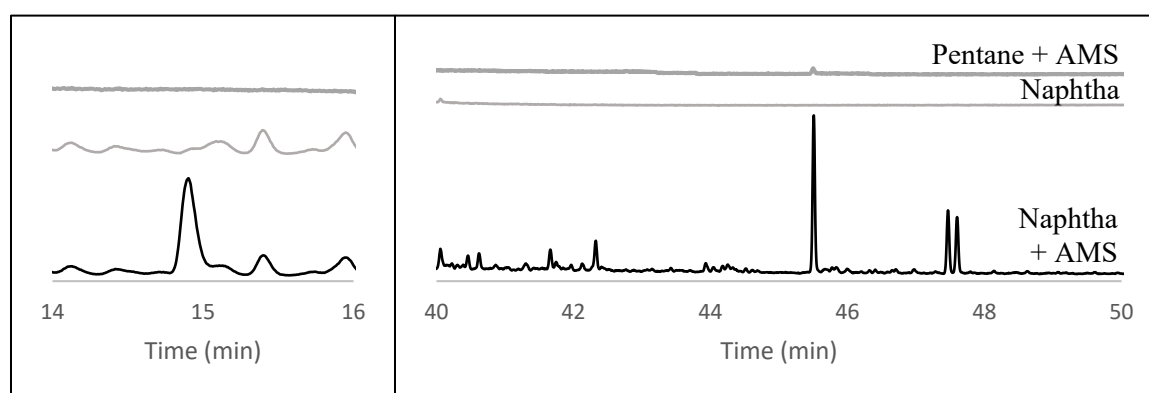


Figure A9. Reactions at 300 °C

## Appendix B: Support information for Chapter 5.

### B1. Dimerization products from the reaction of cyclopentene and Siral30.

The chromatogram of the products and their highlighted retention time are shown in Figure B0.1. The product identification was done using the MS search library and the authentic compounds when available. Table B6 lists the most likely structures for such compounds, as well as key information from the mass spectra, like the molecular ion and the base peak ion (highest intensity peak). The molecular ion would correspond to the higher molecular mass ion that could form upon fractioning of the molecule, and the highest intensity ion corresponds to the most stable ion that can be formed upon fractioning in the mass spectrometer.

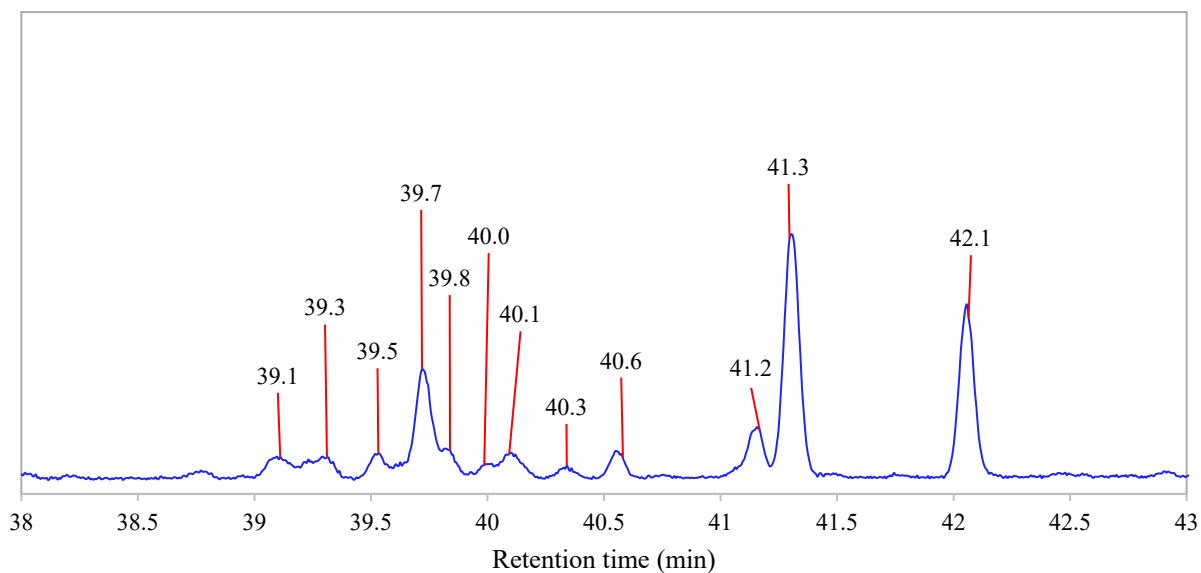
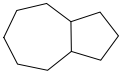
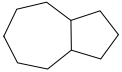
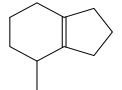
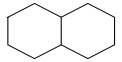
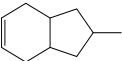
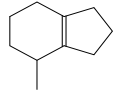
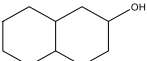
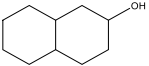

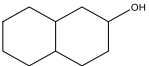
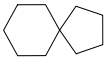
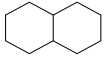
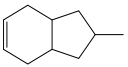
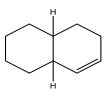


Figure B0.1. Chromatogram of dimerization products from reaction of cyclopentene on Siral30 at 300 °C.



Table B6. Suggested compounds for the main dimerization products from reactions of cyclopentene on Siral30.

| <b>Retention time (min)</b> | <b>Suggestions</b>                     | <b>Structure</b>                                                                    | <b>Probability</b> | <b>Molecular ion</b> | <b>Base peak ion</b> |
|-----------------------------|----------------------------------------|-------------------------------------------------------------------------------------|--------------------|----------------------|----------------------|
| 39.1                        | Bicyclo[5.3.0]decane (cis)             |    | 30.4%              | 138                  | 81                   |
| 39.3                        | Bicyclo[5.3.0]decane (cis)             |    | 12.5%              | 138                  | 95                   |
| 39.5                        | 2-Methylbicyclonon-1(6)-ene            |    | 36.2%              | 136                  | 121                  |
| 39.7                        | Decahydronaphthalene                   |    | 18.4%              | 138                  | 138                  |
| 39.8                        | 2-Methyl-cis-3a,4,7,7a-tetrahydroindan |   | 12.7%              | 136                  | 79                   |
| 40.0                        | 2-Methylbicyclo[4.3.0]non-1(6)-ene     |  | 16.1%              | 136                  | 121                  |
| 40.1                        | Decahydro-2-naphthalenol               |  | 34.1%              | 136                  | 121                  |

|             |                                           |                                                                                    |       |     |     |
|-------------|-------------------------------------------|------------------------------------------------------------------------------------|-------|-----|-----|
| <b>40.3</b> | Decahydro-2-naphthalenol                  |   | 28.6% | 136 | 95  |
| <b>40.6</b> | Spirodecane                               |   | 14.9% | 138 | 68  |
| <b>41.2</b> | Decahydro-2-naphthalenol                  |   | 9.2%  | 136 | 79  |
| <b>41.3</b> | Spirodecane                               |   | 26.8% | 138 | 138 |
|             | Decahydronaphthalene                      |   | 21.6% |     |     |
| <b>42.1</b> | 2-Methyl-trans-3a,4,7,7a-tetrahydroindane |   | 10.4% | 136 | 136 |
|             | Octahydronaphthalene                      |  | 8.5%  |     |     |

Although it is difficult to determine the structure of a compound based on this information, the molecular ion and the most stable ion can be used to discard the possibility of certain structures. A methyindene type molecule, for instance, has a molecular weight of 130 g/mol that corresponds to the molecular ion on its mass spectrum (i.e. 130 m/z). In this case, the molecular ion is also the most stable ion (base peak), being the peak with the highest intensity. Upon fractionating, the second most stable ion formed a methyindene type molecule would be an indene ion with a m/z=115. This would yield a spectrum where the highest intensity peak would be at 130 m/z, followed by the peak at 115 m/z.

From the molecular ion peak and base peak information of the products from the reactions of cyclopentene on Siral30, listed in Table B6, we can conclude that methyindene type molecules are not among them.